The role of hippocampal calcium-permeable AMPA receptors in network activity and behaviour

Matthew Cooper

A thesis submitted for the degree of Doctor of Philosophy

Department of Physiology, Anatomy and Genetics

Green Templeton College

University of Oxford

Michaelmas Term, 2018

Abstract

Parvalbumin-expressing (PV+) interneurons within the hippocampus play important roles in controlling spike timing and spike rates in circuits within the hippocampus, a brain region widely associated with various aspects of memory and spatial navigation. Due to minimal expression of the GluR2 AMPA receptor subunit, excitatory synapses onto PV+ interneurons are dominated by inwardly rectifying, Ca^{2+}-permeable AMPA receptors (CP-AMPARs); in contrast, many other cell types, including principal cells, predominantly express GluR2-containing receptors. In addition to contributing to rapid excitation of these fast-spiking cells, CP-AMPARs are capable of mediating synaptic plasticity independent of NMDA receptors, with LTP following anti-Hebbian rules. Given the central role of PV+ interneurons in multiple aspects of hippocampal network function, including theta- and gamma-frequency oscillatory patterns of activity, the work in this thesis explored what impact manipulating neuronal recruitment and synaptic plasticity mediated by these receptors would have on the function of the hippocampal network and associated behaviour.

Initial experiments focused on application of different antagonists with varying selectivity for GluR2-lacking CP-AMPARs over other AMPARs to *in vitro* slice preparations, which reduced the power of carbachol-evoked gamma oscillations whilst variably affecting oscillation frequency. *In vivo* infusion of one such antagonist, NASPM, into dorsal hippocampus resulted in a dose-dependent impairment in spatial working memory in mice, further supporting the widely-reported link between PV+ interneuron activity, hippocampal network function, and short-term spatial memory.

Subsequent experiments aimed to more selectively manipulate Ca^{2+} flow through CP-AMPARs whilst conserving overall excitability (charge transfer), via transfection of PV+ interneurons with a virus driving Cre-dependent artificial expression of the Q/R-edited GluR2 subunit. Selective transfection of hippocampal PV+ interneurons in PV-Cre mice altered various single-cell and network properties *in vitro*, including reductions in synaptically-evoked dendritic calcium signals, resistance to the effects of NASPM on hippocampal gamma oscillations, and impairments in induction of anti-Hebbian plasticity.

After determining viral expression and functionally validating the AMPAR manipulation *in vitro*, a behavioural characterisation of the effects of removing Ca^{2+} permeability from hippocampal PV+ interneurons was performed, with a cohort of mice given bilateral, complete (dorsal and ventral) hippocampal injections of the floxed GluR2 virus or a control Cre-dependent GFP virus. The GluR2-transfected animals exhibited impairment in spatial reference memory acquisition. However, the GluR2-transfected animals exhibited a substantial, delay-dependent impairment on the spatial working memory, rewarded alternation T-maze task compared to controls. They also exhibited worsening performance with accumulating trials across a session, independent of delay. Additionally, the GluR2-transfected animals took longer to learn new locations of an escape platform in a serial reversal water maze task. The results from the behavioural characterisation suggest that substitution of CP-AMPARs in hippocampal PV+ interneurons with GluR2-containing AMPARs leads to memory impairments due to interference between competing memory traces, potentially as a consequence of impaired AMPAR-mediated plasticity.

Acknowledgements

The work in this thesis would not have been possible without the guidance, insight, advice, support, and eagerness to buy rounds at the pub of my two supervisors, Ed Mann and David Bannerman. Additionally, this project was possible only due to funding from the Wellcome Trust via the OXION studentship, for which I am very grateful.

I thank Ed for his support, both through my rotation project in his lab and the work described in this thesis, his expertise and willingness to teach, both with electrophysiological techniques and programming in IGOR, his availability for consultation, and his friendship throughout the past 3.5 years. I also thank him for contributing to the plasticity experiments reported in section 4.3.5.

I thank David for his support, again during both my rotation project and primary project, expertise and guidance regarding all things concerning animal behaviour, boundless enthusiasm, willingness to find time to meet, friendship, and keenness to discuss sports and A Song of Ice and Fire/Game of Thrones.

I thank Mina Moniri, a project student from the MSc Neuroscience programme, for her contribution to the plasticity experiments reported in section 4.3.5, and enthusiastic approach during her time in the lab.

I would like to thank Dennis Kaetzel for guiding me throughout the viral development process and providing the plasmid backbone used to generate the floxed GluR2 construct.

I thank Professor Colin Akerman and members of his lab for kindly donating breeding animals from the PV-Cre and Ai9 lines from which the animals used throughout this thesis were generated.

I would like to thank many former and currents members of the Mann lab from my time in Oxford. In particular, I thank: Pantelis Antonoudiou for his tutelage and reliable assistance during *in vitro* field recording experiments, as well as his inspiring ignorance of current events worldwide; Sofia Deleniv for personal support and office camaraderie; Sonia Spitzer for her friendship and introducing me to the joys

of dissections; Martin Kahn for his sensible shower policy during our time as housemates; and Julian Bartram for introducing me to the world of psytrance.

I would also like to thank many former and currents members of the Bannerman lab from my time in Oxford. In particular, I thank: Chris Barkus for assisting surgery and infusions performed in Chapter 3, as well as introducing me to, and assisting set-up of, nearly all behavioural experiments in Chapter 5; Marios Panagi for assisting infusions performed in Chapter 3 and advising me regarding statistics; and Stephen McHugh for supervising surgeries performed in Chapter 3. Additionally, I thank: Thomas Börner for supervising my first rotation project in Oxford, introducing me to animal behavioural work, and providing wonderfully cynical company during my first 2 years in Oxford; Alexei Bygrave, for introducing me to the T-maze and enlightening me about the world of carp fishing; and Amy Wolff, for her friendship throughout my time in Oxford.

I would like to thank Louise Upton for co-supervising my second rotation project in Oxford with Ed, advice and training regarding histology and *in vivo* electrophysiology techniques, and political discussion during my time in Oxford.

I would like to thank the staff in the BSB, particularly the technicians, and the BNU manager Katie Hewitt for accommodating my various room booking requests during 2018.

I thank Liam Argent and Sam Nayler, for reliable Friday evening pub company and keeping me sane during the last couple of years in Oxford, as well as my other friends during my time here.

I would like to show my appreciation to the many bands and directors whose music and movies have motivated, uplifted, and emotionally stirred me in the past few years, and who give me the inspiration to succeed in my endeavours. I would also like to thank King Stannis for inspiring me to persevere, regardless of the odds.

Finally, I want to show my immense appreciation to the support my parents have provided me, through good and bad times, in the past decade, and enabled me to tackle every obstacle I have encountered along the way.

Table of contents

Abbreviations

AAV – adeno-associated virus

aCSF – artificial cerebrospinal fluid

AMPAR – α-amino-3-hydroxy-5-methyl-4-isoxazoleproprionic acid receptor

ANOVA – analysis of variance

AP – anterior-posterior

AP5 – 2-amino-5-phosphonopentanoic acid

CA – *Cornu ammonis*

CCK+ – cholecystokinin-positive

CNS – central nervous system

CP-AMPAR – Ca^{2+}-permeable AMPAR

DAPI – 4',6-diamidino-2-phenylindole

DG – dentate gyrus

DMTP – delayed matching-to-place

DV – dorsal-ventral

E-I – excitatory-inhibitory

(s)EPSC – (spontaneous) excitatory post-synaptic current

EPSP – excitatory post-synaptic potential

ER – endoplasmic reticulum

GABA($_A$R) – gamma-aminobutyric acid ($_A$ receptor)

GFP – green fluorescent protein

G-G – Greenhouse-Geiser

H-F – Huynh-Feldt

hSyn – human synapsin 1

I-I – inhibitory-inhibitory

IC_{50} – half-maximal inhibitory concentration

ING – interneuron gamma model

IPSP – inhibitory post-synaptic potential

LMA – locomotor assay

LTD – long-term depression

LTP – long-term potentiation

ML – medial-lateral

NASPM – 1-naphthylacetylspermine

NBQX – 2,3-dihydroxy-6-nitro-7-sulfamoyl-benzo[f]quinoxaline

NMDAR – N-methyl-D-aspartate receptor

NHS – normal horse serum

OGB-488 – Oregon Green 488 Bapta-1

O-LM cell – oriens lacunosum-moleculare cell

PBS – phosphate buffered saline

PFA – paraformaldehyde

(m)PFC – (medial) prefrontal cortex

PhTx(-433/-74) – philanthotoxin(-433/-74)

PING – pyramidal-interneuron gamma model

PV+ – parvalbumin-positive

PV-Cre – Cre recombinase expression under PV promoter

Q/R substitution – glutamine-to-arginine

R/G substitution – arginine-to-glycine

RI – rectification index

SOM+ – somatostatin-positive

SPW-R – sharp-wave ripple complex

TBS(-T) – tris buffered saline(-triton X-100)

Table of figures

1 Introduction

1.1 A brief overview of the project

The focus of the work performed within this thesis is synaptic transmission and plasticity at excitatory inputs onto hippocampal parvalbumin-expressing interneurons, and the consequences of interfering with these processes (via pharmacological and viral manipulations) on hippocampal-dependent memory processes and behaviour. In performing these manipulations, I aim to demonstrate the importance of transmission at these synapses via AMPA receptors to network activity and short-term memory, and explore how manipulating calcium flow and resulting synaptic plasticity mediated by these receptors affects memory processes believed to require flexible recruitment of these interneurons. In order to explain the purposes of this work, I will first discuss various topics related to this area of interest, including the structure, neuronal composition, and functions of the hippocampus, the receptor-dependent properties of excitatory transmission and plasticity at synapses in distinct cell types within the hippocampus, patterns of network activity observed within the hippocampus and the cellular components that enable these patterns of activity to arise, and finally the research tools and techniques that can be used to investigate how manipulations of the cells of the hippocampus and their synaptic inputs can result in impairments at a cellular, network, and behavioural level.

1.2 The hippocampus

1.2.1 Hippocampal structure

The hippocampus is a bilateral structure in the mammalian brain, located within the limbic system (Bird and Burgess, 2008). The structure is widely connected to numerous brain regions, interactions with which are important to many hippocampal functions (van Groen et al., 2003). The hippocampus is extensively connected with the entorhinal cortex, both of which are located within the medial temporal lobe of mammals; projections from multiple entorhinal cortical layers project to many hippocampal sub-fields (Canto et al., 2008). The entorhinal cortex forms part of a set of cortical areas termed the parahippocampal region, which closely associates with both the hippocampus as well as a number of association cortices, and as part of this formation the entorhinal cortex is believed to act as a hub, utilising its extensive reciprocal connections with the hippocampus to interface between it and the neocortex (Buzsáki, 1996; Kiernan, 2012; Kloosterman et al., 2004; Lavenex and Amaral, 2000; Witter et al., 2000, 1989). Distinct layers of the entorhinal cortex project to different sub-fields of the hippocampus, ultimately connecting the cortical region to the entire structure (Canto et al., 2008).

The basic structure of the hippocampus is well-defined and broadly conserved across all mammalian species, notwithstanding some inter-species variation (Amaral and Lavenex, 2007; Moser and Moser, 1998). The region receives a vast array of connections from various brain regions (e.g. thalamus), but for the purposes of this thesis this introduction will only cover circuits within the medial temporal lobe.

Layer II of entorhinal cortex acts as the primary excitatory input to the dentate gyrus (DG), a wedge-shaped layer tightly packed with granule cells, through projections called the perforant pathway (Amaral and Lavenex, 2007; Andersen et al., 2006; Canto et al., 2008). Alongside the DG is a curved layer of pyramidal cells termed the ram's horn, or *cornu ammonis* (CA), which is subdivided into CA1-4; CA4 extends towards the open side of the DG wedge (Amaral and Lavenex, 2007; Insausti and Amaral, 2004). Granule cells from DG unilaterally project towards CA3, where they synapse onto pyramidal cells (Amaral et al., 2007). These pyramidal cells then project both locally to other CA3 pyramidal cells, and also towards pyramidal cells within area CA1 via projections called Schaffer collaterals, as well as to CA1 cells in the contralateral hippocampus via the associational commissural pathway (Collingridge et al., 1983; Insausti and Amaral, 2004). CA1 pyramidal cells, which also receive inputs from layer III of entorhinal cortex along the temporoammonic pathway, then send projections along the output pathways of the hippocampus, including towards the subiculum, which acts as the major output region of the hippocampus (Amaral et al., 2007; Andersen et al., 2006; Canto et al., 2008; Insausti and Amaral, 2004). Both area CA1 cells and subiculum send projections to deep layers of entorhinal cortex, primarily layer V, which then project to cortical and subcortical regions, in addition to deep-to-superficial interlaminar connections within entorhinal cortex (Canto et al., 2008; Kloosterman et al., 2003). The layer II entorhinal cortex→DG→CA3→CA1 relay of synaptic transmission forms what is called the trisynaptic loop, and acts as the primary pathway of excitatory transmission through the hippocampus, with substantial behavioural abnormalities arising in rodents in which the circuit has been disrupted (Insausti and Amaral, 2004; O'Reilly et al., 2014).

1.2.2 Functions of the hippocampus

One of the earliest hypotheses proposed to explain the role of the hippocampus was that it acted as a component of response inhibition, or response 'braking', a theory summarised by Altman, Brunner and Bayer in 1973 (Altman et al., 1973). Amongst the observations underpinning this idea were the hyperactive phenotype of animals carrying hippocampal damage, and the reported difficulty of these animals to learn to inhibit previously taught behaviours in several studies, particularly in tests that required inaction on the part of the animals. However, the theory was not universally accepted, with Nadel, O'Keefe and Black authoring a comprehensive critique of Altman et al.'s ideas (Nadel et al., 1975). Nadel et al. posited that the response-inhibition hypothesis was contradicted by studies excluded from Altman et al.'s literature review, and required misleading interpretation of studies used as supporting evidence. The critique expanded to state that the Altman model failed to take into account, amongst other things, the role of spatial factors in reversal deficits, the nature of exploratory deficits, and the equivocal nature of passive-avoidance deficits based upon the literature. Nowadays, the inhibition theory has very limited popularity.

The discovery by O'Keefe and Dostrovsky in 1971 of rat hippocampal neurons exhibiting spatially-related activity fuelled the emergence of the highly influential 'cognitive map' theory (O'Keefe and Dostrovsky, 1971; O'Keefe and Nadel, 1978). These cells were later dubbed place cells, and the firing of these cells within a particular spatial environment could be correlated to the location of the rodent within said environment; these locations where cells became active are called the 'place fields' for these cells (Moser et al., 2008). The locations of place cells in the hippocampus do not necessarily correlate to their spatial representations, i.e. cells with adjacent place fields are not likely to be adjacent within the hippocampus. Similar observations of spatially-activated hippocampal neurons have been found in monkeys when moved around whilst restrained in a chair, whilst epileptic patients undergoing invasive surgery whilst navigating a virtual 'town' exhibited cells in the hippocampus with location-specific firing patterns (Ekstrom et al., 2003; Matsumura et al., 1999;

Rolls, 1999). Since the discovery of place cells, a number of other cell types with spatial, directional, or boundary-driven firing patterns have been found in rodent hippocampus or parahippocampal regions, namely grid cells, head direction cells, and boundary cells (Moser et al., 2008; Solstad et al., 2008; Taube et al., 1990). Further support for spatial theories of hippocampal function can be drawn from the substantial impairments of hippocampally lesioned rodents on spatial behavioural tasks (Duva et al., 1997; Moser et al., 1993, 1995).

However, purely spatial hypotheses fail to account for a substantial number of reported hippocampally-related phenotypes. The contribution of the brain region towards memory became widely apparent following the observations made by Scoville and Milner of Henry Molaison, an epileptic who underwent surgical destruction of his hippocampus in an attempt to relieve his condition (Scoville and Milner, 1957). Molaison, who came to be known as "Patient H.M.", suffered severe anterograde and partial retrograde amnesia following this surgery; however, he retained memories that occurred significantly prior to the operation. Patient H.M. became widely studied, as did many other patients who suffered hippocampal damage from one cause or another. The findings from Patient H.M. and similar individuals have catalysed a strong focus into the role of the hippocampus and associated regions in different aspects of memory; however, even today there is no clear consensus over the exact roles the region plays in different memory types.

One type of memory that has been strongly linked to hippocampal function is termed episodic memory, referring to memories of specific events with spatial and temporal properties (i.e. where and when something happened). The spatial context in which a memory occurs is an important component of episodic memory, and having a functional representation of space is paramount to this, demonstrating a tight link between the two leading proposed ideas of hippocampal function (Smith and Mizumori, 2006). There is a strong consensus that the human hippocampus is important

to episodic memory, including the failure of episodic memory in people with hippocampal damage and the decline in retention of episodic memories in people with probable Alzheimer's disease (Burgess et al., 2002; Kramer et al., 2004; Vargha-Khadem et al., 1997). There are disagreements over the extent to which the human hippocampus contributes to episodic memory; some posit that such memories always rely on the hippocampus, whilst other suggest that these memories only temporarily reside in the hippocampus before consolidation in the neocortex (Rasch and Born, 2013).

There is also substantial evidence from rodent studies of the importance of hippocampal function for encoding episodic memories, although there are suggestions that distinct memory representations are localised to the separate hemispheres, with this lateralisation enabling each hemisphere to serve complementary roles in episodic memory (Iglói et al., 2010; Shipton et al., 2014). Furthermore, a study targeting specific pathways connecting the hippocampus to extrahippocampal cortical regions has potentially uncovered subdivisions of function of CA1 neurons towards different aspects of episodic memory within distinct subnetworks (Barker et al., 2017). In addition, spatial memory tasks, which can often depend upon episodic-like memory, have been regularly used to study the function of the hippocampus and pathways within it. Rodents with dorsal hippocampal lesions have been found to be impaired at spatial learning on the Morris water maze, perform poorly at the rewarded alternation T-maze task, and fail to show learning on an elevated Y-maze reference memory task (Deacon et al., 2002; Gould et al., 2002; Hock and Bunsey, 1998; Moser et al., 1993). Therefore, an intact dorsal hippocampus is necessary for both spatial working (or short-term) memory, where one must use memory of recent spatial locations to inform on choices in the near future, and spatial reference (long-term) memory of the fixed location of a goal.

As a result of decades of such findings, the importance of temporal lobe activity in spatial and episodic memory is of little dispute nowadays. However, there are also many reports, if occasionally conflicting, of the requirement of a functioning hippocampus in non-spatial, non-episodic memory. Recognition memory is the ability to recognise previously encountered people, objects, events, etc., and is considered to involve two components – familiarity with a previously encountered entity, and recollection of the details of the previous encounter (Brown and Aggleton, 2001; Jeneson et al., 2010). Patients with temporal lobe damage have been found to be impaired at recognition memory tasks, although there are some conflicting findings depending on the onset of the lesion (Holdstock et al., 2002; Mayes et al., 2004, 2002; Vargha-Khadem et al., 1997; Yonelinas et al., 2002). Some people have hypothesised that the hippocampus and surrounding cortex of the temporal lobe differentially contribute to recollection and familiarity; however, one study found that patients carrying hippocampal damage were similarly impaired at tests more dependent on one or other component, indicating a role for the region in both aspects (Jeneson et al., 2010). Object recognition has been tested in numerous rodent studies, using the non-spatial visual novel object recognition (NOR) task, in which after presentation of an object and subsequent delay, an animal must be able to recognise a novel object from the previously presented object. Lesion studies have provided contrasting evidence either for or against a role for the hippocampus in familiarity-based object recognition (Broadbent et al., 2010a, 2004; Clark et al., 2000; Good et al., 2007; Winters et al., 2004).

Studies such as those covered above have built an idea that rather than being restricted to spatial and episodic memory, that the hippocampus can be more broadly classified as underpinning what is termed declarative memory, an umbrella term for all forms of conscious and explicit memory that includes episodic, semantic, visual, and familiarity-based recognition memory (Burgess et al., 2002; Squire and Zola-Morgan, 1991). In contrast, implicit memory, unconsciously acquired memory such as procedural memory that aids performance on tasks without consciously thinking about the

activity performed, is generally believed to be minimally influenced by hippocampal function, particularly given its typical sparing following hippocampal damage in humans, although there is some debate over this (Hannula and Greene, 2012).

The idea of the hippocampus as a site of purely mnemonic and spatial importance became challenged by the relatively recent knowledge that hippocampal function contributes to proper expression of both contextual and unconditioned anxiety and fear. Lesions of the ventral, but not dorsal, hippocampus in rodents have been shown to impair appropriate fear-driven responses to contextual clues, as well as reducing neuroendocrine responses and dampen anxiety-associated behaviours in stressful situations (Bannerman et al., 2003b; Kjelstrup et al., 2002; Richmond et al., 1999; Selden et al., 1991). The dissociation of the mnemonic and spatial functions of the dorsal hippocampus and role in anxiety of the ventral hippocampus is intriguing, particularly given the common anatomical organisation of the hippocampus along the septotemporal axis.

To find common ground between the myriad roles of the hippocampus spread along this axis, Gray and McNaughton proposed a hypothesis of the hippocampus as (part of) a comparator system that responds to situations of conflict or ambiguity, and alters attention, increases arousal, and suppresses motor activity to resolve the conflict (Bannerman et al., 2014; Gray and McNaughton, 2000). Anxiety, a response to potential danger, is associated with competition between approach and avoidance choices (Gray and McNaughton, 2000). Similarly, one could predict that accurate retrieval of, and decision-making based upon, episodic memories would require some system of disambiguation due to the level overlap between the composition of memories. The behavioural inhibition aspect of this hypothesis ties into the early theories of hippocampal function mentioned at the beginning of this subsection, but the concepts of mismatch detection and disambiguation can

find more modern support in both human and rodent studies (Altman et al., 1973; Fyhn et al., 2002; Honey et al., 1998; Kumaran and Maguire, 2006).

Whilst the exact portfolio of functions the hippocampus subserves or underpins is unlikely to be fully established in the immediate future, it is clear that, despite its clear contributions to spatial cognition and episodic memory, the hippocampus likely has roles that expand beyond just these components. Furthermore, whilst lesions studies have been highly useful in gaining understanding of the complex functions of this brain region, the network, cellular, and molecular mechanisms contributing to each aspect of hippocampal function require more refined tools and greater knowledge of the components of the hippocampus.

1.2.3 Dorsal and ventral hippocampus

As mentioned in the previous section, dorsal and ventral hippocampal activity have been associated with distinct psychological processes, with dorsal hippocampus implicated in spatial navigation and memory, whilst ventral hippocampus is linked to anxiety processes. Aside from functional separation, differences in intrahippocampal connectivity and projections to entorhinal cortex and other regions suggest that the two regions are distinct regions (Fanselow and Dong, 2010). Furthermore, gene expression analysis has indicated separation of activity within the two regions; gene expression in dorsal hippocampus has been correlated with cortical regions implicated in information processing, whilst ventral hippocampal expression was correlated with amygdala and hypothalamus (Dong et al., 2009; Lee et al., 2017). The different hippocampal sub-regions are not isolated, however, with interactions via several routes, including perirhinal and postrhinal cortical areas; such interactions may enable emotional processes to support memory consolidation (Fanselow and Dong, 2010; Malin and McGaugh, 2006; Shi and Cassell, 1999).

Despite these and other reported differences, there are clear similarities between the sub-regions. Both dorsal and ventral hippocampus contain trisynaptic loops containing DG, CA3, CA1, and entorhinal interactions (Lanselow and Dong, 2010). Furthermore, the range of different neuronal subtypes (see 1.2.4) and patterns of network activity (see 1.4) have been observed in both dorsal and ventral hippocampus, albeit with some differences (Czéh et al., 2015; Mikulovic et al., 2018). To

the best of my knowledge, the properties of certain neuronal classes of interest have not been reported as substantially different between dorsal and ventral hippocampus, and despite the focus on the role of the hippocampus in cognition and memory, properties of hippocampal neurons and networks have commonly been explored *in vitro* in horizontally-cut sections containing ventral hippocampus (Le Roux et al., 2013; Mann et al., 2005a; Mann et al., 2005b; Nissen et al., 2010). In the case of network function, the preservation of intra-regional activity facilitates the generation of particular patterns of network activity in horizontally-cut ventral hippocampal preparations compared with in dorsal hippocampal preparations. Whilst application of observations in ventral hippocampal circuits to the study of dorsal hippocampal behavioural roles carries an element of risk in terms of misinterpretation, the fundamental components of the circuits appear to be sufficiently similar to render the comparisons valid.

1.2.4 Neurons and circuits of the hippocampus

As described in 1.1.1, the core excitatory circuits of the hippocampus are composed of granule cells in the dentate gyrus receiving entorhinal inputs, pyramidal cells in CA3 receiving perforant path inputs from granule cells, as well as local recurrent connections from other CA3 pyramidal cells, and CA1 pyramidal cells receiving inputs from entorhinal cortex, Schaffer collaterals from CA3, and local recurrent connections from other CA1 pyramidal cells. Beyond these cells, however, there are a number of other neuronal cell types distributed throughout the hippocampus that impinge upon network function in the region, in particular numerous classes of interneuron.

Interneurons are regularly categorised based upon such factors as their shape (basket cell, chandelier cell, trilaminar cell), axonal targets (axon initial segment, dendrites, cell soma), spiking properties (fast spiking, regular spiking, bursting), and expression of neurochemical markers (parvalbumin, somatostatin, calbindin, calretinin). Cell subtypes that share one of these properties are likely to share further properties; for example, parvalbumin-expressing (PV+) interneurons are typically fast-spiking, perisomatic-targeting cells, whilst somatostatin-expressing (SOM+)

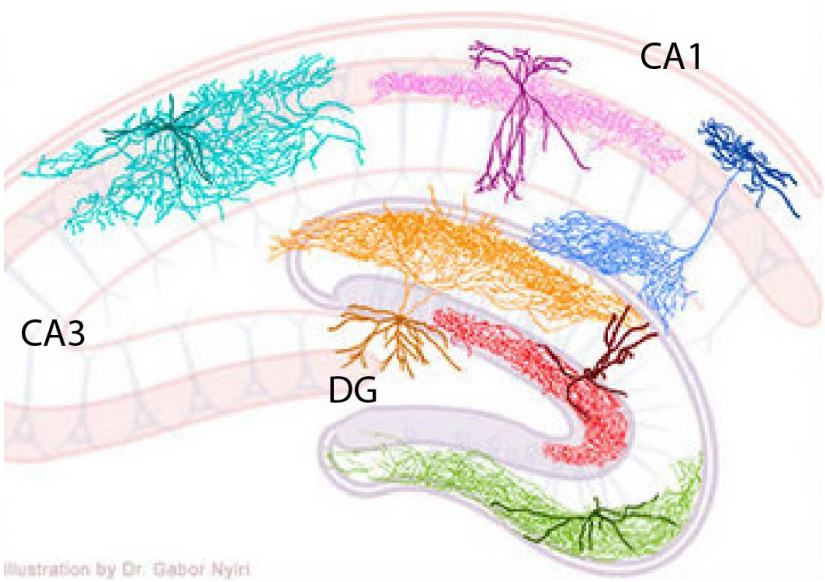

Figure 1.1. Structure and neuronal diversity of the hippocampus. Illustration of the dorsal hippocampus, demonstrating the different subfields (DG, CA3, CA1) and the array of distinct interneuronal types located within the region, with distinctive dendritic and axonal projections and laminal somatic locations. Figure taken from an illustration by Dr. Gabor Nyiri on the 'Interneurons' page of www.scholarpedia.org.

interneurons commonly innervate dendritic regions (Hu et al., 2014; Maccaferri, 2005; Yuan et al., 2017). I will briefly overview the various classes of interneuron found within the different sub-fields of the hippocampus to underline the heterogeneity within the region, as well as identifying common features between different neuronal subtypes within the separate sub-fields, but with a particular focus upon PV+ cells.

The dentate gyrus is the initial stage of the trisynaptic loop, and functions by preprocessing incoming information from, amongst other locations, entorhinal cortex, and transforming similar inputs into different output patterns sent to area CA3, a process termed 'pattern separation' (Andersen et al., 1969; Jonas and Lisman, 2014). Through its processing, the DG is critically involved in learning, memory and spatial coding. The functions of the DG, both pattern separation as well as other processes, are accomplished by modulation of granule cell activity by a variety of different neurons. Mossy cells in the hilus form local excitatory loops, whilst a number of interneuron types provide both feedforward and feedback inhibition (Amaral, 1978). Perisomatic-targeting basket cells,

predominantly pyramidal in nature and many expressing PV as a neurochemical marker, are found in large numbers on the granule cell:hilus border – these cells receive inputs from granule cells and the perforant path, and perisomatic inhibition from precise recruitment of these cells governs the sparse activity patterns of granule cells necessary for pattern separation (Amaral et al., 2007; Jonas et al., 2004; Jung and McNaughton, 1993; Leutgeb et al., 2007; McHugh et al., 2007; Nitz and McNaughton, 2004; Ribak, 1992; Ribak et al., 1978; Ribak and Seress, 1983; Sik et al., 1997; Struble et al., 1978; Treves and Rolls, 1994). Plasticity at excitatory inputs onto these basket cells is considered important for appropriately adjusting inhibition levels in order to maintain sparse activity and improve signal:noise ratio within the DG network (Sambandan et al., 2010). Beyond these cells, there are an array of other interneurons spread throughout the DG. Within the hilus, hilar perforant-path-associated cells (HIPP cells) target granule cell distal dendrites and express SOM, whilst in the molecular layer of DG there are axo-axonic chandelier cells innervating granule cell axon initial segments (AIS), molecular layer perforant path-associated cells (MOPP cells) involved in feedforward inhibition from the perforant path, and outer molecular layer (OML) interneurons that send long-range projections from the DG to the subiculum and that are proposed to mediate feedforward inhibition within a cross-regional interneuron network, necessary for synchronising principal cells spatially distributed across the hippocampus (Amaral, 1978; Amaral et al., 2007; Ceranik et al., 1997; Han et al., 1993; Li et al., 2013; Sancho-Bielsa et al., 2012; Soriano and Frotscher, 1989).

The *cornu ammonis* region of the hippocampus is composed of multiple distinct layers, going, from the hippocampal fissure to the outer edge: strata lacunosum-moleculare; radiatum; lucidum (in CA3 only); pyramidale; oriens; and alveus. Stratum pyramidale is composed of pyramidal cells, whilst the other strata contain fibres projecting to and from these cells (e.g. stratum lucidum is composed of mossy fibres from granule cells projecting to CA3, stratum radiatum in area CA1 contains Schaffer collaterals projecting from CA3 pyramidal cells, stratum alveus contains projections from CA1

pyramidal cells to subiculum and from entorhinal cortex to CA1 pyramidal cells, etc.) (Deller et al., 1996; Insausti and Amaral, 2004; Knowles and Schwartzkroin, 1981). In addition to the excitatory cells and pathways of the hippocampus, all of these layers typically contain one or multiple classes of interneuron; even stratum lucidum, primarily composed of mossy fibres, contains at least two types of calretinin-expressing interneuron contributing to local inhibitory circuits in CA3 (Spruston et al., 1997).

Many of the cell types found in DG share important characteristics with the interneurons found within the layers of the CA regions. For example, like HIPP cells, SOM+ cells such as oriens lacunosum-moleculare (O-LM) cells and oriens bistratified cells predominantly target (distal) dendrites and spines of principal cells, and appear to receive most of their excitatory input from local collaterals of CA1 cells (Blasco-Ibáñez and Freund, 1995; Maccaferri, 2005). By targeting dendrites of excitatory cells, SOM+ interneurons are suited for regulating the input of excitatory information into area CA1; experiments on O-LM cells have demonstrated a capacity to gate information flow by differentially facilitating/muting the influence of distinct inputs from CA3 and entorhinal cortex into CA1 pyramidal cells (Leão et al., 2012).

Perisomatic-targeting cells such as basket cells and axo-axonic cells throughout the hippocampus often express PV as a marker (Boyett and Buckmaster, 2001; Howard et al., 2005; Meyer et al., 2002; Tallent, 2007). PV+ basket cells in the DG and CA regions share other properties, such as fast spiking as a result of high expression of K_v3-type potassium channels with rapid deactivation kinetics, dendritic gap junctions formed of connexin 36 that permit electrical coupling of cells, and extensive innervation of the perisomatic regions of many target principal cells – these properties together enable PV+ basket cell populations to have widespread simultaneous control over the excitatory output of a large number of pyramidal/granule cells (Amaral et al., 2007; Chow et al., 1999; Freund

and Buzsáki, 1996; Fukuda and Kosaka, 2000; Hu et al., 2014; Koh et al., 1995; Meyer et al., 2002; Rudy and McBain, 2001; Venance et al., 2000). PV+ basket and axo-axonic cells can be found in stratum pyramidale, with some also in stratum oriens, and both can receive excitatory input from the major afferent sources in CA1 and CA3 (as well as other inhibitory interneurons) due to dendrites spanning most hippocampal layers; for example, PV+ basket cells in CA1 can receive excitation both from CA3 Schaffer collaterals as well as local recurrent connections from CA1 pyramidal cells (Buhl et al., 1994; Freund and Buzsáki, 1996; Ganter et al., 2004; Gulyás et al., 1999, 1993; Le Roux et al., 2013; Sik et al., 1995; Somogyi et al., 1983).

In contrast, some interneurons that share similarities in one of the aforementioned categories may differentiate in others. For example, in the hippocampus there have been found to be basket cells that exhibit either PV or cholecystokinin (CCK) (Nissen et al., 2010). Both cell types target the perisomatic region of target cells; however, CCK+ basket cells do not share the fast spiking properties of PV+ basket cells, and the two cells exhibit differences in receptor expression and subcortical innervation (Freund and Katona, 2007; Mátyás et al., 2004). CCK+ basket cells receive far less synaptic input than PV+ cells; however, the inhibitory drive is stronger onto these cells (Mátyás et al., 2004). It is believed that the properties of CCK+ basket cells, such as cannabinoid receptor expression and subcortical modulatory inputs, may leave these cells more suited to fine-tuning the activity of hippocampal networks based on mood and behavioural states, whilst PV+ cells are more involved in general network synchronisation due to locally driven excitation and high interconnectivity via gap junctions (Mátyás et al., 2004; Venance et al., 2000).

Another way in which CCK+ basket cells and PV+ cells diverge is in their expression of excitatory glutamate receptors. However, to properly understand the significance of their respective expression patterns, it is necessary to summarise the differences in distinct subtypes of ionotropic

glutamate receptors in the central nervous system, and how their separate properties impinge upon cellular function.

1.3 Ionotropic glutamate receptors

1.3.1 Glutamate receptors in the CNS

Within the central nervous system (CNS), the primary excitatory neurotransmitter is glutamate, which can mediate its actions through ionotropic and metabotropic receptors. Metabotropic receptors bind glutamate and transmit the signal to intracellular signalling partners, the downstream pathways of which can modulate neuronal excitability and subsequent transmission at the synapse (Niswender and Conn, 2010). Conversely, ionotropic receptors are ion channels that open in response to glutamate, permitting the flow of ions into the cell and enabling fast transmission of signals at synapses by exciting the post-synaptic terminal (Dingledine et al., 1999).

Important types of ionotropic glutamate receptors include AMPA receptors, NMDA receptors, and kainate receptors (Wright and Vissel, 2012). Of these, kainate receptors have undergone the least research, with more limited distribution compared to the other two receptor types and less well-defined functions (Contractor et al., 2011). They are found pre- and post-synaptically, and whilst they are known to contribute to functionality at the synapse, at most synapses they appear to play a restricted, more modulatory role in transmission and signalling, only contributing a small percentage of the overall current (Castillo et al., 1997; Contractor et al., 2011; Frerking et al., 1998; Lerma, 2003). Of arguably greater interest in relation to this project are AMPARs and NMDARs, due to their

more widespread distribution, and distinctive properties that enable them to function co-operatively in synaptic activity and plasticity.

1.3.2 Fast transmission at the glutamate synapse

AMPARs and NMDARs are both tetrameric channels activated by glutamate, composed of subunits with extracellular N-termini and intracellular C-termini; however, the requirements for channel opening, and capacity for mediating flow of currents, differs between the two (Anggono and Huganir, 2012; Dingledine et al., 1999; Punnakkal et al., 2012). At resting membrane potentials, binding of glutamate to AMPARs is sufficient for channel opening and fast influx of sodium ions (Na^+), but the same binding is insufficient for activation of NMDARs (Edmonds et al., 1995). In addition to glutamate, NMDARs also require co-activation at a glycine-binding site to open (Johnson and Ascher, 1987). Furthermore, at resting membrane potentials, NMDARs are blocked by magnesium ions (Mg^{2+}) from the extracellular fluid (Mayer et al., 1984). This block is relieved by depolarisation of the post-synaptic membrane; therefore, NMDARs act as 'co-incident receptors', requiring glutamate and glycine binding alongside membrane depolarisation to function (Lüscher and Malenka, 2012).

When glutamate arrives at the post-synaptic terminal, it binds to both AMPARs and NMDARs, but only the former type of receptor is activated. However, as AMPARs open and facilitate large, rapid inward cation currents, the terminal is depolarised, alleviating the Mg^{2+} block (Ruppersberg et al., 1994). Now relieved of the block, NMDARs can facilitate the flow of ions, and whilst slower to activate than AMPARs, NMDARs have higher glutamate affinity and carry longer-lasting inward

currents (Davies and Morris, 2004). These currents allow greater excitation of the post-synaptic cell and promote signal transduction through the CNS.

1.3.3 NMDAR-mediated excitatory plasticity

Plasticity, the process by which the strength or excitability of a synapse is altered in an activity-dependent manner, can occur at both excitatory and inhibitory synapses, and result from a range of pre- and/or post-synaptic membrane changes (Gaiarsa et al., 2002; Gerrow and Triller, 2010). However, influx of calcium ions (Ca^{2+}) is a common trigger for the induction of activity-dependent plasticity, and NMDARs, unlike the majority of AMPARs, are permeable to Ca^{2+} (Lüscher and Malenka, 2012; Neher and Sakaba, 2008). Long-term potentiation (LTP) of post-synaptic responses following stimulation of afferents was first described in the DG of the hippocampus, and throughout the subsequent years it was reported in area CA3, area CA1, and eventually extrahippocampal brain regions (Alger and Teyler, 1976; Andersen et al., 1977; Bliss and Lomo, 1973; Martin et al., 2000). It was later found that induction of this form of plasticity in area CA1 could be prevented by blockade of NMDARs, indicating their vital role in the process (Collingridge et al., 1983). NMDAR-dependent excitatory plasticity has been reported in a number of cell types throughout the CNS, including CA1 pyramidal cells; however, it is not a universal mechanism, as plasticity at mossy fibre inputs onto CA3 pyramidal cells occurs independent of post-synaptic NMDAR activation (Nicoll and Schmitz, 2005).

Following AMPAR-mediated depolarisation and NMDAR opening, inward Ca^{2+} flow activates Ca^{2+}/Calmodulin-dependent protein kinase II, resulting in phosphorylation of AMPARs, altering channel properties (Lee et al., 2003; Soderling and Derkach, 2000; Wang et al., 2005). Furthermore,

phosphorylation promotes the insertion of more AMPARs into the synapse (Henley and Wilkinson, 2013). These changes increase the number and conductance of recruitable AMPARs in the post-synaptic membrane, resulting in greater excitability. These changes can last for extended periods of time, hence the name LTP (Barnes, 1979).

The discovery of LTP was soon followed by the proposal that it might be a contributing factor to long-term memory (Lynch and Baudry, 1984). Assumptions that information storage is underpinned by changes at the synaptic level have existed since the time of Ramón y Cajal, and the discovery that levels of high activity at synapses within the hippocampus can bring about strengthening of said synapses leads credence to the idea that stimulus-driven activity could result in strengthening of connections that represent the memory of that stimulus (Bliss and Collingridge, 1993). Supporting these ideas were findings that pharmacological blockade of NMDARs and knockouts of NMDAR subunits impaired spatial learning (Morris et al., 1986; Sakimura et al., 1995). Furthermore, hippocampal region-specific knockouts of NMDARs have been performed, resulting in ablation of LTP from the targeted regions and selective impairments in different aspects of memory (McHugh et al., 1996; Nakazawa et al., 2003; Tsien et al., 1996). However, there is some contention on this matter, with other groups reporting successful spatial encoding following intracerebral infusion of NMDAR antagonist under certain conditions, and after full-brain and hippocampal region-specific ablation of NMDAR subunits (Bannerman et al., 2012, 2008, 1995).

There is also evidence that low levels of activity at synapses can result in synaptic weakening, a process known as long-term depression (LTD), and that this process also contributes to memory processes (Bear and Abraham, 1996; Zeng et al., 2001). The role of synaptic weakening in learning and memory has been less widely studied, but ablation of phosphatases necessary for LTD has been

shown to impair performance on hippocampus-dependent working and episodic-like memory tasks (Zeng et al., 2001).

Due to the coincident properties of NMDAR activation, LTP mediated by these receptors requires both pre-synaptic (glutamate release) and post-synaptic (depolarisation) activity simultaneously. This combination of activity for plasticity has been labelled 'Hebbian' LTP based upon Hebb's postulates (Hebb, 1949). The postulate states that when an axon of one cell is sufficiently close to excite second cell and persistently contributes to the second cell's firing, changes occur in either or both cells such that the efficiency of cell 1 driving the firing of cell 2 is increased; the postulate is commonly simplified to 'cells that fire together, wire together'. NMDAR-mediated LTP exhibits several properties, including: associativity (weak stimulation of one pathway occurring simultaneously with strong depolarising stimulation of a second pathway onto the same cell will induce LTP at both pathways); coopravity (LTP can be induced by strong stimulation of a single pathway to a synapse, or cooperatively by weak stimulation of many convergent pathways that collectively trigger sufficient post-synaptic depolarisation for LTP to occur); and input specificity (LTP induced at one synapse does not spread to other synapses, and is only propagated according to the rules of associativity/cooperativity) (Hao et al., 2018; Kitajima and Hara, 1991).

Similarly, Hebb's postulate contains the complementary statement that persistent failure of a presynaptic axon from cell 1 to excite post-synaptic cell 2, changes take place such that the efficiency of cell 1 to trigger firing of cell 2 is reduced (Hebb, 1949; Stent, 1973), and is supported by the observation that weak pre- or post-synaptic activity at NMDAR-expressing hippocampal synapses results in LTD, as the small Ca^{2+} currents passing through transiently unblocked NMDARs activate phosphatases and result in AMPAR endocytosis (Bi and Poo, 2001; Bliss and Collingridge, 1993; Bloodgood et al., 2009; Jahr and Stevens, 1993; Lisman, 1989; Lüscher and Malenka, 2012).

Experimental induction of LTP *in vitro* requires either sufficiently strong pre-synaptic stimulation to induce post-synaptic depolarisation (e.g. high-frequency tetanic stimulation), or combination of pre-synaptic stimulation with experimentally-induced post-synaptic depolarisation (Chen et al., 1999; Larson and Munkácsy, 2015). These requirements align with the known properties of NMDARs, but raise the possibility of alternative learning rules at synapses dominated with Ca^{2+}-permeable channels with different activation requirements.

1.3.4 Ca^{2+}-permeable AMPARs

AMPARs play clear roles in NMDAR-dependent plasticity, by generating the post-synaptic depolarisation necessary for removal of the Mg^{2+} block, and by being the target of enzymes and intracellular protein trafficking machinery in response to Ca^{2+} signals (Henley and Wilkinson, 2013; Huganir and Nicoll, 2013; Lee et al., 2003). However, they are not typically believed to contribute to the generation of the Ca^{2+} signal directly. This is due to the properties imbued upon AMPARs by the presence of one particular subunit.

AMPARs are homomeric or heteromeric tetramers created from combinations of four different subunits – GluR1, GluR2, GluR3 and GluR4 (Nakagawa, 2010). The most common receptors, depending on cell type, are GluR1 homomers, and GluR1/GluR2 and GluR2/GluR3 heteromers. All these subunits contain four hydrophobic domains (M1-M4), yet have extracellular N-termini and intracellular C-termini (Isaac et al., 2007). This is because, whilst M1, M3, and M4 form transmembrane helices, M2 forms a re-entrant loop (Fig.1.2). A glutamine found in this re-entrant loop is edited selectively in GluR2 subunits; transcribed GluR2 mRNA undergoes hydrolytic editing of an adenosine in the codon encoding residue 607, converting it to an inosine that encodes an

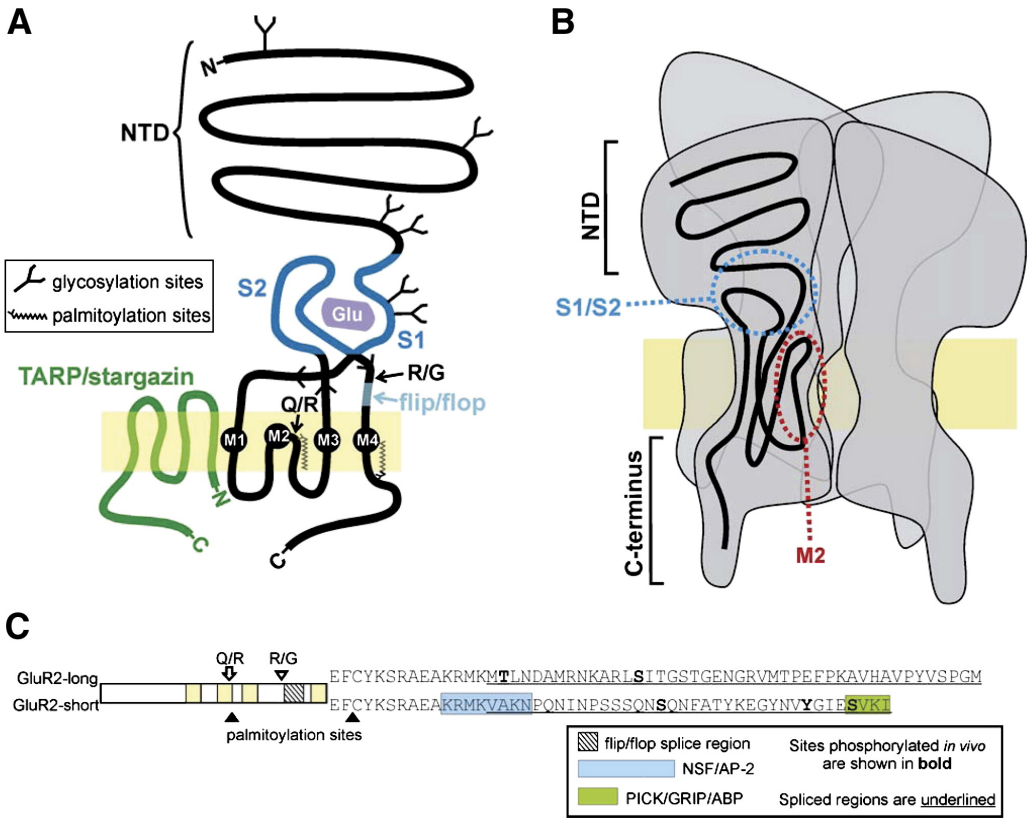

Figure 1.2. GluR2 subunit structure and modifications. The GluR2 subunit undergoes an mRNA edit substituting a glutamine with an arginine in the M2 re-entrant loop. The subunit can also undergo further RNA modifications, including an arginine-to-glycine substitution and alternative splicing of a flip or flop exon. Figure taken from Isaac et al., 2007.

arginine instead of a glutamine (Sommer et al., 1991). This Q607R substitution is performed for over 99% of GluR2 subunits post-natally, and results in a subunit with distinctive properties that can overrule those of other AMPAR subunits (Geiger et al., 1995; Isaac et al., 2007).

AMPARs in which glutamine has not been edited form a carbonyl ring of negative charge in the channel pore, whilst the Q607R substitution disrupts this ring (Fig. 1.3) (Jonas and Burnashev, 1995; Swanson et al., 1997). Disruption of this ring has significant consequences. First, it prevents the entry and binding of polyamines to this site (Swanson et al., 1997). Following membrane depolarisation, positively charged intracellular polyamines move down the electrochemical gradient outwards and attach to the negative charges in the membrane pore arising from glutamine and aspartate residues. Consequentially, channels lacking edited GluR2 exhibit inward rectification of currents, as polyamine block prevents the flow of ions at positive membrane potentials (Bowie and Mayer, 1995; Donevan

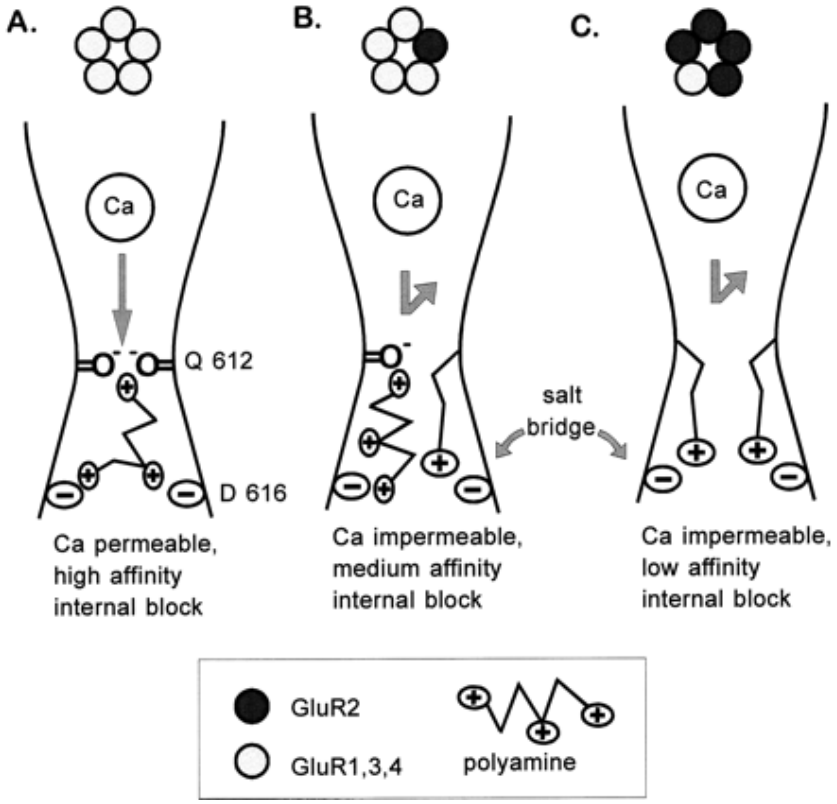

Figure 1.3. Dependence of calcium permeability and polyamine-induced block on expression of Q/R-edited GluR2 subunit. (A) In the absence of the GluR2 subunit, an intact carbonyl ring within the channel pore facilitates calcium ion flow through the channel and binding of positively-charged polyamine molecules. (B, C) Inclusion of increasing numbers of GluR2 subunits progressively abolishes both these properties. Figure taken from Washburn et al., 1997.

and Rogawski, 1995; Kamboj et al., 1995). In contrast, GluR2-containing AMPARs do not undergo this block, and thus exhibit linear current-voltage relationships (Bochet et al., 1994; Boulter et al., 1990). GluR2-containing AMPARs are resistant to block by extracellular polyamines, such as those found in certain spider and wasp toxins (Anis et al., 1990; Jones et al., 1990). Furthermore, GluR2-lacking AMPARs exhibit larger and faster single-channel conductances, as they have rapid gating kinetics and lack a positive charge impeding cation flow through the channel pore (Geiger et al., 1995; Lawrence and McBain, 2003; Oh and Derkach, 2005; Swanson et al., 1997; Verdoorn et al., 1991).

However, arguably the most functionally significant consequence of the GluR2 edit is the removal of Ca^{2+} permeability through AMPARs (Isaac et al., 2007). The presence of a positive charge at this point of the channel pore prevents the movement of divalent cations through GluR2-containing AMPARs,

rendering them impermeable to Ca^{2+} (Geiger et al., 1995; Jonas and Burnashev, 1995). However, the absence of GluR2 removes this problem, therefore GluR2-lacking AMPARs such as GluR1 homomers are referred to as Ca^{2+}-permeable AMPARs, or CP-AMPARs (Jonas and Burnashev, 1995; Szabo et al., 2012). These channels are inwardly rectifying, and are sensitive to block by polyamine-derived toxins such as philanthotoxin-433 (PhTx-433) and 1-naphthylacetylspermine (NASPM), rendering these compounds useful for probing the GluR2 content of AMPA receptors within cells of interest, as well as studying the impact of manipulating CP-AMPAR function on cellular properties (Bowie and Mayer, 1995; Conrad et al., 2008; Kumar et al., 2002; Liu and Cull-Candy, 2002; Nissen et al., 2010; Terashima et al., 2004; Washburn et al., 1997). Whilst other polyamine-modulated receptors can also act as targets for these drugs, including NMDA receptors, they demonstrate varying selectivity for CP-AMPARs over others (Washburn and Dingledine, 1996).

1.3.5 CP-AMPAR expression profiles and properties of expressing cells

A publication from Bochet et al. in 1994 reported two different types of cells within the hippocampus that could be differentiated based on their expression of AMPAR subunits and their electrophysiological properties, with cells dubbed either 'type I' or 'type II' cells (Fig. 1.4) (Bochet et al., 1994). Type I cells exhibited high levels of GluR1 and GluR2 mRNA expression and low levels of GluR3 and GluR4, whilst type II cells had minimal GluR2 expression and were instead dominated by GluR1 and GluR4 mRNA expression. As a consequence, the current-voltage relationship of AMPAR-mediated evoked responses was linear in type I cells, whilst type II cells exhibited large conductances at resting membrane potentials, but rectification at positive potentials, in line with the known properties of CP-AMPARs. These findings indicate that the composition of AMPARs is cell type-specific, and subsequent studies indicated that in cells that express GluR2, the majority of AMPARs

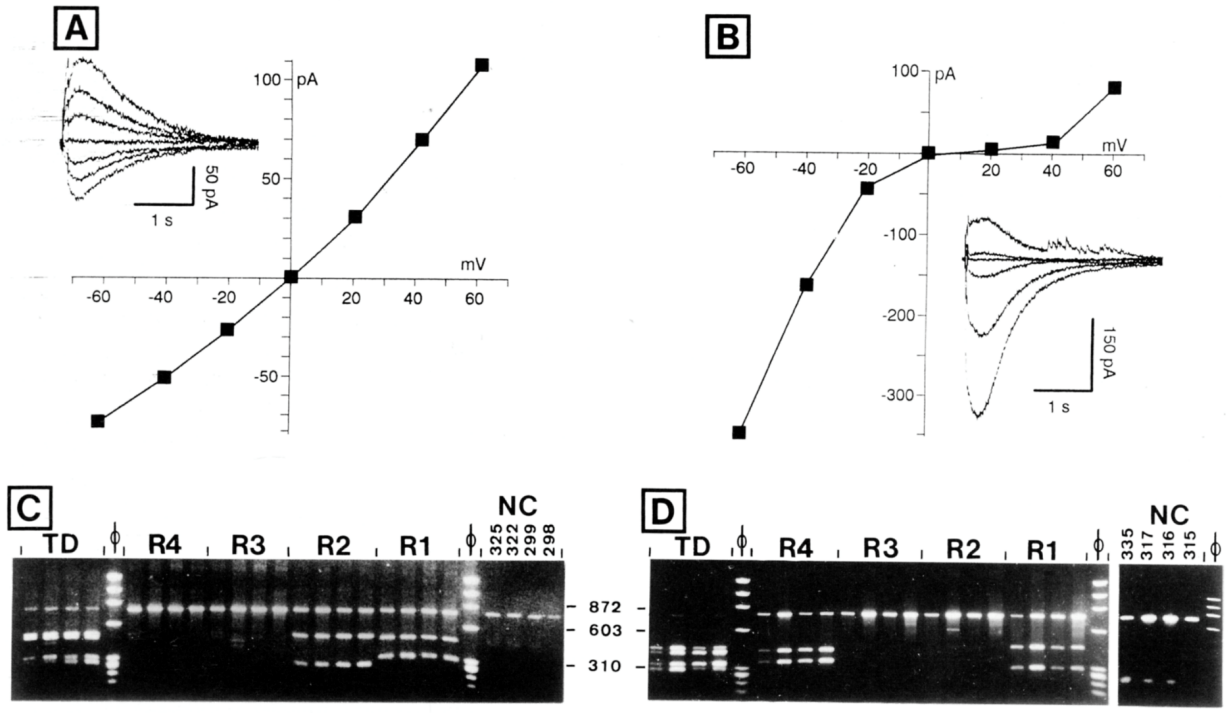

Figure 1.4. Rectification properties of AMPAR-mediated currents in cells depend on GluR2 expression. (A) 'Type I' cells (indicative of pyramidal cells) had linear relationships between the holding membrane potential and the amplitude of evoked currents, whilst (B) 'type II' cells (representative of PV+ interneurons) had larger-amplitude currents at negative membrane potentials, but exhibited marked rectification at positive potentials. (C) Type I cells exhibited high levels of GluR1 and GluR2 mRNA transcription, whilst (D) type II cells lacked GluR2 mRNA. Figure taken from Bochet et al., 1994.

were composed of GluR2 and one other subunit in symmetrical heteromers (Mansour et al., 2001; Wenthold et al., 1996).

Research later revealed that the type I cells mentioned in the above study were likely to be principal cells including pyramidal cells; however, this is temporally dependent. A transition from high CP-AMPAR expression to high GluR2 expression has been seen in the early post-natal days and weeks in pyramidal cells in multiple layers of cortex and in the hippocampus (Brill and Huguenard, 2008; Ho et al., 2007; Kumar et al., 2002; Monyer et al., 1991; Wisden and Seeburg, 1993). Inward rectification and philanthotoxin sensitivity of synaptic events have been seen in hippocampal CA3 pyramidal cell synapses in rodents up to P17 (Ho et al., 2007; Lei et al., 2003). Once in adulthood, principal cells typically express minimal numbers of CP-AMPARs, with estimates of up to approximately 95% of AMPARs in adult pyramidal cells lacking Ca^{2+} permeability (Isaac et al., 2007; Lu et al., 2009). Beyond

this point, CP-AMPAR expression in adult pyramidal cells has been reported in a range of different situations, including transient expression during NMDAR-dependent LTP, stress, sleep, and drug exposure (Guire et al., 2008; Shepherd, 2012; Whitehead et al., 2013; Wolf and Tseng, 2012). In relation to LTP, rapid incorporation of CP-AMPARs into CA1 pyramidal neuron synapses has been observed, lasting briefly before replacement by GluR2-containing AMPARs; this phenomenon has not been universally observed, however, with other groups failing to find evidence of transient CP-AMPAR insertion immediately following LTP (Adesnik and Nicoll, 2007; Plant et al., 2006).

In contrast to principal cells, there are a subset of GABAergic interneurons that do not exhibit the increase in GluR2 expression into adulthood, and express functionally significant levels of CP-AMPARs across all stages of development (Geiger et al., 1995; Koh et al., 1995; McBain and Dingledine, 1993). These cells exhibit electrophysiological profiles matching the 'type II' cells from the Bochet study, with inwardly rectifying evoked currents, large, rapidly decaying excitatory post-synaptic potentials (EPSPs), and polyamine-based toxin sensitivity (Bochet et al., 1994; Carter and Regehr, 2002; Geiger et al., 1997, 1995; Lawrence and McBain, 2003; Oh and Derkach, 2005; Walker et al., 2002). The interneurons that fall into this group include PV+ and SOM+ interneuron cells in the hippocampus such as basket cells, chandelier cells, and O-LM cells, but not CCK+ basket cells (Nissen et al., 2010; Szabo et al., 2012). The benefit of expressing faster-conducting AMPARs can be seen when considering the role these cells play within neuronal circuits; fast-spiking cells such as PV+ basket cells deliver rapid, widespread inhibition enabling coordination of precisely timed principal cell output, and as such require rapid, precise firing kinetics (Isaac et al., 2007; McBain and Fisahn, 2001). Activation of CP-AMPARs in interneurons during current-clamp conditions has been shown to result in precise firing of action potentials within narrow temporal windows (Jonas et al., 2004; Lawrence et al., 2004; Vida et al., 2006).

1.3.6 AMPAR assembly and trafficking

AMPAR assembly occurs by initial production of 'dimer-of-dimers' in the endoplasmic reticulum (ER), a process dependent upon N-terminal domain interactions, followed by further dimerisation controlled by both ligand binding, as well as membrane domain interactions, which can be affected by the Q/R substitution on GluR2 (Ayalon and Stern-Bach, 2001; Greger et al., 2003; Mayer, 2006). As mentioned earlier, the availability of subunits, particularly GluR2, appears to be the primary deciding factor determining AMPAR composition – cells that express GluR2-containing AMPARs typically have large pools of edited GluR2 subunits within the ER, likely to ensure that this subunit dominates the AMPAR profile within these cells (Greger et al., 2003; Isaac et al., 2007). Further supporting the idea that subunit availability is a primary determinant of receptor composition is the evidence from studies showing that artificial overexpression of edited GluR2 in cell types dominated by CP-AMPARs, such as glioblastoma cells and Bergmann glia, results in a switch in AMPAR expression and electrophysiological profile to one closer to that of principal cells (Iino et al., 2001; Ishiuchi et al., 2002).

The Q/R substitution appears to be highly influential upon the formation of complete AMPARs, however it also appears to influence the transport of GluR2 prior to receptor formation, as Q/R reversion has been shown to result in rapid GluR2 release from the ER and elevated GluR2 surface expression (Greger et al., 2002). Furthermore, additional edits and alternative splicing of the subunit influence aspects of AMPAR expression (Fig. 1.2). Aside from the Q/R edit, AMPAR subunits can undergo an adenosine-to-inosine RNA edit that converts an arginine to a glycine; this R/G edit occurs in the ligand binding site, and the edit seems to reduce the self-assembly competence of GluR2, slowing maturation within the ER (Greger et al., 2006). This edit occurs at higher levels as development progresses towards adulthood, and by increasing the time the subunit dwells within

the ER, may work to encourage heteromer formation (Greger et al., 2006; Lomeli et al., 1994; Penn and Greger, 2009). Finally, AMPAR subunits undergo alternative splicing, with a difference of four residues between flip and flop exons (Sommer et al., 1990). The expression of either exon is also developmentally linked, with the default flip replaced by flop as the brain develops (Penn and Greger, 2009). The increase in dwell time from the Q/R and R/G edits, as well as the inclusion of the flop exon, may all work together to promote GluR2 inclusion into heteromeric AMPARs, and given that part of this RNA processing is under developmental control, there is a clear basis for the developmental switch in AMPAR expression from early post-natal period to adulthood (Greger et al., 2007; Monyer et al., 1991; Penn and Greger, 2009; Sommer et al., 1990).

However, the evidence that some neuronal populations can express functionally relevant levels of both CP-AMPARs and GluR2-containing AMPARs with differential targeting to distinct synapses dependent upon afferent input suggests that there must be greater regulation of receptor composition and expression beyond subunit availability and processing (Tóth and McBain, 1998).

1.3.7 CP-AMPARs and plasticity

As has already been mentioned, AMPARs play a role in NMDAR-dependent plasticity, as both an instigator of depolarisation, and as a substrate of the downstream signalling cascades recruited following NMDAR activation (Henley and Wilkinson, 2013; Lee et al., 2003). Furthermore, CP-AMPARs themselves are suggested to have transient expression and, presumably, activity, during LTP, albeit with some debate on this matter (Adesnik and Nicoll, 2007; Plant et al., 2006). However, the fact that these receptors are capable of mediating Ca^{2+} influx raises the possibility that they may

be capable of mediating plastic changes in conjunction with, or even independent of, other Ca^{2+} channels at the synapse.

Whilst CP-AMPARs do allow passage of Ca^{2+} ions into the cell when open, their permeability is low relative to NMDARs, a combination of their lower single channel conductance, different channel kinetics, and a fivefold reduction in the Ca^{2+}:Na^{+}/K^{+} permeability ratio (Dingledine et al., 1999; Geiger et al., 1995; Köhr et al., 1993; McBain and Mayer, 1994; Rozov et al., 2012; Swanson et al., 1997). As such, with a similar AMPAR:NMDAR ratio to that seen in principal cells one might expect NMDAR activity to dominate Ca^{2+} currents and hence mediate the primary forms of plasticity within the cell. However, some of the interneuron populations that highly express CP-AMPARs have a divergent NMDAR profile, with low levels compared to principal cells, as well as unusually high ratios of the GluN2A subunit relative to GluN2B, with inclusion of the former subunit into NMDARs resulting in shorter excitatory currents with lower Ca^{2+} flux (Gonzalez-Burgos and Lewis, 2012; Kinney et al., 2006; Nyíri et al., 2003). Together, these differences suggest that CP-AMPARs may serve as a primary mediator of Ca^{2+} flux at synapses onto interneurons such as PV+ basket cells, and therefore that plasticity at synapses onto these cells may be mediated by CP-AMPARs, in addition to, or instead of, NMDAR-dependent LTP/LTD.

Some of the first reports of CP-AMPAR-mediated LTP came from experiments on interneurons in the amygdala (Mahanty and Sah, 1998). However, like with NMDAR-dependent plasticity, many studies into AMPAR-dependent plasticity have focused on the hippocampus. In 2005 and 2007, Lamsa et al. published reports of both NMDAR-dependent LTP and CP-AMPAR-mediated LTP from interneurons in the hippocampus, albeit recorded from different layers (Fig. 1.5) (Lamsa et al., 2005, 2007). They observed differences in the properties of cells either conducive or resistant to CP-AMPAR-mediated plasticity, as well as differences in the properties of, and criteria for, the two types of LTP (Lamsa et

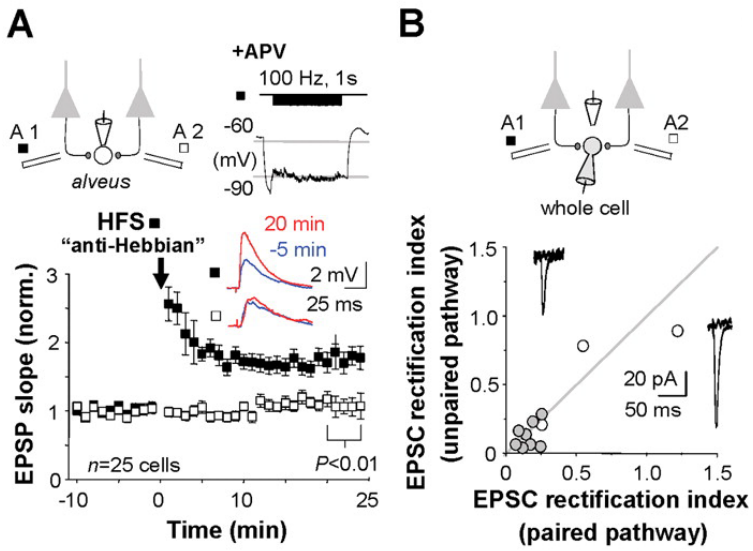

Figure 1.5. Long-term potentiation of excitatory post-synaptic potentials in rectifying interneurons occurs in the absence of NMDAR activity. (A) Induction of potentiation following high-frequency stimulation in the presence of the NMDAR antagonist AP5. (B) Cells that had potentiated responses with this protocol exhibited rectifying AMPAR-mediated currents. Figure taken from Lamsa et al., 2007.

al., 2007). Perhaps most notably, whilst NMDAR-dependent LTP is well known to require both pre- and post-synaptic depolarisation simultaneously for NMDAR activation (Hebbian plasticity), due to the depolarisation-induced block of CP-AMPARs by polyamines, CP-AMPAR-mediated plasticity could only be induced when pre-synaptic activity and glutamate release occurred in the absence of post-synaptic depolarisation. Furthermore, in contrast to NMDAR-mediated LTP, it did not exhibit associativity, as weak stimulation of one pathway paired with strong depolarising stimulation of a second pathway failed to induce LTP at either synapse. This AMPAR-mediated mechanism has been termed 'anti-Hebbian', due to the reversed requirements for LTP and LTD compared to traditional Hebbian plasticity. The authors posited that such plasticity could occur in interneurons that remain silent during periods of intense pyramidal cell firing (e.g. sharp waves), resulting in altered activation later on.

In the subsequent decade since these findings, knowledge of anti-Hebbian LTP in hippocampal interneurons has expanded, with occasionally conflicting results emerging. CP-AMPAR-dependent plasticity was successfully induced in both PV+ and SOM+ interneurons in feedforward and feedback

inhibitory pathways, with philanthotoxin-433 able to block the expression of disynaptic potentiation of inhibitory post-synaptic responses (Nissen et al., 2010; Szabo et al., 2012). Conversely, CCK+ interneurons, which do not express CP-AMPARs in functionally significant numbers, were incapable of expressing CP-AMPAR-dependent LTP. In PV+ interneurons in area CA1, CP-AMPAR-dependent anti-Hebbian plasticity was induced by stimulation of either feedforward inputs from CA3 pyramidal cells, or feedback inputs from CA1 pyramidal cell local collaterals (Le Roux et al., 2013). However, this study did also manage to induce NMDAR-dependent LTP at feedback inputs only, not feedforward inputs, suggesting input-specific learning rules enabling distinct inputs to be differentially responsive to patterns of activity with different frequencies.

Inhibitory plasticity has been increasingly studied as an essential response to excitatory plasticity, to maintain excitatory-inhibitory balance and preserve fidelity within a network (Lamsa et al., 2005). Should long-term potentiation of excitatory connections between pyramidal cell assemblies underpin memory formation, it might be expected that compensatory measures need to be taken to avoid excessive activation of said memory, and modelling work suggests that inhibitory plasticity leading to increased inhibition was necessary to re-establish global excitatory-inhibitory balance (Vogels et al., 2011). The simplified model predicted that this re-organisation of balance was due to plasticity following Hebbian rules, albeit occurring at inhibitory synapses onto excitatory cells; however, different inhibitory cell types exhibit distinctive receptor expression and consequentially plasticity rules (Lamsa et al., 2005, 2007). The importance of rapid, precise recruitment of cells such as PV+ and SOM+ interneurons for optimal network activity makes the incorporation of AMPARs with faster kinetics a logical ‘design choice’ for these cells. How the distinct properties of these receptors, relative expression of different glutamatergic receptors, and resultant criteria set for plastic changes at their synaptic inputs affect recruitment of these cells during different types of

network activity and behavioural states, and how flexible recruitment of these cells affects the flow of information through the hippocampal network, is far less clear.

1.3.8 Ionotropic glutamate receptors and hippocampus-dependent behaviour

Pharmacological and genetic approaches have been used to explore the contribution of NMDARs and AMPARs, both across the hippocampus and restricted to specific sub-fields or cell types, to hippocampal function and behavioural output, enabling further understanding of the cellular and network mechanisms underpinning aspects of different hippocampus-dependent behaviours.

Infusions of the NMDAR antagonist D-AP5 into dorsal and ventral hippocampus has been shown to impair working and recognition memory, and measures of anxiety, respectively (Baker and Kim, 2002; McHugh et al., 2008; Nascimento Häckl and Carobrez, 2007). Knockout of NMDARs selectively in area CA1 impaired spatial memory (but not non-spatial learning) in one study, whilst ablation of NMDAR obligatory subunit NR1 in CA3 pyramidal cells was found to impair acquisition of novel spatial memory and non-cued memory retrieval (Nakazawa et al., 2003, 2002; Tsien et al., 1996). In contrast, a separate study combining NR1 knockout in CA1 and DG found that animals could successfully acquire a particular platform location in a water maze spatial reference memory task, but had impairments in learning a new location following a change in the platform position (Bannerman et al., 2012).

Similar glutamate receptor knockouts have also been performed with non-principal cells. One study ablated NR1 globally from PV+ cells, and reported impairments in spatial representations and working memory (Korotkova et al., 2010). NMDAR dysfunction in PV+ cells has become a recent

topic of interest in the pathophysiology of schizophrenia, and a separate study post-natally ablating NMDARs from cortical interneurons (albeit not only PV+ cells) similarly reported spatial memory deficits, as well as changes in anxiety-like behaviours and social activity (Belforte et al., 2010; Lewis et al., 2005). However, the impairments reported by Korotkova et al. were not replicated by others when using an alternative Cre recombinase-expressing PV+ cell genetic line to ablate NR1 from PV+ cells, so this research topic still has many questions to answer (Billingslea et al., 2014; Bygrave et al., 2016).

Infusion of AMPAR antagonists into hippocampus impairs encoding and retrieval of spatial memory (as well as long-term storage) and expression of fear memory (Bianchin et al., 1993; Izquierdo et al., 1993; Pierson et al., 2015; Riedel et al., 1999). There were no clear published data regarding region-specific knockouts of GluR1; however, global knockout of the GluR1 subunit selectively impairs performance on spatial working memory tasks, with hippocampal-specific, virally-induced re-expression of GluR1 partially rescuing these phenotypes (Freudenberg et al., 2016; Sanderson et al., 2010). Additionally, the same group that observed memory impairments following PV+ cell-specific knockout of NR1 used the same PV+ Cre recombinase line to ablate GluR1 selectively in PV+ cells, and observed impairments on spatial working memory but not reference memory (Fuchs et al., 2007). Alongside this, global and local knockouts of GluR4, selectively expressed in interneuron subpopulations including PV+ cells, similarly affected working memory (Caputi et al., 2012; Fuchs et al., 2007). Lastly, modulation of levels of brevican, a protein that forms perineuronal nets that enwrap PV+ cells, affects synaptic plasticity and impairs working memory (Favuzzi et al., 2017). These findings indicate that reducing the excitatory drive onto PV+ interneurons (in addition to affecting synaptic plasticity) results in changes in the network that affect working memory. To understand how one might lead to the other, one requires a greater understanding of some of the different classes of network activity observed in the hippocampus.

1.4 Oscillations

1.4.1 Patterns of hippocampal activity

The diverse array of interneurons within the hippocampus, combined with the complex excitatory connectivity of the region, raises the potential for a range of different patterns of activity to arise (Buzsáki et al., 2003). In particular, rhythmic, repetitive patterns of neural activity at different frequencies arising from synchronised output of cell sub-populations have been widely observed within and outside of the hippocampus (Butler and Paulsen, 2015). These patterns of activity can be detected by recording from single cells using patch-clamp techniques, or they can be recorded by the placement of extracellular electrodes (either *in vivo* or *in vitro*) that detect local field potentials generated by large currents passing through extracellular space (e.g. in/out of populations of active cells) (Buzsáki et al., 1983; Fisahn et al., 1998; Florez et al., 2015; Mann et al., 2005b; Tsintsadze et al, 2015). The synchronised activity of large neuronal ensembles appears in the local field potential as macroscopic oscillations of varying wavelength, which can also be detected at a cellular level (Buschman et al, 2012).

Amongst the lowest-frequency oscillations observed in the brain are slow waves (<1 Hz), in which alternative 'down' states of neuronal silence and 'up' states of intense firing enable synchronisation of neuronal assemblies across brain regions, in a process proposed to support memory consolidation (Buzsáki and Draguhn, 2004; Mölle et al., 2006). Slow waves are not generated within the hippocampus (Hahn et al., 2006). Instead, the hippocampus exhibits a unique pattern of activity during immobility and sleep, known as the sharp-wave ripple complex (SPW-R), a brief, recurring

event that is composed of a combination of large sharp waves alongside 100-300 Hz oscillations called ripples (Cutsuridis and Taxidis, 2013; Eschenko et al., 2008; Sullivan et al., 2011). Sharp depolarising events generated in area CA3 are superimposed over ripples generated in area CA1 from Schaffer collateral excitation; thousands of neurons discharge synchronously during the SPW-R time window, with neurons participating in SPW-Rs typically active during the previous awake phase, a phenomenon referred to as compressed replay (Buzsáki, 1986; Cutsuridis and Taxidis, 2013; Sullivan et al., 2011). Artificial interference with SPW-Rs impairs spatial learning and memory in rodents, indicating a functional role in memory consolidation (Ego-Stengel and Wilson, 2010).

Ripples are generated within area CA1 via rich excitatory connectivity as well as extensive interneuron regulation (Cutsuridis and Taxidis, 2013). Axo-axonic cells, O-LM cells, basket cells, and bistratified cells are active at distinct phases of the ripple cycle – axo-axonic cells fire before the onset of the ripple episode, basket and bistratified cells fire alongside pyramidal cells in phase with the ripple, and O-LM cells only at the end of the SPW-R (Cutsuridis and Taxidis, 2013). Modelling suggests that axo-axonic cells silence the CA1 network to prepare for relay of information, before interneuron-targeting interneurons silence axo-axonic cells and disinhibit basket and bistratified cells, with basket cells synchronising with each other and bistratified cells through recurrent inhibition to provide synchronous perisomatic and dendritic inhibition that hyper-synchronises CA1 pyramidal cell firing during ripples (Cutsuridis and Hasselmo, 2011; Cutsuridis and Taxidis, 2013; Ellender et al., 2010). Dynamic recruitment and activity of various CP-AMPAR-expressing interneuron populations results in the high-frequency synchrony seen in SPW-Rs. It has also been proposed that SPW-Rs may offer up conditions suitable for anti-Hebbian LTP in certain interneurons; notably, O-LM cells are generally inactive during SPW-Rs while pyramidal cells, many of which may input onto O-LM cells, fire at high frequency (Klausberger et al., 2003; Lamsa et al., 2007). Long-term alterations in

excitability of O-LM cells, active during exploratory behaviour, may contribute to (spatial) memory formation.

A typical pattern of hippocampal activity seen during awake exploration is the theta rhythm (6-10 Hz) oscillation (Buzsáki, 2002). Theta oscillations are seen during either REM sleep or active motor behaviour, and have been proposed to contribute to voluntary movement and/or learning and memory. There are multiple reported generators of hippocampal theta rhythms; excitatory drive from entorhinal cortex is thought to play a major role in entraining theta rhythms in area CA1 (Buzsáki, 2002). However, theta can still be generated within the hippocampus following surgical removal of entorhinal cortex; this separate oscillator requires cholinergic activation, as the remaining theta activity following entorhinal removal is abolished by atropine (Kocsis et al., 1999; Montoya and Sainsbury, 1985). Cholinergic projections to pyramidal cells and basket cells arise from an extrahippocampal structure called the medial septum; additionally, there are GABAergic cells within this region that project to and inhibit interneurons including basket cells (Colgin, 2013; Fox et al., 1986; Hangya et al., 2009; Stewart and Fox, 1990; Tóth et al., 1997). Theta oscillations generated by inputs from the medial septum are believed to involve a combination of phasic GABAergic inhibition of PV+ basket cells and cholinergic activity, potentially via tonic activation of interneurons (Stewart and Fox, 1990). Lesions to the medial septum result in spatial memory task impairments correlating with reductions in theta rhythm (Givens and Olton, 1994; Winson, 1978). It is proposed that periods of high basket cell activity and low septal inhibition exist during memory encoding, whilst septal inhibition and pyramidal cell disinhibition occur during retrieval (Kunec et al., 2005).

Perhaps the most extensively studied neural oscillation in recent decades, however, is the gamma wave oscillation, high-frequency (30-80 Hz) synchronous oscillatory activity proposed to be highly important in information processing (Gloveli et al., 2005b). Unlike SPW-Rs and (to a lesser extent)

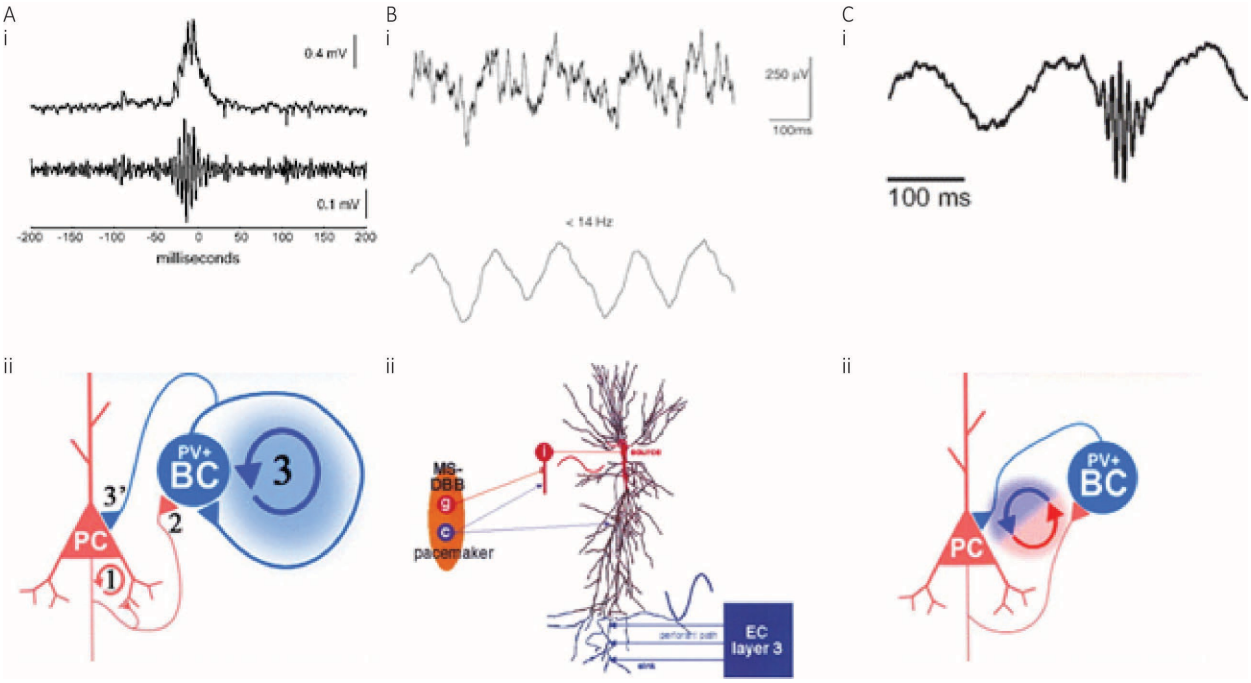

Figure 1.6. Oscillations of the hippocampus. (A) (i) A sample sharp-wave ripple (unfiltered, top; high-pass filtered, bottom). (ii) Diagram the generation of SPW-R resulting from rich excitatory connectivity and interactions with interneurons. (B) (i) Sample wide-band (top) and low-pass filtered (bottom) traces of theta oscillations. (ii) Model of hippocampal theta oscillations generated by medial septal inputs, with GABAergic hyperpolarisation of basket cells and cholinergic depolarisation of pyramidal cells promoting pyramidal activity. (C) (i) Local field potential trace illustrating gamma activity nested in theta oscillations. (ii) An illustration demonstrating the proposed loop of excitation and inhibition between pyramidal cells and PV+ interneurons during gamma-frequency activity. Figure produced from figures taken from: Rex et al., 2009 (Panel A(i)); Schlingloff et al., 2014 (Panels A(ii) and C(ii)); Dragoi et al., 1999 (Panel B(i); Buzsáki, 2002 (Panel B(ii)); Tort et al., 2008 (Panel C(i)).

theta oscillations, gamma activity is not restricted to the hippocampus, with bursts of gamma frequency oscillations promoting rapid principal cell coordination across brain regions (Colgin and Moser, 2010). Gamma is faster than theta, but less stable, occurring in bursts commonly nested within theta oscillations that persist throughout active behaviours (Bragin et al., 1995; Canolty et al., 2006; Jensen and Colgin, 2007). The theta/gamma coupling is hypothesised to form a code for ordered representations of multiple items or ideas, as well as coordinating communication between brain regions (Lisman and Jensen, 2013).

1.4.2 Generation of hippocampal gamma oscillations

Early work investigating the mechanisms of gamma oscillations noted high correlation between the phase of gamma oscillations and spike timing of interneurons, and found that gamma frequency currents recorded from pyramidal cells were inhibitory currents composed of chloride and bicarbonate ions (Buzsáki et al., 1983; Soltesz and Deschênes, 1993). Further work indicated that the peaks of gamma oscillations reflect rhythmic inhibitory post-synaptic potentials in pyramidal cells mediated by $GABA_A$ receptors (Penttonen et al., 1998). The first GABAergic cells implicated in generating these rhythmic inhibitory currents were PV+ basket cells, which were shown to fire at gamma frequency phase-locked to field oscillations.

Gamma oscillations are believed to represent alternating activity of interneurons and principal cells, and the properties of basket cells make them ideal candidates for the drivers of oscillations. Basket cells innervate the perisomatic regions of large numbers, or ensembles, of pyramidal cells, inhibiting the output of these neurons by blocking action potential generation (Mann et al., 2005a). When a basket cell is activated, it will impose this inhibition on its target pyramidal cells. When the basket cell subsequently inactivates, the target cell population is simultaneously relieved from this inhibition and can now fire in synchrony (Meyer et al., 2002). The fast spiking kinetics, high dendrodendritic interconnections through gap junctions, and dense collateralization of axons make PV+ basket cells well suited for coordination of pyramidal cell activity on a rapid timescale.

There have been at least two models proposed as to how interneurons generate gamma oscillations, namely inhibitory-inhibitory (I-I) and excitatory-inhibitory (E-I) models (Fig. 1.7) (Buzsáki and Wang, 2012). I-I models require mutually connected interneurons, as well as sufficient drive to induce

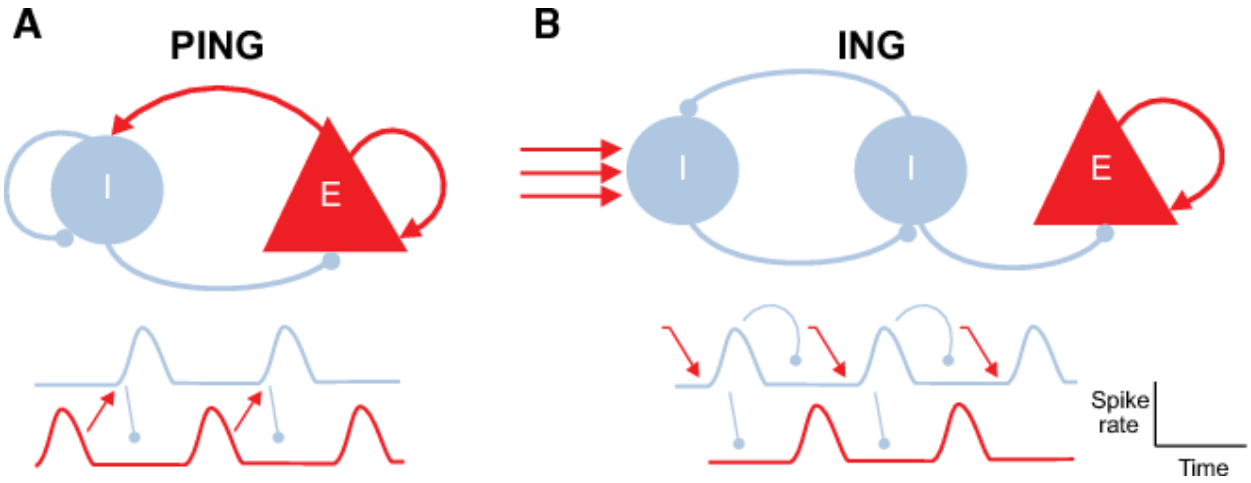

Figure 1.7. Two separate models of gamma oscillations. (A) The pyramidal-interneuron gamma model (PING, or E-I) proposes that reciprocal connectivity between pools of inhibitory interneurons and excitatory cells enables the generation of high-frequency oscillations via recruitment of fast-spiking interneurons, rapid perisomatic inhibition of excitatory cells mediated by these interneurons, eventual disinhibition of excitatory cells, and subsequent recruitment of interneurons. (B) The interneuron gamma model (ING, or I-I) proposes that mutually connected interneurons, under sufficient excitatory drive, exert rhythmic inhibition on adjacent populations of excitatory pyramidal cells, as well as reciprocal inhibition of interneurons. Taken from Bosman *et al.*, 2014, which was in turn adapted from Tiesinga and Sejnowski, 2009.

interneuron spiking (Wang and Buzsáki, 1996; Whittington et al., 1995). When these interneurons receive stochastic inputs that drive irregular spiking, strong recurrent synaptic interactions stabilise the network – a subset of interneurons fires together, generating inhibitory potentials in partnered interneurons, which subsequently discharge following decay of inhibition, triggering a repeating cycle that leads to the emergence of oscillations (Ardid et al., 2010; Brunel, 2000; Brunel and Hakim, 1999; Brunel and Wang, 2003; Geisler et al., 2005). Conductance through $GABA_A$ receptors, determined by subunit composition, governs the duration of inhibitory potentials, thus shaping the frequency of oscillations (Farrant and Nusser, 2005; Whittington et al., 1995).

In the E-I model, on the other hand, oscillations are generated by reciprocal connections between pyramidal cells and interneurons, with two pools of neurons alternating between fast excitation of interneurons by pyramidal cells, and subsequent inhibition of excitatory cells by interneurons (Börgers and Kopell, 2003; Ermentrout and Kopell, 1998; Geisler et al., 2005). Axon conduction and synaptic delays result in a shift between principal cell and interneuron spiking, with the extent of these delays determining the frequency of the generated rhythm, in addition to the synaptic decay

time (Bragin et al., 1995; Brunel and Wang, 2003; Csicsvari et al., 2003; Hájos and Paulsen, 2009; Hasenstaub et al., 2005; Mann et al., 2005a; Tiesinga and Sejnowski, 2009). It has been widely shown that spikes of putative fast-spiking cells, as well as subsequently identified, PV+ basket cells rapidly follow the firing of pyramidal cells during hippocampal gamma oscillations both *in vivo* and *in vitro* (Bragin et al., 1995; Csicsvari et al., 2003; Hájos and Paulsen, 2009; Mann et al., 2005a). Furthermore, weakening E-I connections by genetically knocking down AMPARs on PV+ interneurons is reported to reduce the amplitude, or power, of gamma oscillations (Caputi et al., 2012; Fuchs et al., 2007). E-I models indicate that both excitation and inhibition are necessary for generating and sustaining gamma frequency oscillations. Evidence indicates that the responsibility for generating these oscillations falls primarily on PV+ interneurons, as optogenetic stimulation of PV+ cells, but not pyramidal cells, has entrained cortical networks at gamma frequency, whilst optogenetic silencing of PV+ cells substantially reduced the power of oscillations (Cardin et al., 2009; Sohal et al., 2009).

The role of other interneurons in generating or shaping gamma oscillations cannot be entirely discounted, however. CCK+ basket cells do not have the firing kinetics to generate gamma frequency rhythms, and typically fire episodically during oscillations, unlike the regular, rapid firing of PV+ basket cells locked to the descending phase of gamma oscillations (Gulyás et al., 2010; Klausberger et al., 2005; Tukker et al., 2007). However, the fluctuating, imprecise inhibitory signal from CCK+ cells may regulate the balance of E-I activity, implementing gain control and offsetting the excitatory drive necessary to reach the action potential threshold in pyramidal cells, working to shape the neuronal ensembles active on each gamma cycle (Gulyás et al., 2010; Klausberger et al., 2005; Klausberger and Somogyi, 2008; Mitchell and Silver, 2003; Tukker et al., 2007). Inhibition of weakly active, but not strongly recruited, principal cells could enhance the signal-to-noise ratio at a network level, and support appropriate processing/encoding of information in pyramidal cell assemblies (Bartos and Elgueta, 2012; Klausberger and Somogyi, 2008; Tukker et al., 2007).

There is also some evidence pointing towards a contribution of unknown significance of SOM+ interneurons during hippocampal gamma oscillations. Bistratified cells in area CA1 have been shown to exhibit strong phase-locking to field gamma oscillations in CA3, and GABAergic input from these cells could explain gamma-frequency oscillations in CA1 pyramidal dendrites (Csicsvari et al., 2003; Penttonen et al., 1998; Tukker et al., 2007). SOM+ interneurons have been reported as critical for context-dependent gamma rhythms in visual cortex (Veit et al., 2017). It was further proposed that gamma-modulated bistratified cell firing could generate precise windows of excitability at sites of innervation in pyramidal cells, and in doing so contribute to temporal compression of pyramidal cell assembly firing (Klausberger et al., 2004; Pouille and Scanziani, 2004; Tukker et al., 2007). Dynamic changes in dendritic excitability driven by SOM+ interneuron activity could contribute to the regulation of which pyramidal cell assemblies are active during rhythmic network activity (Müller and Remy, 2014).

A significant proportion of these findings have been made through recording oscillations *in vitro* in area CA3 of hippocampus. Oscillations generated within this region are typically within the slow gamma sub-band; however, faster oscillations have been seen elsewhere in the hippocampus (Colgin et al., 2009). Slow gamma oscillations recorded in area CA1 are entrained by inputs from CA3, but mid/fast gamma-frequency oscillations (65-140 Hz) have been observed within this region (Colgin et al., 2009). These faster oscillations appear to be entrained by inputs from medial entorhinal cortex, as blocking synaptic transmission from layer III of medial entorhinal cortex caused a reduction in observed fast but not slow gamma oscillations in area CA1 (Colgin et al., 2009; Yamamoto et al., 2014). There is also evidence that in the absence of activation by CA3 or entorhinal cortex, area CA1 generates fast gamma oscillations, with the suggestion that area CA3 inputs ‘override’ the default setting of CA1 activity (Pietersen et al., 2014).

1.4.3 Functions of gamma oscillations

By facilitating the transfer of pertinent stimuli and information during an experience via synchronised activity of pyramidal cells, gamma oscillations could promote the encoding of memory. Intracranial recordings from humans found a positive correlation between hippocampal gamma power and probability of word recall, and a separate study using electroencephalography found that words during the presentation of which gamma showed higher synchronisation between the hippocampus and rhinal cortex were more likely to be remembered (Fell et al., 2001; Sederberg et al., 2007). It has been proposed that fast gamma synchronisation between CA1 and medial entorhinal cortex facilitates memory encoding; the entorhinal-to-CA1 projection conveys information about an animal's current position within its environment, and fast oscillations may transmit information regarding environmental stimuli (Brun et al., 2002; Colgin et al., 2009; Fyhn et al., 2004). The fast successive inputs to CA1 cells from entorhinal cortex may lead to spiking and spike timing-dependent plasticity that promotes encoding (Bi and Poo, 1998).

In addition to encoding of memory, gamma-frequency oscillations have been implicated in mechanisms underpinning memory retrieval, by temporally linking activity of spatially distributed cells that represent a memory episode (Bi and Poo, 1998). The rewarded alternation T-maze task first places an animal in the home arm of a T-maze, and then forces it to enter one of two reward arms and receive a reward. The animal is then returned to the home arm, and given a choice of entering either of the reward arms; however, it will only receive a reward if it enters the previously unexplored arm, so it must learn to remember which arm it previously entered and use that information to receive a reward. Local field potentials recorded from the hippocampi of rodents performing the task showed increases in power and coherence of gamma oscillations between CA3

and CA1, specifically when the animals entered the choice zone of the maze (Montgomery and Buzsáki, 2007). This suggests that the coherent oscillations may have transmitted information allowing the animal to retrieve the memory of the previous experience and modify its behaviour accordingly. Other studies have shown CA3-to-CA1 connections as necessary for retrieval, and reported increases in CA3 gamma power during accurate performance on retrieval-dependent tasks (Gilbert and Kesner, 2006; Nakashiba et al., 2008; Tort et al., 2009). Based upon these and other findings, it has been proposed that coherent slow gamma activity within the CA3-CA1 network promotes memory retrieval (Colgin et al., 2009; Steffenach et al., 2002).

These findings suggest that fast and slow gamma entrained by entorhinal cortex and CA3, respectively, may have competing functions in memory processes. Segregation of these inputs with differing frequencies has been proposed by one group to be a mechanism allowing dynamic routing of the flow of information, in order to prevent interference from previously learned associations whilst encoding new associations, and conversely restricting formation of new memories whilst retrieving already encoded memories (Colgin et al., 2009). Gamma oscillations may be an ideal mechanism for this segregation of inputs by facilitating transfer of information from one region whilst filtering out inputs from other regions (Hasselmo et al., 2002). Fast and slow gamma oscillations preferentially occur during different phases of theta in CA1, and excitatory currents from CA3 and entorhinal cortex are reported as maximal during different theta phases, raising the possibility that underlying theta oscillations regulate gamma-mediated dynamic routing of information to CA1 (Brankack et al., 1993; Colgin et al., 2009; Hasselmo et al., 2002; Kamondi et al., 1998a, 1998b).

Long-term potentiation is most easily induced at a particular phase of theta, specifically that at which entorhinal input is maximal, suggesting that entorhinal inputs arrive in CA1 at the time during

which memory encoding occurs optimally (Hasselmo et al., 2002; Huerta and Lisman, 1995; Jutras et al., 2009). $GABA_AR$-mediated control of spike timing during theta activity may contribute to temporal coding via organisation of pre- and post-synaptic spiking to regulate plasticity, and provide a mechanism for retrieval through spike timing-based neuronal interactions (Kwag and Paulsen, 2009). Retrieval is believed to occur during the theta phase in which CA3 input to CA1 is maximal and entorhinal signals are suppressed (Hasselmo et al., 2002). Expanding upon this, Bieri et al. found that slow gamma spikes occurred earlier in place fields than fast gamma spikes, and that cell ensembles retrieved upcoming positions during slow gamma and encoded past positions during fast gamma (Bieri et al., 2014). This supports the idea that non-overlapping inputs from CA3 and entorhinal cortex driving different-frequency gamma states enable switching of hippocampal mode between encoding and retrieval whilst preventing interference. However, work from *in vitro* studies has suggested that entorhinal input is insufficient to directly drive fast gamma oscillations; rather, hypotheses built on these findings suggest that the fast gamma state is the default mode of CA1, and represents a status quo such that in the absence of retrieval driven by CA3, memory encoding is the dominant state (Colgin and Moser, 2010; Remondes and Schuman, 2002; Zemankovics et al., 2013).

Working memory has been defined as short-term internal maintenance of information that is required for upcoming actions or choices but is no longer present in the external environment, and likely relies upon distributed networks of brain regions (D'Esposito, 2007; Fuster, 2000). Intracranial recordings in humans have reported increases in hippocampal gamma power correlating with increases in working memory load, and enhanced hippocampal theta-gamma coupling during maintenance periods of working memory tasks (Axmacher et al., 2010; van Vugt et al., 2010). It has been hypothesised that changes in hippocampal gamma profile during working memory in humans may involve synchronisation of the hippocampus with other brain regions implicated in working memory operations, such as prefrontal cortex (Ranganath, 2006; van Vugt et al., 2010).

There is evidence, both indirect and direct, implicating gamma oscillatory activity in working memory in rodents, particularly using spatial working memory tasks. Interfering with the excitation or output of PV+ interneurons has been shown to selectively impair spatial working memory performance on rewarded alternation tasks whilst preserving spatial reference memory (Caputi et al., 2012; Fuchs et al., 2007; Murray et al., 2011). As previously mentioned, the rewarded alternation T-maze requires an animal to remember immediate prior experience of being in the maze during the forced sample phase of a trial in order to inform upon choice-making when given the choice between the two now-open arms. Two separate mutations (crossbreeding animals with a floxed GluR1 gene with a PV-Cre line, and a constitutive GluR4 deletion) disrupting AMPAR expression in PV+ interneurons, caused reductions in correct choice-making on the task, whilst sparing reference memory (Caputi et al., 2012; Fuchs et al., 2007). Additionally, viral-driven expression of tetanus toxin light chain in PV+ interneurons in area CA1 of hippocampus, a transfection that prevents vesicle fusion and synaptic output, again affected spatial working memory but not reference memory (Murray et al., 2011).

Yamamoto et al. placed electrodes into area CA1 and medial entorhinal cortex of mice and trained them on the T-maze task, observing incidences of strong fast-gamma synchrony between dorsal CA1 and entorhinal cortex during the choice phase of trials, restricted to when the animal entered the choice zone preceding the turning into the reward arms, but only on trials where the animal successfully alternated from the sample phase (Yamamoto et al., 2014). Ablation of inputs from medial entorhinal cortex layer III, or optogenetic silencing of these inputs when entering the choice zone, inhibited emergence of synchronised fast gamma in area CA1 and reduced performance to chance levels. These results indicate that synchronous gamma-frequency activity within these two regions is necessary for successful choice-making on a working memory-dependent task.

Intriguingly, these results contrast with previous observations reported by Montgomery and Buzsaki on a similar task, where they detected increases in power and coherence of slow gamma oscillations at the interface between CA3 and CA1 when approaching the junction of the T-maze (Montgomery and Buzsáki, 2007). As this portion of the task requires the animal to remember where it has been previously to inform on current behaviour, it would seem more apt for the route of information flow more commonly associated with memory retrieval (CA3 to CA1) to be active at this point, so the findings from Yamamoto et al. are surprising. However, both studies do point towards an important role for gamma frequency activity in working memory processes and associated choice-making.

1.4.4 Dynamics of gamma oscillations

As generators of gamma and theta rhythms, it is believed that activity of PV+ interneurons is a key component underpinning the power and frequency of oscillations (Colgin and Moser, 2010). The oscillations recorded by extracellular electrodes are believed to reflect rhythmic IPSPs in pyramidal cells mediated by $GABA_A$ receptors (Penttonen et al., 1998). Following from this, the amplitude of gamma-frequency oscillations are believed to represent the number of PV+ interneurons that fire per gamma cycle (Buzsáki and Wang, 2012; Sohal et al., 2009). This is supported by observations that optogenetically inhibiting PV+ cells decreases gamma power, as does reducing the excitatory drive onto PV+ cells by knocking out AMPAR subunits (Caputi et al., 2012; Fuchs et al., 2007; Sohal et al., 2009).

As $GABA_A$ receptor-mediated currents are the primary driving force of gamma oscillations, the time course of GABAergic inhibition via these receptors is expected to be the core determining aspect of

oscillation frequency (Farrant and Nusser, 2005; Wang and Buzsáki, 1996; Whittington et al., 1995). As GABAergic hyperpolarisation of principal cells decays, these cells will have an increasing probability of spiking, and in doing so activating PV+ cells to re-inhibit them. Therefore, the activation and deactivation properties of $GABA_A$ receptors, which are influenced by the component subunits, and the excitation of PV+ cell populations, likely have greatest influence over oscillation frequency in an E-I model featuring PV+ interneurons (Ardid et al., 2010; Brunel, 2000; Brunel and Hakim, 1999; Brunel and Wang, 2003; Geisler et al., 2005). However, in a loop of excitation and inhibition, the rate of excitation of PV+ interneurons following disinhibition of principal cells is likely to also have some influence. This will be influenced by how quickly principal cells spike once inhibition is relieved, along with the excitation properties of PV+ cells, particularly the kinetic properties of their AMPARs, which are predominantly fast due to the lack of GluR2.

NMDARs have received some focus within the study of hippocampal gamma oscillations, but have generally been shown to be a minor contributor to oscillatory activity, as pharmacological blockade of NMDARs did not influence the persistence of carbachol- or potassium-evoked gamma oscillations (in contrast, AMPAR antagonism blocked carbachol-evoked oscillations) (Fisahn et al., 1998; LeBeau et al., 2002). One study observed increases in the frequency of carbachol-evoked gamma oscillations following NMDAR activation under certain conditions, and found that this modulation of frequency resulted from balance between tonic excitation and inhibition of interneurons (Mann and Mody, 2010). Overall, the contribution of NMDARs to the properties of gamma oscillations, at least those recorded *in vitro*, are relatively minor.

In contrast, AMPAR activity, particularly in PV+ interneurons, has been clearly shown as necessary for hippocampal gamma oscillations, at least in some models, as AMPAR antagonism blocks oscillations, and knockout of AMPAR subunits in PV+ interneurons selectively reduces gamma power

in vitro and impairs performance of oscillation-dependent behaviour *in vivo* (Caputi et al., 2012; Cunningham et al., 2003; Fisahn et al., 1998; Fuchs et al., 2007). However, whilst the general importance of AMPAR activity has been established, the relative influence of some of the distinctive properties of AMPARs in different neuron types remains to be investigated.

Distinct, often largely non-overlapping ensembles of neurons are active on different cycles of theta and gamma oscillations; this raises the opportunity for various items of information to be represented in a defined pattern (Lisman and Jensen, 2013). Furthermore, ensembles representing distinct spatial maps or patterns of spatial information can emerge or fade in prominence during the formation or reconfiguration of cognitive maps depending on the presence of new information within the environment (Fig. 1.8) (Dupret et al., 2013, 2010). Different pyramidal cell assemblies representing old and new spatial maps were found to be expressed on non-overlapping theta and gamma cycles during learning of new reward locations on a spatial memory task, with expression flickering between the two assemblies, and expression of new assemblies increasing in strength during the course of learning. In general, appropriate processing of information likely requires flexibility within the network in order for correct formation and selection of cell assemblies, particularly as assembly formation within oscillatory periods is dynamic and dependent on environmental context (Nissen et al., 2010).

Due to the leading influence that PV+ interneurons have upon network activity during gamma and theta oscillations, it has been previously predicted that plastic changes in synaptic strength at excitatory inputs onto PV+ interneurons occur over behaviourally relevant time scales in order to enable appropriate ensembles to optimally transmit relevant, up-to-date environmental information and correctly guide behaviour (Csicsvari et al., 1998; Nissen et al., 2010). There has been little work exploring this; however, one study found that reconfiguration of cognitive maps whilst learning new

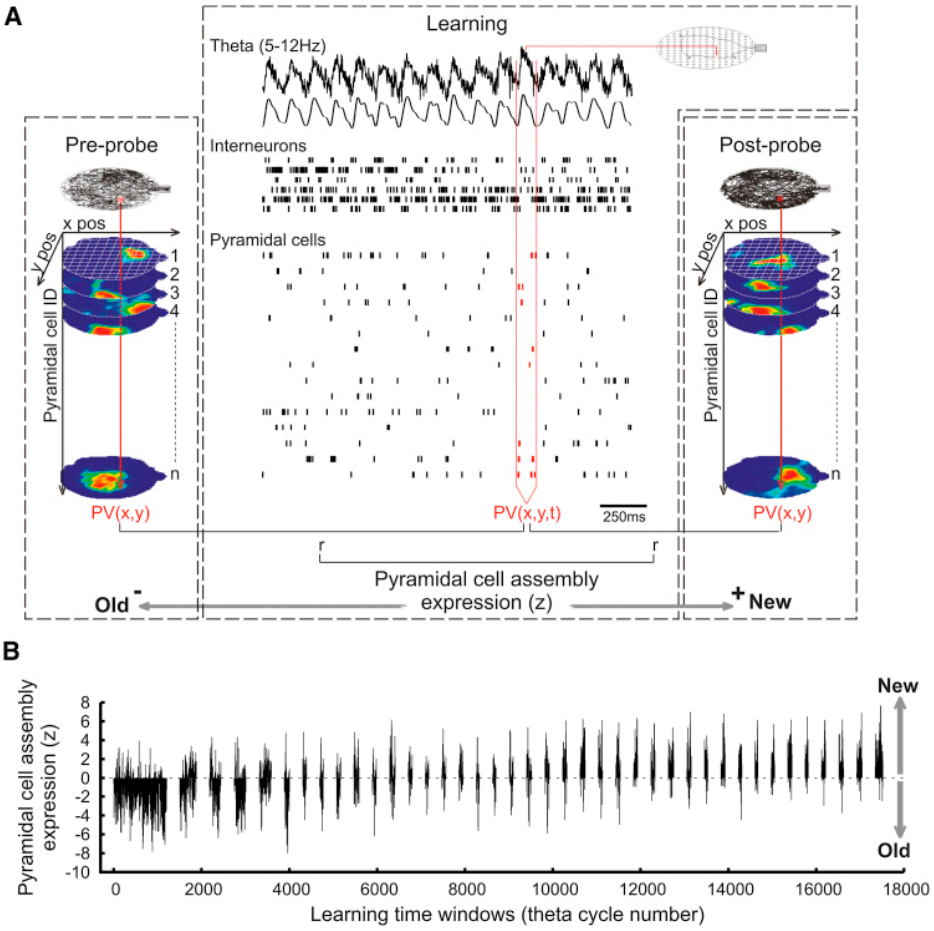

Figure 1.8. Flickering of pyramidal assemblies across theta cycles and fluctuating expression across learning. (A) Theta cycles used as time windows to calculate interneuron firing rate and identify ongoing hippocampal spatial maps expressed by pyramidal cell ensembles. (B) Pyramidal cell assembly expression shifts during a learning session. Taken from Dupret et al., 2013.

reward locations in a familiar environment was associated with the emergence of prominent new ensembles (and fading of ensembles reflecting old reward locations), as well as both positive and negative changes in the strength of synaptic connections from excitatory cells onto interneurons (Dupret et al., 2013). Another group found that manipulating expression of a surface protein important in regulating interneuron plasticity altered performance on the working memory-dependent T-maze task, amongst other behavioural changes (Favuzzi et al., 2017).

As previously mentioned, PV+ interneurons express high levels of CP-AMPARs. Whilst the properties of these AMPARs contribute to the fast excitation of these fast-firing cells, they can also mediate NMDAR-independent excitatory plasticity at synapses onto these cells (Lamsa et al., 2007). Indeed,

some studies suggest that plasticity mediated by these receptors is the primary mechanism of plasticity within these cells (Nissen et al., 2010). However, it is worth noting that one study found a distinction in PV+ interneurons in area CA1, where feedforward inputs from CA3/entorhinal cortex could only mediate CP-AMPAR-dependent plasticity, while higher levels of NMDARs meant that feedback inputs from local CA1 pyramidal cell collaterals could induce plasticity mediated by either type of receptor (Le Roux et al., 2013). The relative importance of each input or type of plasticity to dynamic changes in synaptic strength during gamma oscillatory activity is uncertain. The depolarisation-dependent properties of each type of receptor lends them more or less suitable to responding to certain types of input; the high-frequency stimulation occurring during gamma oscillations is more likely to promote potentiation of synapses via NMDARs, or depression via CP-AMPARs, if the interneuron is depolarised whilst receiving the input. Depending on the mechanisms of gamma oscillation dynamics, it is possible that plasticity in CA1 interneurons is mediated by NMDARs. However, it has been proposed that, at least with slow gamma entrained by CA3, the primary driver of CA1 interneuron discharge is excitatory input from CA3, based on the time differences between discharge of CA1 and CA3 pyramidal cells and CA1 interneurons, as well as the greater number of synapses onto CA1 basket cells from CA3 pyramidal cells than CA1 pyramidal cells (Csicsvari et al., 2003; Freund and Buzsáki, 1996). As far as CA3 interneurons go, there is much less experimental evidence on the subject; however, one study did find a higher NMDAR:AMPAR current ratio at synapses onto stratum lucidum interneurons formed by recurrent pyramidal cell collaterals compared to mossy fibre inputs, similar to what was seen with CA1 PV+ cells (Lei and McBain, 2002).

Overall, there has been little work done to explore what influence plasticity at excitatory synapses onto hippocampal PV+ interneurons has on optimal network activity and behavioural output. Furthermore, there has been no work done that I know of that investigates the contribution of each type of Ca^{2+}-permeable receptor to the plasticity profile of these interneurons during behaviour. I

wish to explore the contribution hippocampal CP-AMPAR activity to hippocampal function and behavioural output, specifically CP-AMPAR-mediated Ca^{2+} conductance and resultant anti-Hebbian plasticity, with a particular focus on hippocampus-dependent behaviours associated with oscillatory activity.

1.5 Research techniques

1.5.1 In vitro models of gamma oscillations

Studies of mechanisms underpinning gamma oscillations in the hippocampus have made extensive use of *in vitro* models of oscillogenesis in area CA3 of hippocampus, due to the ability to pharmacologically induce intrinsic generation of oscillations through the highly reciprocated connectivity within the region compared to CA1. Oscillations have been generated by applying a range of compounds, including cholinergic agonists such as carbachol and kainate receptor agonists (Bartos et al., 2007). GABA-mediated inhibition is necessary for oscillogenesis in all models, although it is sufficient only for glutamatergic models; carbachol-induced oscillations require a combination of phasic inhibition and excitation. The properties of oscillations in all models can be modulated using compounds that influence $GABA_AR$ gating (Fisahn et al., 2004; Traub et al., 1996a; Whittington et al., 1995). As my project is focussing upon manipulation of glutamatergic activity within the hippocampus, I will use carbachol-evoked CA3 gamma oscillogenesis as a model for investigating gamma oscillations, both due to the E-I nature of the model and also to avoid cross-over between two compounds that interact with glutamate receptors. As such, I will briefly cover some of the translatability of findings from *in vitro* carbachol-evoked oscillations to gamma oscillations generated in the hippocampus *in vivo*.

Cholinergic induction of gamma oscillations is intended to mimic the high levels of acetylcholine reported *in vivo* during exploratory behaviour when gamma oscillations are present, and is believed to function by elevating the excitability of pyramidal cells in area CA3, shifting the excitation:inhibition balance such that field oscillations emerge within the region (Bragin et al., 1995; Csicsvari et al., 2003; Fisahn et al., 1998; Hájos and Paulsen, 2009; Marrosu et al., 1995; Müller and Misgeld, 1986; Nabekura et al., 1993). The current source density profiles of oscillations are similar in the model and *in vivo*, with local field potential phase reversal between strata pyramidale and radiatum (Fig. 1.9) (Csicsvari et al., 2003; Hájos et al., 2004; Hájos and Paulsen, 2009). Further electrophysiological similarities can be observed with the firing patterns of neurons; the firing probabilities of CA3 pyramidal cells are highest at the negative peak of gamma cycles recorded in stratum pyramidale, and this firing is followed by firing of inhibitory neurons in the region with a delay consistent with monosynaptic excitation, a pattern seen both *in vivo* and *in vitro.* In both situations, individual pyramidal cells average a firing rate of 2-4 Hz, whilst perisomatic interneurons fire on most gamma cycles, with both cell types' firing patterns phase-coupled to field oscillatons (Csicsvari et al., 2003; Fisahn et al., 1998; Gloveli et al., 2005a; Hájos et al., 2004; Hájos and Paulsen, 2009; Senior et al., 2008; Tukker et al., 2007). Overall, whilst there will naturally be discrepancies between an *in vitro* model driven by continuous pharmacological stimulation and *in vivo* oscillations generated by natural network activity, there is sufficient overlap between the activity profiles of the two situations to lend credence to the translatability of *in vitro* discoveries to *in vivo* scenarios.

As the majority of *in vitro* experiments have studied slow gamma-band oscillations in the CA3 region, the majority of what is known about oscillation mechanisms may only be applicable to these slow oscillations (Colgin et al., 2009). This issue extends to *in vivo* recordings performed under urethane anaesthesia, which similarly feature gamma oscillations dominated by slow band oscillations

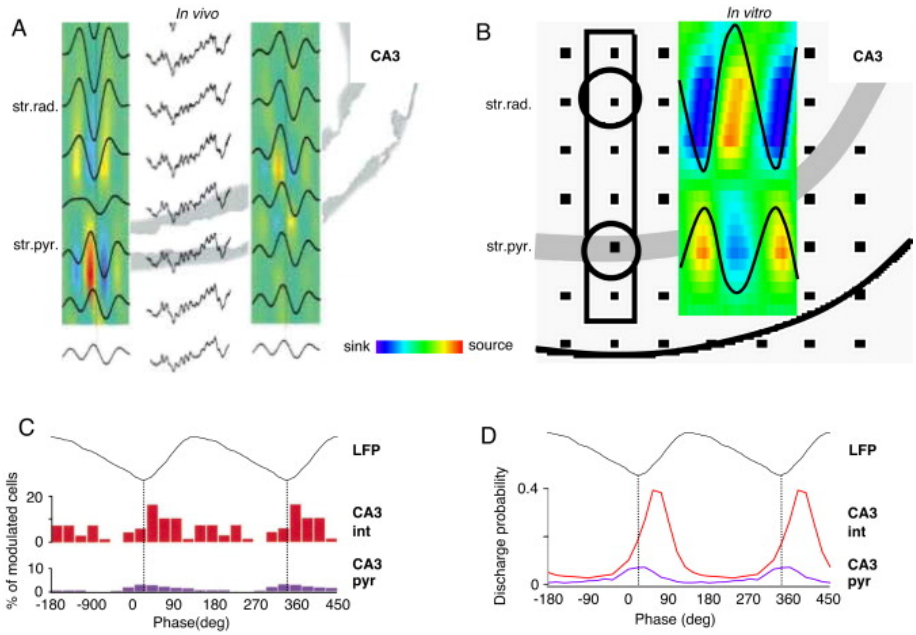

Figure 1.9. Similarities between hippocampal gamma oscillations recorded in CA3 *in vivo* in a behaving rat and recorded *in vitro* in rat hippocampal slices following cholinergic activation. (A, B) In both cases, reversal of the field potential is observed between stratum pyramidale and stratum radiatum, i.e. the cell soma and apical dendritic layers of pyramidal cells. (C, D) The spike phase of pyramidal cells and interneurons are similar in both situations. Taken from Hájos and Paulsen, 2009, which in turn reproduced panels from Csicsvari et al., 2003, and Hájos et al., 2004.

generated in CA3 and entrained in CA1, as the anaesthetic attenuates entorhinal inputs (Buzsáki et al., 1983; Penttonen et al., 1998; Tukker et al., 2007; Ylinen et al., 1995). Therefore, caution must be taken in applying any findings in these situations to mid/fast gamma-band oscillations entrained by entorhinal cortex or independently generated in CA1.

1.5.2 AMPA receptor antagonists

AMPARs, as previously covered, exhibit heterogeneity in their properties depending on their subunit composition. There are a range of many different competitive AMPARs that have been developed with variation in potency, receptor selectivity, and more (Catarzi et al., 2007). NBQX, a mixed AMPA/kainate receptor antagonist, has been shown to abolish gamma oscillations in CA3 and medial entorhinal cortex, and infusion of another AMPAR antagonist, CNQX, has been shown to impair

memory retrieval in rodents *in vivo* (Broadbent et al., 2010b; Catarzi et al., 2007; Cunningham et al., 2003; Fisahn et al., 1998; Riedel et al., 1999; Wiltgen et al., 2010).

Compounds that selectively inhibit CP-AMPARs have been derived from toxins from several animals (Brackley et al., 1993). These compounds typically contain polyamines, such as philanthotoxin-433, refined from wasp venom, which has been shown in xenopus oocytes to exhibit approximately 100-fold greater affinity for AMPARs lacking rather than containing GluR2. An array of philanthotoxin derivatives with a range of different receptor potencies and selectivities have been generated, with varying availability (Kromann et al., 2002; Poulsen et al., 2014). Other compounds exist outside of philanthotoxin; 1-naphthyl acetyl spermine (NASPM), a synthetic analogue of Joro spider toxin, is highly selective for CP-AMPARs, as mutating AMPAR subunits to remove Ca^{2+} permeability abolishes NASPM binding to receptors (Blaschke et al., 1993). These compounds have found use *in vitro* and (to a far lesser degree) *in vivo*, for such purposes as investigating interneuron excitation and plasticity, and receptor expression during memory retrieval (Hong et al., 2013; Le Roux et al., 2013; Nissen et al., 2010). However, their effects on hippocampal network activity have not been tested tomy knowledge.

1.5.3 Viral transfection of GluR2

Adeno-associated viruses (AAVs) have become a highly valuable research tool, particularly in neuroscience, for their ability to transfer genes to transfected cells and drive stable protein expression for extended periods of time without triggering a strong immune response (McCown et al., 1996; Miyake et al., 2015, 2011). In the virus, a transgene is incorporated into a plasmid construct taken up by the virus as its genome, along with promoter elements to drive the

transgene's expression (for example, the human synapsin (hSyn) promoter, which drives high levels of transgene expression specifically in neuronal cells) (Kügler et al., 2003; Miyake et al., 2015). Following transfection of cells, adenoviral DNA is retained in cells, typically in the form of an episome, a circular extrachromosomal DNA element that enables expression of the gene of interest; however, certain forms of AAV can undergo site-specific integration into the human host DNA at a unique locus on chromosome 19 (Colosimo et al., 2000; Ehrhardt et al., 2003; Kotin et al., 1990). As well as regional specificity conferred from the site of injection, cell type specificity can be achieved through several ways, such as placing the gene under the control of a promoter for a protein only expressed in certain cells (e.g. parvalbumin), or flanking the gene with loxP sites and inverting its sequence so that only cells expressing Cre recombinase can express the protein (e.g. PV+ interneurons in PV-Cre mice) (Murray et al., 2011). The efficiency of AAV transduction and gene expression can vary depending on the viral serotype used and region of interest; for example, one study found that AAV8-serotype led to best transgene expression in hippocampal interneurons, whilst AAV9 led to best expression in cortical interneurons (Aschauer et al., 2013).

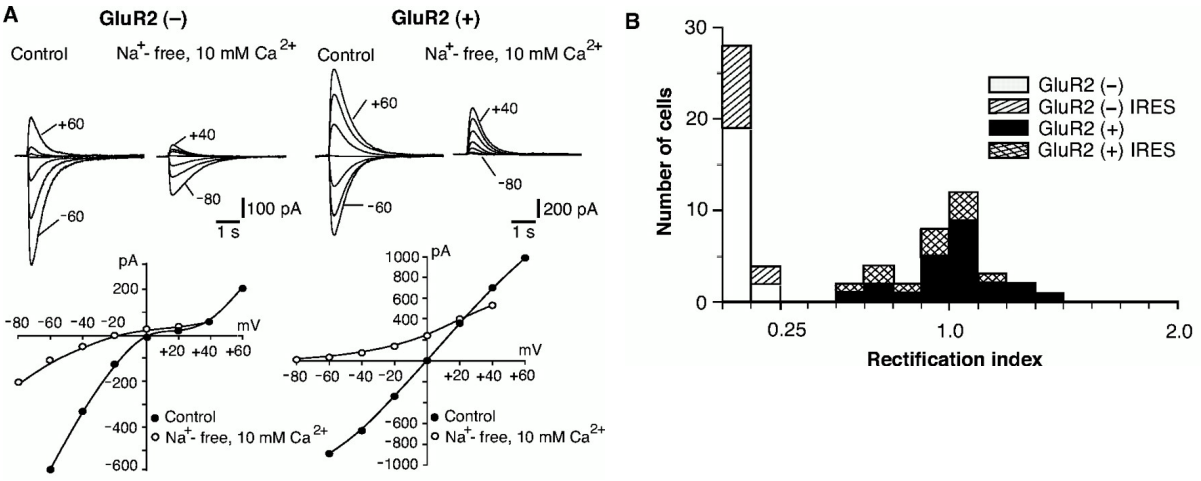

Figure 1.10. Shift in rectification properties of Bergmann glia cells transfected with a virus driving expression of edited GluR2. (A) Bergmann glia cells, typically dominated by CP-AMPAR expression, exhibit inwardly rectifying AMPAR-mediated currents, but following transfection by a virus driving artificial expression of the Q/R-edited form of the GluR2 subunit, shift towards a linear current-voltage relationship. (B) Histogram demonstrating strong shift in rectification properties of transfected cell population compared to controls. Taken from Iino et al., 2001.

AAV vectors can be used to express a wide variety of proteins, including light-activated channels, fluorescent proteins, and receptor subunits e.g. GluR2. Several studies from a group in Japan used an AAV construct carrying cDNA encoding the Q/R-edited form of GluR2 to transfect multiple non-neuronal cell types, including Bergmann glia and glioblastoma cells, and in doing so managed to replace CP-AMPARs with GluR2-containing AMPARs, substantially influencing the properties of these cells (Fig. 1.10) (Iino et al., 2001; Ishiuchi et al., 2002). However, to my knowledge, no one has done the same in neuronal cell types such as PV+ interneurons.

1.5.4 Behavioural tests

There are fundamental challenges to attempting to model aspects of human behaviour in rodents, due to the limited capacity for interaction with rodents and limited complexity that can be incorporated into tasks. However, many tests have been developed to try and replicate aspects of human behaviour and memory processes, enabling researchers to introduce manipulations and observe changes in these tasks in order to link said manipulation with psychological consequences.

Spontaneous locomotor activity and exploratory behaviour can be easily assessed using tracking equipment or photobeam equipment that detects movement in the form of beam breaks. Such assays have been used to assess locomotor impairment in models of neuromuscular disease, changes in activity following exposure to various compounds (including antipsychotics), and other alterations in movement and behaviour following a variety of manipulations (Pratt et al., 2012; Raben et al., 2000). Manipulations of glutamatergic receptor expression in PV+ cells have been found to bring about alterations in baseline locomotor activity; in addition, there are conflicting reports of desensitisation to the effects of psychosis-inducing drugs following PV+ specific knockout

of the NMDAR subunit NR1 (Belforte et al., 2010; Bygrave et al., 2016). One can also assess rearing behaviour with the same assay, which is considered to be a risk assessment response to potential danger in a novel environment (Piras et al., 2013).

Novelty recognition or preference can be assessed in various ways, including novel object recognition and spatial novelty preference tests. Spatial novelty preference is performed with a Y-shaped maze, and involves exposing an animal to two out of three arms on the maze for a period of time, before unblocking the third arm and replacing the animal in the maze, with animals typically preferring to spend more time in the novel arm rather than the previously explored arms. Hippocampal lesions decreased novelty preference in mice, as did animals with knockdown or knockout of the perineuronal net protein brevican (Favuzzi et al., 2017; Sanderson et al., 2007).

Working memory can be tested in humans using several tasks, such as the N-back test, in which subjects are exposed to a sequence of stimuli, and then must respond when a stimulus is presented that matches the stimulus presented 'n' number of steps previously; a higher value of 'n' leads to a greater working memory load (Miller et al., 2009). In contrast, working memory is often tested in rodents in the form of spatial working memory, using win-shift, or rewarded alternation, tasks such as the T-maze task previously covered.

The rewarded alternation T-maze task involves placing an animal in the home arm of a T-shaped maze, with the two branches at the 'top' of the T acting as reward arms (Deacon and Rawlins, 2006). The animal is first forced to enter one of the arms and receive a reward; it is then removed from the maze, the previously blocked arm is made accessible, and the animal is again placed in the home arm. The reward in the arm sampled first is not replaced, so the animal must learn to enter the

previously unexplored arm to receive a second reward. Working memory is tested as the animal must remember during the period between the initial sample phase and the subsequent choice phase which arm it has entered (intra-trial period), and flexibly alter its choice on a trial-by-trial basis. The task can be made more difficult by extending the intra-trial period to increase the working memory load, or by reducing the period between separate trials to increase the overlap in memories and interference with current choice-making.

It is entirely possible that spatial working memory represents a different set of psychological processes to human working memory tested in humans (Sanderson and Bannerman, 2012). Furthermore, simple spatial working memory tasks, such as the rewarded alternation T-maze, may be confounded by unconditioned habituation to recently explored stimuli and locations, meaning animals alternate their arm entries based on familiarity rather than purely rule learning and working memory.

Spatial working memory varies from spatial reference memory, which can be tested using apparatus such as a Y-shaped maze or the Morris water maze. In these tasks, the location of a reward is constant in a radially symmetrical shape, but the animal is placed in at different points, and must use extra-maze cues to remember where the reward location is. Compared to the rewarded alternation T-maze task, the animal must learn to find its way from different start points to the same location, instead of going to different reward locations depending on recent trial-specific information. Whilst performance on both of these tasks is dependent on having an intact hippocampus, the processes underpinning them are different, as animals with knockouts (e.g. GluR1 deletion in PV+ interneurons or whole brain) that impair working memory often have intact reference memory (Deacon and Rawlins, 2006; Fuchs et al., 2007; Morris et al., 1982; Reisel et al., 2002; Sanderson and Bannerman, 2012).

A more complicated version of the Morris water maze reference memory task is called the delayed matching-to-place (DMTP) task, and involves moving the location of the platform on a day-to-day basis (Steele and Morris, 1999). On each day, the animal must reconfigure its cognitive map to encode the new location. Whilst healthy animals rapidly learn the new location, animals with hippocampal lesions are unable to effectively learn the new location at the same rate as controls. A more complicated version of this task, a 'matching-to-multiple-places' task, is set on a 'cheeseboard' apparatus with holes that can conceal food rewards (Dupret et al., 2010). Multiple holes are baited each day, and these holes stay consistent across trials on each day, but change between days. Animals must again learn the new locations and stop revisiting locations from previous days that are no longer baited. Electrophysiology performed during this task showed the emergence of new prominent cell assemblies across theta and gamma oscillations during each day, alongside changes in synaptic strength at potential monosynaptic connections between pyramidal cells and interneurons in CA1 (Dupret et al., 2013).

These tasks are dependent on the hippocampus, specifically the dorsal hippocampus. Destruction of dorsal, but not ventral, hippocampus, has profound effects on spatial learning and memory, and ventral hippocampus cannot fully compensate for dorsal hippocampal damage, although whether dorsal hippocampal lesions occur before or after acquisition of a task has an influence on performance (Bannerman et al., 2003b; Moser and Moser, 1998). In contrast, ventral hippocampal activity is associated with measures of anxiety, as ventral hippocampal lesioned animals exhibit reduced anxiety on several tests (Bannerman et al., 2003b). These tests often involve the animal being exposed to, and avoiding, situations of potential danger, such as an open field in which the animals stay at the edges rather than the middle, or an elevated plus maze in which the animals stay in the two arms that are walled and sheltered (closed) rather than the two arms with no side walls

(open). In these tasks, ventrally lesioned animals will often show a greater willingness to move into the 'dangerous' locations of these apparatus, demonstrating a reduction in, or failure to express, anxiety. Anxiety can also be tested with a food neophagia assay, in which a food-restricted animal in placed in a novel environment with a novel foodstuff (Modlinska and Stryjek, 2016). Avoidance of the food arises from a need for the animal to assess the relative value of the food against the risk of toxicity or being exposed to other harm. Animals with full or ventral hippocampal lesions were quicker to approach and consume the novel food, a further indication of diminished anxiety in these animals (Bannerman et al., 2002).

1.6 Aims and hypotheses

I have mentioned in this introduction about the role of PV+ interneurons in hippocampal network activity, the links between hippocampal and PV+ interneuron functionality and behavioural impairments, and the distinctive receptor profile and plasticity mechanisms at excitatory connections onto these cells. I have spoken about the possibility that flexibility at these excitatory connections may be necessary for optimal information processing in the hippocampus by modulating activity of appropriate cell assemblies representing current information, and that Ca^{2+} currents mediated by CP-AMPARs may be necessary to achieve this flexibility. To my knowledge, the activity of CP-AMPARs within the context of hippocampal gamma activity and the contribution of Ca^{2+} currents through these receptors to network activity and hippocampus-dependent behaviour has not been investigated to date. As such, using pharmacological and viral approaches both *in vitro* and *in vivo*, over the next 4 chapters I will address the following questions:

- Chapter 2: is the activity of hippocampal CP-AMPARs necessary for optimal gamma activity? I will test this *in vitro* by acutely blocking CP-AMPARs using pharmacological agents with varying affinity for CP-AMPARs over GluR2-containing AMPARs. I will apply these agents *in vitro* to slices following carbachol-evoked generation of gamma oscillations and observe the effects of these agents on oscillation properties including power and frequency.

- Chapter 3: is the activity of hippocampal CP-AMPARs necessary for optimal performance on a gamma oscillation-associated task? I will test this by training animals to perform a working memory-dependent task (the rewarded alternation T-maze), and then directly infusing a CP-AMPAR-selective antagonist into dorsal hippocampus to observe the effects of acute CP-AMPAR blockade in this region on performance of the task.

- Chapter 4: can viral introduction of GluR2 into PV+ interneurons be used to transform the AMPAR profile of the cell? I will generate an adeno-associated viral vector containing a floxed form of Q/R-edited GluR2 and inject it into the hippocampus of PV-Cre animals, and, following histological confirmation of viral expression, I will perform several *in vitro* validation tests to demonstrate a change in the properties of the transfected cells indicative of a transition from a predominantly GluR2-lacking to GluR2-containing AMPAR profile, as well as observing the effects of such changes on the properties of carbachol-evoked gamma oscillations.

- Chapter 5: does a reduction in the calcium permeability of the AMPAR population of PV+ interneurons influence behavioural output of transfected animals, including on tasks dependent on hippocampal function and associated with oscillatory activity? Depending on successful validation of the uptake and incorporation of GluR2 into AMPARs expressed in hippocampal PV+ interneurons, I will perform a batch of behavioural tests assessing a range

of phenotypes in mice injected with the virus, including behaviours dependent on dorsal hippocampal function and oscillatory activity, ventral activity, and those reported to involve dynamic changes in interneuron activation, likely dependent on synaptic plasticity.

By answering these questions, I aim to further elucidate the role of CP-AMPAR-expressing interneurons in E-I models of hippocampal gamma oscillations, and reveal the significance of CP-AMPAR-mediated plasticity in PV+ interneurons in the optimal functioning of hippocampal networks within relevant behavioural contexts. This body work will provide a much-needed insight into the previously unexplored role of anti-Hebbian plasticity at pyramidal-to-PV+ interneuron connections in hippocampal activity and hippocampal-dependent memory processes, and expand knowledge regarding how the dynamic nature of the hippocampal network underpins its myriad reported functions.

2 AMPAR activity and antagonism in hippocampal network activity

2.1 Introduction

As discussed in the introduction chapter, gamma-frequency oscillations are widely believed to arise from rhythmic perisomatic inhibition generated by parvalbumin-positive fast-spiking interneurons (Mann et al., 2005a). PV+ interneuron activity appears to be critical to the emergence and maintenance of optimal gamma activity, as optogenetic silencing of these interneurons suppresses oscillatory activity *in vivo* (Sohal et al., 2009). Conversely, gamma-frequency optogenetic stimulation of PV+ interneurons can entrain and amplify oscillations (Cardin et al., 2009; Sohal et al., 2009).

The excitatory-inhibitory model of oscillation generation posits that reciprocal connectivity between pools of PV+ interneurons and pyramidal cells results in the generation of oscillations via alternating excitation of interneurons and inhibition of pyramidal cells (Börgers and Kopell, 2003; Mann et al., 2005a; Mann and Mody, 2010). The role of fast excitation in gamma activity can be demonstrated by the abolition of oscillations recorded in area CA3 of hippocampus *in vitro* in the presence of the AMPAR antagonist NBQX (Cunningham et al., 2003). In contrast, application of NMDAR or metabotropic glutamate receptor antagonists has been shown to not alter the power or frequency of oscillations (Zarnadze, 2016).

Activity in both pools of neurons is necessary for the emergence of gamma-frequency oscillations in the E-I model; however, only PV+ cells are capable of entraining the network at such high frequencies; optogenetic stimulation of pyramidal cells was only able to generate or amplify low-frequency oscillations (Cardin et al., 2009). Therefore, excitatory recruitment of PV+ cells is essential for optimal network activity in this model, and blockade or interference with fast excitatory currents restricted to these cells is likely to reduce or abolish gamma-frequency activity, such as is seen with NBQX exposure. In support of this hypothesis is the discovery of reduced power of gamma-frequency oscillations recorded *in vitro* from animals with a PV-specific knockout of the GluR1 AMPAR subunit, and a global GluR4 knockout (Caputi et al., 2012; Fuchs et al., 2007). However, the PV-Cre line used for the GluR1 knockout was also used for a PV-specific knockout of the NR1 NMDAR subunit that produced conflicting phenotypes to those seen with an alternative PV-Cre line by a separate group, raising some questions regarding the relative neuronal coverage of each line (Bygrave et al., 2016; Fuchs et al., 2007; Korotkova et al., 2010). Additionally, an acute manipulation of interneuronal AMPAergic activity may offer a distinct perspective upon the dynamics of network function than a constitutive subunit knockout, and any compensatory changes resulting from this.

NBQX is an AMPAR antagonist, but also targets kainate receptors, and doesn't show significant selectivity for different subclasses of AMPARs. In contrast, polyamine-based compounds such as philanthotoxin and NASPM have far greater affinity for CP-AMPARs over GluR2-containing AMPARs (Blaschke et al., 1993; Brackley et al., 1993). This capacity to selectively target CP-AMPARs, which are only expressed in large amounts on certain neuronal subpopulations such as PV+ interneurons, permits selective study of the consequence of AMPAR blockade of these cells, and have been used to study plasticity in PV+ cells, amongst other uses (Le Roux et al., 2013; Nissen et al., 2010). However, to my knowledge, these tools have not been used to study the consequences of acute

inhibition of excitatory input onto PV+ interneurons on network activity, including what effects this has on hippocampal gamma oscillations.

Gamma-frequency oscillations can be generated *in vitro* with a variety of agents, including glutamatergic and cholinergic agonists (Bartos et al., 2007). As I am planning to target glutamate receptors during this project, I will use a cholinergic model, involving the application of carbachol to horizontally-sectioned ventral hippocampal brain slices, which results in the generation of robust gamma-frequency oscillations in area CA3 (Mann et al., 2005b). Despite the focus on the dorsal-dependent roles of the hippocampus in spatial navigation and memory, studies investigating gamma oscillations in hippocampus *in vitro* commonly use horizontally cut sections of ventral hippocampus, as oscillations are more easily stimulated in these sections due to greater preservation of intra- and inter-regional activity along the septo-temporal axis of the hippocampus, although earlier studies used slices sectioned transversely (Fisahn et al., 1998). I will then apply CP-AMPAR-specific antagonists to slices and observe the consequences on gamma activity.

The future aims of this project are to selectively manipulate interneuronal AMPAR subunit expression and receptor Ca^{2+} permeability; however, performing these current experiments will both confirm an ability to show a direct link between CP-AMPAR function and hippocampal network activity in-house, and reveal the parameter space in which I may observe smaller effects with a more refined approach. Ultimately, the purposes of these experiments are to provide an alternative insight into the contribution of acute CP-AMPAR recruitment to hippocampal gamma activity, to confirm or contradict observations following PV+ cell-specific genetic reductions in AMPAR expression, and to provide proof-of-concept of the essential nature of functional expression of these receptors for fast hippocampal network activity, prior to later experiments specifically investigating the contribution of AMPAR-mediated calcium currents to the same network function.

2.2 Materials and methods

2.2.1 Animals

Experimentally naïve adult (8 weeks and older) C57Bl6 wild-type mice were used for field recordings. For the voltage-clamp recordings, *Pvalb*$^{tm1(cre)Arbr}$ (PV-Cre; JAX stock no. 008069; Hippenmeyer et al., 2005) mice expressing Cre recombinase in parvalbumin-positive (PV+) cells and *Gt(ROSA)26Sor*$^{tm9(CAG-tdTomato)}$ (Ai9; JAX stock no. 007909; Madisen et al., 2010) mice expressing tdTomato in a Cre-dependent manner (breeding animals of both strains kindly provided by Professor Colin Akerman, University of Oxford) were crossed to produce double heterozygous offspring. Brain slices from these animals contained PV+ interneurons filled with tdTomato that was visible under the microscope used for recordings. Animals were housed in group cages, and maintained at the Biomedical Sciences Building (University of Oxford), on a 12 hour:12 hour light-dark cycle in a temperature- and humidity-controlled room, with *ad libitum* food and water. All animals were housed according to Home Office regulations, with procedures carried out under a UK Home Office project licence (30/2897, Professor Ed Mann) and personal licence (IE1E0DB60, myself) in accordance with the United Kingdom Animals (Scientific Procedures) Act, 1986. All procedures were performed during the light phase of the light-dark cycle.

2.2.2 Electrophysiology

2.2.2.1 Slice preparation

Horizontal brain sections of 350 µm thickness containing ventral hippocampus were prepared from adult mice (8 weeks and older) using a sucrose-based cutting solution as described by Kuenzi et al., performed under heated conditions as described by Huang and Uusisaari, in attempts to maximise the yield of useable cells within slices (Huang and Uusisaari, 2013; Kuenzi et al., 2000). In brief, animals were anaesthetised with isoflurane and decapitated. The brain was removed from the skull, and positioned on a microtome cutting stage (Leica) whilst immersed in a heated (~34 °C) sucrose solution (composition of solution (in mM): 150 sucrose, 15 glucose, 34.5 NaCl, 25 $NaHCO_3$, 3 KCl, 1.25 NaH_2PO_4, 1 $CaCl_2$, 10 $MgSO_4$) and gassed with 5% CO_2/95% O_2. Slices were then transferred to an interface chamber submerged in a heated water bath and filled with oxygenated artificial cerebrospinal fluid (aCSF) (composition (in mM): 10 glucose, 126 NaCl, 24 $NaHCO_3$, 3.5 KCl, 1.25 NaH_2PO_4, 2 $CaCl_2$, 2 $MgSO_4$) and incubated at ~31 °C.

2.2.2.2 *In vitro* field recordings

After incubation in the interface chamber for a minimum of 1 hour, slices were transferred to an interface recording chamber, in which they were maintained at ~34 °C and superfused with a continuous stream of oxygenated aCSF, plus 5 µM carbachol to stimulate the generation of gamma oscillations. An extracellular recording electrode filled with aCSF (borosilicate, 1 MΩ) was used to record oscillations in stratum pyramidale of the CA3 region of the hippocampus, and field activity was recorded with a sampling rate of 10 kHz and digital low-pass filtering of 1 kHz.

The power of recorded oscillations (the amplitude of oscillatory activity within the 20-80 Hz frequency band; this frequency range was used throughout this thesis) in the early period following placement within the recording chamber would increase rapidly for a sustained period of time; slices

were left until this transitioned into a more gradual increase in power before recordings were initiated (typically within 30-45 minutes following initial placement). However, oscillation power would continue to increase for an extended period of time (multiple hours) without plateauing; therefore, recordings and drug application experiments were performed before a plateau was reached.

Once this point was reached, field oscillations were recorded for approximately 5 minutes, then experimental drugs (dissolved in dH_2O) were introduced into perfusing solution (at a drug solution:aCSF volume ratio of at least 1:1000, i.e. 10 µl of drug solution in 10 ml of perfusing solution) and washed into the slice. Throughout the study, the following drugs and concentrations were used: philanthotoxin-433 (PhTx-433; Sigma Aldrich), 10 µM; philanthotoxin-74 (PhTx-74; Tocris), 500 nM, 1 µM, 2 µM, and 10 µM; 1-napthylacetylspermine (NASPM; Tocris), 10 µM, 20 µM, 50 µM, and 100 µM; as well as control recordings during which equivalent volumes of dH_2O were applied. Slices were recorded for 15 minutes; recordings in which oscillations disappeared or collapsed dramatically before this time point were discarded during quantification and analysis. At the end of recordings, slices were removed from the recording chamber and discarded, whilst the chamber was washed with dH_2O and then aCSF plus carbachol before further slices were inserted.

Data were acquired and amplified (x10) by Axoclamp 2A (Molecular Devices), and further amplified (x100) and low-pass filtered (1 kHz; LPBF-48DG, NPI Electronic). Signals were digitised at 5k samples/second by an ITC-16 acquisition board (InstruTECH) and recorded by Igor Pro software (Wavemetrics).

2.2.2.3 Single-cell voltage-clamp recordings

For single-cell voltage clamp recordings, after incubation in the interface chamber for a minimum of 1 hour, PV-Cre/Ai9 double heterozygous slices were transferred to a submerged chamber maintained at ~31 °C mounted on an upright microscope (Olympus BX51W1) and superfused with aCSF (plus 25 µM bicuculline to block GABA receptors). Whole-cell patch-clamp recordings were made using recording electrodes (borosilicate, 4-7 MΩ) filled with a caesium methanesulfonate-based internal solution containing (in mM): 140 $CsCH_3SO_3$, 5 NaCl, 10 HEPES, 2 EGTA, 2 Mg-ATP, 2 Na-GTP, 5 QX-314, 0.1 spermine, 10 biocytin.

Due to the relatively greater yield of cells, recordings were made from neurons in CA1 rather than CA3. Despite the different location, the relative AMPA receptor profiles of PV+ cells and pyramidal cells within CA1 were suitable for investigating relative inhibition of CP-AMPARs and GluR2-containing AMPA receptors (He et al., 1998; Nissen et al., 2010; Sans et al., 2003). Recordings were taken from PV+ interneurons (in strata pyramidale or oriens) to measure CP-AMPAR currents, and from pyramidal cells (in stratum pyramidale) to record GluR2-containing AMPA receptor currents. Cells were patched in whole-cell mode and recording were made in voltage-clamp, with cells clamped at -70 mV to maintain voltage-dependent block of NMDA receptors whilst enabling activation of AMPA receptors.

A stimulation electrode was used to stimulate excitatory afferents synapsing onto target neurons; the electrode was placed in stratum radiatum to stimulate Schaffer collateral projections onto, and evoke EPSCs in, pyramidal cells, and into stratum oriens to stimulate projections onto PV+ cells; previous studies in the field had successfully reduced the amplitude of AMPA currents in CA1 PV+

interneurons generated from electrical stimulation of stratum oriens using PhTx-433 (Nissen et al., 2010). Throughout recording, stimuli were delivered at a rate of 1 per 15 seconds. After a typical set of two recording sessions of 20 stimuli to establish a consistent baseline EPSC response, a long-duration recording was initiated, with stimuli delivered once every 15 seconds throughout. Once a stable baseline had been recorded, either drug solution (10 µM PhTx-74, 100 µM NASPM) or, for control recordings, an equivalent volume of dH_2O, was introduced into the superfusing solution and washed into the submerged chamber. During the subsequent recording period, holding current and series resistance were monitored alongside EPSC amplitude. Series resistance and whole-cell capacitance were estimated and compensated to 60-70%, with a 7-µs lag. Series resistance compensation was manually altered, and recordings were terminated if the series resistance varied by >15% of the initial series resistanced, as well as if there were substantial shifts in the holding current. Additionally, recordings were terminated if series resistance went higher than 30 MΩ. No correction was made for liquid junction potentials. All recordings included in the results ran for a minimum of 15 minutes after the introduction of drug.

Delivery of stimuli was controlled by, and changes in EPSC size over time were recorded by IGOR Pro. Signals were acquired using a Multiclamp amplifier (Axon Instruments) and ITC-18 interface (Instrutech).

Following the end of recordings, cells were resealed through the slow movement of the patching electrode away from the cell. Slices were then retrieved from the patching rig and stored in 4% paraformaldehyde (PFA) in 0.1 M phosphate buffer for future histological analysis. The rig was washed thoroughly with aCSF to eliminate any drug solution before a new slice was added. Slices were always replaced after any exposure to drug solution.

2.2.3 Histology

During voltage-clamp recordings, neurons were filled with biocytin within the internal solution. Following recordings, slices were kept in 4% PFA for a minimum of 24 hours for preservation. Post-recording histology was performed to confirm the identity of recorded cells as interneurons or pyramidal cells. Slices were washed twice in PBS, and bathed in PBS 0.4% Triton-X100 for 2-3 hours. Following this, they were bathed in PBS 0.4% Triton-X100 plus Fluorescein Avidin D or Amca Avidin D (Vector, both 1:1000) and DAPI, and incubated overnight at 4 °C. The following day, the slices were washed several times with PBS, and then mounted using Fluoroshield mounting medium (Sigma Aldrich).

Sections were imaged using a Leitz DRMD Fluorescence Microscope (Leica), and either a DXM1200 digital camera (Nikon) or a Retiga 2000R CCD camera (QImaging). Images of fluorescence were taken using Ocular software.

2.2.4 Analysis and statistics

All statistical tests were performed using SPSS. Within- and between-subjects data was analysed using ANOVAs, with Dunnett's two-tailed t-tests used for *post hoc* analysis. In conditions where assumption of sphericity was violated, the Huynh-Feldt (H-F) or Greenhouse-Geiser (G-G) corrections were used to adjust the reported degrees of freedom in order to reduce Type I error (when $\varepsilon > 0.75$, Huynh-Feldt was used, and when $\varepsilon < 0.75$, Greenhouse-Geiser was used). Throughout this thesis, the

two-tailed significance value for all tests was set at 0.05 unless specified otherwise, meaning that a probability of 1 in 20 or greater was set to define a result as statistically significant.

Significance indicators used in figures in this chapter represent, unless otherwise stated: * = $p < 0.05$, ** = $p < 0.01$, *** = $p < 0.001$, n.s. = $p \geq 0.05$. For statistical comparisons, when mean values for two groups are provided (i.e. X ± a vs Y ± b), unless stated otherwise, the first value (i.e. the X value) represents the control group, and the second value (i.e. the Y value) represents the specified experimental group. Error bars on all figures represent the standard error of the mean.

Field activity data was analysed using IGOR Pro. In order to characterise and analyse gamma oscillations, power spectra were calculated as the normalised magnitude square of the FFT. The purpose of the normalisation was to ensure that the signal of A*cos(2*pi*f*t) resulted in a value of A^2 in the bin associated with frequency f. The power spectra were filtered with an 11-point median filter, and power area (the area below the power spectrum plot) was determined for the 20-80 Hz band range. Power area data were calculated in V^2 and normalised for comparison via conversion to $\log_{10}$ values. The peak frequency of oscillations was acquired by measuring the frequency at which the peak of the power spectrum occurred in the gamma-band range. Power area and peak frequency values were generated for each 5-second recording sweep, and averaged across 5 consecutive sweeps for each minute following introduction of drug/control treatment.

One-way repeated-measures ANOVAs were used to determine significant effects of time on log power area and frequency for control recordings. To compare changes in gamma oscillation power and frequency following drug treatment in relation to control treatment, the 'baseline' (value at the point of drug/control introduction) peak frequency and $\log_{10}$(power area) values were subtracted

from the values at 10 minutes. Subtracting one log value from another generated a log value of the second value divided by the first, as so:

$$\log_{10}(10\ \text{minutes}) - \log_{10}(0\ \text{minutes}) = \log_{10}(\frac{10\ \text{minutes}}{0\ \text{minutes}})$$

Therefore, the calculated values represented the logarithmic of the relative power area at 10 minutes compared to at 0, normalising changes in power across the different groups. One-way ANOVAs were used to observe the effects of treatment on change over time. Dunnett's two-tailed t-tests were used to compare changes in power and frequency across the first 10 minutes following treatment in drug groups compared to controls.

Analysis of EPSCs recorded in voltage-clamp was done based upon the peak amplitude of EPSCs. Evoked EPSC amplitudes were normalised to the baseline period (the 3 minutes prior to first addition of drug/control treatment to the superfusing solution), and averaged across each minute of recording. These mean amplitudes were averaged across recordings for each cell type and drug/control condition by aligning recordings to time point 0. For analysis purposes, the percentage change in response size at 15 minutes compared to baseline was used to judge the effects of different conditions. A two-way ANOVA was used to assess significant effects of drug treatment, cell type, and interactions between the two variables, with *post hoc* Dunnett's two-tailed t-tests used to assess the nature of any interactions.

Properties of spontaneous EPSCs recorded in voltage-clamp were analysed, including mean amplitude, median amplitude, median area, and median inter-event interval (IEI) of currents

recorded in each cell. EPSCs with a minimum amplitude of 5 pA deviation from the baseline holding current were detected on each recording sweep in a 2-second window 300 ms after delivery of the stimulus. Mean and median sEPSC values were calculated for events recorded in each cell for the 3-minute pre-treatment baseline period, and the final 3 minutes of each recording (i.e. 12-15 minutes post-application). Changes in these variables 15 minutes following treatment with drug or control were calculated as a percentage of the baseline value, and significant changes in mean percentage values between each treatment group were detected by performing one-way between-subjects ANOVAs with treatment group as the independent variable. The nature of any significant changes were further investigated using post-hoc Dunnett's two-tailed t-tests.

2.3 Results

2.3.1 Temporal evolution of carbachol-evoked gamma oscillations during recordings

Horizontal brain sections containing ventral hippocampus were extracted from adult wild-type mice, and placed in an interface field recording chamber, in which they were exposed to carbachol. The placement of a recording electrode into area CA3 enabled detection of carbachol-evoked gamma oscillations (Fig. 2.1A). During the first half-hour following placement within the recording chamber, oscillations slowly emerged, before increasing in regularity and amplitude. Oscillations were monitored until the rate of increase of gamma power decreased, typically taking 40-60 minutes following initial placement in the recording chamber. At this point, control recordings were taken that would be compared against subsequent drug recordings. These involved arranging the recording set-up in preparation for adding drug solution, but instead adding an equivalent volume of

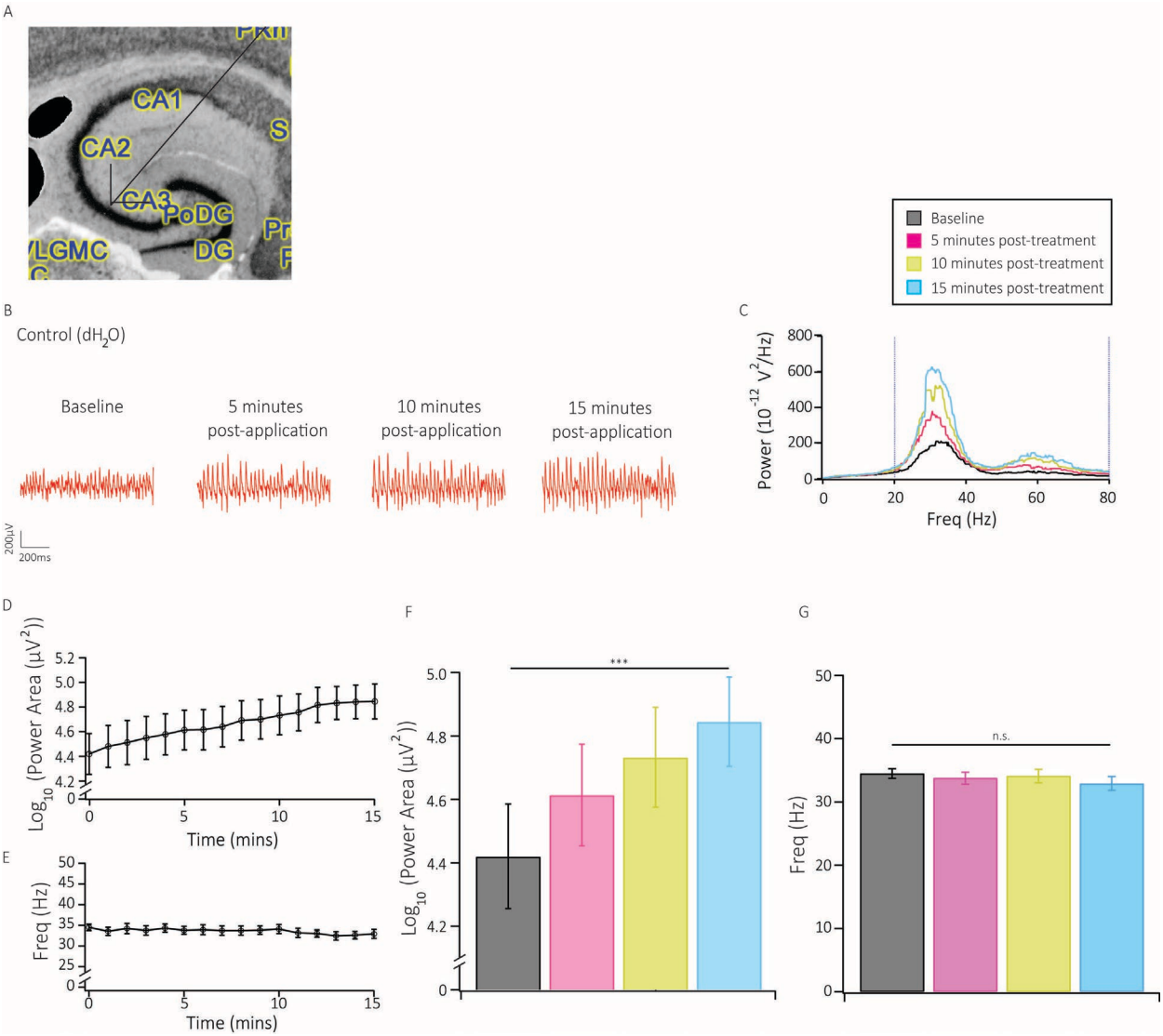

Figure 2.1. The temporal evolution of carbachol-evoked hippocampal gamma oscillations *in vitro*. (A) The set-up for field recordings from slices, with a recording electrode (1 MΩ) placed in area CA3 of ventral hippocampus (image taken from the C57BL/6J horizontal mouse brain atlas, Mouse Brain Library). (B) Sample 1-second oscillation traces from one slice, recorded at 0, 5, 10, and 15 minutes post-introduction of control dH_2O into the perfusing solution. (C) Power-frequency spectra generated by normalising Fast Fourier transform with 11-point median filtering at the time points and from the slice shown in (B). The dashed lines demonstrate the window in which power area is calculated for section D & F. (D) A minute-by-minute display of the changes in log(power area) during the 15 minutes post-introduction of control treatment, averaged across slices (n = 7 slices); each time point represents the average of 5 consecutive sweeps. (E) A minute-by-minute display of changes in peak frequency post-control introduction. (F) Carbachol-evoked gamma oscillations increased in power across the recording period. Comparison of mean $\log_{10}$(power area) values at 0, 5, 10, and 15 minutes reveals a strongly significant effect of time on oscillation power. Furthermore, the differences in power area from Baseline (4.42 $\log_{10}(mV^2)$) to 5 (4.61 $\log_{10}(mV^2)$), 10 (4.73 $\log_{10}(mV^2)$), and 15 minutes (4.85 $\log_{10}(mV^2)$) were significant. (G) The frequency of carbachol-evoked gamma oscillations does not substantially vary over time. There was no main effect of time on oscillation frequency, and the peak frequency of oscillations was not significantly different at baseline (34.49 Hz) compared to 15 minutes later (32.92 Hz). * = $p < 0.05$; ** = $p < 0.01$; *** = $p < 0.001$. n.s. = $p \geq 0.05$. Error bars indicate standard error of the mean.

dH_2O, the drug solvent used in this chapter. Following addition of this control treatment, oscillations were recorded for 15 minutes.

Throughout this 15-minute period, oscillations exhibited a consistent increase in power (Fig. 2.1B-F). Sample 1-second oscillation traces recorded from one slice at 0, 5, 10, and 15 minutes post-application of dH_2O demonstrate the substantial changes in power over time (Fig. 2.1B). Fast Fourier transforms were applied to 5-second recording sweeps; the power-frequency plots generated from this highlight the changes in oscillation properties over time (Fig. 2.1C).

Despite prolonged equilibration periods pre-treatment, recorded oscillations showed significant monotonic increases in power across the recording session following application of control treatment, as defined by the power area (Fig. 2.1D). Taking the values at 0, 5, 10, and 15 minutes post-application and performing a one-way repeated-measures ANOVA reveals a strongly significant effect of time on oscillation power (n = 7 slices; no assumption of sphericity ($\chi^2(7) = 14.162$, $p = 0.017$, G-G $\varepsilon = 0.419$); $F_{(1.258,7.55)} = 27.839$, $p < 0.001$; Fig. 2.1F). This effect was carried by the large increase in power area from the 'baseline' time point (4.42 ± 0.2 $\log_{10}(mV^2)$) to 15 minutes later (4.85 ± 0.1 $\log_{10}(mV^2)$). However, despite the strong changes in oscillation power, peak frequency (frequency showing peak power) was generally unchanged across the recording period (Fig. 2.1E). A one-way repeated-measures ANOVA across the same time points reveals no effect of time on oscillation frequency (no assumption of sphericity ($\chi^2(7) = 14.499$, $p = 0.015$, G-G $\varepsilon = 0.42$); $F_{(1.261,7.568)} = 0.882$, $p = 0.469$; Fig. 2.1G).

In summary, gamma oscillations generated in hippocampal slices *in vitro* using the cholinergic agonist carbachol display a continual trend towards increasing power across a prolonged period of time (>1 hour; the maximum period between first placement in field rig and cessation of recording during this DPhil study was approximately 1.5-2 hours), referred to elsewhere as 'temporal

evolution', in the absence of significant changes in oscillation frequency (Zarnadze, 2016). Similar findings have been observed using kainate, suggesting that the changes in activity within the network underpinning this evolution in power are separate from the effects of the oscillating-inducing pharmacological agent.

2.3.2 Exposure to different philanthotoxin derivatives and NASPM results in consistent decreases in gamma power with varied distinct effects upon oscillation frequency

Once establishing the dynamic properties of carbachol-evoked oscillations and their tendency to increase in power, I set out to investigate the effects of CP-AMPAR-blocking pharmacological agents on gamma oscillations *in vitro*. I first tested the effects of PhTx-433, with a 10 µM starting dose decided upon due to common use in previous studies (Nissen et al., 2010).

Exposure to PhTx-433 resulted in a visible decrease in the amplitude of oscillations (n = 5; Fig. 2.2). This reduction typically occurred within the first 10 minutes post-drug application, by which point the mean power area had dropped from 4.18 ± 0.3 $\log_{10}(mV^2)$ immediately pre-drug application, down to 3.92 ± 0.2 $\log_{10}(mV^2)$ (Fig. 2.2A-C). In contrast to the power, oscillation frequency stayed generally stable throughout recordings (38.42 ± 3.5 Hz at 0 minutes vs 41.21 ± 3 Hz at 10 minutes; Fig. 2.2D). These trends were consistent across all 5 recordings.

PhTx-433 reliably reduced the power of gamma oscillations; however, the price per quantity of the compound was prohibitive to long-term use. As a consequence, I looked for alternative, more cost-effective compounds. A range of philanthotoxin derivatives have been synthesised, each with

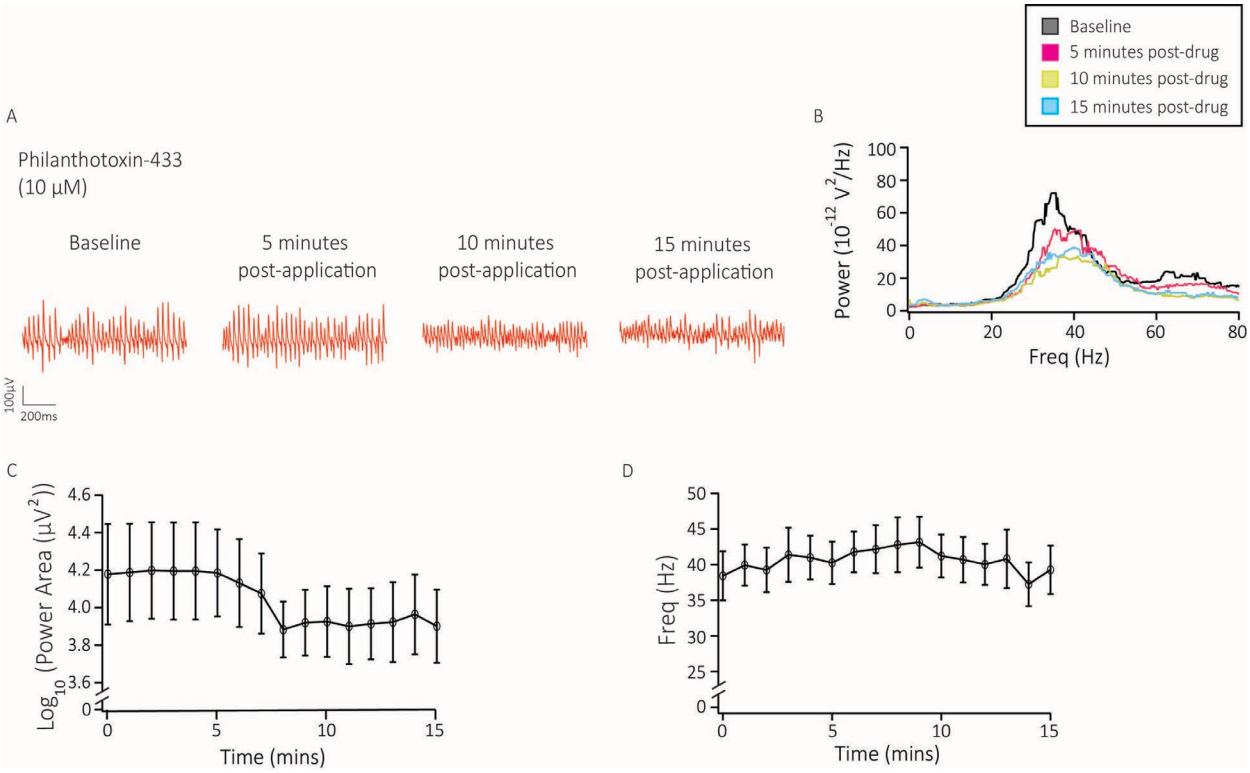

Figure 2.2. The effects of philanthotoxin-433 on carbachol-evoked hippocampal gamma oscillations *in vitro*. (A) Sample 1-second oscillation traces at 0, 5, 10, and 15 minutes post-introduction of 10 µM PhTx-433 into the perfusing solution. (B) Power-frequency spectra calculated for the same time points and from the slice shown in (A). (C) A minute-by-minute display of the changes in power during the 15 minutes post-introduction of PhTx-433 (n = 5 slices). (D) A minute-by-minute display of changes in frequency post-PhTx-433 introduction.

different affinities for CP-AMPARs against other glutamate receptors (Kromann et al., 2002). Amongst these, the only one readily available from suppliers was PhTx-74, which was far more affordable for long-term use than PhTx-433. This compound has a similar affinity ratio for CP-AMPARs compared to GluR2-containing AMPA receptors based upon IC_{50} data from previous pharmacological studies, with roughly 100-fold greater affinity for CP-AMPARs than for other AMPA receptors. Over 20 years ago, PhTx-433 was reported to have an IC_{50}(CP-AMPARs) of 2.8 µM, and an IC_{50}(other AMPA receptors) of 270 µM, whilst a recent study reported for PhTx-74 an IC_{50}(CP-AMPARs) of 0.25 µM, and an IC_{50}(other AMPA receptors) of 20 µM (Brackley et al., 1993; Poulsen et al., 2014). The 10 µM concentration used for PhTx-433 is approaching the IC_{50} for GluR2-containing AMPA receptors; therefore, I reduced the starting concentration for PhTx-74 to something closer to its IC_{50}(CP-AMPARs).

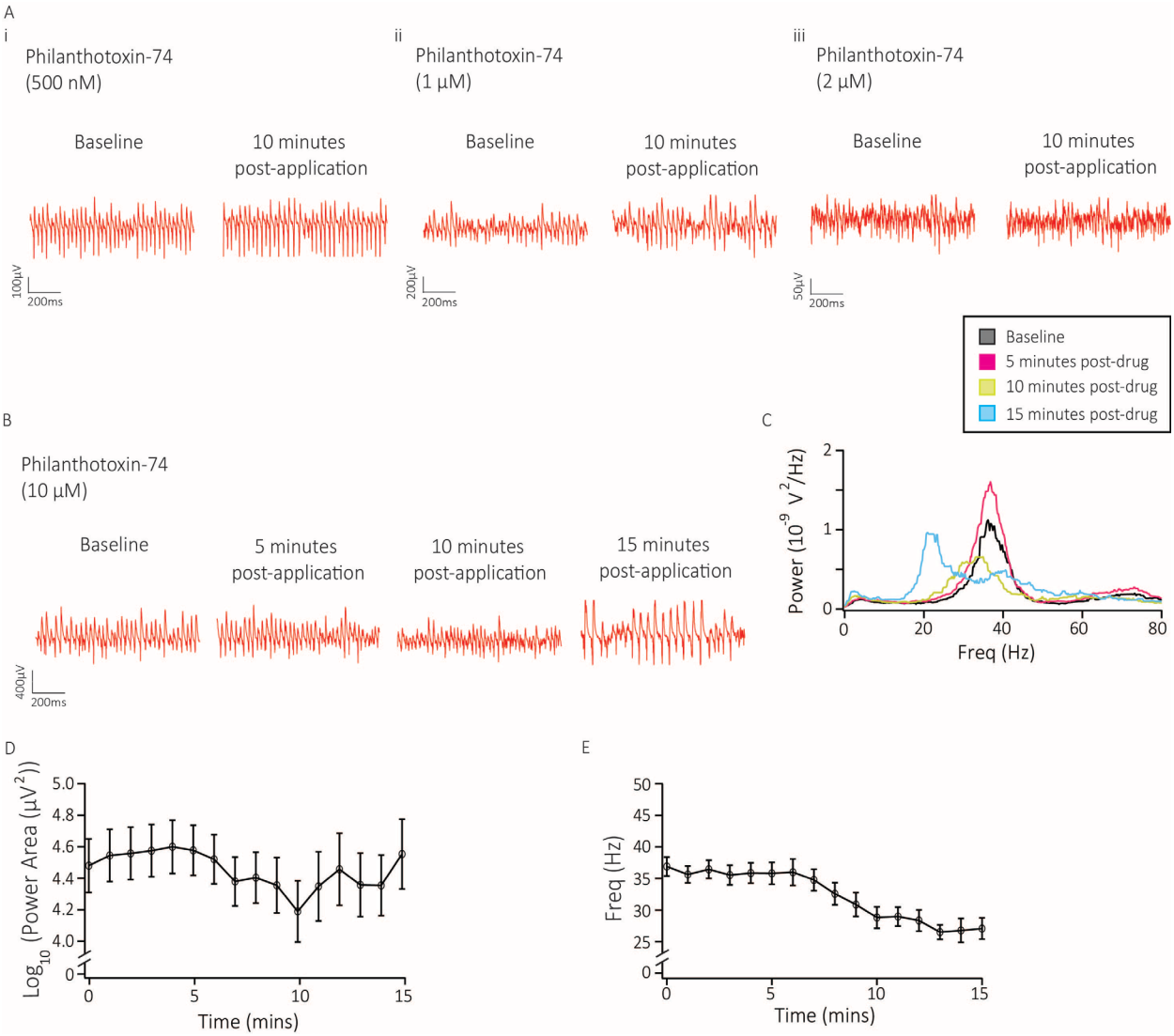

Figure 2.3. The effects of philanthotoxin-74 on carbachol-evoked hippocampal gamma oscillations *in vitro*. (A) Exposure to 0.5, 1, or 2 µM concentrations of PhTx-74 had no detectable effect upon gamma oscillations. (B) Sample 1-second oscillation traces recorded at 0, 5, 10, and 15 minutes post-introduction of 10 µM PhTx-74 into the perfusing solution. (C) Power-frequency spectra calculated for the time points and from the slice shown in (B). (D) Application of PhTx-74 first decreases, then increases the power of hippocampal oscillations (n = 11 slices). (E) PhTx-74 application reduces oscillation frequency.

Exposure to 0.5, 1, or 2 µM concentrations of PhTx-74 failed to reliably induce any detectable changes in carbachol-evoked hippocampal gamma oscillatory activity (Fig. 2.3A). As a result, I decided to shift to the same concentration used for PhTx-433. 10 µM PhTx-74 exposure resulted in reliable changes in gamma activity in a distinctive sequence (n = 11 slices; Fig. 2.3B-E). PhTx-74 application resulted in an initial reduction in the oscillation amplitude within 10 minutes, followed by the emergence of large-amplitude, lower-frequency oscillations by 15 minutes, which were typically erratic and unstable (Fig. 2.3B). The shift towards beta-frequency oscillations correlated with the

initial reduction in oscillation power (Fig. 2.3D, E). Out of 11 slices treated with 10 µM PhTx-74, 9 exhibited a reduction in gamma power within 10 minutes compared to baseline (overall mean: 4.48 ± 0.2 $\log_{10}(mV^2)$ at baseline vs 4.19 ± 0.2 $\log_{10}(mV^2)$ at 10 minutes), and 7 exhibited a revival in oscillation power by 15 minutes to above-baseline levels (4.56 ± 0.2 $\log_{10}(mV^2)$ at 15 minutes for population); all 11 exhibited decreases in frequency within 10 minutes (36.9 ± 1.4 Hz immediately pre-treatment vs 28.81 ± 1.7 Hz at 10 minutes).

Inactive at lower doses, when applied at the same concentration as PhTx-433, its derivative PhTx-74 has a more substantial effect upon hippocampal network activity *in vitro*, reducing the frequency of carbachol-evoked oscillations recorded in area CA3, alongside its effects on oscillation power.

Given the previously reported IC_{50}s for PhTx-74's interactions with different classes of AMPA receptors, I hypothesised that the more transformative effects of the drug could be a consequence of interactions with receptors other than CP-AMPARs. In an attempt to more closely investigate the consequences of CP-AMPAR block with an affordable compound, I turned to NASPM, a drug with a high affinity for CP-AMPARs (reported IC_{50} of 0.33µM) that is reported in the literature to be extremely selective, as substitution of the glutamine residue determining Ca^{2+} passage through AMPARs abolishes binding to GluR1 homomers (Blaschke et al., 1993; Koike et al., 2000). Several different concentrations ranging from 10 µM to upwards of 100 µM have been previously used for *in vitro* experiments in the literature, so a starting dose of 10 µM was used, and the concentration increased consistent effects on oscillation activity were observed.

There were no notable effects on carbachol-evoked gamma oscillations observed when slices were exposed to 10, 20, or 50 µM doses of NASPM (Fig. 2.4A); however, when 100 µM NASPM was

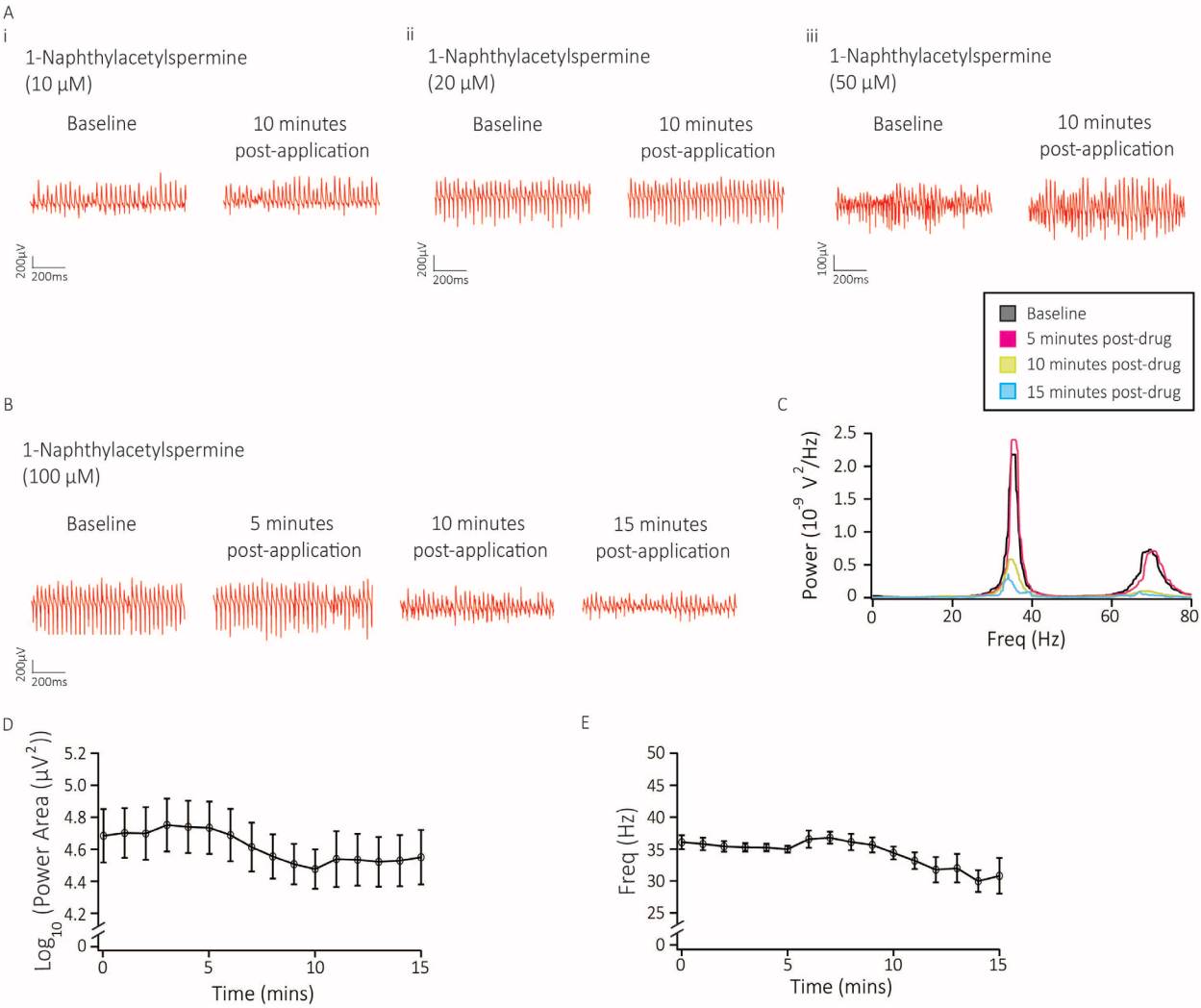

Figure 2.4. The effects of NASPM on carbachol-evoked hippocampal gamma oscillations *in vitro*. (A) Exposure to 10, 20, or 50 µM concentrations of NASPM had no noticeable effect upon gamma oscillations. (B) Sample 1-second oscillation traces recorded at 0, 5, 10, and 15 minutes post-introduction of 100 µM NASPM into the perfusing solution. (C) Power-frequency spectra calculated for the time points and from the same slice as in (B). (D) A minute-by-minute display of the changes in power during the 15 minutes post-introduction of NASPM (n = 6 slices). (E) A minute-by-minute display of changes in frequency post-NASPM introduction.

introduced into the perfusing solution, recordings showed either a decrease in oscillation power or a complete collapse of oscillatory activity within 10 minutes (Fig. 2.4B-D). Oscillations collapsed in 3 slices, which were discarded from analysis. With data from the remaining 6 slices, a baseline mean power area of 4.68 ± 0.2 $\log_{10}(\mu V^2)$ was observed, which fell to 4.47 ± 0.1 $\log_{10}(\mu V^2)$ by 10 minutes (Fig. 2.4D). In contrast, peak frequency remained broadly stable within the first 10 minutes (36.08 ± 1.1 Hz immediately pre-drug application vs 34.4 ± 1 Hz at 10 minutes; Fig. 2.4E). By eliciting a reduction in gamma power whilst not substantially altering oscillation frequency, the effects of NASPM were closer to PhTx-433.

A side-by-side comparison of effects of each of the three drugs on oscillation power and frequency further highlights the dissociation between the effects of PhTx-433/NASPM and PhTx-74 with respect to control conditions (Fig. 2.5). For analysis purposes, relative differences in power between 0 and 10 minutes were calculated for the different treatment groups by subtracting the $\log_{10}$(power area) value at 0 minutes from the value at 10 minutes, effectively calculating $\log_{10}$(power area (10 minutes)/power area (0 minutes)). A one-way ANOVA comparing this average subtracted $\log_{10}$ value for each of the treatment groups revealed a significant effect of drug condition on change in oscillation power ($F_{(3,25)} = 4.219$, $p = 0.015$; Fig. 2.5A, B). To further explore the basis of this effect, Dunnett's two-tailed t-tests were performed to compare the change in power 10 minutes following treatment with each of the drugs with respect to control. Compared to the increase in oscillation power 10 minutes after baseline seen for control recordings (+0.31 ± 0.04 $\log_{10}(\mu V^2)$), there was a significant drop in power within 10 minutes following PhTx-433 application (-0.25 ± 0.11 $\log_{10}(\mu V^2)$; $t(10) = 2.586$, $p = 0.042$) and NASPM application (-0.21 ± 0.13 $\log_{10}(\mu V^2)$; $t(11) = 2.508$, $p = 0.049$), and a strongly significant drop in power following PhTx-74 application (-0.29 ± 0.16 $\log_{10}(\mu V^2)$; $t(16) = 3.341$, $p = 0.007$).

To investigate frequency, much like for power, peak frequency values at baseline were subtracted from those at 10 minutes. A one-way ANOVA for treatment revealed a significant effect of drug treatment on frequency ($F_{(3,25)} = 14.182$, $p < 0.001$; Fig. 2.5C, D). As before, Dunnett's two-tailed t-tests were performed to judge the significance of changes in frequency 10 minutes following drug exposure compared to controls. A very mild decrease in frequency was observed after 10 minutes for control recordings (-0.4 ± 0.6 Hz); compared to control conditions, the decrease following PhTx-74 was strongly significant (-8.09 ± 1.3 Hz; $t(16) = 4.603$, $p < 0.001$; Fig. 2.5D). The differences in

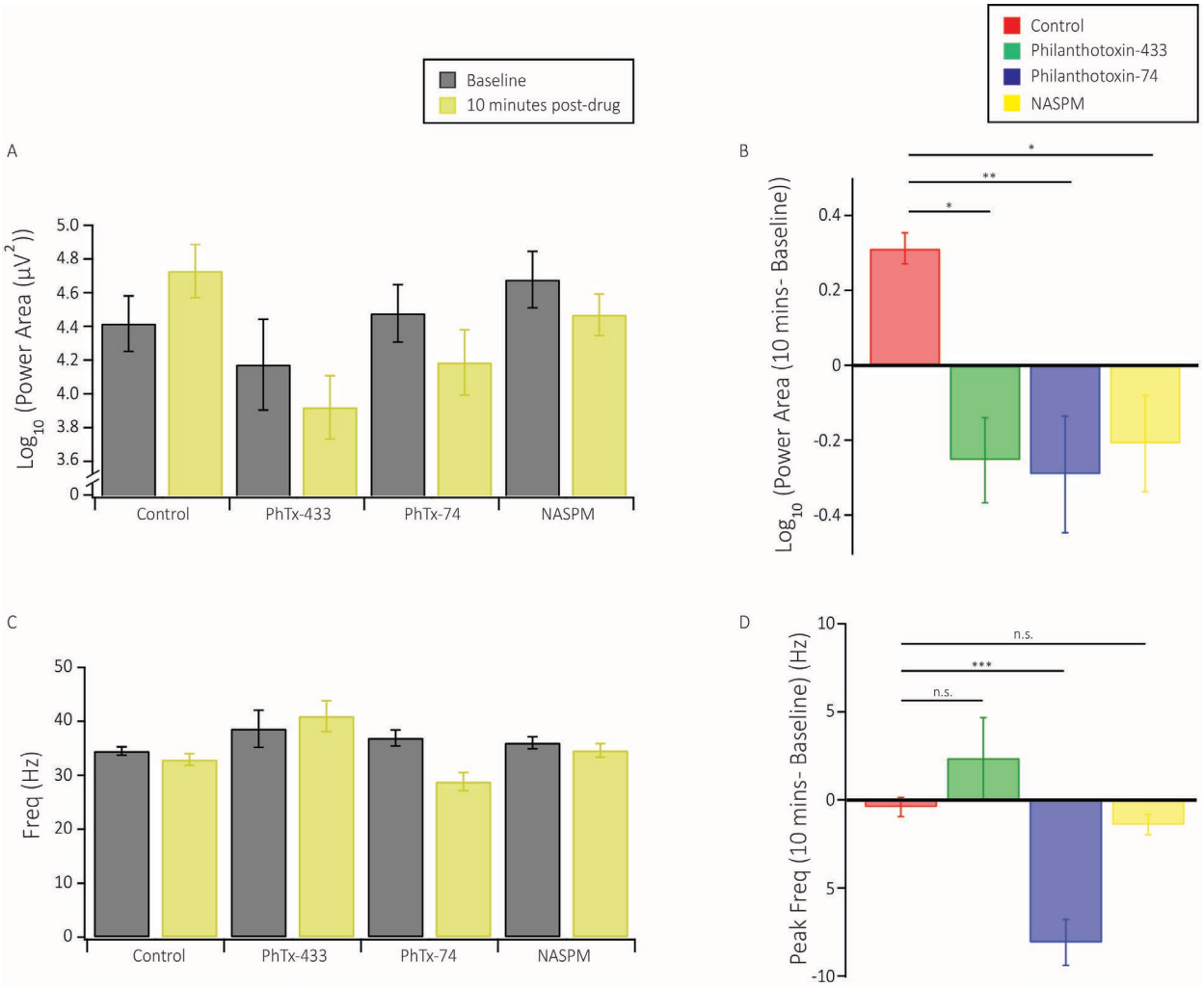

Figure 2.5. Effects of different CP-AMPAR-blocking drugs on carbachol-evoked oscillation power and frequency *in vitro*. (A) Mean log_{10}(power area) values at 0 and 10 minutes post-treatment introduction for control recordings and each of the CP-AMPAR-blocking drugs used in the study. (B) CP-AMPAR blockade reduces the power of gamma oscillations. Log_{10} differences between baseline and 10 minutes later; whilst control recordings demonstrated a large increase in power during this time window (0.31, n = 7 slices), PhTx-433 (-0.25, n = 5) PhTx-74 (-0.29, n = 11), and NASPM (-0.21, n = 6) application resulted in a significant reduction in oscillation power in comparison. (C) Mean peak frequency values at 0 and 10 minutes post-treatment introduction for control recordings and CP-AMPAR-blocking drugs. (D) PhTx-74 caused a reduction in oscillation frequency not present following application of other CP-AMPAR-blocking drugs. Differences in peak frequency at 10 minutes compared to baseline reveal a small decrease in frequency during this time window for control recordings (-0.4 Hz), but a strongly significant reduction following PhTx-74 application in comparison (-8.1 Hz); treatment with PhTx-433 (+2.37 Hz) or NASPM (-1.4 Hz) did not significantly alter oscillation frequency within this time window.

frequency following PhTx-433 (+2.37 ± 2.3 Hz) and NASPM (-1.4 ± 0.6 Hz) application were not significant ($p = 0.292$ and $p = 0.846$, respectively).

Overall, the data from these three different drugs indicate that blockade of CP-AMPARs in the hippocampus results in a reduction in the power of carbachol-evoked gamma oscillations.

Furthermore, one CP-AMPAR antagonist (PhTx-74) affected the frequency of oscillations; this change in frequency, along with the rebound increase in gamma power, could be a consequence of off-target effects beyond CP-AMPAR antagonism.

2.3.3 CP-AMPAR selectivity of NASPM and non-specific antagonism of AMPA receptors on pyramidal and PV+ cells by philanthotoxin-74

The above data reveal a separation in the effects of PhTx-433 and NASPM compared to PhTx-74 on hippocampal gamma oscillations. This could be explained by differing levels of blockade of CP-AMPARs compared to other AMPARs; whilst PhTx-433 is reported to be highly selective for CP-AMPARs at the dose used in the present study, and NASPM is reported to have minimal interaction with GluR2-containing AMPARs, the concentration at which PhTx-74 had its effects in this study is close to its IC_{50} for GluR2-containing AMPARs, as reported in a study using HEK cells (Blaschke et al., 1993; Brackley et al., 1993; Poulsen et al., 2014). As such, there is the possibility that PhTx-74 is imposing its effects on oscillation frequency via off-target effects on GluR2-containing AMPARs on cell types other than PV+ interneurons, such as pyramidal cells. Therefore, I investigated the relative selectivity of PhTx-74 and NASPM for CP-AMPARs and GluR2-containing AMPA receptors.

The selectivity of NASPM has previously been established through whole-cell patch-clamp experiments. Stimulating AMPAR currents onto 'type I' and 'type II' rat hippocampal cells demonstrated strong inhibition of AMPAR currents on 'type II' cells with minimal inhibition on 'type I' cells (Koike et al., 1997). The properties of these 'type I' and 'type II' cells have since been identified to reflect pyramidal cells and PV+ interneurons, respectively, and similarly selective effects on AMPAR currents in each of these cell types have been observed following application of PhTx-433

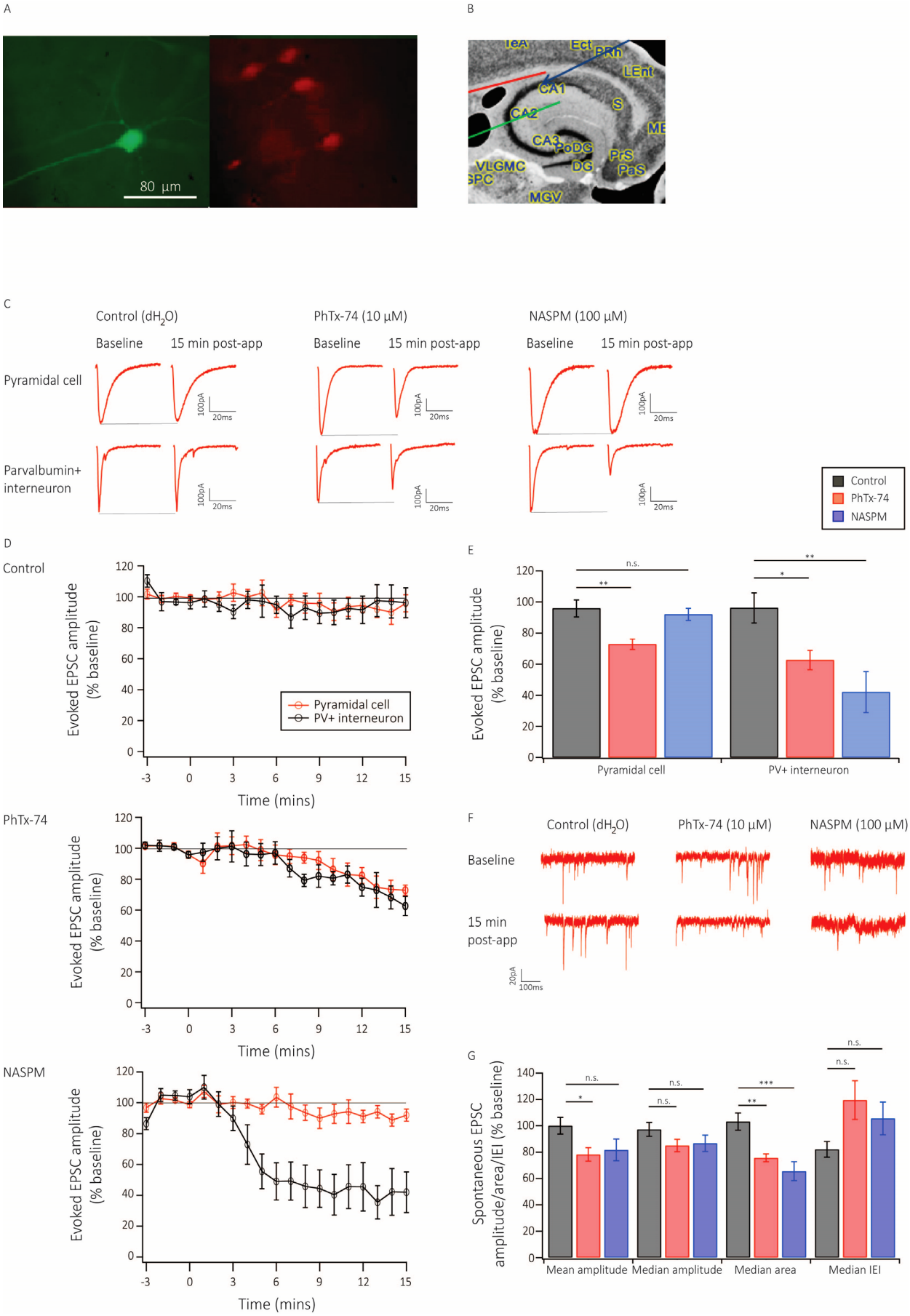

(Nissen et al., 2010). Therefore, to investigate the AMPAR selectivity of the drugs used in this study,

Figure 2.6 (previous page). CP-AMPAR-blocking drugs with distinct effects on *in vitro* gamma oscillations differentially alter evoked and spontaneous EPSCs in PV+ and pyramidal neurons. (A) Mice expressing Cre recombinase in PV+ cells were crossed with mice carrying a gene for Cre-dependent expression of tdTomato, resulting in mice expressing fluorescent tdTomato in PV+ cells. A recorded CA1 PV+ interneuron (labelled with Fluorescein Avidin D; top) exhibits co-expression of tdTomato (bottom). (B) Recorded pyramidal and PV+ cells in stratum pyramidale/oriens (blue) were held at -70mV and AMPAR currents were evoked by electrical stimulation of afferents in stratum radiatum onto pyramidal cells (green), or of afferents in stratum oriens projecting onto PV+ cells (red; image taken from the C57BL/6J horizontal mouse brain atlas, Mouse Brain Library). (C) Example evoked EPSCs in pyramidal and PV+ cells immediately before and 15 minutes after exposure to control conditions, or either 10 µM PhTx-74 or 100 µM NASPM. (D) Minute-by-minute displays of changes in EPSC amplitude with respect to baseline (calculated over the three-minute window directly preceding drug/control application) for each cell type following treatment with each condition. (E)% changes in amplitude with respect to baseline 15 minutes following application of control treatment, PhTx-74, or NASPM. In pyramidal cells, control-treated cells showed minimal reduction in AMPAR-mediated currents (95.8% of baseline amplitude); as did cells exposed to NASPM (92%). However, pyramidal cells treated with PhTx-74 showed on average a 27.2% reduction in evoked current amplitude within 15 minutes post-application of the drug. In contrast, whilst control-treated PV+ cells showed little change in response amplitude (96.2%), treatment with either PhTx-74 or NASPM resulted in a significant reduction in evoked amplitude within 15 minutes (62.6% and 42.1% respectively). (F) Example traces of spontaneous EPSCs recorded from PV+ interneurons immediately before and 15 minutes following application of control or drug treatment. (G)% changes in the mean amplitude, median amplitude, median area, and median inter-event interval (IEI) of spontaneous EPSCs in PV+ cells 15 minutes following exposure to control, PhTx-74, or NASPM treatment. Amplitude and area of EPSCs in control cells did not notably vary over the 15-minute period (100%, 97.2%, and 103.2% of baseline mean and median amplitude and area, respectively), whilst the IEI decreased (82.1%). In comparison, PhTx-74 exposure resulted in significant reductions in mean amplitude and area 15 minutes post-application (78.2% and 75.7%, respectively), but without significant changes in median amplitude and IEI (85% and 119.4%). NASPM treatment resulted in a significant reduction in area compared to controls (65.5%), but no significant changes in amplitude (81.7%/86.7% for mean/median) and IEI (105.6%).

mice were bred to be heterozygous for both PV-Cre and Ai9, resulting in PV+ interneurons expressing tdTomato that were easily identifiable for patch-clamp recordings (Fig. 2.6A). A stimulating electrode was placed in either stratum radiatum to stimulate Schaffer collaterals projecting onto CA1 pyramidal cells or stratum oriens to stimulate local collaterals projecting onto PV+ cells (Fig. 2.6B). After entering whole-cell patch-clamp mode with either pyramidal cells or PV+ interneurons in CA1, cells were held at -70mV and inputs were stimulated to evoke AMPA receptor-mediated currents in the patched cells. Once a stable baseline was achieved, either 10 µM PhTx-74, 100 µM NASPM, or an equivalent volume of dH_2O as a control were added to the superfusing solution, and changes in AMPAR current amplitude were observed over the subsequent 15 minutes, with response amplitude normalised to the mean baseline amplitude and binned for each minute.

NASPM and PhTx-74 affected evoked AMPAR currents in a cell type-specific manner; whilst PhTx-74 decreased the amplitude of AMPAR currents recorded from both pyramidal cells and PV+ interneurons compared to control conditions, NASPM only reduced current amplitude in PV+ interneurons, having no significant effect on currents recorded from pyramidal cells (Fig. 2.6C-E). Recordings from 40 cells were included in the study, 18 from pyramidal cells (n = 6 for control, PhTx-74-treated and NASPM-treated) and 22 from PV+ interneurons (n = 8 for controls and PhTx-74-treated, n = 6 for NASPM-treated). A 2 (cell type) * 3 (treatment) two-way ANOVA analysing the change in response size at 15 minutes as a % of baseline revealed significant main effects of cell type ($F_{(1,34)} = 9.254$, $p = 0.005$) and treatment ($F_{(2,34)} = 8.694$, $p = 0.001$), as well as a significant interaction between the two factors ($F_{(2,34)} = 5.24$, $p = 0.01$). Investigating the dissociation between the drug effects on pyramidal and PV+ cell AMPAR currents, Dunnett's two-tailed t-tests were used to compare the change in response amplitude following application of each drug with respect to control conditions. In pyramidal cells, application of PhTx-74 caused a significant reduction in response size within 15 minutes compared to control conditions (95.8 ± 5.5% vs 72.8 ± 3.3%; $p = 0.002$); however, there was no significant difference between NASPM application and control conditions (95.8 ± 5.5% vs 92 ± 3.9%; $p = 0.404$). In contrast, in PV+ interneurons, compared to control conditions (96.2 ± 9.7%), there was a significant reduction in evoked AMPAR current amplitudes following application of either PhTx-74 (62.6 ± 6.2%; $p = 0.032$) or NASPM (42.1 ± 13.2%; $p = 0.002$).

In addition to evoked responses, the effects of exposure to CP-AMPAR-blocking compounds on spontaneous EPSCs in recorded PV+ cells were also investigated. Mean and median values for EPSC amplitude, area, and frequency (as represented by inter-event interval, or IEI) were generated for each cell for events recorded the 3-minute baseline period, and the corresponding period 15 minutes later, following drug/control treatment conditions (Fig. 2.6F). Effects of each treatment on

these properties were determined by calculating the relative change for each variable with respect to the baseline value, and taking the mean across the recorded cell populations.

To analyse the significance of any changes in these properties, one-way ANOVAs assessing percentage change after 15 minutes for each of the four variables were performed for the three treatment groups. A one-way ANOVA revealed a significant effect of treatment group on relative change in mean amplitude of spontaneous EPSCs in PV+ cells ($F_{(2,19)} = 3.558$, $p = 0.049$), which Dunnett's two-tailed t-tests revealed resulted from a significant reduction in amplitude following PhTx-74 treatment compared to control conditions (100 ± 6.3% vs 78.2 ± 5.1%; $t(14) = 2.514$, $p = 0.039$); the decrease following NASPM treatment was not significant (100 ± 6.3% vs 81.7 ± 8.2%; $t(12) = 1.955$, $p = 0.117$), although it was numerically similar to the significant drop following PhTx-74 exposure.. In contrast, there was no effect of treatment group on changes in median amplitude of spontaneous EPSCs ($F_{(2,19)} = 1.643$, $p = 0.22$). Whilst median amplitude of spontaneous EPSCs remained broadly stable in control cells (97.2 ± 5.2%), neither PhTx-74 nor NASPM caused a significant reduction in comparison (85 ± 4.6% and 86.7 ± 6.2%, respectively).

Changes in median area, an alternative variable to assess changes in EPSC size, showed a strongly significant effect of treatment group ($F_{(2,19)} = 11.928$, $p < 0.001$). Dunnett's two-tailed t-tests revealed that reductions in response area were strongly significant with respect to control cells following treatment with either PhTx-74 (103.2 ± 6.5% vs 75.7 ± 3%; $t(14) = 3.617$, $p = 0.004$) or NASPM (103.2 ± 6.5% vs 65.5 ± 7%; $t(12) = 4.584$, $p < 0.001$). Finally, median IEI was investigated as an indicator of effects of the compounds on the frequency of spontaneous EPSCs. A one-way ANOVA revealed a non-significant trend towards an effect of treatment group on changes in IEI over time ($F_{(2,19)} = 2.896$, $p = 0.08$), likely due to the relative changes in IEI following control or PhTx-74 treatment (82.1 ± 5.9% vs 119.4±14.7%), with IEI remaining broadly stable following NASPM treatment (105.6 ± 12.4%).

Overall, treatment with either PhTx-74 or NASPM reduced the size of spontaneous EPSCs in PV+ cells, whilst drug treatment resulted in a non-significant trend towards reduction of EPSC frequency. Similar analyses were attempted with the data from pyramidal cell recordings. There were no significant effects of either compound compared to control; however, the low frequency of spontaneous EPSCs meant there were insufficient samples to enable any robust conclusions to be drawn (data not shown).

2.4 Discussion

The results from this chapter reveal a dissociation in the effects of different AMPA receptor antagonists, that may be dependent upon their relative selectivity for AMPARs with distinct subunit composition. These findings produce a clearer picture of the specific contribution that currents carried by CP-AMPARs make to gamma rhythms in the hippocampus, and may provide a greater insight into the particular dynamics of network activity.

For the present study, I used an *in vitro* model of gamma oscillation activity that involves persistent exposure to carbachol, a cholinergic agonist (Mann et al., 2005b). I consistently observed that carbachol-evoked oscillations in area CA3 of ventral hippocampus would continually increase in power over prolonged periods of time in the absence of any additional compounds. These observations are similar to those seen in another model of *in vitro* hippocampal oscillogenesis involving application of the glutamatergic agonist kainate (Zarnadze, 2016). This reliable pattern of activity has been dubbed 'temporal evolution' of gamma oscillations, and has been hypothesised to result from the gradual yet continual recruitment of additional pyramidal and PV+ neurons into the oscillatory network over a prolonged period of persistent, robust gamma activity. The contribution

of excitatory plasticity, at least in pyramidal neurons, to this process is unclear, as neither NMDAR nor metabotropic glutamate receptor antagonists affected this process in the kainate model.

Following the application of any of the AMPAR antagonists used during this study, the power of gamma oscillations reliably decreased. This reduction in power happened on a similar timescale with all three compounds, occurring within the time window 5 to 10 minutes following initial introduction of each compound. For philanthotoxin-433 and NASPM, this decline typically bottomed out by 10 minutes, with a mean decline of 45% and 41%, respectively. This is comparable to (if less pronounced than) the reduction in gamma power observed following a PV-specific knockout of the GluR1 subunit and a full-brain knockout of GluR4, and contrasts to the complete abolition of activity following *in vitro* application of the non-selective AMPAR antagonist NBQX (Caputi et al., 2012; Cunningham et al., 2003; Fuchs et al., 2007). Whilst it cannot be said for certain that the effects of NASPM and PhTx-433 are entirely or primarily due to antagonism of CP-AMPARs specifically on PV+ interneurons, when placed in the context of prior genetic experiments and established knowledge of the cellular mechanisms of hippocampal gamma oscillations, these results further point towards the important role of CP-AMPAR-mediated excitation and recruitment of PV+ interneurons in maintaining high-power gamma-frequency oscillations in the hippocampus. The lesser reduction in power may be a consequence of reduced coverage of the PV+ interneuron population with a pharmacological approach compared to a genetic knockout. Conversely, it may be a consequence of activity-dependent unblock of receptors; particularly in the case of NASPM, where power begins to recover to some degree after 10 minutes, the reversible nature of blockade combined with continued pyramidal cell activity may prevent a full, sustained blockade of receptors on interneurons (Rozov and Burnashev, 1999).

It should also be noted that the effects of NASPM were only reliably observed with a large concentration of NASPM. I did not observe drug effects with application of 10, 20, or 50 µM NASPM. However, NASPM has been reported to have an IC_{50} substantially lower than 100 µM; indeed, Koike et al. observed reductions in AMPAR-mediated currents in type II cells (see Fig. 1.4) following NASPM treatment with an IC_{50} of 0.33 µM. Therefore, it is possible that there is a substantial degree of redundancy built into the network, such that large proportion of receptors or CP-AMPAR-expressing neurons need to be affected in order to sufficiently alter activity within the network at large.

Treatment of oscillating slices with PhTx-74 also caused a reduction in gamma power within 10 minutes following initial introduction. However, this decline coincided with a decrease in the frequency of recorded oscillations, with an 8 Hz fall in peak frequency within the same time window. This decline would often continue to the 15-minute time point, with oscillations shifting into the beta-frequency range and the oscillation power rebounding. The single-cell patch-clamp pharmacology suggests that these additional influences upon network activity could result from inhibitory effects on GluR2-containing AMPARs, including those on pyramidal cells. In order to explain how the distinct AMPAR selectivity of PhTx-74 compared to NASPM or PhTx-433 could result in this dissociation of effects, one must consider the contribution of each cell type and synaptic connection to the maintenance of oscillatory activity.

In a pyramidal-interneuron network gamma (PING) model of gamma-frequency hippocampal activity, oscillations exist as a consequence of excitation at inputs onto both pyramidal cells and PV+ interneurons, and inhibition from PV+ cells on pyramidal cells. The amplitude of oscillations, and hence gamma power, is related to the number of cells that are active per gamma cycle (Buzsáki and Wang, 2012). Additionally, the peaks of gamma oscillations reflect $GABA_A$ receptor-mediated currents in pyramidal cells resulting from PV+ interneuron activity (Penttonen et al., 1998). In a

situation where excitatory drive onto PV+ cells is decreased, either by AMPAR subunit knockout or by selective blockade of CP-AMPARs, fewer cells will reach firing threshold on a given cycle, resulting in smaller currents within a population and oscillations with lower power. Models of PING-based gamma oscillations indicate that the strength of drive to inhibitory neurons, or to a connected excitatory-inhibitory network as a whole, is the primary influencer on oscillation power (Bartos et al., 2007; Tiesinga and Sejnowski, 2009; Whittington et al., 2011). However, whilst ING models report significant changes in oscillation frequency with changes in network drive, PING models show far less sensitivity of frequency in relation to degree of excitation (Hormuzdi et al., 2001; Traub et al., 1996a, 1996b; Whittington et al., 2011). With the fast-spiking properties of PV+ interneurons still intact, the rate of overall population activity may be preserved, resulting in the minimal changes in frequency seen with PhTx-433 and NASPM, at least during the period of decline in power.

The mechanisms influencing peak frequency are less clear, but besides the relationship with power indicated by some studies, it has also been shown by some groups to be affected by synaptic kinetics and conductance, as well as excitatory-inhibitory balance and cortical feedback (Brunel and Wang, 2003; Kang et al., 2010; Traub et al., 1997, 1996a; Wang and Buzsáki, 1996; Whittington et al., 2011, 1995). In a situation where only excitatory drive onto PV+ cells is affected, pyramidal cells will still be similarly excitable following disinhibition, so should be able to fire as previously. Provided the PV+ cell population is able to maintain similar rates of firing at a population level, the frequency of oscillations should remain stable. However, if PhTx-74 is also inhibiting AMPARs on pyramidal cells, they may be slower to activate following relief of perisomatic inhibition, having a knock-on effect on the excitatory drive onto PV+ cells. By reducing excitatory drive at two separate inputs within the excitatory-inhibitory network, this may be sufficient to slow down the network in the manner observed following PhTx-74 application in this study. The reduced excitatory drive onto PV+ cells

resulting from reduced pyramidal excitation may also explain the slightly greater reduction in gamma power observed within 10 minutes post-drug application compared to PhTx-433 or NASPM.

It has previously been shown that increases in the decay time at $GABA_A$ synapses results in a decrease in oscillation frequency, due to an accumulation of slowly decaying inhibition over time that results in tonic hyperpolarisation, counteracting external depolarisation (Wang and Buzsáki, 1996). Whilst there is not any suggestion that PhTx-74 directly manipulates $GABA_A$ receptor kinetics, it is possible that reducing external depolarisation of pyramidal cells by partially inhibiting AMPARs has a similar outcome. As the rate of firing decreases, it is likely that more cells become available to fire on a given cycle, resulting in the rebound in oscillation power as frequency decreases into the beta-frequency range.

Our patch-clamp recordings showed a highly selective effect of NASPM on evoked EPSCs in CP-AMPAR-expressing PV+ cells but not pyramidal cells expressing GluR2, whilst PhTx-74 significantly reduced evoked EPSC amplitude in both cell types. Given the greater effect on gamma power by PhTx-74, it might be surprising that it produced a smaller reduction in EPSC amplitude in PV+ cells compared to NASPM; however, its effects on pyramidal cells may contribute to this. The compounds also influenced the size of spontaneous EPSCs recorded in PV+ cells, as determined by current amplitude and area. PhTx-74 treatment resulted in decreases in both amplitude and area; however, NASPM only significantly reduced area, not amplitude. This may just be a consequence of the relatively small number of cells recorded from, as there appeared to be a trend towards reduced sEPSC amplitude following NASPM treatment.

In summary, the experiments performed in this chapter have demonstrated an ability to affect hippocampal network function using CP-AMPAR-selective agents, and demonstrated the extent to which manipulating these receptors can disrupt oscillatory activity. This both provides incentive for further investigating hippocampal CP-AMPAR activity in a more refined and cell-specific manner, and reveals a window within which one might expect to see changes following a more restricted manipulation. Furthermore, my results provide support to findings from genetic studies targeting AMPAR subunit expression in PV+ interneurons regarding their impact upon hippocampal activity, whilst offering a novel insight into the consequences of acute reduction of excitatory drive onto CP-AMPAR-expressing hippocampal cells (including PV+ cells) on network activity, as well as potentially providing novel insights into the relative contributions of excitatory drive at separate synapses within the excitatory-inhibitory hippocampal network. The combination of network and synaptic pharmacology reveal a dissociation between the effects of different AMPAR antagonists based upon their receptor selectivity, and identify NASPM as a more appropriate compound for probing CP-AMPAR activity *in vivo*. I can now build upon these findings and move towards investigating CP-AMPAR function within a behavioural context, and assess whether acute, selective CP-AMPAR blockade *in vivo* will influence performance on behavioural tasks associated with hippocampal function and oscillatory network activity.

3 The role of CP-AMPAR activity in behaviour

3.1 Introduction

The activity of PV+ interneurons within the hippocampus has been shown to contribute to memory function and behavioural performance within several different paradigms, with cellular dysfunction or impairments in their excitatory recruitment eliciting multiple selective phenotypes. Reduced numbers or silencing of hippocampal PV+ cells has been shown to alter anxiety expression and disrupt fear memory consolidation (Godavarthi et al., 2014; Ognjanovski et al., 2017). They have also been considered as necessary for optimal expression of working memory. Working memory describes the capacity to retain recently acquired information; recall of said information can then be used to inform upon current choice-making in conditional tasks relying upon this information (Lisman, 2010). Gamma-frequency oscillations are believed to be important in the organisation of information necessary for maintaining working memory, with gamma oscillations correlated with working memory load in humans (Howard et al., 2003). Hippocampal gamma-frequency oscillatory activity has been observed during successful performance on spatial working memory-dependent behavioural tasks in rodents, and optogenetic interference with inputs entraining CA1 gamma activity has been shown to impair performance on these tasks (Montgomery and Buzsáki, 2007; Yamamoto et al., 2014). Hippocampal gamma oscillations require activity in PV+ interneuron populations, and purported PV+ interneuron-specific ablation of AMPAR subunits has been reported to impair spatial working memory (Fuchs et al., 2007).

The rewarded alternation T-maze task is a commonly used test to assess working memory in rodents (Deacon and Rawlins, 2006). The task involves an animal being placed in a start arm, forced to enter one of two reward arms to receive a reward (with the other blocked off), removed from the maze and then returned to the start arm with the previously blocked arm now available. The animal must learn to enter the previously unvisited arm to receive a reward (i.e. to 'alternate' its turning based upon recent memory of its previous arm entry). Working memory load can be increased by increasing the delay between (i) the initial sample of the first reward during the forced run, or 'sample' phase, and (ii) the subsequent 'choice' phase in which it chooses which arm to enter when given a choice.

Successful performance of the task requires an intact dorsal hippocampus, as animals carrying lesions in the region perform at chance levels (Bannerman et al., 1999). Additionally, hippocampal gamma activity seems necessary for correct choice-making on the task, as increases in gamma peak and coherence across hippocampal sub-fields were observed in the start arm on the choice run when entering the choice zone, but only on successful trials (Montgomery and Buzsáki, 2007; Yamamoto et al., 2014). AMPAergic recruitment of PV+ cells, necessary for optimal hippocampal gamma activity, appears necessary for successful execution of the T-maze task, as PV+ cell-specific GluR1 knockout, as well as both whole-brain and hippocampus-specific GluR4 knockout, caused impairments in performance on the task, whilst other forms of spatial memory were retained (e.g. spatial reference memory) (Caputi et al., 2012; Fuchs et al., 2007). As such, one would anticipate that a CP-AMPAR-selective pharmacological blockade within the hippocampus to result in similar and selective impairments in performance on the task.

There are several methods one can use to test the impact of a given compound on performance in a behavioural task or assay. However, amongst the most practical, particularly if one wants to restrict

the effects of the drug to a specific brain region, is to infuse the compound via implanted intracerebral cannulae targeted to the region of interest (Gleeson et al., 1980). One can surgically implant guide cannulae, which can be used multiple times for repeated infusions into the region of interest. This system has been used to infuse various compounds intrahippocampally, with impairments in performance on the T-maze following infusion of D-AP5 or muscimol (McHugh et al., 2008).

Despite their use *in vitro* in studying, amongst other things, interneuronal CP-AMPAR expression and PV+ interneuron plasticity, there has been minimal use *in vivo* of CP-AMPAR-selective antagonists (Le Roux et al., 2013; Nissen et al., 2010). Studies have infused NASPM into areas such as the amygdala and nucleus accumbens, but not the hippocampus, whilst no studies were found that used any form of philanthotoxin (Goffer et al., 2013; Hong et al., 2013). The lack of prior use of these compounds gives me limited guidance regarding optimal doses for infusions; the study in the amygdala used doses of approximately 1.6 and 16 mM, but whether these doses would be applicable for safe usage in the hippocampus is unclear. There are concerns that using a compound that selectively reduces excitation of inhibitory cells such as PV+ interneurons could result in excessive excitation within the hippocampus and the risk of seizures occurring; therefore, it is necessary to be cautious, whilst at the same time aiming to use a dose at which there is a good chance of seeing behavioural effects.

The aims of these experiments will be to use NASPM, a highly selective pharmacological agent, to specifically target CP-AMPARs, and to ascertain the contribution of activity at CP-AMPAR-expressing synapses (including those on PV+ interneurons) in performance on a behavioural task dependent on hippocampal function and associated with gamma oscillatory activity. Whilst the knockout studies previously covered have targeted AMPARs in PV+ interneurons, genetic knockouts could impact

development and induce compensatory responses, in addition to previously mentioned concerns regarding the Cre line used to establish the knockout. Furthermore, optogenetic approaches affect neuronal activity levels rather than specifically targeting synaptic recruitment.

Our pharmacological approach, whilst not accomplishing the same type of cellular specificity, provides an opportunity to investigate CP-AMPAR activity in the absence of compensatory changes, and explore acute consequences of impairing the function of these channels and the synapses they are expressed at. The experiments will also provide me an opportunity to explore whether I can impair working memory via manipulating hippocampal CP-AMPAR function ourselves, and provide a positive control for the more refined transgenic approaches I aim to perform in later chapters, providing possible limits for any potential impairments I may expect to see following a more targeted manipulation. The hope is that the study will demonstrate the translatability of my *in vitro* results from the previous chapter, and confirm the necessity of hippocampal CP-AMPAR activity for functionality of the brain region before proceeding with experiments specifically studying Ca^{2+} currents through these channels.

3.2 Materials and methods

3.2.1 Animals

Experimentally naïve, age-matched adult male and female mice, heterozygous for both PV-Cre and Ai9 on a C57BL/6 background (as described in Chapter 2), were initially housed in group cages, and maintained at the Biomedical Sciences Building (University of Oxford), on a 12 hour:12 hour light-dark cycle in a temperature- and humidity-controlled room. For the rewarded alternation T-maze

task, animals within the cohort were approximately 16 weeks of age or older; the cohort was initially comprised of 16 mice (n = 8 male, n = 8 female). All animals were housed according to Home Office regulations, with procedures carried out under a UK Home Office project licence (30/3068, Professor David Bannerman) and personal licence (IE1E0DB60, myself) in accordance with the United Kingdom Animals (Scientific Procedures) Act, 1986. All procedures were performed during the light phase of the light-dark cycle.

Animals were provided with *ad libitum* access to water throughout. Following initiation of pre-surgical behavioural training, *ad libitum* food was replaced with a restricted food diet with the aim of maintaining body weight between 85-90% of the animals' free feeding weights. The animals' diet consisted of 2916 food, plus any condensed milk reward consumed during behavioural training or testing. Following this, *ad libitum* food was only restored prior to surgery, during post-surgical recovery until re-commencement of behavioural training, and before perfusions. Following surgery, animals were separated into singly housed cages with elevated lids to prevent contact of the headcaps/cannulae with the cage lid.

3.2.2 Pre-surgery T-maze habituation and rewarded alternation training

Spatial working memory was assessed using an elevated (1 m) T-maze, made of wood, painted grey, with a start 'home' arm (47 x 10 cm), two reward arms (35 x 10 cm), and a perimeter wall (10 cm in height). Plastic wells were located at the end of each reward arm, placed centrally at a 3 cm distance from the end of the arms. Sliding plastic doors were fixed into grooves lining the entrances to the reward arms, and could slide to completely block off each reward arm or allow unrestricted access

to the arms. During each phase of testing, the maze was placed in a dimmed but well-lit room with distinct extramaze cues (cabinets, posters, door).

The rewarded alternation T-maze task was chosen in favour of the spontaneous alternation T-maze task due to the consistent level of motivation maintained during testing sessions in response to receiving a reward. Mice are known to satiate and lose their motivation to solve alternating tasks, rendering short testing sessions essential (Pioli et al., 2014). As the possibility of performing longer testing sessions during infusion experiments was intially considered to maximise data acquisition per infusion, the rewarded alternation task was selected in the hope of maintaining motivation throughout sessions.

During the experiment, a 50:50 condensed milk:water mix was used as a reward for correct choices. Mice were first introduced to this reward in their home cages. Following this, mice began to be habituated to both the T-maze, and eating within the T-maze. They were first exposed to the T-maze in cage groups, and learned to explore the maze and consume the milk reward from the plastic wells, before subsequently being individually habituated to the maze. Mice were individually habituated to the maze for 4 days before being trained at the rewarded alternation T-maze task. They received regular further habituation sessions throughout the study to overcome anxiety at performing the task.

Mice were first trained on the rewarded alternation task on the T-maze prior to implantation of cannulae. During this period, a training session consisted of 10 trials. During a trial, a mouse was placed at the end of the home arm and permitted access to only one arm, with the other arm blocked by the plastic sliding door. When the mouse reached the end of the only accessible reward

arm and consumed the milk reward, it was removed from the maze for a 5-second period, during which the previously blocked arm was opened up. As the milk consumed during the 'forced' arm entry was not replaced, the only remaining reward was located at the end of the previously blocked (i.e. unvisited) arm. After 5 seconds, the mouse was replaced at the end of the home arm, and given a free choice to enter either arm. If the mouse successfully 'alternated' and entered the previously inaccessible arm, it would receive a milk reward, whilst if it re-entered the arm it had already drank from, it would not receive a second reward. Each trial was separated by a 45-second inter-trial interval (ITI).

During training, mice learned to enter the previously blocked arm during the 'choice' period of the trial; for example, if the mouse was first forced to enter the left arm of the T-maze, it would have to learn to enter the right arm when replaced in the maze following the 5-second period. Such a scenario would be classed as a 'correct' choice. A choice (whether correct or incorrect) was counted as when all 4 paws had entered one of the reward arms. The latency for both forced arm entry and choice arm entry was timed as the period from initial placement into the home arm until full torso entry into a reward arm. Sessions of 10 trials included 5 trials in which the animal was initially forced left (a 'left' trial) and 5 in which it was initially forced right (a 'right' trial). These trials were delivered in a pseudorandom sequence, produced by a random sequence generator, with the restriction that no more than 3 successive trials could be of the same type (i.e. sequences containing 4 or 5 successive 'left' or 'right' trials were forbidden). Performance at the task was calculated as the percentage of correct choices made across a training/test session.

As mice habituated towards the maze at different rates, not all animals could be run for 10 trials in each session; however, sessions including 5 or more trials were counted towards the pre-surgery training scores. Animals managed to complete 5 or more trials on between 3 and 11 separate days,

depending on the animal. Once a majority of the animals were consistently achieving scores of 70% correct choices or higher, the cohort underwent surgery.

3.2.3 Surgical implantation of guide cannulae

Mice were implanted with guide cannulae, such that when injector cannulae were inserted into them, they would project into the dorsal hippocampus. Following the lead of former members of the lab group that had previously infused into the dorsal hippocampus, guide cannulae were implanted with coordinates (relative to bregma) of: anterior-posterior (AP) -1.3 mm, medial-lateral (ML) ±1.3 mm, and dorsal-ventral (DV) -1.0 mm. Insertion of the injector cannulae was such that the tip of the cannulae would reach DV -1.8 mm. For this chapter only, the DV coordinates were set relative to the skull surface at bregma instead of the brain surface at the site of insertion, due to the inability to see the brain surface when the guide cannula pedestal was in position.

Mice (20-30 g in weight) were anaesthetised with isoflurane (3.5% in 4 L/min O_2 for induction, 1-1.5% in 1 L/min O_2 for maintenance; IsoFlo, Abbott Laboratories) and given subcutaneous injections of meloxicam (0.1-0.15 ml, 5 mg/kg; Metacam, Boehringer-Ingelheim), buprenorphine (0.05-0.08 ml, 0.08 mg/kg; Vetergesic, Sogeval UK Ltd.) and physiological saline (0.5 ml, 0.9% w/v NaCl, Aqupharm; Animalcare UK), as well as a topical injection of bupivacaine (0.2 ml, 2 mg/kg; Marcain; AstraZeneca UK). The scalp was shaved to expose the skin, and was wiped with iodine. The mouse was mounted into a stereotaxic frame (David Kopf Instruments), and a rectal temperature probe inserted to regulate body temperature, aiming to maintain a body temperature of 37 °C using a homeothermic blanket (Harvard Apparatus). Lacrilube (Allergan UK) was applied to the eyes to prevent drying.

An incision was made in the scalp along the midline, and the underlying connective tissue was scraped off to expose the skull surface, into which six holes were drilled; two holes for the guide cannulae to be inserted at AP -1.3 mm, and ML ±1.3 mm, plus two holes towards the front and back of the skull into which anchor screws were inserted. These holes were positioned sufficiently anterior/posterior of the cannulation holes such that the pedestal of the guide cannulae would not catch on the screws (e.g. the posterior screws were posterior to lambda), and were positioned as to form two roughly parallel lines. Following insertion of the screws, the guide cannulae (Plastics One Inc.) were inserted into the brain. The cannulae came as a single bilateral unit, with two stainless steel 26-gauge cylinders fixed within a cylindrical plastic pedestal, with a centre-to-centre distance between the centre of each cylinder measuring at 2.6 mm, and the cylinders extending 2 mm from the pedestal. The guide cannulae were lowered into the brain using a probe holder (David Kopf Instruments) such that the tips of the cannulae were at DV -1.0 mm, and then suspended in this position using the probe holder whilst dental cement (Simplex Rapid, Kemdent) was applied to the area, covering the anchor screws and cannula pedestal in a dome-like shape to secure the cannulae at these coordinates. The edges of this dome were designed to prevent irritation of the surrounding skin, through the separation of skin and cement and the smoothing down of edges. Once the cement had dried, loose skin around the implant was sutured (Vicryl Rapide, Ethicon) to close up the wound. The guide cannulae were fitted with a complementary bilateral dummy cannula (length 2.0 mm, Plastics One Inc.) that fit inside the guide cannulae, and topped with a screw-on brass dust cap, to prevent blockage of the cannulae whilst not in use.

At the end of surgery, a second 0.5 ml dose of saline was injected subcutaneously, and anaesthesia was removed, with oxygen still supplied. Once the animal had begun recovering from anaesthesia (regaining toe pinch and righting reflexes), it was moved to a heated (30 °C) recovery chamber for 1+ hours until full movement had returned. The animal was then given an additional dose of Vetergesic,

equivalent to that given at the start of surgery, plus a 0.5 ml dose of glucose saline, before being transferred to a new home cage with an elevated lid. 24 hours later, the animal was given another dose of glucose-containing saline, plus a dose of Metacam equivalent to that given at the start of surgery. Recovery was subsequently monitored for the next two weeks by measuring body weight and assessing wound appearance and behavioural activity, with any additional fluids or drugs provided if necessary.

3.2.4 Post-surgical habituation and training

Animals were first reintroduced to food deprivation and habituation to the T-maze 2 weeks after surgery. For all post-surgery habituation, training, and testing, the T-maze apparatus was moved into a different room from the one used for pre-surgery habituation and training. For all animals, they were first re-exposed to the T-maze with several sessions of non-contact habituation, in which the animal was placed within the maze and allowed to explore arms to obtain food rewards without any human contact. The sliding doors would be alternated after one or two rewards were obtained from a certain arm to try and avoid any preference developing for either arm, and the food wells would always be refilled with food once the animal moved away from them. Depending on the animal's level of performance, this would run for either a certain period of time, or until a certain amount of milk reward was consumed. Following this, the animals would also receive brief human exposure outside the maze on occasions, in which the animal was handled extensively by the experimenter, including walking over the hands and latex gloves, to build familiarity and reduced anxiety towards handling with the gloves.

Once animals were consistently moving freely throughout habituation sessions immediately following initial placement in the maze, re-training was initiated. Like before, training sessions entailed providing animals with 10 trials, of which 5 began with forced entry of the left arm, and the other 5 with forced entry of the right arm, with no more than 3 of either trial in succession. Again, the interval between consumption of the first reward and replacement in the home arm for the choice trial was approximately 5 seconds, and the inter-trial interval was 45 seconds. Depending on the latencies of animals throughout the trial and performance levels, animals were given habituation sessions between training sessions to try and reduce anxiety. All animals received a minimum of four training sessions during this period. At this point, all animals either scored 80% or higher during at least one of the final two training sessions.

3.2.5 Mock infusions and T-maze testing

The next stage involved exposing the animals to the practicalities of the infusions process, specifically the restraint necessary to insert the injectors, and the sensation of movement with the infusion tubing attached to their head. To this end, animals were first given a training session immediately following exposure to the restraint required for attachment of the injector. This restraint involved placing a sheet of blue roll paper in the open palm, and placing the mouse onto the paper. Then, the hand was quickly closed around the animal, with the head restrained between the thumb and forefinger and the body covered by the remaining fingers. The blue roll was used as it made animals calmer in comparison to restraint with just a latex gloved hand, meaning a looser restraint was possible for successful connection of the infusion assembly. Once the animal was adequately restrained, the dust cap on the headcap could be easily unscrewed and removed, the dummy cannulae removed, and the infusion assembly inserted and attached. The restraint was effective for quick removal/insertion of dummy cannulae and infusion assemblies without damaging

the equipment or animals, and the animals quickly became accustomed to the procedure and typically behaved calmly whilst restrained.

Subsequently, animals received two training sessions immediately preceded by 'mock' infusions. Mock infusions entailed performing the entire set-up and sequence of events for intrahippocampal infusions, but excluding the actual infusion of liquid into the hippocampus. In brief, two pairs of Microlitre Syringes (10 µl, Hamilton Company) were filled with saline (0.9% w/v NaCl, Aqupharm; Animalcare UK), and attached to a double connector assembly (40 cm, Plastics One Inc.), such that the whole distance from each syringe injector to the tip of the connector assembly was filled with saline. The syringes were fixed into an automated Nanoliter Infusion Pump (World Precision Instruments), set to infuse 0.5 µl over 2 minutes. Once set up, double internal cannulae (additional projection beyond guide cannulae 0.8 mm, Plastics One Inc.) were attached to the free ends of the connector assembly, and saline pushed through the tips. The set-up now permitted the insertion of injectors through the implanted guide cannulae such that the tips resided in the dorsal hippocampi of implanted mice. To insert these internal cannulae, animals were restrained as previously described, and the dust cap/dummy cannulae removed. The internal cannulae were inserted inside the guide cannulae, and a screw attachment at the end of the connector assembly was screwed onto the pedestal of the headcap, fixing the internal cannulae at the desired location. During mock infusions, animals were not infused with saline or drug solution; however, the animals were placed in cage boxes without lids (infusion boxes) to freely roam for 3 minutes, equating to the 2 minutes of infusion time plus an additional 1 minute to permit fluid diffusion throughout the hippocampus during actual drug/vehicle injections. Due to the weight of the connector assembly, this tubing was manually elevated to reduce force on the animal's head and neck. After 3 minutes, the animals were re-restrained, the infusion assembly removed and new, sterile dummy cannulae inserted, with the

dust cap subsequently replaced onto the headcap. After an additional 5 minutes, the animals were run on the rewarded alternation T-maze task.

Following restraint/mock infusions, animals were left for 5 minutes in the infusion boxes before being run on the task. During these experiments and during the next phase of testing, animals were run two at a time, as drug-infused and control saline-infused animals in the next phase would be run in pairs. Animals were assigned into pairs based upon past performance scores and running latencies. The two animals would be run in alternation, with the first animal running a trial, then the second one running a trial, then the first one running another trial, and so on. Additionally, in order to maximise data output following each drug infusion, the plan was to increase the number of trials per session to 20 trials per animal. As such, following each mock infusion, two animals would in alternation receive 20 trials. As in the previous section, each animal received an equal number of 'left' and 'right' trials, with no more than 3 of each type of trial in succession. Furthermore, there were an equal number of 'left' and 'right' trials in both the first and second halves of sessions. The interval between sampling the food reward in the 'forced' arm to replacement in the home arm would, like before, be approximately 5-10 seconds. In order to accommodate running two animals at the same time, the inter-trial interval was increased to a minimum of 2 minutes, or longer if the other animal had not finished its trial by the time 2 minutes had passed. After 20 trials, animals were returned to their home cages, and, depending on performance, were given additional habituation sessions on subsequent days if required.

Each animal received one restraint session without involvement of the infusion equipment, and then subsequently two mock infusions. Based on the performance of some of the slower animals, and based on previous use of the experimental drug NASPM in the literature, it was felt that 20 trials

would extend beyond the active window of the drug following infusion (Goffer et al., 2013). As such, for the infusion experiments, the number of trials per session was restored to 10 trials.

3.2.6 Drug infusions and T-maze testing

Each animal was to receive two infusions; a saline infusion as a control condition and an infusion of NASPM dissolved in saline. Counterbalanced based upon the performance scores from the mock infusions, animals in each pair were assigned either control or drug infusion for their first infusion. For their second infusions, animals received the other treatment. The set-up of equipment and insertion of injector cannulae was the same as for mock infusions; once the infusion assembly was in place, animals were left to roam free in the infusion boxes (with the connector assembly manually elevated) for 3 minutes (2 minutes for infusion and 1 minute for diffusion of fluid away from the injection site) before the internal cannulae were removed and new sterile dummies inserted. After removal of the infusion assembly, animals were left in the infusion boxes for 5 minutes, and then were given 10 trials with an inter-trial interval of 2 minutes, with two animals run together as in 3.2.5. After 10 trials, animals were returned to their home cages. On the following day, animals were given a 're-acquisition' day, in which they would receive 10 trials run in the same manner as on infusion days but without infusion. The animals would be placed under the previously described restraint, and the dummy cannulae 'jigged' up and down within the guide cannulae without being removed to avoid blockage of the guide cannulae, before the dust cap was reattached. After this, animals were left for 5 minutes before being tested on the T-maze.

As NASPM had not previously been infused into dorsal hippocampus, there was limited precedent within the literature to base doses on. Based on past use of the drug in other brain regions,

concentrations of 1 mM and 10 mM NASPM (Tocris Biosciences) dissolved in saline were used during the study (Hong et al., 2013). Similar to previous dorsal hippocampal infusion studies, a dose volume of 0.5 µl/hemisphere was used, infused for 2 minutes at a rate of 0.25 µl/min (McHugh et al., 2008).

3.2.7 Histology

At the end of behavioural testing, animals were returned to free feeding, and once they had reached normal free feeding weight, they were culled and their brains were extracted. In brief, animals received a 0.4 ml (200 mg/ml) intraperitoneal injection of pentobarbital (Euthatal, Merial Animal Health Ltd.), before being transcardially perfused with first physiological saline, followed by paraformaldehyde (PFA, 4% in 0.1 M phosphate buffer). Fixed brains were extracted from the skull and stored at 4 °C in PFA. 24 hours before brains were to be sectioned, they were moved from PFA to a 30% sucrose-in-0.1 M phosphate buffer solution.

Brains were mounted at -25 °C using OCT Compound (VWR) on an SM2000R freezing-stage microtome (Leica), and slices of 40 µm thickness containing dorsal hippocampus were cut. Slices were placed in 0.1 M phosphate buffer in a 96-well plate, and DAPI (1 µg/ml) was applied to stain sections. Slices were mounted on slides and coverslips applied, with Fluoroshield (Sigma-Aldrich) used as mounting medium to preserve DAPI fluorescence.

Sections were imaged using a Leitz DRMD Fluorescence Microscope (Leica), and either a Retiga 2000R CCD camera (QImaging) for images of light-illuminated sections or tdTomato fluorescence from PV+ interneurons, or a Dino-Eye eyepiece camera (Dino-Lite) for images of DAPI fluorescence

and gliosis. Cannula positions were illustrated using images from the Mouse Brain Reference Atlas (Allen Brain Atlas).

3.2.8 Statistical analysis

All statistical tests were performed using SPSS. Within-subjects (e.g. 1 mM infusion experiments) and between-subjects (e.g. 10 mM infusion experiments) data were analysed across sessions and infusion treatment groups using repeated-measures analyses of variance (ANOVAs) and t-tests, whilst correlation between variables was assessed using bivariate (Pearson) correlation tests. The two-tailed significance value was set at 0.05 for all tests, except tests of simple main effects corrected for multiple comparisons.

To allow for a coherent test of simple effects whilst controlling for multiple comparisons, a Dunn-Sidak correction was used, where the p-value threshold for a comparison was defined as (where α was the per-family error rate for the nominal number of families tested, and k was the number of contrasts tested) (Gabriel, 1969):

$$p = 1 - (1 - \alpha)^{(\frac{1}{k})}$$

The nominal number of families tested was defined as α = 0.05 for each main effects family; as simple effects analyses spanned both the main effect family and interaction family, simple effects on one factor (e.g. treatment) had a nominal familywise error rate of 0.1, whilst tests of simple effects for both factors had a familywise error rate of 0.15 (Bird, 2004; Harris, 2001).

As in Chapter 2, significance indicators used in figures in this chapter represent, unless otherwise stated: * = $p < 0.05$, ** = $p < 0.01$, *** = $p < 0.001$, n.s. = $p \geq 0.05$, with error bars representing the standard error of the mean. For statistical comparisons, when mean values for two separate groups are provided (i.e. $X \pm a$ vs $Y \pm b$), unless stated otherwise, the first value represents the control group (for example, the vehicle-treated group), whilst the second value represents the experimental group (for example, the NASPM-infused group).

Performance of animals across sessions during the mock infusion phase was assessed using one-way repeated-measures within-subjects ANOVAs. As in Chapter 2, in conditions where assumption of sphericity was violated, the Huynh-Feldt (H-F) or Greenhouse-Geiser (G-G) corrections were used to alter degrees of freedom in order to reduce Type I error. Influence of habituation sessions on performance of the rewarded alternation task was assessed using a two-way repeated-measures ANOVA to assess effects of session and use of habituation on performance. Correlation between mean latency and performance was tested for using a Pearson correlation test.

During the infusion phase of testing, two-way ANOVAs were used to assess the effect of session type and infusion treatment on performance and latency to choice; analysis was performed within-subjects for 1 mM NASPM treatment as the cohort was infused with both drug and vehicle treatment, and between-subjects for 10 mM NASPM, as infusions of both treatments was not completed for the cohort (see 3.3.4). The interaction between session and treatment was further explored with *post hoc* simple main effects tests adjusted for multiple comparisons. As simple main effects were used to compare treatment at each level of session, $\alpha = 0.1$, and $k = 3$, setting the significance value at 0.035.

3.3 Results

3.3.1 Placement of cannulae and confirmation of dorsal hippocampus as site of infusion

Bilateral guide cannulae were implanted into the dorsal hippocampus of 16 mice (n = 8 male, n = 8 female), such that the tips of the cannulae were positioned relative to bregma at -1.3 mm AP, ±1.3 mm ML, and -1.0 mm DV, with 0 mm DV set at the height of the skull surface at bregma. Of these animals, 13 mice (n = 5 male, n = 8 female) survived long enough to receive intrahippocampal infusions, during which internal cannulae would be inserted, with additional length such that their tips would extend to -1.8 mm DV. At the end of the study, the animals were perfused and their brains extracted for histological analysis of cannula placement following fixation and sectioning into 40 µm slices. The slices were stained with the nucleus-staining fluorescent marker DAPI; however, the staining was weak in the slices, meaning useful images at appropriate magnification could not be acquired for DAPI fluorescence using the microscopes available within the department. Consequentially, images of sections were taken to observe tdTomato fluorescence from PV+ cells, or grayscale images of hippocampal appearance under illumination by white light.

In the majority of sectioned brains, the site of infusion through internal cannulae was clearly visible by the presence of substantial reactive gliosis (Fig. 3.1A). Whilst the shapes of the gliosis varied between animals, its position was consistently found either within or on the edge of the dorsal hippocampus (Fig. 3.1B). Imaging for tdTomato fluorescence also reveals that the PV+ interneurons outside of the area of gliosis are still present in physiologically relevant numbers. A minority of brains did not exhibit obvious gliosis; however, comparison of the position of the guide cannulae between these brains and those that exhibited clear gliosis suggests that the internal cannulae in

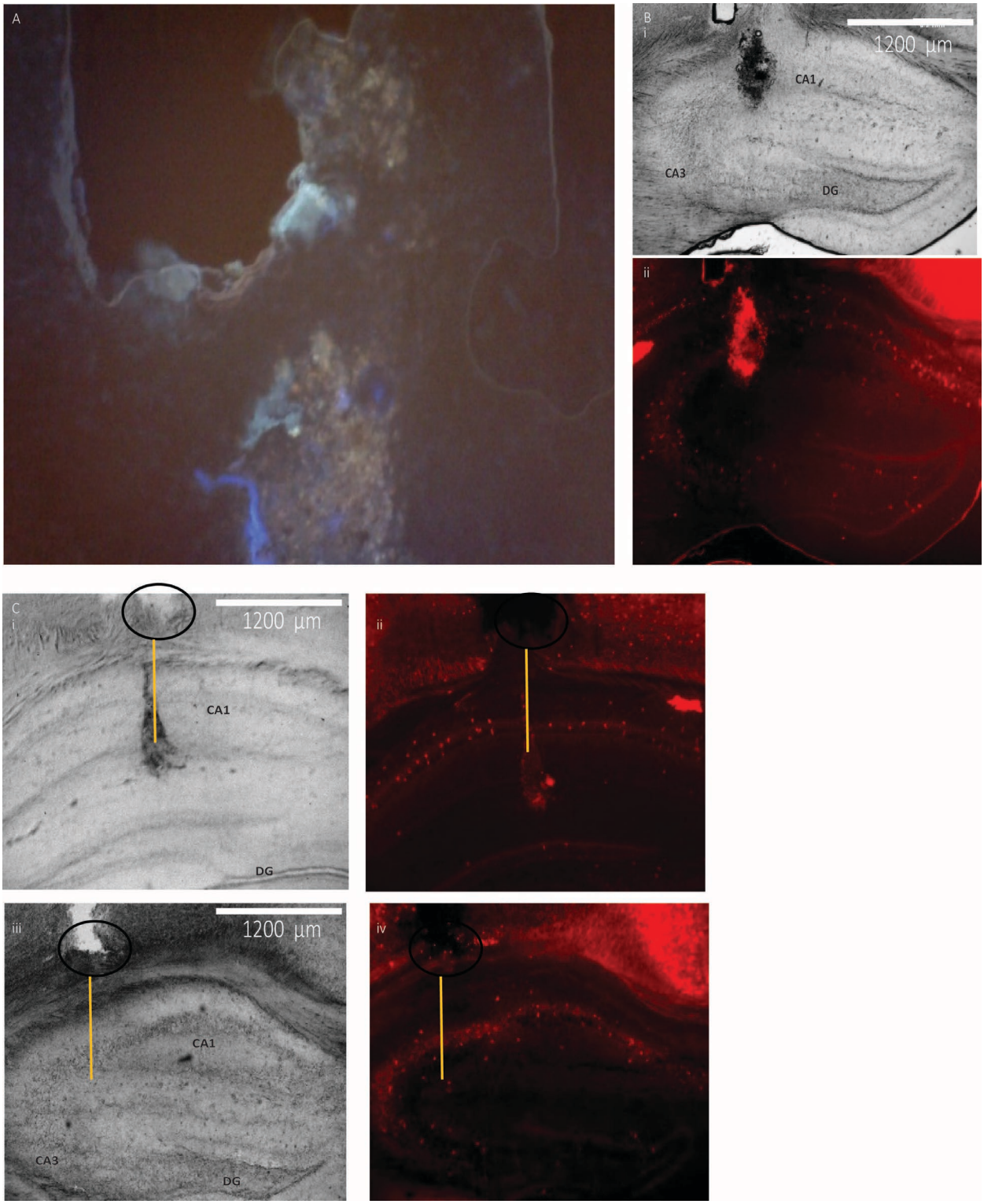

Figure 3.1. Sites of infusion into the dorsal hippocampus. (A) Appearance of reactive gliosis in the dorsal hippocampus following multiple infusions of saline and drug solution, as ween whilst visualising DAPI fluorescence. (B) Gliosis in the dorsal hippocampus of cannulated mice. Grayscale image (i) and tdTomato fluorescence (ii) revealing the position of gliosis in the hippocampus, and the condition of surrounding PV+ interneurons. (C) The presence (I, ii) and absence (iii, iv) of gliosis in brain sections from cannulated animals. The position of the end of the guide cannula tract is highlighted with a black circle; the distane from the tip of the guide cannula to the point of infusion as predicted by gliosis is highlighted in yellow. Images were acquired under 10x (DAPI) or 5x (grayscale, tdTomat) magnification, with 1 ms (grayscale), 10 ms (DAPI) or 1000 ms (tdTomato) exposure.

these brains also terminated within or on the edges of the hippocampal formation (Fig. 3.1C). From

this, it is possible to assume that within all animals, infused solutions entered and diffused through the dorsal hippocampus. However, the borderline positioning of the cannulae in some animals makes it possible that the solution also entered extrahippocampal regions of the brain; as such, one cannot rule out that behavioural responses to drug infusions in these animals could be a consequence of extrahippocampal receptor interactions.

3.3.2 Rapid acquisition of the rewarded alternation T-maze task

Before implantation of cannulae, mice were first habituated to and subsequently trained on the T-maze. Following several sessions of exposure to the T-maze, animals were introduced to the rewarded alternation T-maze task (Fig. 3.2). As described in the introduction, the task requires an animal to use memory of previous forced arm entry and reward consumption (in this study, a 50:50 condensed milk:water solution) during the 'sample' phase of a trial in order to enter the opposite arm during the 'choice' phase (Fig. 3.2A). Across training and testing sessions, animals would receive 10 sample-and-choice trials in a pseudorandom order, with an even split of trials in which the animal was forced into either the right or left reward arm during the sample phase. No more than 3 successive trials would have the same sample reward arm.

Rodents are known to spontaneously alternate without reinforcement, therefore one would expect a starting level of performance above chance levels in the absence of hippocampal damage (Sanderson and Bannerman, 2012). Aside from tdTomato expression in PV+ cells, the PV-Cre/Ai9 mice used in the study were generally similar to wild-type mice, which are known to quickly learn the task and consistently score highly across sessions (Schaefers and Winter, 2011). As such, I expected the animals in the study to quickly learn how to successfully perform this task. In actuality,

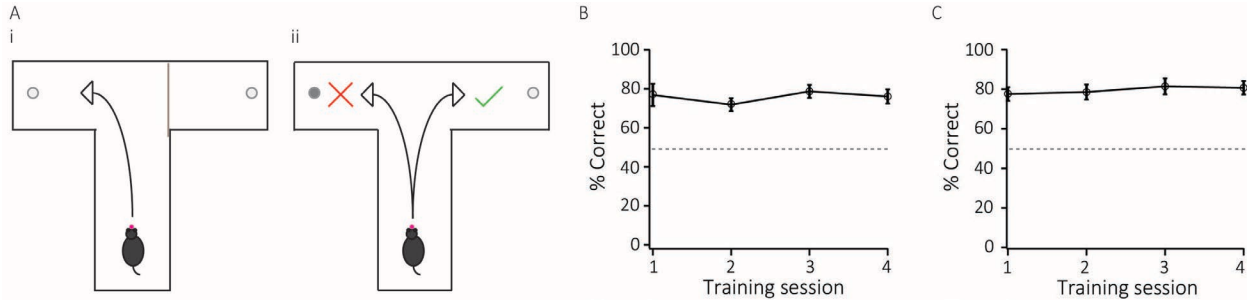

Figure 3.2. Learning of the rewarded alternation task during pre- and post-surgery training sessions. (A) Animals are trained to perform the rewarded alternation task on the T-maze. (i) During the sample phase, the animal is placed in the home arm, and allowed access to only one of the two reward arms, each of which have a food well at the end filled (white) with a milk reward. The animal learns to run to the junction between the home and reward arms, and to the end of the available 'sample' arm to receive a reward. (ii) During the choice phase, the animal is removed from the maze, and the previously blocked arm is made available; however, the previously consumed reward in the sample arm is not replaced. The animal is then replaced at the end of the home arm, and given a choice between the two arms. To successfully complete the task and receive a second reward, the animal must 'alternate' which arm it enters during the choice phase from the one it entered during the sample phase. (B) Prior to surgery, animals (n = 16) across the cohort performed consistently highly on the task, even from the very first exposure to the task. (C) After recovery from implantation surgery, animals (n = 14) continue to perform consistently highly across training sessions. Data averaged over 10 trials per session per animal. Error bars indicate standard error of the mean. Horizontal dashed lines represent chance (50%).

the animals scored an average of 77% across the cohort during the very first training session, and maintained average scores of over 70% during the remainder of the pre-surgery training (Fig. 3.2B; n = 16 mice, n = 8 male and n = 8 female). Following surgery, animals were re-habituated and then re-trained at the task. The remaining cohort (n = 14 mice, n = 6 male and n = 8 female) averaged 78% correct across the first session and just under 80% across four sessions (Fig. 3.2C). This demonstrated that the animals within the cohort were capable of learning the task quickly, and whilst performance for some animals dropped substantially for one or two successive sessions, the average across the cohort remained consistently high across the training sessions. The initial high performance in the very first training session also suggests that the requirements of the task may be compatible with the innate behavioural tendencies of mice.

3.3.3 Mock infusion protocol did not affect performance on the T-maze task

Following post-surgical retraining, the animals were first introduced to the restraint technique required to insert infusion equipment, and then subjected to 'mock' infusions, in which the equipment necessary to infuse solutions was set up and inserted into the animal, without solution actually being infused. This would prepare the animals for the procedure when solutions were infused, to ensure they were comfortable enough to perform the rewarded alternation task following infusion to avoid wasting drug solution. After the animals were unrestrained and the equipment removed, the animals were left alone for a 5-minute period, and then subjected to testing sessions of 20 trials in a pseudorandom order. All animals completed 20 trials in all 3 sessions, except for one mouse that only completed 16 trials following its second mock infusion (trials were aborted if an animal took more than 2 minutes to leave the start arm, and sessions were ended after 2 aborted trials).

Three animals were lost from the cohort before mock infusions; one during surgery, one during post-surgical recovery, and one following post-surgical re-training. Performance following restraint was high across the remaining cohort (72.69 ± 5.8% correct; n = 13 mice, n = 5 males and n = 8 females), and remained high following both mock infusions (79.6 ± 3.1% and 82.2 ± 2.1% for mock infusions 1 and 2, respectively; Fig. 3.3A). A one-way repeated-measures within-subjects ANOVA across the three sessions revealed no significant difference in average performance across the cohort across sessions (no assumption of sphericity ($\chi^2(2) = 6.96$, $p = 0.031$, G-G $\varepsilon = 0.681$); $F_{(1.362,16.339)} = 1.929$, $p = 0.183$). Given this high level of performance following multiple mock infusions, I was confident that the process of infusing solutions by itself would not cause a significant reduction in performance, giving me a useful window in which I could observe any drug effects on performance.

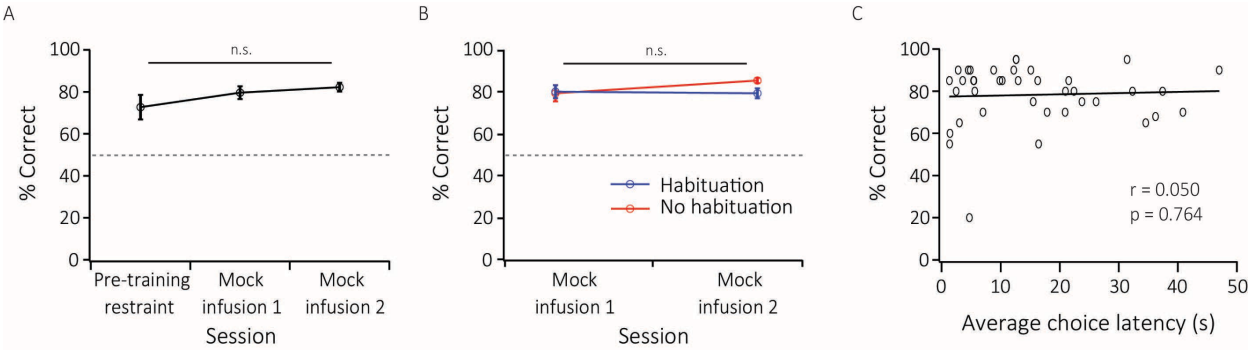

Figure 3.3. Profile of animal performance of the rewarded alternation T-maze task following mock infusions. (A) Animals score highly on the rewarded alternation task following restraint and insertion of mock infusion equipment. Average performance across the cohort (n = 13 animals) over 70% correct in each session. There is no significant improvement in performance across the three sessions. (B) Habituation of animals to the T-maze does not significantly affect performance on the T-maze. Animals that received additional habituation sessions between the two mock infusions (blue, n = 8) showed a very minor decrease in average cohort % correct score, whilst those animals that did not receive additional habituation sessions (red, n = 5) showed a slight increase in average cohort % correct score. However, these changes were not statistically significant. (C) There is no correlation between the average time taken to make a choice across a testing session and the number of correct choices made across a session. A 2D scatter plot of average choice latency plotted against % correct score for all 13 animals in each 3 sessions (n = 39 points). There was found to be no correlation between average choice latency and % correct score. All data averaged over 20 trials per session per animal (with one exception of 16 trials). * = $p < 0.05$; n.s. = $p \geq 0.05$.

The initial plan was to avoid doing further habituation sessions during the mock and actual infusion testing phases of the study to avoid any confounds in learning. However, following the restraint day and first mock infusion I saw a notable build-up in anxiety in some animals reflected in increased latencies whilst performing the task. To try and prevent latencies becoming impractically long, and in doing so inadvertently increasing the memory demands of the task by increasing the sample-choice delay period, habituation sessions were re-introduced between the first and second mock infusions. To ensure these sessions would not interfere with performance during the drug infusion phase of the study, changes in performance between the first and second mock infusions were compared for those anxiety-prone animals that were given additional habituation sessions (n = 8 animals) against those that had consistently short latencies and did not receive further habituation (n = 5 animals) (Fig. 3.3B). The group of 5 animals that did not receive habituation sessions averaged 79 ± 6.2% correct choices during the first mock infusion, which increased to 87 ± 2% during the second mock infusion; in contrast, the group of 8 animals that did receive habituation sessions averaged 80 ± 3.5%

during the first mock infusion, which fell slightly to 79.1 ± 2.7% during the second mock infusion. A 2 (session) * 2 (use of habituation) two-way ANOVA comparing performance across the two mock infusion sessions showed no significant main effect of habituation ($F_{(1,11)} = 0.669$, $p = 0.431$), nor a significant habituation x session interaction ($F_{(1,11)} = 1.739$, $p = 0.214$). Overall, subjecting animals to additional T-maze habituation sessions to alleviate anxiety when performing the rewarded alternation task did not have a significant effect on performance on the task; therefore, it was considered safe to include habituation sessions during the drug infusion phase of the study when deemed necessary to avoid the build-up of excessive anxiety in animals.

As a consequence of the aforementioned anxiety, trial latencies (defined as the time from placement in the home arm to full entry into a reward arm) varied substantially between animals (Fig. 3.3C). Across 20 trials (or 16 trials in one instance) the average choice latencies varied from 1 second up to 47 seconds. To ascertain whether there was a correlation across the animals between average choice latency during a session and % correct score for the session, a bivariate (Pearson) correlation test were performed to assess the relationship between the two variables. With an n of 39 data points (13 mice, 3 sessions), there was found to be no correlation between choice latency and % correct score ($r = 0.05$, $n = 39$ sessions, $p = 0.764$). High % correct scores (≥70%) were consistently achieved by animals across sessions with average choice latencies of both sub-5 seconds and above 25 seconds. Overall, although consistently very long latencies are undesirable, and habituation sessions are used to try and avoid this, within a fairly large window (up to 50 seconds) there was no notable influence of average choice latency on performance of the rewarded alternation task.

3.3.4 Dose-dependent impairment on rewarded alternation T-maze task following intrahippocampal infusion of NASPM

Once the cohort had exhibited an ability to perform the rewarded alternation task with a high degree of accuracy following insertion of the infusion equipment, they were moved forward to the infusion phase of testing, during which either control saline solution or NASPM solution was infused intrahippocampally prior to testing on the T-maze. The testing schedule was similar to the mock infusion phase of the study; animals were run in pairs, with the two animals taking turns after the infusions to perform trials. Whilst animals were subjected to 20 trials per session during the mock infusion phase, due to the variable latency speeds of animals and concerns over the duration of activity of the drug, animals were only subjected to 10 trials per session during this phase of the study (Ding et al., 2014).

On the day immediately following infusion days, animals were given 're-training' days to ensure there were no lasting effects of drug infusion on performance on the task, as well as to confirm animals were performing sufficiently well at the task as to observe any potential subsequent drug effects. On the retraining day, animals were exposed to the restraint used to insert/remove infusion cannulae, and the dummy cannulae already inside the guide cannulae were jiggled around to ensure the infusions had not caused any blockages before being reinserted and the headcaps reattached. Following a 5-minute waiting period, animals were again subjected to 10 trials. Animals that scored lower than 70% received additional re-training days until they reached 70%. Additionally, animals with slow latencies continued to receive additional T-maze habituation sessions throughout this phase of the study.

As mentioned previously, there was no precedent in the literature for infusion of NASPM into rodent hippocampus; therefore, doses were determined based on studies infusing the compound into other brain regions. One study infused NASPM into rat lateral amygdala at doses corresponding to 1.6 mM and 16 mM, at 0.5 µl/side (Hong et al., 2013). Other studies have infused different compounds into

dorsal hippocampus at a rate of 0.25 µl/min, 0.5 µl/side (McHugh et al., 2008). As such, I decided to begin testing using a dose of 10 mM NASPM, infused at 0.25 µl/min for 2 minutes. Following complete solution infusion and removal of the infusion cannulae, mice were subjected to a 5-minute delay before the first trial of the rewarded alternation testing session, based on the introduction of a similar delay between infusion of the compound into nucleus accumbens and commencement of behavioural testing in a different study (Ding et al., 2014).

Animals were infused as described above in pairs, with one animal receiving saline solution and one animal receiving 10 mM NASPM. For the first six drug infusions, animals showed no clear visible phenotype unrelated to task performance. However, following this, two consecutive infusions into drug-naïve animals resulted in the onset of spasms and, in the case of the second animal, an extended period of seizure-like activity, necessitating culling of the animal. As a result of this, experiments using 10 mM NASPM were terminated and the dose was decreased to 1 mM for the remainder of the study. However, from the data acquired from the 10 mM infusions prior to the onset of spasms, a between-subjects comparison of the effect of drug on performance on the rewarded alternation T-maze task in comparison to control saline infusion was conducted (n = 9 vehicle-infused animals, n = 6 NASPM-infused animals; Fig. 3.4A).

A 2 (treatment) * 3 (session) two-way ANOVA comparing performance of drug- and saline-infused animals across three sessions (the session prior to infusion, the session immediately following infusion, and the session one day after infusion) revealed a significant within-subjects main effect of session ($F_{(2,26)} = 10.626$, $p < 0.001$), plus a significant interaction between session and infusion treatment ($F_{(2,26)} = 6.833$, $p = 0.004$). To explore the nature of the interaction, simple main effects of treatment at each level of session were tested, with an adjusted significance value of 0.035. These tests revealed a significant difference in performance on the task between the drug-treated and

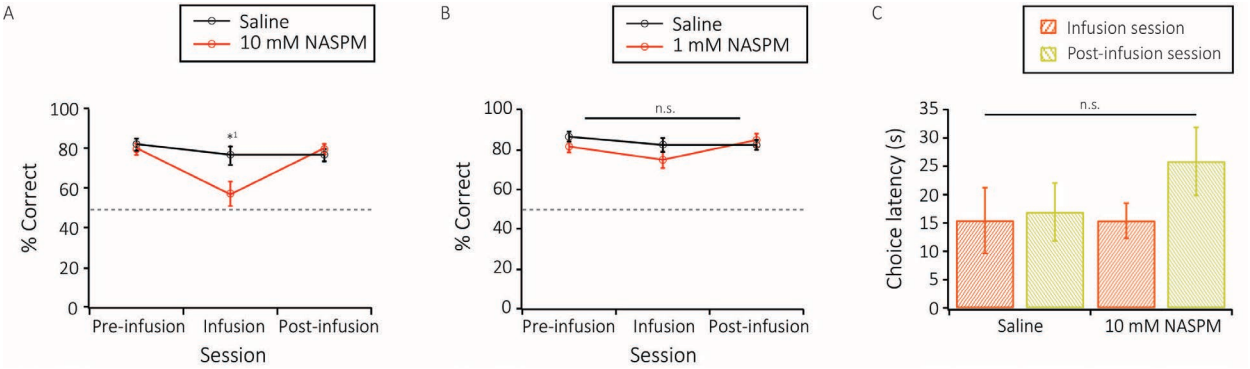

Figure 3.4. Dose-dependent effects of intrahippocampal infusion of NASPM on animal performance on the rewarded alternation T-maze task. (A) Infusion of 10 mM NASPM into dorsal hippocampus resulted in fewer correct choices made on the rewarded alternation task, restricted only to the day of infusion. The mean correct score of drug-infused animals (57%, n = 6) was significantly lower than that of saline-infused control animals (77%, n = 9). This impaired performance was independent of prior performance of animals at the task, and effects did not last beyond the day of testing. (B) Infusion of 1 mM NASPM did not replicate the effects of 10 mM NASPM, as there was no significant effect of infusion on correct choice-making behaviour during the task (n = 12, within-subjects study). (C) Infusion of 10 mM NASPM did not cause significant changes in trial latency. The mean choice latency was similar on the day of infusion for saline-treated and NASPM-treated animals (15.44 s vs 15.4 s), and latency did not significantly change between the day of testing and the following day (15.44 s vs 16.92 s for saline, 15.4 s vs 25.85 s for NASPM). All data averaged over 10 trials per session per animal. $*^1$ = $p < 0.035$.

saline-treated groups on the day of infusion (76.67 ± 4.8% vs 56.67 ± 5.9%; $F_{(1,13)} = 6.849$, $p = 0.021$), but not on the day prior to (80 ± 3.2% vs 82 ± 2.6%; $F_{(1,13)} = 0.232$, $p = 0.638$) or following infusion (80 ± 3.6% vs 76.67 ± 2.9%; $F_{(1,13)} = 0.52$, $p = 0.484$). Thus, infusion of 10 mM NASPM into the dorsal hippocampus of mice impaired performance on the rewarded alternation T-maze task, restricted only to the period immediately following infusion, in a reversible manner independent of prior performance of animals on the task. However, due to the risk of this drug dose inducing spasms or seizure-like activity, subsequent infusions were performed using a 1 mM drug dose.

As before, animals were run in pairs, with one animal in each session infused with 1 mM NASPM and one infused with saline. As there were no complications with spasms or seizures, each animal underwent 2 infusions, such that 12 animals received both NASPM and saline solution infusions. This enabled within-subjects analysis of performance on the task (n = 12 animals; Fig. 3.4B). A 2 (treatment) * 3 (session) within-subjects ANOVA revealed a non-significant trend towards an effect on task performance of treatment ($F_{(1,11)} = 3.474$, $p = 0.089$), no significant effect of session (no sphericity assumed ($\chi^2(2) = 8.811$, $p = 0.012$, G-G $\varepsilon = 0.631$); $F_{(1.261,13.874)} = 2.001$, $p = 0.179$), and no

significant interaction between the two variables ($F_{(2,22)} = 1.175$, $p = 0.327$). Therefore, intrahippocampal infusion of 1 mM NASPM into mice does not seem to produce the impairments in performance on the spatial working memory-dependent rewarded alternation T-maze task elicited with 10 mM NASPM infusion.

Due to unexpected effects that emerged in two animals following infusion of 10 mM NASPM, I decided to investigate whether there was a more general impact upon locomotor activity in the cohort. I took the mean latencies during the choice phase of trials from the day of infusion and the testing session on the day after infusion (Fig. 3.4C). A 2 (treatment) * 2 (day) ANOVA revealed no effect of drug on trial latency ($F_{(1,13)} = 0.367$, $p = 0.555$), nor a significant interaction between session and drug ($F_{(1,13)} = 3.298$, $p = 0.093$). As such, the decline in performance following infusion of 10 mM NASPM does not appear to be a consequence of impaired locomotion during the task.

Overall, acute pharmacological blockade of CP-AMPARs in the dorsal hippocampus by NASPM impairs performance on a spatial working memory task in a dose-dependent manner; however, there is an overlap between the dose necessary to impair working memory task performance and doses capable of eliciting potential seizure-like activity in mice.

3.4 Discussion

The results obtained in this chapter reveal a necessity for CP-AMPAR activity within the dorsal hippocampal region in order for optimal expression of spatial working memory. NASPM resulted in a dose-dependent, reversible decrease in performance to approaching chance levels, with the

impairment restricted to the day of infusion. Whilst the action of NASPM is not cell type-specific, the observed results are consistent with the reported effects of PV+ interneuron-specific disruption of AMPAR expression (a cell type with high CP-AMPAR expression) and of optogenetic disruption of hippocampal gamma oscillatory activity (a pattern of activity involving PV+ interneurons and associated with working memory) (Fuchs et al., 2007; Yamamoto et al., 2014).

The experiments performed within this chapter involved intracerebral implantation of guide cannulae, and repeated intrahippocampal infusions of drug solution. There are pitfalls to this method; the surgery and implantation of the guides will cause some damage to the cortex, whilst repeated insertion of the infusion cannulae and injection of the studied compound can cause the build-up of reactive gliosis at the site of infusion, with the knock-on effect of reducing the efficiency of subsequent infusions (Cunningham et al., 2008; Gleeson et al., 1980). Nevertheless, the system has found widespread use for restricted exposure of specific brain regions to compounds of interest. Given that both experimental and control animals underwent the same procedure, there is little reason to suspect that the difference between the two groups following infusion of 10 mM NASPM was notably influenced by these factors, rather than actions of the drug.

During the study, 1 mM and 10 mM doses of NASPM were used, with the impairment in performance on the working memory-dependent T-maze task emerging only with the higher dose. These doses were partly based on previous work in the amgydala, which used doses of similar volume with concentrations equivalent to 1.6 mM and 16 mM as low and high doses, respectively (Hong et al., 2013). The study in the amygdala only observed significant behavioural impairments with the higher dose, similar to in this chapter. In Chapter 2, I observed reductions in gamma power in hippocampal sections *in vitro* when exposed to 100 µM, but not 10-50 µM. The *in vitro* interface set-up involves sections being superfused with the drug solution, with direct contact of the tissue

with the solution, permitting easy access for the compound to interact with target receptors. In contrast, *in vivo* cannulation requires diffusion of the fluid from the point of infusion throughout the surrounding brain tissue. As a result, there is likely to be uneven spread of the drug solution in the hippocampus and variable exposure of CP-AMPARs to this drug concentration. As such, concentrations used for cannulation experiments *in vivo* are typically higher than those that would be used for *in vitro* experiments, but there is no defined rule for conversion that enables me to compare the doses at which I elicited abnormalities *in vitro* and *in vivo*.

Working memory is a form of short-term memory that involves active retention of recent information, and requires persistent neuronal activity (Fuster and Alexander, 1971). Both theta and gamma oscillatory activity are biomarkers of working memory load, with increases in gamma power observed with increasing demands, i.e. more information, or a greater period of time over which to retain said information (Howard et al., 2003; Raghavachari et al., 2001; Tallon-Baudry et al., 1999). High-frequency oscillations enable the separation of information and memories into distinct cycles, and thus allow ordering of said memories. Memory capacity is thought to be limited by the number of gamma cycles within a given theta cycle (Lisman, 2010). Within the context of the T-maze, different cell ensembles were shown to fire on distinct gamma cycles as an animal approached a choice point in a familiar maze, with this segregated firing proposed to allow recall of past memory of moving through the maze (Johnson and Redish, 2007). Furthermore, in the rewarded alternation T-maze task, synchronised gamma activity (whether between CA1 and CA3 or CA1 and entorhinal cortex) has been shown to occur immediately prior to reaching the choice point during trials in which a correct choice was made (Montgomery and Buzsáki, 2007; Yamamoto et al., 2014). The segregated cellular firing facilitated by gamma oscillatory activity enables recall of recent experience to inform on current choice-making within the maze.

CP-AMPARs are expressed on a subset of neuronal cell types in the hippocampus, including PV+ interneurons, the function of which is associated with working memory and oscillatory activity (Nissen et al., 2010). The data indicate that synaptic recruitment via CP-AMPARs, most likely of hippocampal interneurons, is necessary for optimal expression of working memory. The contribution of NASPM inhibiting receptors on other cell types, including SOM+ interneurons, to this working memory impairment cannot be discounted, but arguably the most likely points at which NASPM brings about working memory impairments are excitatory synapses onto PV+ interneurons. Ablation of AMPAR subunit expression in PV+ interneurons has previously been reported to elicit substantial impairments in performance on the T-maze (Caputi et al., 2012; Fuchs et al., 2007).

By interfering with excitatory drive onto hippocampal interneurons, NASPM is likely to alter the timing and/or rate of interneuron firing. *In vitro*, NASPM caused a reduction in the power of gamma oscillations, likely due to reduced recruitment of PV+ interneurons. *In vivo*, this impaired excitability may disrupt or impair the effectiveness of information transmission through the hippocampus by decreasing the degree of control or organisation interneurons have over pyramidal cell ensembles, resulting in the impairment observed in this chapter. My results are similar to those demonstrating an impairment on the T-maze task following optogenetic disruption of hippocampal gamma oscillation synchrony (Yamamoto et al., 2014). Overall, the data reported in the current and previous chapter further point towards a connection between hippocampal interneuron recruitment, optimal function of the hippocampal network, and effective retention and expression of working memory.

At this higher concentration of NASPM, I also observed the emergence in a subset of animals, either transient or sustained, of spasms and epileptic-like seizures. Due to the selective expression of CP-AMPARs on inhibitory cells in the hippocampus, such as PV+ and SOM+ interneurons, blockade of these AMPARs, but not GluR2-containing AMPARs, is likely to cause a relative reduction within the

given brain region of inhibitory activity compared to excitatory activity. This imbalance, and excessive excitatory firing resulting from it, is likely to be the reason for this seizure-like phenotype (Bromfield et al., 2006). In fact, optogenetic suppression of PV+ interneuron firing in visual cortex has been shown to induce seizure-like patterns of discharge in response to visual stimuli (Trevelyan et al., 2013). However, in the absence of these unintended effects, experimental animals appeared broadly normal, and were able to complete the T-maze task at a similar speed to saline-infused animals. Furthermore, animals appeared to exhibit similar appetitive motivation to vehicle-treated animals, as they were equally willing to consume all available rewards during testing immediately post-infusion.

The spasms observed following NASPM infusion represent one of the pitfalls of using pharmacological agents. More importantly, however, whilst the results obtained thus far demonstrate the functional importance of interneuronal GluR2-lacking AMPARs versus GluR2-containing AMPARs to hippocampal function, they do little to clarify what importance calcium permeability through these channels in particular has for activity in the hippocampal network or for hippocampus-dependent behaviour. Antagonists such as NASPM or PhTx-433 bind within the channel pore, and block all conductance through the channel (Washburn et al., 1997). In order to selectively manipulate AMPAR-mediated calcium entry into PV+ cells and resulting plasticity at their excitatory inputs, I required a more targeted approach that can disrupt calcium entry whilst broadly conserving overall conductance. To this end, the experiments performed in the following chapters will use alternative methods to manipulate AMPARs.

4 Virally-driven overexpression of the GluR2 AMPAR subunit in hippocampal PV+ interneurons

4.1 Introduction

The results from my experiments using antagonists selective for CP-AMPARs demonstrate the acute importance of AMPAergic activity mediated by these channels in the maintenance of hippocampal gamma-frequency oscillatory activity, and the requirement for that activity within dorsal hippocampus for effective expression of working memory. These results fit with the widely believed hypothesis that recruitment of CP-AMPAR-expressing interneurons, particularly those expressing parvalbumin, underpins high-frequency hippocampal network activity associated with working memory, and fall in line with studies using genetic approaches to disrupt AMPAR expression in PV+ interneurons (Caputi et al., 2012; Fuchs et al., 2007; Sohal et al., 2009; Yamamoto et al., 2014). However, the pharmacological approach that I have used thus far has flaws, including the potential to elicit seizure-like activity when utilised *in vivo*. It is also limited by the fact that CP-AMPARs are not exclusively expressed on PV+ interneurons in the hippocampus; they are also found at functionally relevant levels in somatostatin-expressing interneurons, and in small numbers in other cell types, including pyramidal cells (Guire et al., 2008; Szabo et al., 2012). Finally, through their mode of action (binding within the channel pore), agents such as philanthotoxin or NASPM block all conductance through CP-AMPARs (Washburn et al., 1997). Whilst this is ideal for studying the functional importance of CP-AMPARs over GluR2-containing AMPARs in hippocampal function, such an approach does not lend itself to specifically isolating calcium currents mediated by these channels. Therefore, it is limited in how much it can enhance understanding of what influence these currents, and any plasticity mediated by them, have upon the hippocampal network, and on the

expression of hippocampal-dependent behavioural phenotypes. In order to more effectively study this, I needed a more targeted approach.

As mentioned in the introduction, AMPARs are tetrameric channels composed from combinations of four distinct subunits, with several properties (including calcium permeability) being governed by the presence or absence of the edited form of the GluR2 subunit (Nakagawa, 2010; Washburn et al., 1997). A post-transcriptional modification that results in a glutamine-to-arginine substitution disrupts a carbonyl ring within the channel pore necessary for calcium entry and polyamine binding (Geiger et al., 1995; Sommer et al., 1991). The subunit can also undergo other modifications, including the incorporation of either a flip or flop exon, that influence the maturation speed of the subunit and subsequent inclusion in AMPARs (Greger et al., 2006; Sommer et al., 1990). As well as altering calcium permeability, inclusion of GluR2 into AMPARs alters conduction properties, including conductance size and channel kinetics (Geiger et al., 1995; Lawrence and McBain, 2003; Oh and Derkach, 2005; Swanson et al., 1997; Verdoorn et al., 1991).

Channels that lack GluR2 are capable of mediating calcium flow, but typically only at negative membrane potentials, due to the depolarisation-induced block mediated by intracellular polyamines (Bowie et al., 1998). This means that plasticity mediated by CP-AMPAR activity can only occur in situations where presynaptic release of glutamate occurs in the absence of post-synaptic depolarisation, a situation dubbed ‘anti-Hebbian’ plasticity (Lamsa et al., 2007). Due to their minimal expression of GluR2, PV+ interneurons express AMPARs predominantly composed of GluR1 and GluR4 subunits, which form CP-AMPARs; anti-Hebbian plasticity has been induced at excitatory inputs onto hippocampal PV+ interneurons (Bochet et al., 1994; Lamsa et al., 2007; Nissen et al., 2010). If one could drive expression of GluR2 in these neurons, it might be possible to convert the

AMPAR profile of these cells to one dominated by GluR2-containing AMPARs, and in doing so diminish or abolish CP-AMPAR-mediated anti-Hebbian plasticity in these cells.

One possible means by which to accomplish this is the use of a viral agent to transfect a cell type of interest with a vector driving artificial expression of the edited GluR2 subunit. This approach has been previously used in non-neuronal cell types, such as Bergmann glia cells and glioblastoma cells (Iino et al., 2001; Ishiuchi et al., 2002). The group performing these studies reported an alteration in cellular properties following transfection with their vector, including a shift in rectification properties from inward rectification to a linear current-voltage relationship (Iino et al., 2001). I explored the possibility of using this approach to drive GluR2 expression in PV+ cells.

Given that the goal was to find an approach that would manipulate calcium permeability whilst broadly conserving overall cellular excitability via AMPARs, I was aware of the possible unintended consequences that driving overexpression of the GluR2 subunit could have. By introducing a large amount of an AMPAR subunit into the neuron, there is the possibility that I could cause a significant increase in the overall number of AMPARs in transfected PV+ cells. However, previous research indicated that GluR2 subunits are stored in a pool of available subunits in the endoplasmic reticulum following translation in order to be incorporated into new AMPARs; based on this, and the fact that GluR2 homomers are not reported physiologically, it might be expected that the subunits will only be included in AMPARs that were going to be produced regardless of their presence, and will not therefore not affect AMPAR population size (Greger et al., 2003; Isaac et al., 2007). Additionally, manipulating the composition of PV+ AMPARs will affect not only Ca^{2+} permeability, but also channel kinetics and conductance. The aim is to develop a method to alter Ca^{2+} permeability and plasticity whilst maintaining synaptic drive; what influence these other changes in receptor properties will have are unclear, but they are an unavoidable consequence of manipulating receptor composition.

There were several factors to consider in the design of my prospective viral agent. As well as including the Q/R substitution, a decision had to be made over what other variable features of the GluR2 to incorporate, including which splice variant to use. Given the goal was to avoid major changes to global AMPAR levels, incorporating features that slowed ER release of GluR2 in a way that should promote the ER subunit pool that appears in pyramidal cells was considered the best option. Additionally, in order to restrict expression to PV+ interneurons, the GluR2-encoding sequence was inverted and flanked with loxP sites, ensuring its expression only in cells expressing Cre recombinase i.e. PV+ cells in my PVCre/Ai9 mice.

There was also the decision over which vector type to use. Recombinant adeno-associated virus (AAV) is a widely used tool for artificial gene delivery, but there was a number of different available serotypes, each with varying capacity to drive expression depending on cell type or brain region (Aschauer et al., 2013). A study that comprehensively investigated relative capacity of different serotypes to drive expression in different cells indicated that AAV8 produced greatest expression in hippocampal interneurons, so this serotype was selected for my agent. Finally, a choice had to be made over whether to include a viral marker, and if so, what type. Incorporating a fluorescent tag such as GFP into a construct is a popular choice, but there were concerns over whether the inclusion of such a bulky protein might interfere in any way with receptor assembly, although a previous study looking at acetylcholine receptors suggested it did not (Gensler et al., 2001). Ultimately, the choice was made to instead insert an AU1 peptide marker into the N-terminus of the GluR2 subunit, in the linker between the signal peptide and the main body of the protein. The AU1 peptide is a small peptide (6 amino acids in length) that has previously been incorporated into constructs for histological processes, and which has been shown to have little, if any, influence on construct expression (Hoffmann et al., 2010; Shevtsova et al., 2006).

After having developed this construct, the aim of this chapter was to confirm its expression in PV+ cells, and validate its efficacy in being incorporated into AMPARs within the cells and altering the AMPAR profile from one dominated by CP-AMPARs into one dominated by GluR2-containing receptors. This included investigating rectification properties, gamma oscillation properties, sensitivity to CP-AMPAR-selective antagonists, dendritic calcium signals, and ability to express anti-Hebbian plasticity. By doing so, I aimed to show this approach was suitable for selectively manipulating calcium permeability of AMPARs in PV+ interneurons, enabling me to use the tool to study the contribution of these calcium currents to network activity and behaviour.

4.2 Materials and methods

4.2.1 Animals

Double homozygous PV-Cre$^{+/+}$/Ai9$^{+/+}$ mice were bred from animals generated for the previous chapters, and a colony composed of this genotype was maintained for this section of the study. Experimentally naïve adult male and female double homozygous mice were housed in group cages, and maintained at the Biomedical Sciences Building (University of Oxford), on a 12 hour:12 hour light-dark cycle in a temperature- and humidity-controlled room. Animals were used for *in vitro* experiments at 8 weeks and older, and viral injections were performed on mice at 6 weeks and older. All animals were housed according to Home Office regulations, with procedures carried out under a UK Home Office project licence (P79A7860C, Professor Ed Mann) and personal licence (IE1E0DB60, myself) in accordance with the United Kingdom Animals (Scientific Procedures) Act, 1986. All procedures were performed during the light phase of the light-dark cycle. Following

surgery, animals were housed individually in recovery cages for up to 1 week to allow stitches to heal, before being rehoused with littermates.

4.2.2 Viral design and production

A DNA plasmid containing the Q/R-edited, 'flop' splice variant form of the mouse GluR2 cDNA was generated with assistance from GenScript and Dennis Kaetzel (Ulm University). The previously mentioned R/G edit was not incorporated into the construct. Using Snapgene software with help from Dennis Kaetzel, a sequence was designed combining the cDNA encoding GluR2 with an AU1 peptide tag attached between the signal peptide and main sequence, to assist with histological

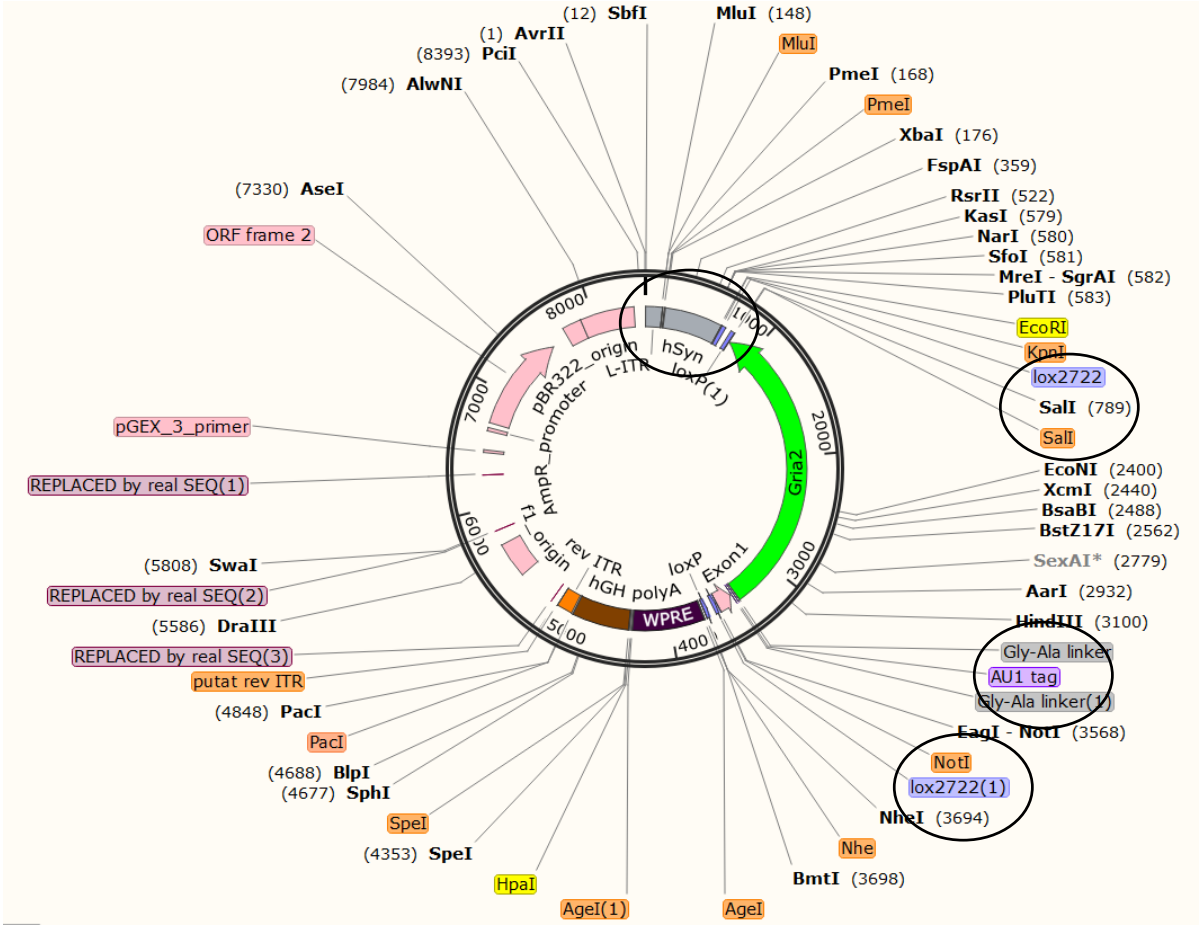

Figure 4.1. SnapGene illustration of the floxed GluR2 construct incorporated into the virus. The Q/R-edited flop form of *Gria2* (with an AU1 tag included in the N-terminus between the signal peptide and the bulk of the protein) was inserted into a plasmid backbone in inverted sequence using NotI and SalI restriction enzymes, flanked by loxP sites. The sequence was placed upstream of the synapsin (hSyn) promoter.

analysis of viral expression. The sequence was written in reverse orientation and flanked by SalI and NotI restriction sites. This sequence was sent to GenScript, along with a plasmid donated by Dennis Kaetzel that contained SalI and NotI sites flanked by loxP sites and an upstream hSyn promoter. Genscript synthesised the sequence and transferred it into this plasmid backbone. The final plasmid contains a hSyn promoter followed by loxP sites flanking the reverse-oriented GluR2 sequence (Fig. 4.1). This plasmid was then sent to UNC Vector Core for amplification and packaging in an AAV8 serotype vector. The virus was received at a concentration of 4.9 x 10^{12} plaque-forming units (PFU), which was used for the duration of the study.

4.2.3 Intracerebral injection

Adult (8 weeks and older) mice were anaesthetised with isoflurane and subcutaneously injected with meloxicam, buprenorphine, and bupivacaine as described in 3.2.3. The scalp was shaved to expose the skin, and was wiped with iodine. The mouse was mounted into a stereotaxic frame (David Kopf Instruments), and a rectal temperature probe inserted to regulate body temperature, aiming to maintain a body temperature of 37 °C using a homeothermic blanket (Harvard Apparatus). Lacrilube (Allergan UK) was applied to the eyes to prevent drying.

An incision was made in the scalp along the midline, and the underlying connective tissue was scraped off to expose the skull surface. One or two craniotomies were made above one or both ventral hippocampal lobes to allow access for viral injection, depending on whether animals were injected unilaterally or bilaterally. The viral vector was injected using a microsyringe (10 µl, Hamilton Company) at a rate of 100 nl/min. Injections were made at 4 sites in each hemisphere, with 600 nl injected at -2.7 mm AP, ±2.75 mm ML, and -2.7/-3.1 mm DV, and -2.9 mm AP, ±2.9 mm ML, and -

2.8/-3.2 mm DV (this was changed to -3 mm AP, -3.25 mm ML, and -2.7/-3.1 mm DV for the calcium imaging and plasticity experiments in 4.3.3/4.3.4). For histology purposes, some animals were also injected into dorsal hippocampus, using the coordinates -1.5 mm AP, ±2.1 mm ML, -1.5/-1.1 mm DV, and -2.8 mm AP, ±3.0 mm ML, -2.1/-1.5 mm DV. After injection at each site, the needle was left in place for 1-2 minutes before being slowly withdrawn in order to minimise backflow of virus and promote spread through the hippocampal tissue.

Once all injections were made, the incision was sutured together (Vicryl, Ethicon) to close the wound, anaesthesia was ceased, and the animal was moved to a heated recovery chamber until full movement had returned. Animals were given an additional dose of meloxicam the following day, and were housed singly for several days until the wound had healed, at which time they were re-housed with their cage mates. Recovery was monitored for 7 days.

4.2.4 Electrophysiology

4.2.4.1 Slice preparation

Following surgery, animals were left for a minimum of 4 weeks to allow sufficient time for optimal expression of the GluR2 construct in ventral hippocampus. After this point, horizontal slices containing ventral hippocampus were generated from injected and non-injected animals as in 2.2.2.1. In brief, animals were decapitated under anaesthesia, and 350 μm sections were cut using a heated sucrose-based solution, before being transferred to an interface chamber filled with aCSF and incubated at ~31 °C.

4.2.4.2 In vitro oscillation recordings

As in 2.2.2.2, slices were kept in the interface chamber for a minimum of 1 hour, and then transferred to an interface recording chamber, and maintained at ~34 °C whilst perfused with aCSF plus 5 µM carbachol. Slices were left for ~30 minutes, and then an extracellular recording electrode filled with aCSF (borosilicate, 1 MΩ) was positioned in/near stratum pyramidale of the CA3 region of the hippocampus to search for gamma-frequency oscillations. Once oscillations were detected, the electrode was positioned and activity was recorded until 1 hour after the slice was first placed in the chamber, at a sampling rate of 10 kHz, with 1 kHz low-pass filtering. If activity was lost, the electrode was moved and recordings restarted.

Once the 1-hour mark was reached, a new recording was started at the same position. Either 100 µM NASPM or an equivalent volume of dH_2O was added to the perfusing solution and washed into the slices. Activity was recorded for 15 minutes, and recordings in which oscillations disappeared or collapsed before this time point were discarded during analysis. Additionally, as the effects of the treatments on oscillation power were of primary interest and the typically upward direction of power size was established in Chapter 2, any recordings in which power decreased within the first 3 minutes (the time taken for the perfusing solution to reach the slice within the interface chamber) were also excluded from analysis. Once recordings were finished, slices were removed from the chamber and the set-up washed with dH_2O and then aCSF plus carbachol before further recordings were made.

As in 2.2.2.2, data were acquired, amplified and low-pass filtered (1 kHz) by AxoClamp 2A and LPBF-48DG, before being digitised by an ITC-16 acquisition board and recorded by Igor Pro software.

4.2.4.3 Current-voltage relationship recordings

As in 2.2.2.3, following a minimum of 1 hour in the interface chamber, slices were transferred to a submerged chamber maintained at ~31 °C mounted on an upright microscope (Olympus BX51W1) and superfused with aCSF (plus 50 µM DL-AP5 and 20 µM gabazine to block NMDA and GABA receptors, respectively). Whole-cell patch-clamp recordings were made using recording electrodes (borosilicate, 4-7 MΩ) filled with a caesium methanesulfonate-based internal solution containing (in mM): 140 $CsCH_3SO_3$, 5 NaCl, 10 HEPES, 0.2 EGTA, 2 Mg-ATP, 2 Na-GTP, 5 QX-314, 1 spermine, 10 biocytin.

Recordings were made from PV+ interneurons and pyramidal cells in the CA1 region of ventral hippocampus. Cells were patched in whole-cell mode and recordings were made in voltage-clamp. AMPA currents were stimulated in pyramidal cells and PV+ interneurons by the placement of a stimulating electrode (FHC) into stratum radiatum and stratum oriens, respectively. To establish a stable response size, following break-in, cells were held at -70 mV and received a series of stimuli, typically 20 stimuli with a 10 s gap. Following this baseline period, series resistance was compensated and cells were subjected to a stimulation-step protocol to determine the current-voltage relationship of AMPA responses within the cells. Starting at -70 mV, cells received two stimuli, with at 15 s gap between stimulation, before the holding potential was moved up to -60 mV. This 2 stimulations, 10 mV step pattern was repeated up to +80 mV. For cells that were still viable at this point, the step protocol was then reversed (+80 mV to -70 mV).

AMPA current rectification was calculated by taking the response to the second stimulation at the voltage steps 40 mV above and below the reversal potential (e.g., at -30 mV and +50 mV for a cell with a reversal potential of +10 mV during recordings) and calculating the +40:-40 ratio, or rectification index (RI). Out of the two recordings made (-70 to +80 and +80 to -70), the one with the lower/more stable series resistance during the -40 to +40 window was used for analysis. Cells were excluded from analysis if the series resistance went above 30 MΩ or varied by >15% between the start and end of this rectification analysis window.

Delivery of stimuli was controlled, and changes in holding current over time were recorded, by IGOR Pro. Signals were acquired using a Multiclamp amplifier (Axon Instruments) and ITC-18 interface (Instrutech).

Following the end of recordings, cells were resealed through the slow movement of the patching electrode away from the cell. Slices were then retrieved from the patching rig and stored in 4% paraformaldehyde (PFA) in 0.1 M phosphate buffer for future histological analysis.

4.2.4.4 Ca^{2+} imaging in PV+ cell dendrites

As in 4.2.4.3, slices were transferred to a submerged chamber in an upright microscope and superfused with aCSF. A silver wire was connected to a stimulation box and placed inside a borosilicate pipette filled with aCSF (minus gabazine and DL-AP5). This stimulation electrode was lowered into the slice near to the target cell. Recordings were made in voltage-clamp with borosilicate pipettes filled with the caesium methanesulfonate solution described in 4.2.4.3. The solution also contained the light-excitable calcium indicator Oregon Green 488 Bapta-1 (OGB-488,

cell-impermeant hexapotassium salt, ThermoFisher Scientific), added at a concentration of 300 µM, and then sonicated and filtered using a centrifuge to remove particulates from the solution. This solution was used to fill the recording pipettes, and PV+ cells (identified by tdTomato fluorescence) were patched in whole-cell mode. Cells were left for a minimum of 15 minutes to allow the cells to fill with the OGB-488 dye. The stimulation electrode was then moved and positioned next to a visible dendrite from the patched cell.

Once in this configuration, cells were stimulated with increasing amplitude by the electrode until a visible current response was detected by the recording electrode. Subsequently, cells underwent a stimulation-recording procedure, during which they were stimulated 3 times at 100 Hz with increasing stimulation amplitude, starting at the minimum threshold for current response detection, and then increasing to 50%, 100%, and 200% of the starting amplitude (hence referred to as 100%, 150%, 200%, and 300% threshold). Whilst stimulated, cells were visualised using 470 nm light and changes in fluorescence were recorded using Micro-Manager imaging software, with snapshots taken continuously at 50 Hz for 3 s. The stimulation was delivered 1 s into this window.

Following this protocol, the stimulation amplitude was returned to the threshold for current response induction (and was adjusted accordingly if this had shifted during the stimulation protocol), and cells were then treated with either 100 µM NASPM or an equivalent volume of control dH_2O, and stimulated for 10 minutes to promote NASPM binding (due to its use-dependent blockade). Following this 10-minute period, the protocol of imaging during burst stimulation of increasing amplitude was repeated. Once 300% threshold stimulation had been reached, recordings were finished from the cell and the recording electrode was withdrawn to reseal the cell membrane. The rig was washed out before further recordings were made.

4.2.4.5 Plasticity in PV+ interneurons

As in 4.2.4.3/4, slices were transferred to a submerged chamber in an upright microscope and superfused with aCSF, with both synaptic excitation and inhibition intact (DL-AP5 and gabazine were absent). Whole-cell patch-clamp recordings were made using borosilicate recording electrodes filled with a potassium gluconate internal solution containing (in mM): 110 KGluc, 40 HEPES, 2 ATP-Mg, 0.3 GTP-NaCl, 4 NaCl. Recordings in this section were made in part by Mina Moniri and Ed Mann.

Recordings were made from PV+ interneurons (identified by tdTomato expression) in strata oriens/pyramidale of area CA1 of ventral hippocampus. Horizontal sections were cut between area CA3 and area CA1 to prevent antidromic activation of CA3 pyramidal cells. Cells were patched in whole-cell mode and recordings were made in current-clamp. Small excitatory post-synaptic potentials were evoked by the placement of a stimulating electrode (same as in 4.2.4.3) in stratum oriens of area CA1, at a moderate distance from the patched cell. Following break-in, slow current was injected into cells to maintain a stable potential for the cell, typically at -70 mV.

Once the cell was in current-clamp mode, stimuli were delivered once every 15 seconds, and the amplitude of evoked EPSPs recorded. Once a stable baseline below 10 mV was reached over a period of 5 minutes for the same input stimulus amplitude, the cell was moved via current injection to -90 mV, and two rounds of 1-second 100 Hz burst stimulation were delivered before the cell was return to the previously held potential. Following this, stimuli were delivered every 15 seconds, with the same stimulation amplitude as before, for 20 minutes. Once 20 minutes of recording had been completed, the recording was typically terminated. The pairing protocol used to induce plasticity in this study was based on the method used by Lamsa et al. to evoke LTP in CP-AMPAR-expressing

hippocampal interneurons, with 1-second 100 Hz stimulation paired with hyperpolarisation to -90 mV (Lamsa et al., 2007). Afterwards, the cell was subjected to a simple step protocol (10 steps of positive and negative current injection, increasing in steps of +/-20 pA) before recordings were completed and a new cell was patched. The criteria for inclusion required that the input resistance did not drift more than 20% throughout the 25 minutes encompassing the baseline and post-pairing stimulation.

4.2.5 Histology

Following a minimum of four weeks post-surgery to leave sufficient time for expression of the viral construct, animals were culled and their brains extracted. In brief, animals received a 0.4 ml (200 mg/ml) intraperitoneal injection of pentobarbital (Euthatal, Merial Animal Health Ltd.), before being transcardially perfused, first with phosphate buffered saline, followed by paraformaldehyde (PFA, 4% in 0.1 M phosphate buffer). Fixed brains were extracted from the skull and stored at 4 °C in PFA.

Brains were sectioned on a VT1000S vibratome (Leica), with horizontal sections (for ventral hippocampus) or coronal sections (for dorsal hippocampus) cut with 60 µm thickness. Sections were washed three times in PBS before spending 20 minutes in 0.15% TBS-Triton X-100 (TBS-T). Following this, sections spent an hour in 20% normal horse serum (NHS) in TBS-T. Slices were briefly washed in TBS-T before incubation at 4 °C for 48 hours with the primary antibody (mouse anti-AU1, BioLegend) diluted 1:1000 in 2.5% NHS in TBS-T. After this incubation, slices were washed thrice in TBS-T before overnight incubation at 4 °C with the secondary antibody (Alexa Fluor-488-coupled goat-anti-mouse, ThermoFisher Scientific) diluted 1:500 in 2.5% NHS in TBS-T. Finally, sections were washed three

times in PBS, once in phosphate buffer, and mounted with Fluoroshield (Sigma Aldrich). All sectioning, incubations, and washes not done at 4 °C were done at room temperature.

Individual slices in which single-cell voltage-clamp recordings were made were stored in 4% PFA at the end of recordings and subsequently stained for both AU1 expression and biocytin. The slices underwent the same histology procedure as above, except in addition to overnight incubation with the secondary antibody, sections were also incubated with AMCA Avidin D (Vector Labs) diluted 1:1000 into the same solution as the secondary antibody. They were then mounted the following day as above.

Mounted sections were imaged at 5x, 20x, and 40x magnification using a Leitz DRMD Fluorescence Microscope (Leica) and a Retiga 2000R CCD camera (QImaging). Images of fluorescence were taken using Ocular software. Additional images were taken using a FV1200 Confocal Microscope (Olympus) fitted with PMT detectors, using FV10-ASW 4.2 Fluoview software, at 40x magnification.

4.2.6 Analysis and statistics

All statistical tests were performed using SPSS. Normally distributed data was tested using t-tests and ANOVAs, with interactions explored *post hoc* using tests for simple main effects. Normality of data was tested using Shapiro-Wilk tests, with differences between groups of non-normally distributed data tested using Kruskal-Wallis tests. Correlations between two variables were tested using bivariate Pearson's correlation coefficients. As before, the two-tailed significance value for all tests was set at 0.05, except for simple main effects tests with multiple comparisons, which were adjusted as in 3.2.8 of Chapter 3.

As previously, significance indicators used in figures in this chapter represent, unless otherwise stated: * = $p < 0.05$, ** = $p < 0.01$, *** = $p < 0.001$, n.s. = $p \geq 0.05$, with error bars representing the standard error of the mean. For statistical comparisons, when mean values for two separate groups are provided, unless stated otherwise, the first group represents the non-injected and/or untreated control group, whilst the second group represents the drug-treated or GluR2 virus-transfected experimental group, depending on the experiment.

For the current-voltage relationship experiments, RIs were calculated by comparing response peak amplitude 40 mV above and below the reversal potential. The peak amplitude was taken from the second out of two stimuli delivered at each voltage step going from -70 to +80 mV. Depending on the condition of recorded cells, stimulus-step protocols were given to some cells both going upwards to +80 mV and going down to -70 mV. Cells were included in the analysis if the series resistance during at least one of these protocols remained within a 15% limit of the series resistance between the beginning and the end of the -40/+40 mV rectification window, and if the series resistance did not go above 30 MΩ during this period.

For cells from which recordings were obtained that passed these criteria, an RI value was calculated by dividing the amplitude recorded at +40 mV above the reversal potential to the amplitude recorded at -40 mV below the reversal potential. The normality of the distributions of RI values in the control and GluR2-injected groups was ascertained using a Shapiro-Wilk test. In the case of non-normal distribution of data, to compare rectification properties of cells across the two treatment groups, a Kruskal-Wallis test was used.

Before recording I-V relationships, cells were subjected to a baseline period of stimulation at -70 mV to establish a stable response size. Spontaneous EPSCs were detected and properties analysed using IGOR scripts as in 2.2.4. The mean wave was calculated for detected spontaneous EPSCs recorded from each cell, and from it the average decay rate of EPSCs was determined. Decay rates of EPSCs were determined by fitting a double exponential to the post-peak waveform and calculating the weighted time constant (tau). In addition, the median amplitude and area of EPSCs for each cell was calculated. Differences in amplitude and kinetic properties of spontaneous EPSCs from PV+ cells from control and injected animals were assessed by performing Kruskal-Wallis tests comparing median amplitude and mean weighted tau values across the two groups, due to the non-normal distribution of data. Furthermore, the relationship between the average spontaneous current amplitude, area, and decay time values, and the rectification properties of cells in each treatment group, was ascertained by calculating the bivariate Pearson's correlation coefficient.

For field recordings, baseline properties of slices were calculated by taking the power area and peak frequency (calculated as in Chapter 2) 1 hour after the slice was placed within the recording chamber, averaged across a 1-minute period. Differences between non-injected and GluR2 virus-transfected slice populations for these properties were calculated using between-subjects t-tests. Effects of age on oscillation frequency within each treatment group were determined with the bivariate Pearson's correlation coefficient.

For the pharmacology experiments, power area and peak frequency were compared between the different viral and drug treatment groups at 7 and 10 minutes, due to the time course of the observed effects. Values for both of these properties were calculated minute-by-minute for each slice and the baseline (0 minutes) value was subtracted from these other values. Taking these (X-0 minutes) values for each of the three time points, differences between the treatment groups were

tested for at each time point by using 2 (virus) * 2 (treatment) ANOVAs, and looking for main effects of either variable or interactions between the two. The nature of any significant effect or interaction for either power or frequency at any time point was explored using simple main effects. Simple effects were tested between each of the two groups (viral group and drug treatment group), giving an alpha of 0.15, k of 4, and significance value of 0.04.

For the calcium imaging experiments, template matching was performed to demonstrate the localised stimulation of dendritic Ca^{2+} signals, visualise the spread of Ca^{2+} signalling, and verify hand-selected regions of interest (ROIs). The method was adapted from a previous study investigating detection of spontaneous synaptic events (Clements and Bekkers, 1997). In brief, a template was derived from the average z projection from a manually selected ROI. Before template matching, each image in the stack was first filtered using a 9 x 9 x 3 point box filter (x y z). For each pixel, the template was then scaled and offset to minimise the sum of squared errors between the template and pixel trace. The detection criterion was then calculated as the scaling factor divided by the standard error of the fit. For quantification, ROIs of equivalent size were manually drawn within reactive dendritic regions (identified from responses following 300% stimulation) and adjacent background regions (see Fig. 4.5iv). Exponential curves were fit to the pre-stimulation baseline and subtracted from traces to account for bleaching effects, and then background fluorescence was subtracted from dendritic fluorescence. Normalised changes in dendritic fluorescence were calculated relative to the mean of the pre-stimulation baseline period ($\Delta F/F$), and the areas of the post-stimulation $\Delta F/F$ signals were used for statistical analysis. The same ROIs were used for all stimulations within a given cell, including pre- and post-NASPM/control treatment.

Significant changes in calcium signal with increasing stimulus amplitude were determined using repeated-measures ANOVAs, with the ANOVAs expanded to include treatment with control or drug,

or different cell types. As previously, in conditions where assumption of sphericity was violated, the Huynh-Feldt (H-F) or Greenhouse-Geiser (G-G) corrections were used to alter degrees of freedom in order to reduce Type I error (when $\varepsilon > 0.75$, Huynh-Feldt was used, and when $\varepsilon < 0.75$, Greenhouse-Geiser was used). To determine the nature of any interactions found by the ANOVAs, simple main effects were used. Main effects between treatment or viral groups were tested at each level of input stimulation, giving a k of 4 and a significance value of 0.026. To determine correlation between current size and calcium signal, the bivariate Pearson's test was used. To compare differences in current size or normalised calcium signal between control and transfected cells, independent-samples t-tests were used.

For the plasticity experiment, the average amplitude of evoked currents was calculated for 1-minute time bins. Current amplitudes were normalised to the mean amplitude of evoked currents during the 5-minute baseline period. Significant differences in post-pairing evoked current amplitudes between the control and virus-injected group were determined using a repeated-measures ANOVA for the post-pairing period. To characterise the response during the induction protocol, the traces were smoothed with an 11 point median filter to remove stimulus artefacts, and the peak depolarisation and the mean depolarisation measured during the 1-second train relative to the baseline. The period between initiation of the plasticity recording run and of the of the pairing protocol was used to represent the period between break-in and induction of plasticity.

4.3 Results

4.3.1 Expression of floxed GluR2 virus in the hippocampus of PV-Cre/Ai9 mice

The first step in assessing the success of my viral transfection was to confirm expression of the construct histologically. The construct includes an AU1 peptide tag in the N-terminus of the GluR2 protein. I perfused PV-Cre/Ai9 mutant mice injected with the virus in either ventral or dorsal hippocampus, as well as C57 wild-type mice. Following extraction, brains were sectioned and stained with antibodies targeted against AU1, as well as GluR2. Despite attempts using multiple different anti-GluR2 antibodies, I was unable to get a successful stain giving me any immunoreactivity within the tissue. However, the anti-AU1 antibody reliably delivered immunofluorescence throughout the injected region (Fig. 4.2). The fluorescence was present in the neuropil of the hippocampus, and appeared in both PVCre/Ai9 and wild-type mice (Fig. 4.2A). The origin of this fluorescence in the neuropil of wild-type mice is unclear, as I observed localised cellular expression in sections from PV-Cre/Ai9 mice only, co-localising with tdTomato expression (Fig. 4.2B). Use of a confocal microscope highlighted the non-nuclear expression of the construct, with the fluorescence typically restricted to the extranuclear areas of the soma and to processes protruding from the somata (Fig. 4.2C). Quantification of co-localisation of tdTomato and anti-AU1 fluorescence in cells from one PVCre/Ai9 animal revealed that approximately half of observed PV+ cells in DG and CA3 (identified by tdTomato expression) exhibited immunoreactivity against AU1, with the proportion decreasing when moving through CA1 (Fig. 4.2D). The images in Fig. 4.2C and quantified in Fig. 4.2D were taken from an animal injected with the coordinates used for result sections 4.3.2/4.3.3; expression in CA1 PV+ cells closer to area CA3 increased following the altering of coordinates to better target area CA1 (used for sections 4.3.4/4.3.5 and Chapter 5).

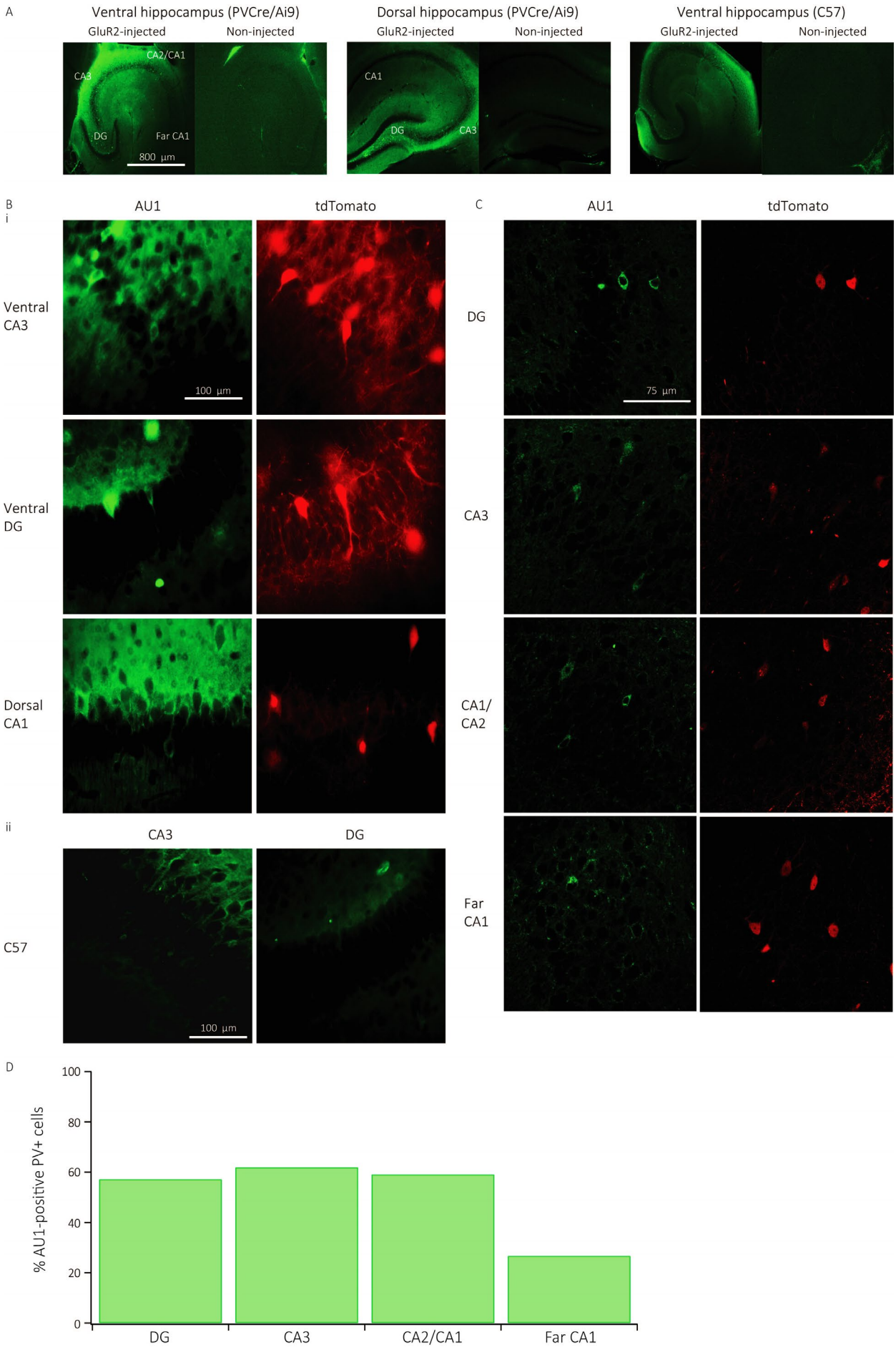
A
Ventral hippocampus (PVCre/Ai9)
GluR2-injected
Non-injected
CA2/CA1
CA3
DG
Far CA1
800 µm
Dorsal hippocampus (PVCre/Ai9)
GluR2-injected
Non-injected
CA1
DG
CA3
Ventral hippocampus (C57)
GluR2-injected
Non-injected
B
i
AU1
tdTomato
Ventral CA3
100 µm
Ventral DG
Dorsal CA1
ii
CA3
DG
C57
100 µm
C
AU1
tdTomato
DG
75 µm
CA3
CA1/ CA2
Far CA1
D
% AU1-positive PV+ cells
100
80
60
40
20
0
DG
CA3
CA2/CA1
Far CA1

Figure 4.2. Expression of the viral construct in hippocampal PV+ cells. (A) Images (5x magnification) acquired from animals injected unilaterally with the floxed GluR2 virus. Left and right panels from each animal present anti-AU1 fluorescence detection in injected and non-injected hemispheres, respectively. From left to right, the images were acquired from: a PVCre/Ai9 mouse injected in ventral hippocampus; a PVCre/Ai9 mouse injected in dorsal hippocampus; and a C57 wild-type mouse injected in ventral hippocampus. (B) (i) Images (40x magnification) exhibiting anti-AU1 immunofluorescence (left) and tdTomato fluorescence (right) acquired from PVCre/Ai9 mice in (from top to bottom) ventral CA3, ventral DG, and dorsal CA1, revealing AU1-immunoreactive PV+ interneurons across sub-fields of both sub-regions. (ii) Anti-AU1 immunofluorescence in wild-type C57 animals in CA3 (left) and DG (right) was weaker than in PVCre/Ai9 animals, without clearly identifiable neurons. (C) Images (40x magnification) acquired using a confocal microscope demonstrating anti-AU1 immunofluorescence (left) and tdTomato fluorescence (right) in a GluR2-injected PVCre/Ai9 animal, taken from (from top to bottom) DG, CA3, CA2/CA1, and far CA1. Fluorescence demonstrates the non-nuclear nature of expression. (D) Quantification of expression across sub-fields using image stacks taken from the section presented in (C). 57.1% (4/7) cells in DG, 61.9% (13/21) cells in CA3, 59.1% (13/22) cells in CA2/CA1, and 26.7% (4/15) in far CA1 exhibited co-expression of tdTomato and AU1.

4.3.2 Transfection of PV+ cells with the floxed GluR2 virus alters rectification properties and spontaneous current kinetics

Following histological confirmation of expression of the viral construct, the next step was to investigate the impact of transfection on the properties of hippocampal PV+ interneurons. One of the clearest identifiers of a cell with an AMPAR population dominated by CP-AMPARs is the marked inward rectification at positive membrane potentials due to depolarisation-induced blockade of channels by polyamine molecules. Transfection of CP-AMPAR-expressing cells with a GluR2-expressing virus has previously shown to reduce rectification of this manner in other cell types (Iino et al., 2001). Therefore, it was believed that investigating the rectification properties of purported transfected interneurons would be a sensible starting point for validating the effectiveness of my viral approach.

TdTomato-expressing PV+ interneurons were patched in stratum oriens of area CA1 of ventral hippocampus in horizontal sections taken from GluR2-injected animals as well as non-injected controls. Additionally, recordings were taken from pyramidal cells in area CA1 of non-injected slices. Due to the nature of the viral construct, I was unable to identify transfected cells prior to patching, as the construct does not contain a fluorescent marker. Unfortunately, I was also unable to identify

transfected cells post-recordings, as the anti-AU1 antibody used for the histology reported in 4.3.1 did not successfully produce a fluorescent signal in any slices stained following *in vitro* experiments performed in this chapter. As such, all cells recorded from slices taken from injected animals were included in the experimental group provided they met the selection criteria (see 4.2.4.3 and 4.2.6 for selection criteria).

Cells were patched in whole-cell voltage-clamp, and were stimulated by an extracellular electrode placed in stratum oriens (for PV+ cells) or stratum radiatum (for pyramidal cells). Following a baseline stimulation period, the cells were subjected to a voltage-step protocol to establish current-voltage relationships. In PV+ interneurons recorded from non-injected control animals (n = 12), a clear reduction in evoked current response amplitude was observed at holding potentials above the reversal potential, whilst pyramidal cells (n = 5) exhibited a linear relationship between holding potential and response amplitude (Fig. 4.3A, B). In contrast, multiple PV+ cells recorded from slices transfected with the GluR2 virus (n = 12) exhibited variable rectification properties, including some cells that expressed a linear current-voltage relationship. The variable viral expression pattern seen in area CA1 in 4.3.1 following injection at the coordinates used in this study may explain the variability in the rectification index (RI) of cells recorded from slices taken from injected animals (Fig. 4.3B). Due to the non-normal distribution of RI values in the experimental group, non-parametric statistics were used to evaluate population changes in rectification properties following injection with the GluR2 virus. An independent-samples Kruskal-Wallis test revealed a significant change in the rectification index of recorded PV+ interneurons from injected animals compared to controls (0.319 ± 0.03 vs 0.557 ± 0.08, $p = 0.013$; Fig. 4.3C).

I was also interested in exploring the amplitude and kinetics of AMPAR-mediated currents. As evoked current amplitudes were determined by arbitrary stimulation parameters, spontaneous

currents were considered more suitable candidates to compare these properties between cells. The decay time, current amplitude, and current area were investigated, as GluR2-containing AMPARs have been shown to exhibit lower peak conductances and slower kinetics than CP-AMPARs (Geiger et al., 1995; Lawrence and McBain, 2003; Swanson et al., 1997; Verdoorn et al., 1991). Kruskal-Wallis tests comparing the median amplitude and mean decay rate (tau) of spontaneous EPSCs detected during the initial 5-minute baseline stimulation period in PV+ cells recorded from control and injected slices did not reveal any significant differences between the two cell types (18.8 ± 2.7 pA vs 14.9 ± 1.1 pA, $p = 0.470$, and tau = 0.0021 ± 0.0003 vs 0.0022 ± 0.0003, $p = 0.862$, respectively; Fig 4.3D). However, given the previously observed variation in rectification properties, it was thought possible that these spontaneous properties might similarly vary, potentially in a way that correlates with the rectification index of each cell.

When plotting median amplitude against rectification index, a significant negative correlation was found, with less rectifying cells exhibiting smaller spontaneous EPSCs ($r = -0.627$, $p = 0.029$; Fig. 4.3Ei). In contrast, the control group showed no correlation between the two variables ($r = -0.166$,

Figure 4.3 (next page). Transfection with floxed GluR2 virus alters rectification properties of AMPA receptor currents in PV+ interneurons. (A) (i) Sample evoked responses from a PV+ interneuron and pyramidal cell from non-injected animals, and a PV+ interneuron from an injected animal, showing responses when held at the reversal potential, and ±40 mV relative to the reversal potential. (ii) Evoked response amplitudes from -70 mV to +70 mV plotted against holding potential for the cells in (i). (B) Histogram plotting rectification index (response amplitude at +40 mV relative to reversal potential:response amplitude at -40 mV relative to reversal potential) of cells in each of the three groups (n = 12, n = 5, and n = 12 cells, respectively), demonstrating the consistent observation of inward rectification in PV+ interneurons from control animals, the typically linear relationship in pyramidal cells, and the diverse spread seen in cells recorded from injected animals, possibly due to transfection of only a subsection of cells. (C) Injection of ventral hippocampus with the floxed GluR2 virus resulted in a significant increase in the population rectification index value of PV+ interneurons recorded from area CA1 compared to those recorded in control slices (0.319 vs 0.557). (D) Sample spontaneous excitatory currents from non-injected and GluR2-injected PV+ neurons (i), and graphs showing the median amplitude (ii) and mean decay rate (iii) of spontaneous currents within each group. The transfected population showed no significant change in amplitude (18.8 pA vs 14.9 pA) or decay rate (0.0021 vs 0.0022). (E) The median amplitude (i), mean decay rate (ii), and median area (iii) of spontaneous events in each cell plotted against rectification index. Control cell population shows no correlation between any of these factors and RI. Injected cells, however, show significant correlation between RI and amplitude ($r = -0.627$) and decay rate ($r = 0.725$). There was no observed correlation between RI and current area in injected cells ($r = -0.294$). * = $p < 0.05$; ** = $p < 0.01$; *** = $p < 0.001$. n.s. = $p \geq 0.05$. Error bars indicate standard error of the mean.

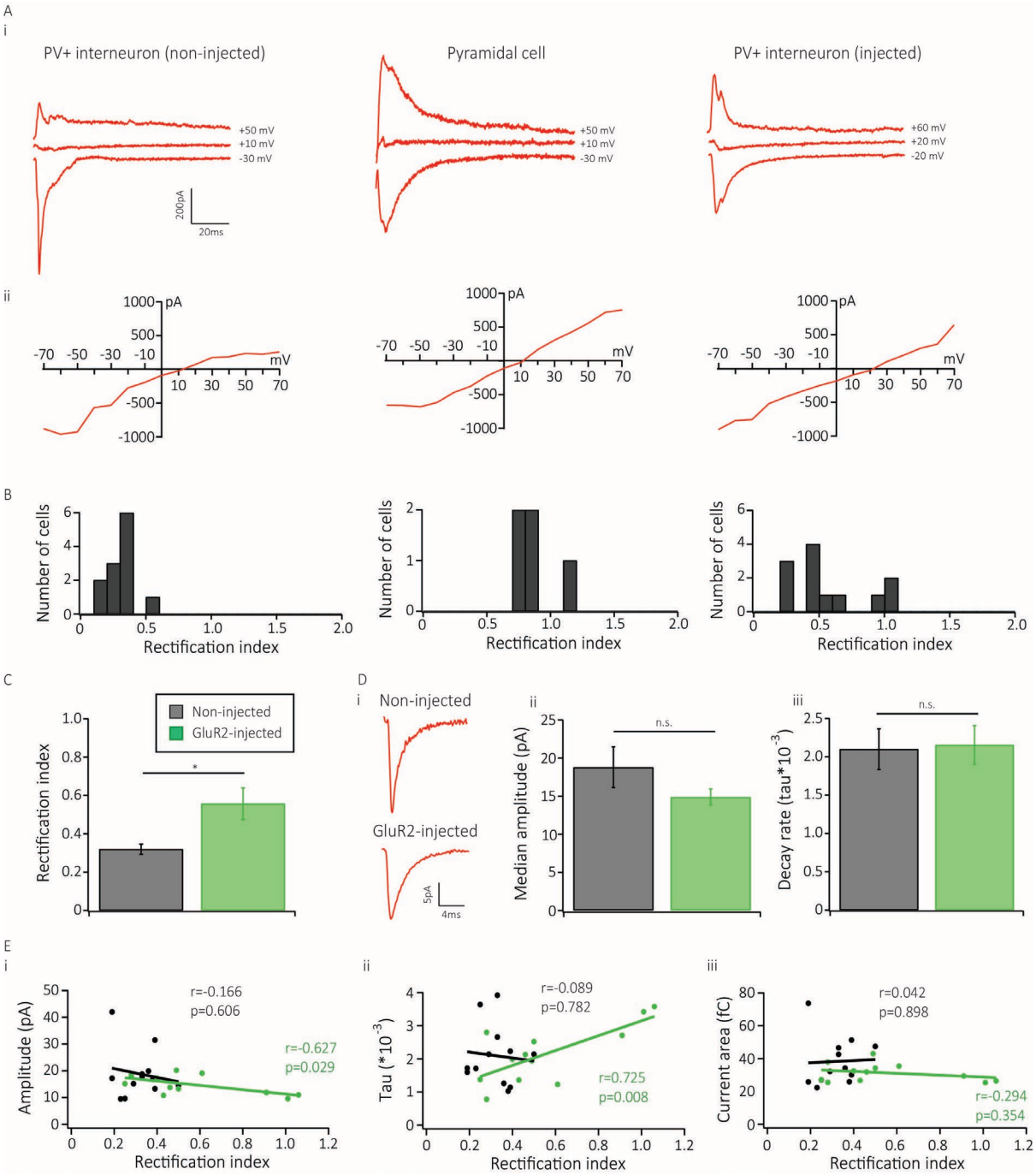

p = 0.606). Similarly, the injected group showed a positive correlation between rectification index and decay rate (r = 0.725, p = 0.008; Fig. 4.3Eii), whilst the control group showed no correlation (r = -0.089, p = 0.782). These results show that interneurons with a rectification profile suggestive of GluR2 incorporation into AMPA receptors also have smaller, slower spontaneous EPSCs than interneurons from injected slices that exhibit a rectification profile typical of CP-AMPAR expression.

The intended goal of the viral transfection approach is to try and reduce calcium permeability through AMPA receptors as much as possible without impacting overall conductance. Whilst peak conductance of spontaneous EPSCs seems to reduce in non-rectifying PV+ cells, the concurrect increase in decay time may work to preserve overall conductance. As such, median area was plotted against rectification index in the same way as for the previous variables, and unlike amplitude and decay rate, was found to not significantly correlate with the RI ($r = -0.294$, $p = 0.354$; Fig. 4.3Eiii); as before, the control group did not show any correlation ($r = 0.042$, $p = 0.898$).

Overall, these findings suggest that transfection with the floxed GluR2 virus generated in this chapter can alter the rectification properties of AMPA currents stimulated in PV+ interneurons in a manner indicative of GluR2 incorporation into AMPA receptors. There is also some evidence that this transfection alters kinetic and dynamic properties of AMPA receptors to reflect those of GluR2-containing AMPA receptors, whilst broadly conserving overall conductance.

4.3.3 Transfection of PV+ interneurons with the floxed GluR2 virus reduces the frequency of gamma oscillations and removes sensitivity to CP-AMPAR-selective pharmacological agents

The contribution of PV+ interneurons to generation of gamma rhythms has been widely studied, particularly *in vitro*. Additionally, the results from Chapter 2 demonstrate the necessity of CP-AMPAR-mediated currents in the maintenance of optimal gamma activity. As such, there were multiple reasons to investigate the properties of *in vitro* gamma rhythms recorded in GluR2 virus-transfected slices. First, any changes in basic oscillation properties may provide insight into any changes seen at a behavioural level. Second, working on the assumption that the changes in gamma power seen following CP-AMPAR antagonist application were, at least in part, mediated by effects

on CP-AMPARs in PV+ interneurons, any resistance to the effects of these compounds would provide further evidence in support of successful replacement of CP-AMPARs with GluR2-containing AMPA receptors following transfection with the virus. Finally, the extent of any resistance would give some insight into the relative contribution of CP-AMPAR activity in hippocampal PV+ interneurons to gamma rhythm maintenance compared to CP-AMPARs in other interneuron classes, e.g. SOM+ interneurons.

As before, horizontal sections of ventral hippocampus were placed in the interface recording chamber and superfused with aCSF containing carbachol, with carbachol-evoked oscillations recorded from area CA3. In order to investigate basic oscillation properties, recordings were taken from slices at a constant time point, 1 hour after first placement in the recording chamber. Baseline data were collected from 33 slices taken from non-injected control mice, and 27 slices from GluR2-injected mice (including multiple slices per animal). No notable change was seen in the baseline power area of gamma-frequency oscillations in the GluR2 slices compared to controls (4.41 ± 0.1 $\log_{10}(mV^2)$ vs 4.45 ± 0.1 $\log_{10}(mV^2)$; $t(58) = 0.413$, $p = 0.681$; Fig.4.4A, B). In contrast, the oscillations recorded from the GluR2 slices had a significantly lower peak frequency than those recorded from controls (35.37 ± 0.6 Hz vs 32.35 ± 0.9 Hz; $t(58) = 3.03$, $p = 0.004$; Fig. 4.4C). The animals from which slices were recorded spanned a range of ages; however, ages were matched between the two groups, and there was no notable correlation found between age and peak frequency in either the control group ($r = 0.262$, $p = 0.14$) or the GluR2-transfected group ($r = -0.075$, $p = 0.709$; data not shown).

After collecting baseline data, the next step was to observe the relative impact of CP-AMPAR antagonism on oscillations recorded from each experimental group. As previously, 100 μM NASPM, or control dH_2O of equivalent volume, was added to the superfusing solution following the 1-hour

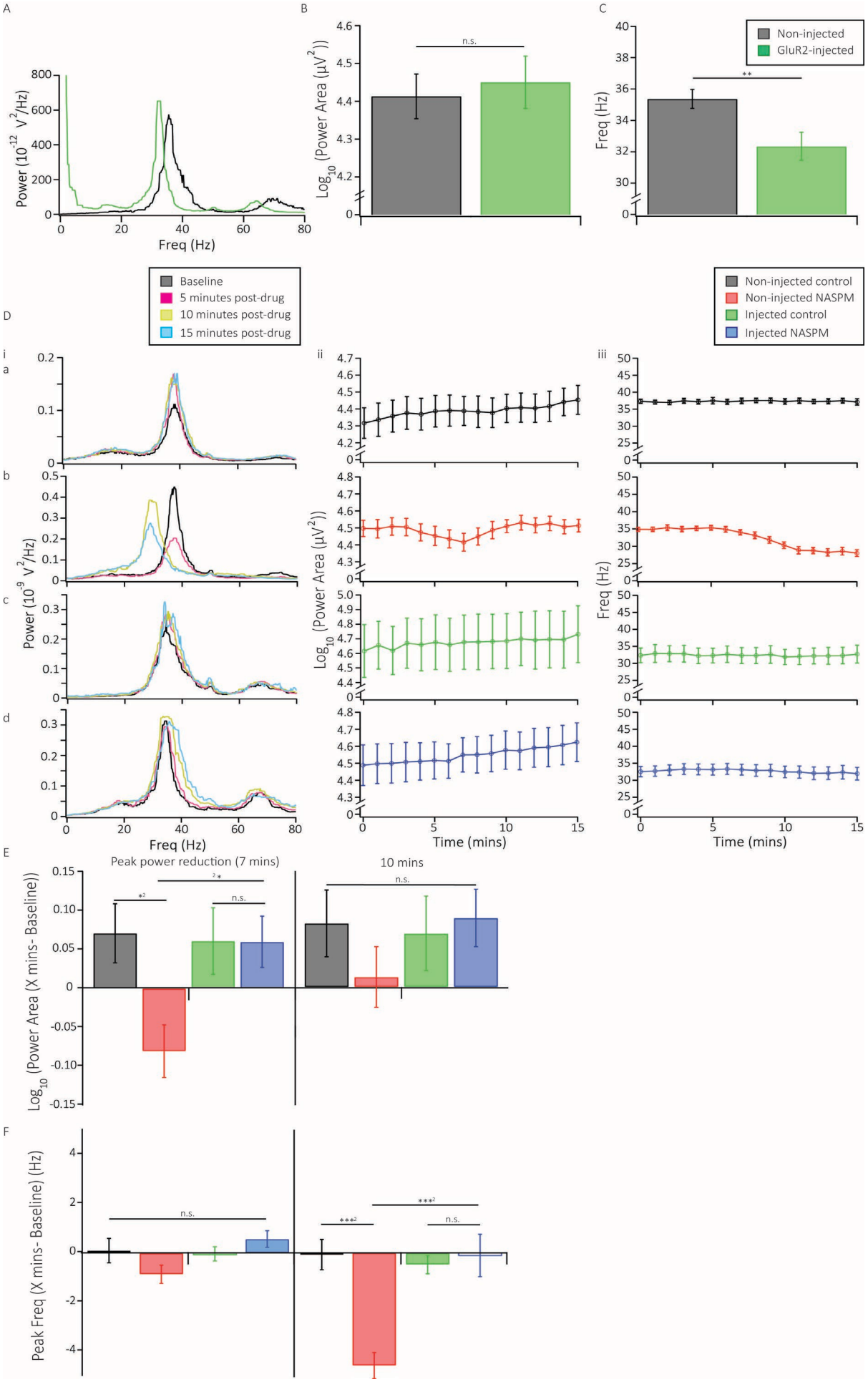
A
B
C
Power (10^{-12} V^2/Hz)
Freq (Hz)
Log$_{10}$ (Power Area (μV^2))
n.s.
Freq (Hz)
**
Non-injected
GluR2-injected
D
Baseline
5 minutes post-drug
10 minutes post-drug
15 minutes post-drug
Non-injected control
Non-injected NASPM
Injected control
Injected NASPM
i
ii
iii
a
b
c
d
Power (10^{-9} V^2/Hz)
Log$_{10}$ (Power Area (μV^2))
Freq (Hz)
Time (mins)
E
Peak power reduction (7 mins)
10 mins
Log$_{10}$ (Power Area (X mins- Baseline))
n.s.
F
Peak Freq (X mins- Baseline) (Hz)
n.s.

Figure 4.4. Transfection of hippocampal PV+ interneurons with the GluR2 virus alters gamma oscillation frequency and removes sensitivity to CP-AMPAR antagonists. (A) Sample power-frequency spectra for a slice from a non-injected animal and one from an injected animal, recorded one hour after first placement in the recording chamber. (B) No significant difference was seen in the power of gamma-frequency oscillations recorded in slices from injected slices (n = 27 slices) compared to controls (n = 33 slices; 4.41 $\log_{10}(mV^2)$ vs 4.45 $\log_{10}(mV^2)$). (C) Oscillations recorded in transfected slices had a significantly lower peak frequency than those recorded from control slices (35.37 Hz vs 32.35 Hz). (D) Sample power-frequency spectra (i), and plots of mean power area (ii) and peak frequency (ii) over 15 minutes following application of either control treatment (a, c) or 100 µM NASPM (b, d) in non-injected (a, b) and GluR2-transfected (c, d) slices. (E) Graph showing changes in gamma power following control or NASPM treatment in the two slice types at 7 and 10 minutes following initial introduction. By 7 minutes, the observed reduction in gamma power recorded from non-injected slices following NASPM application peaked (-0.08 $\log_{10}(mV^2)$), whilst control-treated non-injected slices (+0.07 $\log_{10}(mV^2)$) and both control-treated (+0.06 $\log_{10}(mV^2)$) and NASPM-treated (+0.06 $\log_{10}(mV^2)$) slices showed increases in power compared to baseline. By 10 minutes, the significant reduction in power following NASPM exclusively in non-injected slices had disappeared. (F) Graph showing changes in peak frequency with the same conditions as in (E). No significant changes in frequency occurred in any treatment group during the time period that reductions in gamma power occurred; however, by 10 minutes, a significant reduction in frequency was observed in NASPM-treated non-injected slices (-4.6 Hz) compared to control-treated non-injected slices (-0.1 Hz) or either control-treated (-0.5 Hz) or NASPM-treated (-0.1 Hz) slices taken from injected slices. $*^2$ = $p < 0.04$, $***^2$ = $p < 0.001$.

baseline period. As before, oscillations were recorded for 15 minutes, and changes in power and frequency following drug/control application analysed. 9 non-injected slices were given a control treatment and 11 slices were exposed to NASPM; whilst 7 and 12 GluR2-transfected slices were given the control or drug treatment, respectively. The effects of NASPM on non-injected slices diverged from those seen in 2.3.4 (Fig. 4.4D).

As in Chapter 2, I initially tested the effects of NASPM or control treatment on slices from control and injected animals by subtracting the baseline power area and peak frequency values immediately pre-treatment from the values at 10 minutes post-treatment, and performing an ANOVA on the differentials. A 2 (slice type) * 2 (treatment type) ANOVA did not show a significant main effect of treatment ($F_{(1,35)} = 0.352$; $p = 0.557$) nor slice type ($F_{(1,35)} = 0.555$; $p = 0.461$), nor an interaction between the two variables ($F_{(1,35)} = 1.124$; $p = 0.296$; Fig. 4.4E). However, the results collected in Chapter 2 indicate that exposure to 100 µM NASPM can cause a significant, but somewhat transient, reduction in power of oscillations recorded from slices from non-injected animals, and visual inspection of the minute-by-minute time courses of power area of oscillations recorded from the four groups demonstrate a transient decline in power area exclusively in non-injected slices treated

with NASPM (Fig. 4.4Dii). This transient decline occurred over a faster time course than seen in Chapter 2, with power area bottoming out in NASPM-treated control slices around 7 minutes post-introduction of NASPM.

As a result of this, I repeated the ANOVA with baseline-subtracted power area values at 7 minutes post-treatment, which revealed a significant interaction between slice type and treatment type ($F_{(1,35)} = 4.191$; $p = 0.048$; Fig. 4.5E). Exploring the interaction at 7 minutes further, *post hoc* simple main effects were tested across both viral and treatment groups, setting a significance value of 0.04. These tests revealed a significant decrease in power with respect to baseline following application of NASPM in non-injected slices compared to control treatment (+0.071 ± 0.04 $\log_{10}(mV^2)$ for control treatment vs -0.081 ± 0.03 $\log_{10}(mV^2)$ for NASPM treatment; $F_{(1,18)} = 8.972$, $p = 0.005$); in contrast, there was no significant difference between injected slices treated with control or drug (+0.061 ± 0.03 $\log_{10}(mV^2)$ vs +0.06 ± 0.03 $\log_{10}(mV^2)$, as previously; $F_{(1,17)} < 0.001$, $p = 0.989$). Similarly, whilst there was no significant difference between control-treated non-injected and injected slices ($F_{(1,14)} = 0.029$, $p = 0.865$), NASPM significantly reduced power with respect to baseline in non-injected slices compared to GluR2-transfected slices ($F_{(1,21)} = 9.012$, $p = 0.005$).

In contrast to power area, and the results from Chapter 2, a 2 (slice type) * 2 (treatment type) ANOVA looking at changes in peak frequency at 10 minutes with respect to baseline revealed a strongly significant interaction between slice type and treatment type ($F_{(1,35)} = 12.027$, $p = 0.001$; Fig. 4.4F). Exploring this further with simple main effects revealed a significant reduction in frequency within 10 minutes following NASPM application compared to control treatment in non-injected slices (-0.076 ± 0.7 Hz vs -4.59 ± 0.7 Hz; $F_{(1,18)} = 21.726$, $p < 0.001$) that did not occur with injected slices (-0.49 ± 0.8 Hz vs -0.11 ± 0.6 Hz; $F_{(1,17)} = 0.134$, $p = 0.716$). Additionally, control treatment caused no significant difference in change of frequency between the two slice groups ($F_{(1,14)} = 0.143$,

p = 0.708), whilst NASPM treatment resulted in a significant reduction in peak frequency in non-injected slices compared to injected slices ($F_{(1,21)} = 24.806$, $p < 0.001$). This effect of NASPM upon oscillation frequency had not emerged by 7 minutes, as an ANOVA failed to reveal a main effect of either injection type ($F_{(1,35)} = 2.709$, $p = 0.109$) or drug treatment ($F_{(1,35)} = 0.200$, $p = 0.658$), although a non-significant trend towards an interaction between the two variables was observed ($F_{(1,35)} = 3.869$; $p = 0.057$).

Transfection of hippocampal PV+ interneurons with the GluR2-expressing virus broadly conserves the capacity to generate gamma-frequency oscillations, albeit at lower frequency than in control slices, and protects oscillations from the effects of a CP-AMPAR-selective antagonist. These results provide further evidence that transfection of PV+ interneurons with the virus causes a shift in the cellular AMPAR population towards GluR2-containing receptors, and also suggest that the large majority of the effects of NASPM on hippocampal gamma oscillations are mediated by antagonism of AMPARs on PV+ interneurons.

4.3.4 PV+ interneurons transfected with the GluR2 virus show smaller induced dendritic calcium signals

After establishing the presence of properties indicative of GluR2 incorporation into AMPA receptors (altered rectification properties, NASPM insensitivity), the next step was to more directly investigate the AMPA receptor-mediated calcium conductance in transfected PV+ cells. As mentioned previously, different injection coordinates were used for this section compared to 4.3.2/3, with the intention of targeting greater expression in area CA1. Slices were taken from animals injected with these coordinates as well as non-injected controls and, as in 4.3.2, cells were patched in whole-cell

voltage-clamp with internal solution containing 1 mM spermine. The internal solution also contained 300 µM OGB-488, an indicator that exhibited increased fluorescence following binding with Ca^{2+} ions.

Following entry into whole-cell mode, cells were left until they filled up with OGB-488, such that dendrites were visible. At this point, a stimulating electrode comprising a silver wire electrode located inside a glass micropipette filled with aCSF was positioned next to a fluorescent dendrite. The stimulation amplitude was adjusted until it would consistently evoke a current response above zero (50-150 pA), termed the 'threshold' value. At this point, a protocol was instigated, involving the delivery of three rapid stimuli of increasing amplitude, starting at the threshold value (100%), and subsequently at 150%, 200%, and 300%, with a minimum 1-minute window between each stimulation step. Whilst the stimuli were delivered, the cell was imaged under 470 nm light, and signals resulting from stimulation-induced calcium influx were recorded. Calcium signals were quantified by taking the fluorescence signal from the region of interest next to the stimulation electrode, subtracting the background fluorescence from a non-cellular region during the same time period, and normalising the resultant trace to the signal amplitude in the period immediately pre-stimulation.

Burst stimulation of PV+ cells taken from non-injected animals reliably induced restricted fluorescence indicative of Ca^{2+} entry into dendrites, with increasing stimulation amplitude resulting in larger signals (Fig. 4.5). The signals were typically restricted to the dendritic region immediately next to the tip of the stimulation electrode, as template matching of different cellular sub-regions for changes in fluorescence during the recording window revealed a substantial difference between the fluorescence profile of the region of interest and the rest of the neuron (Fig. 4.5A). Averaged across the recorded cell population (n = 21), the size of the stimulation amplitude had a strongly

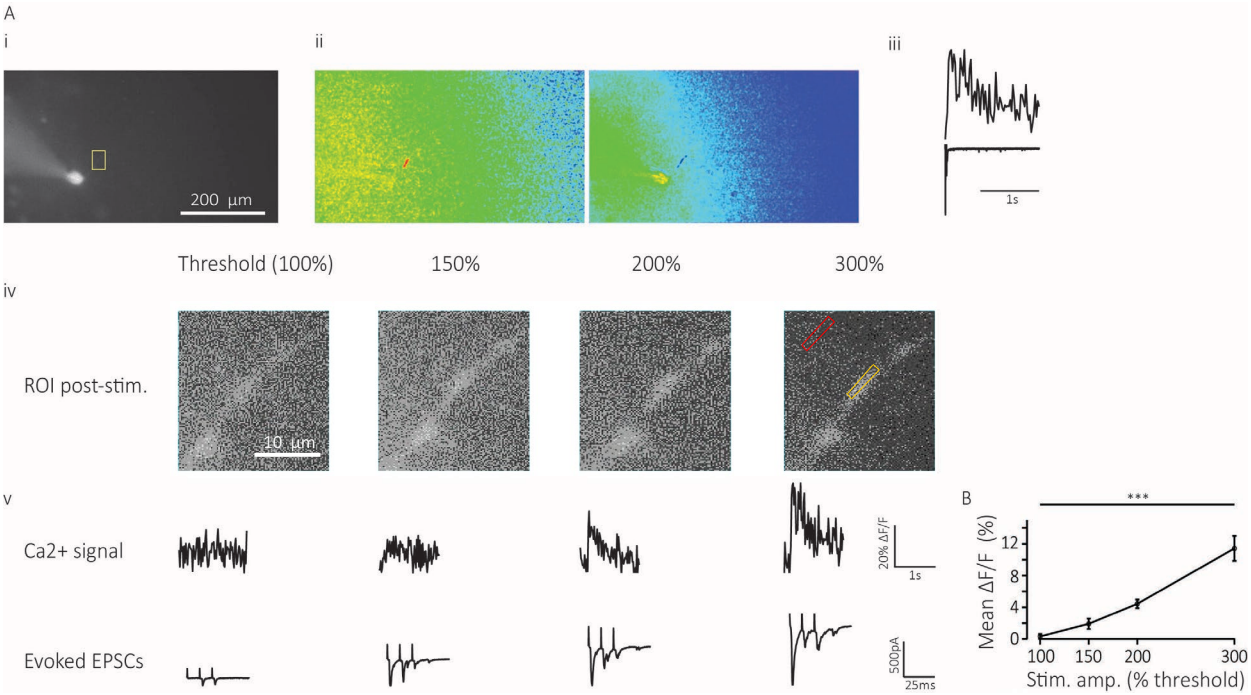

Figure 4.5. Stimulation of calcium signals in PV+ interneuron dendrites with increasing stimulus amplitude. (A) (i) Sample cell filled with OGB-488, with the targeted dendritic region highlighted (yellow box). (ii) Template matching of cellular sub-regions following stimulation at 300% of threshold, demonstrating that the highlighted region in (i) was the only area to exhibit its fluorescence profile during the period of stimulation (left), and was the only region of the cell to substantially diverge from the cell soma (right), revealing the restricted nature of the induced calcium signal. (iii) Relative time course of calcium signal (top) and post-synaptic current (bottom) following 300% stimulation. (iv) Images showing the change in fluorescence of the dendritic region of interest immediately following stimulation at 100%, 150%, 200%, and 300% of the threshold, respectively. The regions of interest used to calculate dendritic and background fluorescence are indicated by yellow and red boxes, respectively. (v) Calcium signals and evoked currents following the same stimulations. (B) Increase in evoked calcium signal with rising stimulation amplitude averaged across the non-injected control PV+ interneuron population. Change in ΔF/F is calculated as area of the evoked calcium signal following baseline fluorescence subtraction.

significant effect on the detected calcium signal (no assumption of sphericity ($\chi^2(5) = 34.999$, $p < 0.001$, G-G $\varepsilon = 0.476$); $F_{(1.428,28.556)} = 46.33$, $p < 0.001$; Fig. 4.5B). The signal increased up until a mean ΔF/F of 11.42 ± 1.6% at 300% stimulation.

After consistently evoking stimulus-dependent calcium signals in PV+ cell dendrites, I next decided to see whether use of a CP-AMPAR-selective antagonist could reduce the signal. Following completion of the initial stimulation protocol, either 100 µM NASPM or control dH_2O was added to the perfusing solution and, due to the reported activity-dependent nature of CP-AMPAR blockade by NASPM, the cells were stimulated at threshold every 15 seconds for 10 minutes to promote inhibition. The cells

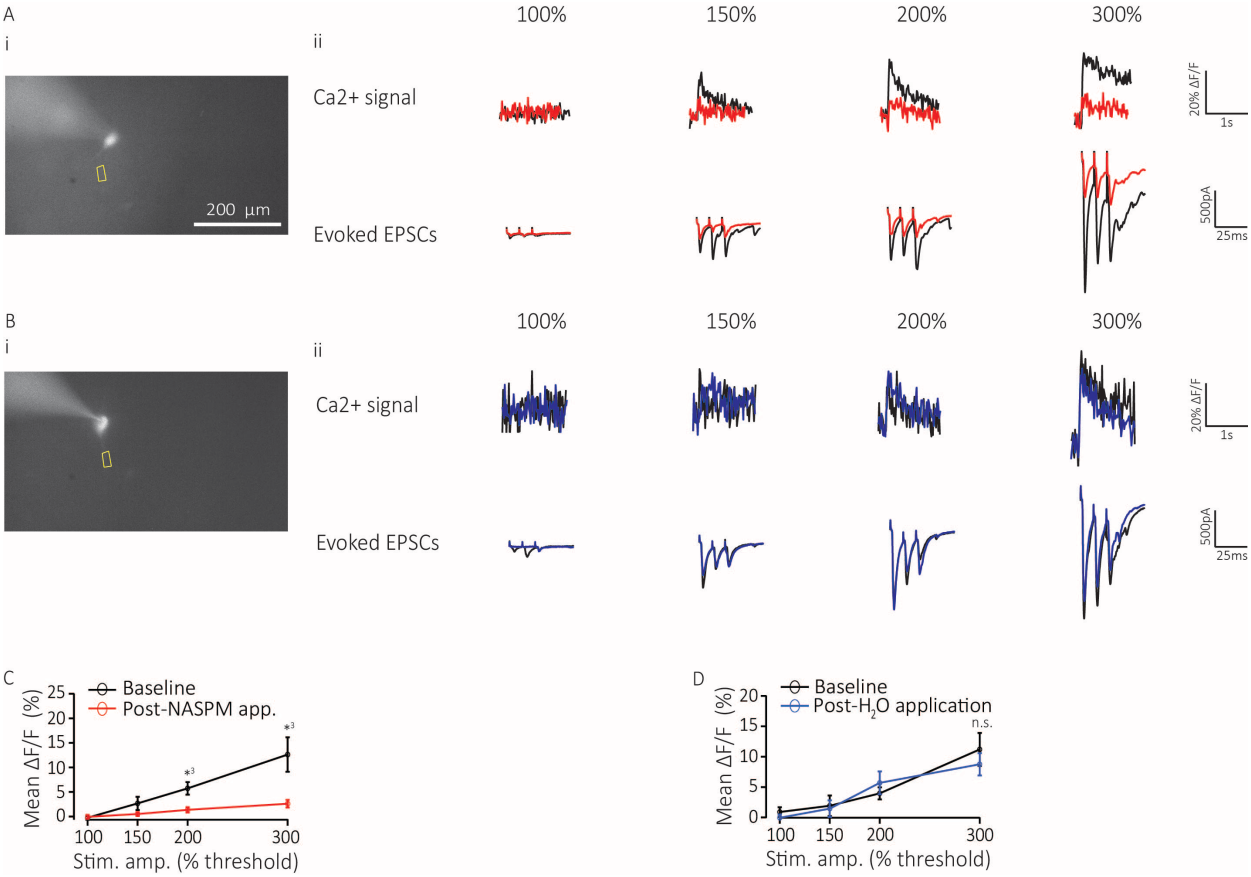

Figure 4.6. The application of a CP-AMPAR antagonist impairs the induction of dendritic Ca^{2+} signals. (A) Sample traces from a cell before (black) and after (red) treatment with 100 µM NASPM. (B) Sample traces from a cell before (black) and after (blue) treatment with an equivalent volume of control H_2O. (C) NASPM treatment significantly reduces amplitude of Ca^{2+} signals stimulated in dendrites, whilst (D) control treatment with H_2O has comparatively little effect. $*^3$ = $p < 0.026$; $***^3$ = $p < 0.001$.

were subsequently subjected to the same stimulation protocol as before, with the 'threshold' stimulation kept at the same amplitude as prior to application of drug/control treatment.

Treatment with NASPM caused a substantial reduction in Ca^{2+} signal amplitude (Fig. 4.6A, C). Averaged across 7 cells, a 2 (before/after treatment) * 4 (stimulation amplitude) within-subjects repeated-measures ANOVA revealed a significant effect of treatment ($F_{(1,6)} = 8.07$, $p = 0.03$), as well as a significant interaction between treatment and stimulus size (no assumption of sphericity ($\chi^2(5) = 15.027$, $p = 0.012$, G-G $\varepsilon = 0.416$); $F_{(1.247,7.48)} = 7.588$, $p = 0.002$). *Post hoc* simple main effects (with a significance value of 0.026) revealed that whilst NASPM treatment did not cause a significant effect to ΔF/F up to 150% stimulation (2.7 ± 1.3% vs 0.5 ± 0.4%; $F_{(1,6)} = 1.855$, $p = 0.222$), by 200%, NASPM

treatment had caused a substantial reduction in the calcium signal (5.7 ± 1.3% vs 1.4 ± 0.5%; $F_{(1,6)}$ = 13.754, p = 0.01). In comparison, control-treated slices (n = 6 cells) did not show an effect of treatment ($F_{(1,5)}$ = 0.179, p = 0.69), nor an interaction ($F_{(3,15)}$ = 1.82, p = 0.187; Fig. 4.6B, D).

After establishing the ability to stimulate calcium transients in PV+ dendrites that are sensitive to CP-AMPAR blockade, the same protocol was then used to attempt to stimulate calcium signals in PV+ cells from virally-injected animals. It was found that repeating the stimulation protocol did not reliably trigger calcium transients in GluR2-transfected PV+ cells, even with similarly large evoked EPSCs as those seen in control cells that exhibited sizeable calcium signals (Fig. 4.7A, B). A subset of cells recorded from injected animals still showed similar calcium profiles to those from control animals, but these were a minority (Fig. 4.7C). Overall, the population of cells from GluR2-transfected slices (n = 16 cells) exhibited significantly reduced calcium signals compared to control slices (n = 21 cells; Fig. 4.7D). A 2 (viral treatment) * 4 (stimulus amplitude) ANOVA revealed a significant main effect of virus ($F_{(1,35)}$ = 11.042, p = 0.002), and a strongly significant interaction between stimulus size and viral treatment ($F_{(3,105)}$ = 10.715, p < 0.001). This interaction was predominantly due to the difference between the two groups that emerged at 300% stimulus amplitude (11.4 ± 1.3% vs 3.4 ± 1.5 mean ΔF/F; $F_{(1,35)}$ = 15.425, p < 0.001).

For both cell types, the initial threshold stimulation amplitude was targeted between 50-150 pA. However, variation between evoked currents between the two groups is possible, and any effects

Figure 4.7 (next page). GluR2 transfection reduces the size of Ca^{2+} transients recorded in PV+ cell dendrites. (A) Sample calcium signals and evoked EPSCs from a control cell at 100%, 150%, 200%, and 300% threshold stimulation, and (B and C) sample traces from transfected cells with the same stimulations. (D) Transfection of PV+ cells with the GluR2 virus causes a significant reduction in calcium signal size at high stimulation amplitudes. (E) (i) The initial stimulation amplitudes were not significantly different between the two groups, however, at 300% (ii) there was a significant difference in the area of evoked currents between the two groups. However, current area and calcium signal were not significantly correlated in either group at 300% stimulation, and (iii) when normalised by the current area, the calcium signal was still significantly larger in control cells compared to transfected cells. (F, G) Neither control treatment or 100 µM NASPM exposure had a significant effect on calcium signals recorded from dendrites of PV+ interneurons transfected with the GluR2 virus. ***[3] = p < 0.001.

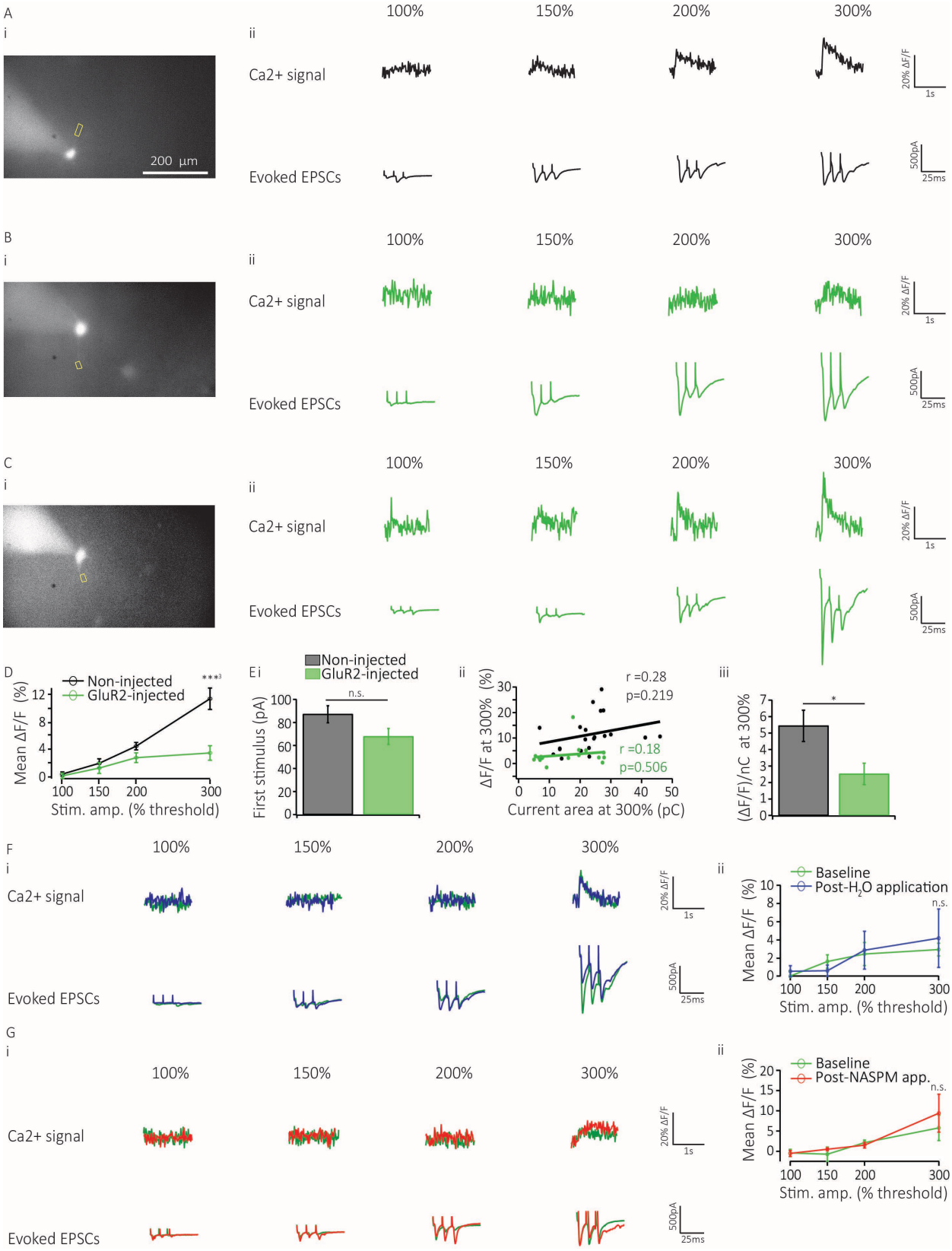

this may have had on the calcium signal amplitudes needs to be controlled for. Taking the first stimulus at 100% threshold stimulation for the two groups, the mean was larger in the control group, but not significantly so (87.1 ± 9.6 pA vs 67.86 ± 7.4 pA; t(35) = 1.504, p = 0.141; Fig. 4.7Ei). By

300% stimulation amplitude, a significant difference had emerged between the sizes of the evoked current responses by area between the two groups (23.26 ± 2 pC vs 15.76 ± 2.2 pC; $t(35) = 2.514$, $p = 0.017$). The lower conductance may be due to the presence of GluR2-containing AMPA receptors compared to CP-AMPARs. However, neither the control group nor the GluR2 group exhibited a significant correlation between current area and calcium signal ($p = 0.219$ and $p = 0.506$, respectively; Fig. 4.7Eii). Furthermore, when normalised for evoked response size (dividing $\Delta F/F$ by current area), the calcium signal was still significantly larger in PV+ cells from control animals compared to those from GluR2-injected animals, underlining the difference in Ca^{2+} conductivity between the two cell types ($t(35) = 2.377$, $p = 0.023$; Fig. 4.7Eiii).

The effect of NASPM on the reduced calcium signal elicited in transfected PV+ cells was investigated, with the same drug/control treatment applied as before (n = 7 cells for control, n = 5 cells for drug recordings; Fig. 4.7F, G). Neither treatment had a significant effect on the calcium signal ($F_{(1,6)} = 0.057$, $p = 0.819$ for H_2O and $F_{(1,4)} = 0.822$, $p = 0.416$ for NASPM), nor were there significant interactions between stimulus size and treatment for either condition (no assumption of sphericity ($\chi^2(5) = 18.714$, $p = 0.003$, G-G $\varepsilon = 0.383$); $F_{(1.149,6.895)} = 0.201$, $p = 0.701$ for control, ($\chi^2(5) = 13.217$, $p = 0.03$, G-G $\varepsilon = 0.363$); $F_{(1.089,4.357)} = 0.471$, $p = 0.544$ for NASPM). The lack of effect by NASPM suggests that the remaining calcium signal in transfected cells may be at least partly mediated by other cellular components than AMPA receptors.

Overall, the results in this section indicate that the transfection of PV+ cells with the Cre-dependent GluR2 virus alters the Ca^{2+} conduction properties of dendrites in these cells, potentially as a result of replacement of CP-AMPARs with GluR2-containing AMPA receptors. Together with the results in the previous sections, the data thus far in this chapter lend support to the hypothesis that my virus is

successfully introducing the edited GluR2 subunit into PV+ cells and causing a physiologically significant shift in the AMPA receptor profile.

4.3.5 PV+ interneuron plasticity

The previous experiments demonstrate that transfection with the GluR2 virus alters the population AMPA receptor properties of PV+ interneurons in a way that is indicative of replacement of CP-AMPARs with GluR2-containing receptors. The final step was to then assess whether removing the calcium permeability of AMPA receptors in PV+ interneurons impaired the induction of excitatory plasticity at inputs onto these cells. Previous studies have shown that, due to the rectification properties of CP-AMPARs, PV+ interneurons exhibit 'anti-Hebbian' plasticity at glutamatergic inputs, i.e. plasticity occurs when there is pre-synaptic activity in the absence of post-synaptic depolarisation (Lamsa et al., 2007). As such, we set out to achieve a set-up in which we could reliably induce potentiation of post-synaptic responses in PV+ cells, and then investigate this potentiation was diminished or absent in PV+ cells from transfected slices. Data acquisition for these experiments was achieved in part by my supervisor, Ed Mann, and in part by a MSc project student in the lab, Mina Moniri.

As in 4.3.2, CA1 PV+ interneurons were recorded in whole-cell mode, with a stimulation electrode positioned in stratum oriens. However, during this study the cells were recorded in current-clamp mode, with slow injection of current used to maintain the membrane potential at approximately -70 mV. The stimulation amplitude was adjusted to reliably evoke excitatory post-synaptic potentials (EPSPs) of less than 10 mV (Fig. 4.8Ai). Once a stable baseline of EPSP amplitude was recorded for 5 minutes (with a 15-second interval between stimulations), the cell was hyperpolarised to -90 mV,

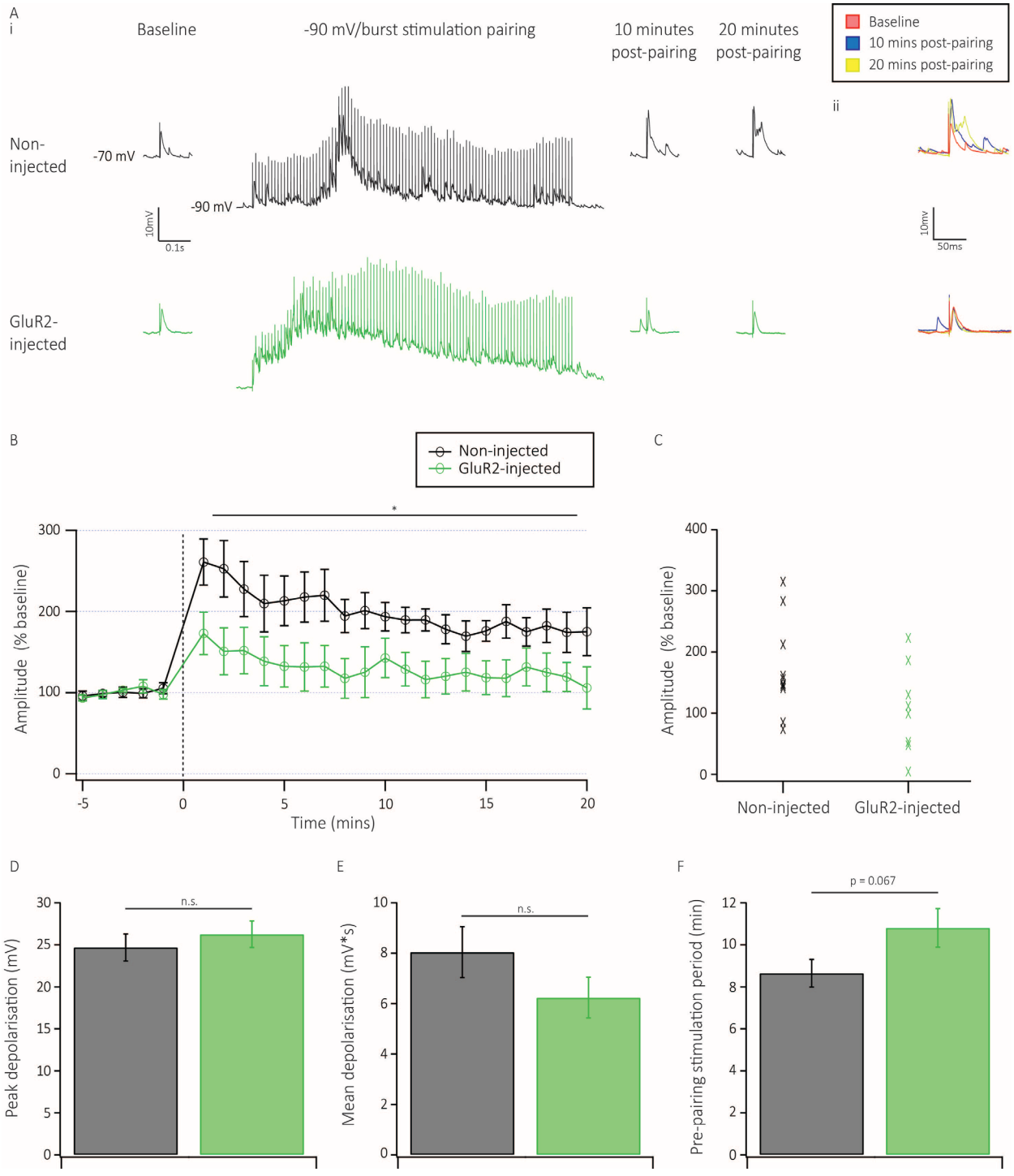

Figure 4.8. Transfection of PV+ cells with GluR2 impairs the ability to induce anti-Hebbian plasticity at excitatory inputs onto these cells. (A) Representative traces from cells taken from non-injected (top) and injected (bottom) animals. (i) Post-synaptic potentials are evoked at -70 mV during the baseline period, before the membrane potential is shifted to -90 mV and paired with burst stimulation. The cell is then returned to -70 mV and stimulated for 20 minutes. (ii) Overlays of example response traces taken from the baseline period, and 10 and 20 minutes post-pairing. (B) EPSP amplitude is normalised to the baseline period and binned into 1-minute time bins, revealing a consistent potentiation of responses in control cells that is absent in cells recorded from animals injected with the GluR2 virus. This potentiation is persistent throughout 20 minutes of post-pairing stimulation (172% baseline amplitude at 20 minutes vs 106.9%). (C) The spread of normalised mean amplitudes of evoked EPSPs 20 minutes post-pairing for each group. (D, E) No significant difference was observed between the (D) peak and (E) mean depolarisation during high-frequency stimulation at -90 mV. (F) A trend towards a significant difference in the duration of the period between initiation of recording and high-frequency stimulation pairing was observed between the two groups (8.65 min vs 10.81 min).

-70 mV. The cell was then stimulated every 15 seconds for 20 minutes.

To assess the effect of this burst stimulation-hyperpolarisation pairing protocol on post-synaptic activity, the peak amplitude of evoked EPSPs was recorded and normalised to the mean baseline amplitude, before being averaged across 1-minute time bins (Fig. 4.8B). PV+ cells from non-injected slices (n = 10 cells) reliably exhibited post-pairing potentiation of responses that persisted throughout the 20-minute post-pairing period (mean response amplitude at 20 minutes is 172 ± 24.6% of baseline). In contrast, PV+ cells from slices taken from animals injected with the GluR2 virus (n = 8 cells) did not reliably replicate this potentiation of post-synaptic potentials (mean amplitude at 20 minutes of 106.9 ± 25.8%). A 2 (virus) * 20 (time bin) repeated-measures ANOVA for the post-pairing period reveals a significant main effect of virus on % change of evoked EPSP amplitude relative to baseline ($F_{(1,16)} = 5.967$, $p = 0.027$), with no interaction between viral group and time bin.

As observed in Fig. 4.8A, a degree of sustained depolarisation was observed during high-frequency stimulation in some cell types. As the pairing protocol relies upon hyperpolarisation of neurons to induce anti-Hebbian plasticity, the potential influence of depolarisation on the difference in potentiation observed between the two groups was explored. As seen in Fig. 4.8D and E, neither the peak (24.68 ± 1.6 mV vs 26.28 ± 1.6 mV) nor mean (8.04 ± 1 mV*s vs 6.24 ± 0.8 mV*s) depolarisation was significantly different between the control and injected groups ($t(16) \leq 1.333$, $p > 0.2$). Additionally, there was no correlation between either variable and the normalised mean amplitude of evoked EPSPs observed 20 minutes following pairing, either for each group individually or together ($p > 0.1$).

The experiments performed in this section of the thesis involved whole-cell recordings from cells; however, plasticity experiments are typically performed using perforated patch clamp, to minimise the impact of washing out cells on the signalling cascades required for induction of plasticity. To attempt to investigate any influence on wash-out of cells on the results of the study, the period between initiation of recordings and induction of plasticity was analysed (Fig. 4.8F); however, as experiments were performed by three individuals, I cannot guarantee that all recordings were begun immediately following break-in, so this is a sub-optimal indicator for this purpose. Nevertheless, a non-significant trend towards an increased time between break-in and stimulation pairing was seen for the injected cell group compared with the control group (8.65 ± 0.7 min vs 10.81 ± 0.9 min; $t(16) = 1.962$, $p = 0.067$); however, no correlation was observed for either group between the duration of the pre-pairing period and the post-pairing evoked amplitude at 20 minutes ($p > 0.2$).

The results from this experiment reveal that transfection of PV+ cells with the GluR2 virus impairs the induction of anti-Hebbian potentiation of responses, in a manner consistent with the loss of calcium permeability of AMPA receptors in these cells. Overall, the data from this series of experiments provide substantial evidence that the virus is successfully transfecting PV+ cells and altering their AMPA receptor composition such that their AMPAergic activity profile is representative of a GluR2-containing AMPA receptor-dominated population. Without having substantial effects on overall conductance, this transfection impairs calcium permeability and resultant plasticity at excitatory inputs onto these cells, enabling me to take this approach *in vivo* to assess the impact of impairing excitatory plasticity in PV+ cells on behaviour and memory.

4.4 Discussion

The work in this chapter involved the creation of a viral construct to drive Cre-dependent expression of the edited form of GluR2, and characterisation of its expression and effects on cellular, synaptic, and network physiology. It was found that the virus could be selectively expressed in Cre-expressing cells, such as PV+ cells in the experimental mouse line used in this study, and caused significant changes to rectification properties of these cells, network sensitivity to selective AMPAR antagonists, dendritic calcium influx, and induction of synaptic plasticity. All these results lend support to my hypothesis that artificial overexpression of GluR2 in PV+ interneurons will lead to incorporation of synthesised GluR2 into AMPARs and a shift in the AMPAR profile of transfected neurons. Following this validation, the next step is to move the experiments *in vivo* and test the consequences of this manipulation on animal behaviour.

The experiments performed within this chapter involved comparison of cells and slices transfected with the previously described floxed GluR2 virus against cells and slices from animals that did not undergo surgery. Whilst the results observed during the various experiments performed in the chapter make logical sense based upon existing knowledge of the properties of GluR2-containing and -lacking AMPARs, the influence of stress, physical damage, or other complications resulting from surgery and intrahippocampal infusion on cellular or network properties cannot be discounted with a naïve control group. As such, repeating the experiments with a control group receiving sham injections or a reporter virus such as the one used in the following chapter would add additional support to the conclusion that the observed significant results were due to alterations in cellular properties resulting from GluR2 expression, rather than surgical confounds.

Additionally, the potential effects of constitutive GluR2 expression on the regulation of other genes merit consideration. The expression of other genes related to AMPAergic signalling was not investigated in transfected neurons, nor in previous studies artificially driving GluR2 expression in different cell types (Iino et al., 2001; Ishiuchi et al., 2002); however, calcium signalling is known to regulate neuronal gene expression (West et al., 2001). Therefore, long-term alterations in the capacity of PV+ interneurons to permit Ca^{2+} influx may alter the Ca^{2+} profile of cells in ways that extend beyond Ca^{2+} signals generated in response to typically plasticity-inducing input, causing more substantial alterations to the expression profile of cells. Additionally, although the limited data regarding spontaneous conductances in transfected cells acquired during the rectification experiments suggest that the effects on overall AMPAR-mediated currents are small, it is possible that artificial, constitutive expression of GluR2 could induce physiologically relevant changes in the expression of other ionotropic glutamate receptor subunits. Nevertheless, I believe that the changes in neuronal activity reported following transfection that are reported in this chapter are primarily due to the altered composition of AMPARs in PV+ interneurons.

The inclusion of an AU1 peptide tag in the N-terminus of the construct enabled histological identification of viral expression. Immunoreactivity against this peptide in animals injected with the virus revealed diffuse immunofluorescence in the neuropil of the hippocampus, even in wild-type animals without expression of Cre recombinase in any cell types. The reason for this apparently leakiness of expression in the neuropil is unclear, given the lack of cellular immunoreactivity in these wild-type mice. Cell-specific fluorescence in PVCre/Ai9 mice co-localised with tdTomato expression, highlighting that these neurons were Cre-expressing PV+ interneurons, indicating that viral expression is Cre recombinase-dependent. The expression was typically absent in cell nuclei, and instead located in the surrounding cytosol, the cell surface, and processes projecting from the cell soma (when visible). This pattern of expression is consistent with the predicted expression pattern

of a subunit synthesised and stored in the endoplasmic reticulum, assembled into AMPARs, and trafficked to synapses in dendrites (Araki et al., 2010; Isaac et al., 2007). The histology offers sufficient evidence to have confidence that any electrophysiological consequences following transfection with my viral agent are the results of expression of the GluR2 construct and its incorporation into AMPARs.

The injection coordinates used for the histology presented in 4.3.1 were also used for the experiments performed in 4.3.2/4.3.3. Figure 4.1 reveals a gradual decrease in the proportion of PV+ cells immunopositive for AU1 when moving from CA3 through CA1. Given that the neurons recorded in 4.3.2 were located in CA1, the split distribution of cells from transfected slices when defined by rectification properties is not a surprise. However, despite this partial coverage, sufficient PV+ interneurons were recorded from that exhibited a linear current-voltage relationship as to deliver a significant effect of the virus. The fact that transfection was capable of converting PV+ cells into expressing a current-voltage relationship comparable to those seen when recording from pyramidal cells within the same region suggests that GluR2 inclusion in AMPARs following transfection is sufficient to replicate the AMPAR profile observed in pyramidal cells, which do not exhibit anti-Hebbian LTP.

The viral expression pattern following transfection with the coordinates used for the rectification experiment was only fully determined after the completion of the experiments. The restricted coverage of CA1 PV+ interneurons, combined with the inability to identify transfected cells either prior to or following recording, added a limitation to the experiment. The experiment was also hindered by the difficulty of reliably recording current-voltage relationships with multiple stimulations at each step. The protocol I initially used involved delivering 5 stimuli at each 10 mV step before moving to the next step; however, the large majority of cells recorded in this manner

were either lost or exhibited excessive drift in series resistance prior to completion of recording. In an attempt to increase the ability to acquire data at positive membrane potentials from cells, the protocol was adjusted such that only two stimuli were delivered at each step. The pitfall of this approach is the decreased reliability of data points at each step, with only one data point included at each step for analysis due to concerns over the influence of adjusting the holding potential on the first stimulated response. As was observed with the pharmacology recordings in Chapter 2, considerable variation can be observed between two individual evoked EPSCs, even with the same holding potential and stimulation amplitude. As such, interpretation of the results in 4.3.2 have clear confounds. Future experiments would be notably improved by altering the experimental set-up such that multiple responses could be detected and averaged across at each step for each cell to minimise the influence of fluctuations in individual responses. One potential approach could be to decrease the number of steps and increase the step amplitude, to reduce the amount of times cells must be recorded from. An increase in the sample size would also be of clear benefit.

The diverse properties of transfected PV+ cells from which recordings were made during the rectification experiment meant that no population differences were detected in the properties of spontaneous excitatory currents when compared to cells recorded from non-transfected slices. However, I observed correlations between the rectification indices of (injected, but not non-injected) PV+ interneurons and both spontaneous current amplitude and decay rate, with smaller amplitudes and slower current kinetics with more linear current-voltage relationships. This is not a surprising finding, given that GluR2-containing AMPARs have been shown to have slower channel kinetics and smaller conductances than CP-AMPARs (Geiger et al., 1995; Lawrence and McBain, 2003; Swanson et al., 1997; Verdoorn et al., 1991). However, these two changes seemed to somewhat cancel out, as the current area of EPSCs did not correlate with rectification index. These results suggest that, despite the inevitable change in channel properties arising from altered subunit

composition, my manipulation may only have a minor impact upon overall synaptic drive to PV+ interneurons.

Transfection of PV+ cells with the edited GluR2 construct did not impair the ability to generate carbachol-evoked gamma-frequency oscillations in area CA3 of hippocampus *in vitro*. Furthermore, there was no notable shift in the power of recorded oscillations in transfected slices compared to control slices. This preservation of network activity suggests that the manipulation has not resulted in substantial changes in the excitability of PV+ cells, given the reductions in gamma power I previously observed in Chapter 2 with pharmacological inhibition of CP-AMPARs, or that other groups reported with PV+ interneuron-specific GluR1 knockout (Fuchs et al., 2007). However, I did see a small but significant shift in the peak frequency of recorded oscillations in GluR2-transfected slices compared to controls. One explanation for this reduced frequency is the fact that GluR2-containing AMPARs have slower kinetics than CP-AMPARs, and as such their presence as the dominant mediator for fast excitation at synapses onto these cells makes them slower to fire, resulting in a decline in oscillation frequency. However, whilst GluR2-containing AMPARs have slower deactivation kinetics than CP-AMPARs, they have been reported as having identical activation kinetics (Grosskreutz et al., 2003).

When I attempted to repeat the experiments from Chapter 2 involving application of NASPM to oscillating hippocampal slices, I saw a discrepancy in the time course and extent of effects compared to previously (possible reasons for this will be discussed in Chapter 6). In comparison to the results in Chapter 2, I saw a faster and shorter decline in gamma power, bottoming out by 7 minutes, with a restoration of power to baseline levels by 10 minutes. These experiments demonstrated the difficulty of performing pharmacological experiments on a non-stable baseline. The 'temporal evolution' reported throughout this thesis and others was a consistent feature of gamma activity in

my set-up (Zarnadze, 2016). Nevertheless, attempts to determine the contribution of drug treatment to changes in power on a dynamic baseline are inherently difficult, due to existing variability occurring with baseline activity. It is possible that the effects of NASPM could become more visible in a more stable set-up.

Furthermore, whilst I had previously seen small, non-significant decreases in oscillation peak frequency in some sections following NASPM, this time I saw reliable and substantial decreases in frequency within 10 minutes. This decline began after the peak decrease in gamma power, so unlike the simultaneous changes observed following PhTx-74 application in Chapter 2, the effects on power and frequency of NASPM do still appear to be at least partially independent processes. Nevertheless, these effects following NASPM treatment were not observed in GluR2-transfected slices, indicating substantial resistance to the effects of this compound. There are multiple implications of this finding; the resistance to NASPM further supports the hypothesis of a significant alteration in the AMPAR profile of PV+ cells such that CP-AMPARs are replaced with GluR2-containing receptors following viral transfection, whilst also indicating that the effects of CP-AMPAR-selective antagonists on hippocampal gamma-frequency oscillations are primarily a result of their antagonism of CP-AMPARs on PV+ interneurons, not on other cell types such as SOM+ interneurons. Additionally, given the partial coverage of PV+ interneurons in area CA3 of injected hippocampus observed in Fig. 4.2, the results may further indicate the potential redundancy within the hippocampal network regarding the effects of CP-AMPAR inhibition. As discussed in Chapter 2, the dose of NASPM required to reliably elicit network changes is substantially larger than the reported IC_{50}; therefore, it was suggested that blockade of a large proportion of the CP-AMPARs or alteration in activity of a large percentage of PV+ interneurons is necessary to transform activity across the network. If transfection of only a portion of the interneurons in area CA3 is sufficient to reduce sensitivity to the effects of NASPM such that the control and drug-treated GluR2 slices are not significantly different, it is possible that

there is substantial redundancy built within to the network to compensate for changes in AMPAergic activity. Overall, these experiments were a demonstration of the selective nature of transfection, in sufficiently conserving overall excitability as to not significantly alter the capacity to generate gamma oscillations or affect oscillation power, whilst still altering AMPAR properties so as to generate insensitivity to the effects of CP-AMPAR antagonists.

In order to stimulate calcium influx in dendrites, I repeated a protocol used elsewhere, involving the delivery of high-frequency bursts of three stimuli, starting at the threshold for evoking post-synaptic currents and progressively increasing the amplitude of stimulation (Camiré and Topolnik, 2014). Using this technique, I was able to reliably induce NASPM-sensitive calcium signals of increasing amplitude with increasing stimulus input size. I did not consistently elicit similar signals in cells from animals injected with my GluR2 virus. One factor to take into consideration was the smaller evoked currents following high-amplitude stimulation in these cells compared to controls, which may have been a consequence of a slightly smaller average threshold response size. However, the difference in response amplitude to threshold stimulation was not significant across the population of recorded cells compared to control cells, and with 300% threshold stimulation there was no correlation between the area of evoked currents and the recorded calcium signal. Furthermore, when normalised for evoked current the calcium signal was still significantly larger for control cells compared to transfected cells. Therefore, there is strong evidence from my work that dendritic calcium currents are substantially reduced following transfection of the virus.

Our final validation step was to see whether this altered rectification profile, NASPM resistance, and impaired dendritic calcium influx translated into a deficit in CP-AMPAR-mediated plasticity induction at synapses onto PV+ cells transfected with my virus. As discussed previously, anti-Hebbian plasticity requires excitatory input in the absence of post-synaptic activity, due to the depolarisation-induced

polyamine block (Lamsa et al., 2007). By pairing hyperpolarisation of PV+ cells with high-frequency presynaptic input, we consistently evoked potentiation of evoked responses in interneurons from control slices, but observed an inability to consistently evoke the same potentiation in PV+ interneurons from transfected slices. The difference between the two groups was apparent within 1-minute post-pairing, and lasted throughout the 20 minutes subsequent to this. It should be noted that the experiments here were performed in the absence of extracellular NMDAR or $GABA_AR$ antagonists, as well as the absence of spermine in the patching solution. Whilst cell somas were hyperpolarised to -90 mV during our anti-Hebbian pairing protocol, it is possible that the dendrites were not equally hyperpolarised. Therefore, I cannot exclude the possibility that NMDARs made some contribution to the potentiation we evoked with our protocol. However, in spite of this, we were able to clearly distinguish between control and virus-transfected PV+ interneurons, suggesting that CP-AMPARs were playing a dominant role in the plasticity processes stimulated by our anti-Hebbian pairing protocol.

In conclusion, we have shown, via a range of experiments, comprehensive evidence that the GluR2 virus delivers the intended effect of altering the AMPAR population profile in hippocampal PV+ interneurons in a way that substantially impairs calcium entry whilst broadly conserving overall activity. The next step is to build upon these promising results *in vitro* and expand these experiments to an *in vivo* setting. In the next chapter, I will perform a comprehensive behavioural characterisation of the consequences of this manipulation on hippocampus-dependent behaviour.

5 Consequences of virally-driven expression of GluR2 in hippocampal PV+ interneurons on behaviour and memory

5.1 Introduction

As discussed in previous chapters, hippocampal activity, PV+ interneuron function, and network oscillations have all been implicated in different aspects of behaviour and memory function. However, the presence of excitatory plasticity at synapses onto interneurons during these processes, and their contribution to expression of memory or other behavioural phenotypes, has received very limited focus. I now have a tool in which I can try to answer some of these questions, and I can use previous research into interneuron plasticity and hippocampus-dependent behaviour to shape expectations under which circumstances I may expect to see any abnormal phenotypes.

Gamma oscillatory activity within the hippocampus appears to be important for the expression of spatial working memory in mice (Montgomery and Buzsáki, 2007; Yamamoto et al., 2014). The restricted activity of distinct neural ensembles on different gamma cycles during periods of oscillatory activity is believed to be necessary for the organisation of information necessary for maintenance of working memory (Howard et al., 2003; Lisman, 2010). It is predicted that the information processing that underpins working memory requires flexible interactions within or between neural ensembles, as cell assembly formation during oscillatory activity is dynamic, enabling representation of distinct memories or contexts (Nissen et al., 2010). As PV+ interneurons exert control over what cells form synchronised assemblies via their perisomatic inhibition, the

capacity to flexibly alter recruitment of these cells via changes in strength at excitatory inputs onto these inhibitory cells across behaviourally relevant time scales is a plausible candidate for achieving this flexibility within the network (Csicsvari et al., 1998; Nissen et al., 2010).

There are questions marks, however, concerning how well the learning rules of plasticity mediated by CP-AMPARs fit with the kinetics of gamma-frequency activity. Given that CP-AMPARs exhibit rectification above 0 mV, high-frequency activation that induces sustained post-synaptic depolarisation may not be favourable to potentiation via this mechanism (Le Roux et al., 2013). However, whilst there may be minimal calcium influx during burst firing, plasticity should occur with subthreshold depolarisation, and CP-AMPAR-mediated spike timing-dependent LTP has been reported in serotonin neurons (Haj-Dahmane et al., 2017). One study found that PV+ interneurons within area CA1 could express distinct forms of plasticity at different inputs; whilst feedforward synapses receiving inputs from area CA3 of hippocampus and entorhinal cortex only expressed anti-Hebbian plasticity, feedback synapses receiving local recurrent connections from pyramidal cells in area CA1 expressed sufficient levels of NMDARs to be capable of undergoing Hebbian NMDAR-mediated plasticity (Lamsa et al., 2007; Le Roux et al., 2013). The same study showed that whilst synaptic potentiation could be mediated via anti-Hebbian pairing with 5-20 Hz input stimulation frequency, only feedback synapses exhibited potentiation with high-frequency (100 Hz) input. As PV+ interneurons are capable of firing on most or every cycle of gamma-frequency oscillations, it is possible that the rate of input may go outside the window for CP-AMPAR-mediated excitatory potentiation (Gulyás et al., 2010). However, given that gamma activity in area CA1 is entrained by CA3 or entorhinal inputs, and that this entrainment has been suggested to occur via CA3 excitatory inputs onto CA1 interneurons, it is possible that the dominant route of excitation of these PV+ interneurons during gamma-frequency activity occurs at feedforward synapses, plasticity at which would appear to require CP-AMPAR-dependent mechanisms (Csicsvari et al., 2003). Possibly as a

result of the multiple forms of excitatory plasticity seen in PV+ interneurons with distinct learning rules, recent *in vivo* experiments have demonstrated the induction of both long-term potentiation and long-term depression in PV+ basket cells in area CA1 following theta-burst stimulation (Lau et al., 2017).

In contrast to spatial working memory, there appears to be minimal contribution of PV+ interneuron activity to spatial reference memory. Manipulations that affect working memory expression often preserve reference memory (Schmitt et al., 2003). Furthermore, neither functional removal of CA1 PV+ interneurons, nor deletion of GluR1/GluR4 from PV+ interneurons, brought about an impairment on a reference memory task, whilst the same manipulations caused significant impairments at performance on working memory tasks (Fuchs et al., 2007; Murray et al., 2011). Whilst reference memory appears to be dependent on hippocampal function, as lesions of the region bring about impairments, it is less sensitive to other manipulations, as even animals with constitutive GluR1 knockouts are capable of performing reference memory-dependent tasks (Deacon and Rawlins, 2002; Reisel et al., 2002). Reference memory appears to represent a form of associative memory, in that it requires formation of a long-lasting association between a given location and an outcome (i.e. a reward) (Bannerman et al., 2012). Working memory, particularly the kind investigated in rodents with spatial working memory tasks, has been suggested to be non-associative, instead requiring short-term recollection of recent experience (Sanderson and Bannerman, 2012). Within the context of rodent studies, spatial-dependent working and reference memory appear to be largely independent processes; however, it has been suggested that instead of operating independently, short- and long-term memory are used complementarily, with retention of information in working memory beneficial to the formation of associatons (Cowan, 2008). Indeed, whilst GluR1 knockout mice were able to learn the reference memory form of the radial maze task without deficits, they were impaired at learning a version of the task that required simultaneous

working and reference memory, with the reference memory errors suggested to arise from interference resulting from working memory deficits (Schmitt et al., 2003).

Whilst GluR1-deficient animals show normal performance on spatial reference memory-dependent tasks, they exhibited mild deficits during 'spatial reversal' trials, in which the reward location was moved to a new location within the familiar environment (Bannerman et al., 2003a). A separate task, in which animals were trained to search for reward locations within a familiar environment, where reward locations remained constant within days but changed on a day-by-day basis, revealed using *in vivo* electrophysiology that the strength of monosynaptic connections from pyramidal cells onto interneurons within the hippocampus changed as new cell assemblies emerged to represent the new reward locations (Dupret et al., 2013). Therefore, whilst PV+ interneuron activity does not appear to be necessary for reference memory for a constant rewarded location, there is evidence that flexibility at inputs onto (unidentified) hippocampal interneurons contributes to learning and/or memory of new locations within familiar environments in response to new information. However, whether these interneurons are PV+ interneurons or other subtypes, and what mechanisms of plasticity occur at these synapses, has not been determined.

As shown in Chapter 3, spatial working memory can be tested in rodents using the rewarded alternation T-maze, a task that is sensitive to manipulations of hippocampal and interneuronal activity (Yamamoto et al., 2014). Spatial reference memory, and day-to-day changes in reward locations, can be tested using apparatus such as the elevated Y-maze, or the cheeseboard task previously used to identify plasticity at pyramidal-to-interneuron connections (Deacon et al., 2002; Dupret et al., 2013). One can also use the water maze, in which learning a static platform location can be used to assess reference memory, whilst consistent movements of the platform location

(termed spatial reversals, or delayed matching to position (DMTP)) can be used to elicit impairments in learning new locations in a familiar environment (Bannerman et al., 2012; Nakazawa et al., 2003).

Whilst the memory processes discussed above have the clearest scientific link with interneuronal plasticity in the hippocampus and are the most likely candidates for observing impairments following PV-specific transfection with my edited GluR2 virus, it was considered pertinent to expand behavioural testing to a fuller characterisation of behavioural phenotypes with my manipulation, to determine the scope and specificity of effects following hippocampal viral injections. Novelty recognition, or specifically spatial novelty preference, can be tested using a Y-shaped maze, and novelty preference on this spatial task has been reduced by hippocampal lesions or knockout of brevican, a perineuronal net protein known to modulate plasticity in PV+ cells (Favuzzi et al., 2017; Sanderson et al., 2007). Locomotor assays can be used as a readout of various spontaneous locomotor abnormalities, including hyperactivity, observed following hippocampal lesions in rodents (Cassel et al., 1998).

The majority of spatial memory impairments are dependent on dorsal hippocampal activity; however, viral validation up to this point has been performed in ventral hippocampal sections, due to the relative ease of performing the intended experiments within this region, in particular *in vitro* gamma oscillation experiments due to high recurrent connectivity. As such, I decided that I would inject my virus into both dorsal and ventral hippocampus, and perform tests for behaviour associated with activity within each sub-region. Whilst dorsal hippocampal activity is widely associated with spatial memory, ventral hippocampal activity is known to be important in expression of anxiety (Bannerman et al., 2003b). Lesions of ventral hippocampus result in abnormal expression of anxiety in behavioural tests, as did chemogenetic alteration of PV+ interneuronal activity in dentate gyrus of hippocampus (Bannerman et al., 2003b; Zou et al., 2016). In contrast, a gain-of-

function in glycine receptor expression in PV+ cells resulted in increased anxiety (Winkelmann et al., 2014). There has been limited research into connections between anxiety and oscillatory network activity, although anxiolytics have been reported to interfere with subcortical control of hippocampal theta activity (McNaughton and Gray, 2000). Despite limited study into the area, there is some evidence to suggest that alterations in excitation of hippocampal PV+ interneurons may affect expression of anxiety.

The aim of the study described in this chapter was to perform a comprehensive investigation into the consequences of artificial introduction of GluR2 into hippocampal PV+ interneurons, and replacement of CP-AMPARs with receptors containing this GluR2 subunit, on animal behaviour and memory. Animals were bilaterally injected in both dorsal and ventral hippocampus with either the GluR2 virus generated in Chapter 4, or a control Cre-dependent GFP virus. I aimed to investigate the translatability of this approach from *in vitro* to *in vivo* applications, and to provide greater insight into the importance for flexible recruitment of fast-spiking perisomatic interneurons in the hippocampus for optimal expression of short- and long-term spatial memory.

For full disclosure, it should be stated that due to time constraints and the lack of available assistance, I performed the surgeries, designed the experimental set-ups, and ran the behavioural experiments by myself. As a consequence, I was unblinded during the acquisition and analysis of data presented in this chapter. The use of automated software for data collection for some experiments could partially mitigate the influence of unconscious experimental bias; however, the influence of bias cannot be discounted.

5.2 Materials and methods

5.2.1 Animals

Experimentally naïve, age-matched adult male and female homozygous PV-Cre$^{+/+}$/Ai9$^{+/+}$ mice bred from animals generated for previous chapters were maintained at the Biomedical Sciences Building (University of Oxford), on a 12 hour:12 hour light-dark cycle in a temperature- and humidity-controlled room. Concerning the cohort used during this study, 24 animals,(12 males and 12 females) were approximately 10-11 weeks old when they underwent surgery, their first procedure. One animal, a female injected with the GFP control virus (see 2.2.2), exhibited an extremely hyperactive locomotor phenotype during the locomotor assay, and as such was excluded from the study, leaving 23 experimental animals in the cohort. All animals were housed according to Home Office regulations, with procedures carried out under a UK Home Office project licence (30/3068, Professor David Bannerman) and personal licence (IE1E0DB60, myself) in accordance with the United Kingdom Animals (Scientific Procedures) Act, 1986. All procedures were performed during the light phase of the light-dark cycle.

Animals were provided with *ad libitum* access to water throughout. Animals were put on food restriction the day prior to food neophagia testing, and *ad libitum* food was subsequently replaced with a restricted food diet during training and testing for the appetitively motivated maze tasks (rewarded alternation T-maze task, reference memory Y-maze task), with the aim of maintaining body weight between 85-90% of the animals' free feeding weights. The animals' diet consisted of 2916 food, plus any condensed milk reward consumed during behavioural training or testing.

5.2.2 Intracerebral injections

Surgery and intracerebral injections were performed as described in 3.2.3 and 4.2.3. In brief, animals were anaesthetised with isoflurane, had their scalps shaved, were subcutaneously injected with meloxicam, buprenorphine and bupivacaine, and mounted into a stereotaxic frame with a rectal temperature probe inserted. An incision was made in the scalp along the midline, the underlying connective tissue scraped away to expose the skull surface, and craniotomies made at the sites for injection. Animals were injected bilaterally into both dorsal and ventral hippocampi.

Out of 24 animals in the cohort, 12 animals, 6 male and 6 female, received intrahippocampal injections of the floxed GluR2 virus described in 4.2.2, and 12 received injections of a control reporter virus, AAV8-CAG-FLEX-GFP, created by Dr. Ed Boyden and acquired via UNC Vector Core. The virus drives Cre-dependent expression of green fluorescent protein (GFP), and is of serotype 8, the same as the floxed GluR2 virus. The GFP virus (as it will now be referred to as) was received at a concentration of 6.2×10^{12} PFU, and was diluted using PBS to 4.9×10^{12} PFU to match that of the floxed GluR2 virus. One animal injected with the GFP virus was subsequently excluded from the study after developing a hyperactive phenotype.

Animals were injected at 8 points in each sub-region; for ventral coordinates injections were made (with respect to bregma) at -2.7 mm AP, ±2.75 mm ML, -2.7/-3.1 mm DV, and -3.0 mm AP, ±3.25 mm ML, -2.7/-3.1 mm DV, whilst for dorsal coordinates, animals were injected at -1.5 mm AP, ±2.1 mm ML, -1.5/-1.1 mm DV, and -2.8 mm AP, ±3.0 mm ML, -2.1/-1.5 mm DV. 600 nl of viral construct was injected at each of these sites at a rate of 100 nl/min, with the needle kept in place for 1-2 minutes

following the completion of injection at each site to promote spread of the virus through the surrounding tissue and prevent diffusion back up the injection tract, before being slowly withdrawn from the tissue. Once all viral injections were made, the wound was sutured (Vicryl, Ethicon), the animals transferred to a heated recovery chamber until full movement returned, and animal recovery was then monitored for 7 days post-procedure in singly housed recovery cages before animals were re-housed with their cage mates.

5.2.3 Behavioural protocols

After a 4-week recovery period post-surgery to allow viral transfection and construct expression to take place, animals were subjected to a battery of behavioural tests, looking at general animal activity as well as performance on tasks associated with dorsal and ventral hippocampal function. These tests were performed in the order listed below. Each test was performed in a different room, with pseudorandom testing orders counterbalanced with respect to groups.

5.2.3.1 Test 1: Anxiety testing – elevated plus maze

A plus-shaped maze elevated 70 cm above the floor consisted of four arms of equal length (35 x 6 cm) radiating from a central square (6 x 6 cm) at right angles. Additionally, two arms opposite each other (the 'closed' arms) were enclosed in a perimeter of 20 cm high walls, with entrances to the two 'open' arms located between the openings of the closed arms. The maze was placed in a quiet, dimly-lit room (15 lux light intensity on the open arms, 9 lux in the centre square).

The experimentally naïve cohort was tested once on a single day in an order counterbalanced for viral treatment, with all males ran before the females. Animals were moved into the experimental room in their home cages a minimum of 5 minutes before testing on the maze. During testing, an animal was placed inside the centre square of the maze and left to explore it for 5 minutes. The experimenter stepped outside the room to leave the animal alone during this period, whilst looking through the window to ensure the animal stayed on the maze. Towels were placed on the floor surrounding the maze to soften any falls from the maze, although no animals ever fell from the maze. After each animal had finished tested, the maze was cleaned and dried before the next animal was placed on the maze.

Animal activity was tracked using a camera and Ethovision XT software (Noldus), which upon detection of the animal would track its position and track its entry into, and time spent inside, predetermined boundaries representing the closed arms, open arms, and centre square. The software calculated time spent in, distance moved in, frequency of entry to, and latency of first entry into each region, as well as total distance moved.

5.2.3.2 Test 2: Locomotor assay

Spontaneous locomotor activity was tested in an illuminated room using a locomotor assay (LMA). Animals were placed in transparent Perspex cages (26 x 16 x 17 cm) surrounded by two photobeam perimeter frames (PAS-Open Field, San Diego Instruments) stacked on top of each other. Horizontal movement of the animal within the cage would break the connection of photobeams on the bottom frame, and accumulations of these beam breaks represent activity levels of the animals. Animal rearing would break photobeams on the top level, enabling distinct detection of this activity.

Animals were run in groups of 6 (the number of available cages), and different animals were run on successive days at the same time point (1 pm start time) to avoid any influence of varying levels of circadian activity on results. Animals were counterbalanced such that at least one animal of each gender injected with each viral type was tested in each of the 6 cages.

Once placed in the cage, animals were left for 2 hours, and horizontal and vertical beam breaks were detected in 24 5-minute time bins. Animals were returned to their home cages at the end of the 2-hour testing period.

5.2.3.3 Test 3: Anxiety testing – anxiogenic open field test

A cylindrical arena (60 cm diameter) with tall white metal walls was brightly illuminated from above, and a camera connected to Ethovision XT tracking software was placed directly above the floor of the arena, connected to the lid of the arena. Using the software, the arena was divided into 3 regions – a central 20 cm diameter circle, surrounded by an outer area of 15 cm thickness and a perimeter area of 5 cm thickness. Animals were separated into individual cages 5 minutes before testing in the arena. Animals were then moved to the testing room and immediately placed into the edge of the open field arena, at which point a testing period of 5 minutes commenced, with the position of the animal in the arena tracked by Ethovision to detect the amount of time in, and entries into, each subdivision of the open field. After 5 minutes was completed, the animal was removed from the arena and rehoused with its cage mates. The arena was cleaned before the next animal was placed into the arena.

5.2.3.4 Test 4: Spatial novelty preference

Spatial novelty preference was tested using a clear Perspex Y-shaped maze with 30 x 8 x 20 cm arms. The floor of the maze was covered with a thin layer of sawdust. Arms could be concealed using a black plastic insert that blocked all visibility of the arm to animals. Animals were assigned a 'start' arm (the arm in which they would be initially placed inside the maze) and a 'novel' arm, entry to which would be blocked during the exposure phase. The start and novel arms were counterbalanced such that equal numbers of animals of each viral treatment and gender would have each combination of start/novel arm.

Animals were moved into individual cages 5 minutes before testing on the maze. They were then moved into the testing room and immediately placed into the start arm. From the moment they completely left the start arm (all four paws outside the arm), they were given 5 minutes of exposure to the two arms available to explore, the start arm and the 'other' arm. Time spent in, and number of entries into, each arm were manually scored using a timer, whilst trials were recorded using a camera and Ethovision for future reference. An arm entry was counted when all four paws were placed inside an arm, and once all four paws were next outside, the animal was considered to have left the arm.

After the 5-minute exposure period, the animal was removed from the maze and returned to its individual cage for a period of 1 minute, during which the time/entry scores were recorded, the timer reset, the black insert removed, and the sawdust brushed around the maze to remove any olfactory cues of previous exposure to an arm. The animal was then replaced in the start arm, and once all four paws had exited the arm, the animal was allowed to explore all three arms of the maze

for 2 minutes, with time spent in, and entries into, each of the three arms of the maze again recorded using the timer. Once this 2 minutes was completed, the animal was removed from the maze and returned to its home cage. A novelty preference ratio for the novel arm over the 'other' arm was calculated with the formula:

$$\frac{\text{Time in novel arm}}{\text{Time in novel arm} + \text{time in 'other' arm}}$$

This value provided a measure of memory for the other arm visited during the exposure phase.

5.2.3.5 Test 5: Anxiety testing – food neophagia

The food neophagia test involves exposure of an animal to a novel foodstuff in a novel environment. The set-up involved a translucent jug of 15 cm diameter, with a spout of 2 cm extra length, placed upturned over the animal, with a 50:50 condensed milk:water reward in a food well positioned underneath the spout. Animals were food restricted from the previous day (approximately 16 hours), to provide an appetitive drive to consume the foodstuff.

Animals were transported into the testing room a minimum of 5 minutes before testing. The food well was filled to the top with the diluted milk, and then an animal was placed in the testing area, with the jug lowered gently around the mouse such that the food well was positioned beneath the spout. They were then left for either 2 minutes, or until they first consumed the milk. The time to (i) first contact with the well, and (ii) first consumption of the milk, were recorded using the timer. If the animal did not drink any milk inside 2 minutes, they were removed from the jug and returned to their home cage. They were then tested again after approximately 2 minutes, once more for up to 2

minutes or until first consumption of the milk. After first drinking the milk, animals were removed from the testing area and not tested again. To prevent social transmission of food preference to remaining untested cage mates, animals exposed to the task were kept separate from untested cage mates until they also performed the task. Performance on the task was measured using latency to first drink, which was combined across runs if an animal did not consume the milk on the first run.

5.2.3.6 Test 6: Rewarded alternation T-maze task

As in 3.2.2, spatial working memory was tested using a wooden elevated T-maze with a 'home' arm (47 x 10 cm), two reward arms (35 x 10 cm), and a 10 cm high perimeter wall. Plastic food wells were located at the end of each reward arm, and plastic sliding doors were used to block entrance to one of the arms during the sample phase. During testing, the maze was placed in a dimly lit room with distinct extramaze cues. The 50:50 milk:water reward drink used in the neophagia test was used throughout the experiment.

To habituate to the demands of the maze, animals received three handling sessions across two days, in which both the whole cage of animals and individuals from the cage were exposed to contact with, and handling by, the experimenter. Habituation to this handling made the animals more comfortable with walking on and off the hand, in and out of the maze. On the second day, each cage of mice was exposed to the T-maze together, receiving 10 minutes to walk around the maze without receiving rewards. On the third day, they received similar habituation, however the food wells were baited with diluted milk and replenished following consumption. Following this session, animals received a further five 10-minute habituation periods during which they individually explored the maze to receive rewards, with no handling except when entering/exiting the maze. The animals also

experienced the sound of the sliding doors to familiarise them with it before testing began. After this extensive habituation period to relieve anxiety towards the T-maze, testing on the task began.

Animals did not have any experience of having to alternate arm entries to receive rewards before the testing phase commenced. During the first testing phase of this experiment, animals received 6 sessions of testing, either on successive days or with a single-day gap in between. Every animal received one session of testing in the same day, and were tested in the same running order such that each session occurred at a similar time of day, with all the males tested before the female. When tested, each animal was removed from its home cage and moved into a single cage before being transported to the testing room. Two animals were run at the same time, one from each viral treatment group, with each one receiving a single trial interleaved with the other animal; the two cages holding these animals were kept on opposite sides of the testing room from each other.

As in 3.2.2, the training/testing sessions consisted of 10 trials in a pseudorandom order, with 5 trials where the left arm was blocked during the sample phase and 5 trials during which the right arm was blocked during the sample phase. No more than 3 of the same trial type were given in succession. Different trial orders were used for each testing session for each animal. A trial consisted of a 'sample' phase, during which the animal was placed at the end of the home arm and had to run to the end of the unblocked arm to receive a milk reward (~30 µl), whilst the other arm was blocked off by the sliding door. Once the sample was consumed, the animal was removed from the maze for 5 seconds, whilst any unconsumed milk was removed from the food well and the previously blocked arm was opened. After the end of this 5-second delay, the animal was replaced at the end of the home arm, and had to choose which arm to enter to receive the reward; the milk consumed during the sample phase was not replenished, so to receive more milk the animal needed to learn to enter the previously blocked arm during the 'choice' phase of the trial. Once the animal had made a choice

to enter one arm (all 4 paws inside the arm), the sliding door was closed on that arm. Once the animal had progressed all the way to the food well, and either drank the reward or found there was no reward, it was removed from the maze and returned to its holding cage for a minimum of 2 minutes before the next trial; during this period, the other mouse would undergo a trial.

After 6 sessions of this testing format, animals were given a single day of no testing before the second phase of the experiment began. As before, animals were run in pairs (in the same running order), receiving 10 trials in a pseudorandom order. However, the delay between the sample and choice phases of trials was extended from 5 seconds to 30 seconds. The testing session format was the same as during the first testing phase aside from this one change (i.e. the inter-trial interval remained at 2 minutes). Animals received two sessions on successive days of this format during this second testing phase.

The third testing phase involved testing sessions containing 12 trials, 6 of which had 5-second sample-choice delays, and 6 of which had 30-second sample-choice delays. These trials were interleaved through the session, with no more than three 5-second or three 30-second delay trials given in succession; as before, no more than 3 left/right sample arm trials were given in succession either. As before, animals were run in pairs in the same running format, with an inter-trial interval of 2 minutes. Animals received two of these sessions on successive days, with the first session on the day following the second session from the second testing phase.

Performance on the task was measured by recording correct and incorrect choices made for each trial. Additionally, the latency from placement in the home arm until consuming the reward during the sample phase, and latency from placement in the home arm until a choice was made in the

choice phase (all 4 paws inside a reward arm), were recorded. After the first session during the first testing phase, a modification was made to the handling of animals during testing to reduce anxiety related to the task and reduce sample and choice latencies. The animals were initially placed in/removed from the maze by being picked up by their tails. However, it was later found that animals would perform the task with much shorter latencies if they were placed in and taken out of the maze by walking on/off the palm of the hand without being picked up. Similar negative responses to tail handling have recently been reported elsewhere (Clarkson et al., 2018). This method was used for the remainder of the study. Finally, during the second phase of testing, performance over time within sessions was tested by looking at correct choices made during the first and second halves (5 trials) of sessions.

5.2.3.7 Test 7: Elevated Y-maze spatial reference memory test

Spatial reference memory was tested using a wooden elevated Y-shaped maze with 3 arms (50 x 9 cm with 0.5 cm high walls), pointing out from a central hexagon (14 cm diameter) at 120° angles from each other. The maze was elevated 80 cm above the ground on a detachable base upon which the arms could be rotated. Food wells were placed 5 cm from the far end of each arm.

Testing on the Y-maze began 2 days after the completion of T-maze testing. Prior to training, animals received one day of habituation to the Y-maze, with one 10 minute session exploring the maze with cage mates (with all food wells continually baited), and then one session in which each animal individually explored the maze, again with all food wells baited, either for 10 minutes or until they had consumed 0.5 ml of the 50:50 milk:water reward used during the experiment.

Following this, animals received 10 sessions of testing, with 10 trials per day. Each animal was assigned a reward arm for the duration of testing, defined by allocentric, extramaze spatial cues (posters, chairs, door, dustbin, etc.), and would only receive rewards in this arm; reward arm assignment was counterbalanced such that 2 animals of each viral treatment and gender had the same reward arm, aside from reward arm 3, which only one GFP-injected female had as their reward arm. They would have to learn to use allocentric spatial cues within the testing room to navigate from variable starting points to a constant reward location. Each day, animals received 5 trials starting from each of the two unbaited arms, delivered in a pseudorandom order with no more than 3 trials in succession starting from either arm. To avoid animals using local intramaze cues (e.g. odor trails), the maze was rotated 120° clockwise approximately every 2 rounds of trials (i.e. after every animal had received 2 trials in the session) so that a different physical arm was in the reward arm position.

The first 9 sessions of training/testing occurred on successive days. On these days, reward arms would be baited, and animals placed into the start arms. From this point, they would be timed until they left the start arm and entered one of the two possible other arms; once their full body had entered the reward arm (all 4 legs), their choice would be scored as either correct or incorrect, and the animal would be allowed to proceed to the food well at the end of the arm, either to consume the reward or observe a lack of reward, before they were removed from the maze. No self-correction was allowed (i.e. if an animal made an incorrect choice, they were not permitted to subsequently enter the reward arm). The latency from initial entry into the arm to contact with the food well was recorded for each trial. Following each trial, animals were returned to their individual holding cages for a minimum of 5 minutes before their next trial. Animals were run in groups of 4, with every member of each gender that shared the same reward arm running together. Each animal received one trial before the first animal had their next trial.

After 5 training sessions, the large majority of animals had not shown any improvement in performance in the task, primarily because they would almost exclusively make the same turning regardless of the start arm, meaning they typically scored 50%. It is possible that past experience on the T-maze task affected their ability to pick up the rules of the new task. In order to counteract this and assess their reference memory capacity, animals scoring 80% or lower on day 5 were given 'supplemental' training at the end of the usual 10 trials. Animals would receive blocks of rapid trials (minimum 1-minute inter-trial interval) starting in the arm from which they would make the incorrect turning. This would continue until the animal began to consistently change their choice-making to enter the baited arm (3 correct trials). Once they had managed this, they would receive trials from the other start arm to ensure they hadn't simply reversed their turning strategy; once they made one correct choice from this arm, they were returned to their home cages. The supplemental training on day 5 brought about an immediate improvement in performance in roughly half the cohort; for those still scoring at approximately chance (60% or lower), after the regular 10-trial training session on day 6, they were given one more session of this supplemental training. Any poor performance following this was considered to be reflective of memory impairments; as such, no further supplemental training was given.

On the final day of testing (day 10), which was 2 days after day 9, the format of the session was slightly altered to previous sessions. To control for any influence olfactory cues from the reward itself were having on animal performance, the well in the reward arm was not baited until animals correctly entered the reward arm during trials; this is termed 'post-choice baiting'. If animals made an incorrect arm entry during a trial, the well was not baited and the animal was removed as usual. In the event of animals performing the trial sufficiently quickly as to reach the reward well before it

was baited, the arm was blocked off using a hand to prevent the animal leaving before it received a reward.

5.2.3.8 Test 8: Reference memory and spatial reversal on the water maze

Following the elevated Y-maze spatial reference memory testing, animals were taken off food restriction and returned to *ad libitum* food conditions. The Morris water maze was used to first test the ability of animals to first acquire a novel spatial reference memory task, and then subsequently learn novel locations within a familiar environment, in a similar way to the cheeseboard task previously discussed. This test involved two separate stages, a simple reference memory task, and subsequently serial spatial reversal.

The water maze was a 2 m diameter, 0.9 m tall circular bath raised 36 cm above the ground. A circular escape platform (21 cm diameter) could be placed in the maze at various positions. The maze is filled with water until the water level was approximately 1 cm above the surface of the platform (an overall depth of around 65 cm). It was then turned opaque using 600 ml white ready-mixed paint (Hobbycraft). During testing, the platform was positioned in one of four positions, assigned 'northwest' (NW), 'northeast' (NE), 'southeast' (SE), and 'southwest' (SW). The coordinates of these positions were such that the platform centre was 50 cm from the wall of the bath, and equidistant from each other and the centre of the bath.

Animals could enter the maze at one of eight points; NW, NE, SE, SW, N, E, S, W. The objective of the task was to learn the location of the platform in order to escape the maze. Once animals were put into the maze, the researcher moved out of the field of vision of the mouse and watched the

performance via a camera positioned directly above the maze. WaterMaze software (Actimetrics, Illinois) was used to track animal position in the bath in relation to the platform location, record and store the path of movement through the water, and detect when the animal had reached the platform. Individual trials would last for a maximum 90 seconds, or until the animal reached the platform. Various properties, including trial latency, path length, swimming speed, time spent in each of the four quadrants of the maze, time spent near walls (thigmotaxis), etc., were recorded by the software for analysis.

The reference memory phase of this test involved 9 successive days of training animals to associate a singular location with escape from the maze. During this period of the task, only SE and NW were used as escape locations; previous studies using this set-up had found least bias towards these platforms (with increased/decreased preference towards SW and NE respectively). Animals were assigned either SE or NW as an escape location, counterbalanced for viral treatment and gender. Each day, animals would receive four trials, with entry positions randomly selected from the eight available options. Once animals had located and mounted the escape platform, they would be given 30 seconds there to associate escape with that location. For animals that failed to find the platform location in 90 seconds, they were guided by the experimenter to the platform and then given 30 seconds there. Once this 30-second period was finished, animals were removed from the maze, quickly dried with a towel, and then placed back into the maze for their next trial. Once four trials were completed, animals were placed in a 31 °C incubator to dry before returning to their home cage.

Additionally, on the day after sessions 6 and 9, animals were given probe tests without the platform present to ascertain whether they had learned the platform location. This entailed removing the platform, and giving animals 60-second trials in which they entered the maze from the opposite

position to the trained platform location (e.g. for animals trained to escape the maze in SE, they would enter the maze at NW). After 60 seconds, the animals were removed from the maze and placed in the incubator; if possible, the animal would be removed near the usual platform location to continue associating this location with escape. Preference for the goal (or training) quadrant was used as an indicator of learning. After the first probe test, animals were then subjected to day 7 of regular training; following the second probe test, animals were not further trained that day, as subsequent testing would involve a new platform location.

Following this, the animals underwent three rounds of testing in which the platform was moved to a new location on each occasion (serial spatial reversals). For the first round, the animals were subjected to spatial reversal testing, where the platform was moved to the position opposite to where they had previously been trained (i.e. animals trained to SE had the platform moved to NW). They then had 3 days of testing (4 trials/day as previously) with this new location, followed by a probe test. Finally, this was followed by two more rounds with the same format (3 days of 4 trials, followed by a probe test), in which the platform was moved first to either SW or NE, and then the other one (NE or SW), in a way that was counterbalanced for virus, gender, and previous platform location (for visual description of task see Fig. 5.7).

5.2.4 Histology

Following this final behavioural test, the animals were perfused and their brains extracted. In brief, animals were intraperitoneally injected with a lethal dose of pentobarbital (Euthatal, Merial Animal Health Ltd.), before being transcardially perfused with phosphate buffered saline and subsequently

4% PFA in 0.1 M phosphate buffer. Fixed brains were extracted from the skull and stored at 4 °C in PFA.

Brains were sectioned on a VT1000S vibratome (Leica); the majority of brains were sectioned coronally to maximise assessment of expression in dorsal hippocampus, due to the dorsal hippocampus-dependent nature of the majority of the tests performed during this study. However, a subgroup was sectioned horizontally to examine ventral hippocampal expression as well. Sections were cut at 60 µm thickness. Following sectioning, slices were washed three times in PBS and were incubated for 20 minutes at room temperature in 0.15% TBS-T. Sections then spent 1 hour incubating in 20% NHS in TBS-T, were briefly washed, and were then transferred into primary antibody (either mouse anti-AU1 from Biolegend or mouse anti-GFP from Abcam, both diluted 1:500 in 2.5% NHS in TBS-T) and incubated for either 24 hours (for anti-GFP) or 48 hours (for anti-AU1) at 4 °C. Slices were then washed three times in TBS-T before overnight incubation at 4 °C in the secondary antibody (Alexa Fluor-488-coupled goat anti-mouse, ThermoFisher Scientific) diluted 1:500 in 2.5% NHS in TBS-T. Finally, sections were washed 3 times in PBS, once in 0.1 M phosphate buffer, and mounted onto slices with Fluoroshield (Sigma Aldrich). All sectioning, incubations, and washes not done at 4 °C were done at room temperature.

Mounted sections were imaged at 5x, 20x, and 40x magnification using a Leitz DRMD Fluorescence Microscope (Leica) and a Retiga 2000R CCD camera (QImaging). Images of fluorescence were taken using Ocular software.

5.2.5 Analysis and statistics

All statistical tests were performed using SPSS. The significance of differences between a group mean and chance-level performance was assessed using one-sample t-tests. Statistically significant differences between the viral and gender behavioural groups during this study were assessed using t-tests, ANOVAs, and *post hoc* simple main effects tests. For t-tests, Levene's test was used to assess equality of variance, with degrees of freedom adjusted in cases of non-equal variance. For ANOVAs, in conditions where assumption of sphericity was violated, Huynh-Feldt (H-F) or Greenhouse-Geiser (G-G) corrections were used to alter degrees of freedom. In cases of skewed distribution of data, normality was tested using a Shapiro-Wilk test. If the data sets for a task were non-normal, a Kruskal-Wallis test was used in place of a t-test. As before, the significance value was set at 0.05 for all tests, except when adjusted for *post hoc* tests with multiple comparisons. Additionally, as mentioned in the introduction, both acquisition and analysis of data within Chapter 5 was performed unblinded by one investigator.

As in previous chapters, significance indicators used in figures in this chapter represent, unless otherwise stated: * = $p < 0.05$, ** = $p < 0.01$, *** = $p < 0.001$, n.s. = $p \geq 0.05$, with error bars representing the standard error of the mean. For statistical comparisons, when mean values for two separate viral groups are provided, unless stated otherwise, the first group represents the GFP virus-injected control group, whilst the second group represents the GluR2 virus-transfected experimental group; when gender groups are compared, the first group represents males, and the second group represents females.

For data from the locomotor assay, overall levels of activity (represented by beam breaks) and rearing were assessed between the two groups. Additionally, differences in locomotor assay over time were assessed using repeated-measures ANOVA to compare data binned into 5-minute blocks.

To explore the nature of any interactions, simple main effects were tested; with 24 time bins, an adjusted significance value of 0.0044 was set.

For anxiety experiments, differences between the two groups for different experimental variables were compared using t-tests, ANOVAs or Kruskal-Wallis tests. In the elevated plus maze, entries into, and time spent in, the open arms were compared between groups, whilst for the open field test, time until first entry into, and time spent in, the central circle of the field were compared. Neophagia was assessed by comparing time to first contact with the novel foodstuff, and time to first consumption.

Differences in spatial novelty preference between the two behavioural groups, and between individual behavioural groups and chance-level performance, were assessed by comparing time spent in the novel arm, novel arm entries, and the relative time spent in the novel arm compared to the previously explored non-start arm, or 'other' arm.

Performance (as judged by % correct choices) during the T-maze study with a 5-second delay was assessed with a repeated-measures ANOVA across the training/testing period, exploring viral treatment, session, and half. Performance with a 30-second delay was assessed by averaging performance across the two days of testing and using ANOVA. Performance across the two halves of testing sessions was assessed using a multivariate ANOVA. Performance during the interleaved 5-second/30-second delay test was assessed with a two-way ANOVA accounting for viral group and delay length. Any interactions were explored with *post hoc* simple main effects tests. For post hoc tests exploring simple effects at two levels (e.g. for both viral group and delay length, or viral group

and half of session), the significance value was adjusted, with an alpha of 0.15, k of 4, and p-value for significance of 0.04.

Differences in performance during the reference memory tasks (Y-maze and water maze) were assessed using repeated-measures ANOVAs across the testing period; performance in the Y-maze was measured by % correct choices, whilst latency to platform, path length, and % time spent near the walls were studied in the water maze acquisition phase. Performance on the probe test was assessed by averaging % time spent in each quadrant across the two probe tests and using t-tests to compare time spent in the target quadrant between the two groups, and between each group and chance-level performance.

Performance during the reversals phase of the water maze study was assessed by testing trial latency and path length for each of the three days across all 3 reversals using repeated-measures ANOVAs. Similarly, time spent in the previous target quadrant when learning a new platform location was tested across reversals with an ANOVA. Time spent in each quadrant was averaged across all three probe tests, and differences in time spent in the target quadrant tested as during the acquisition phase.

5.3 Results

5.3.1 Bilateral full hippocampal expression of virus

Adult PVCre/Ai9 double homozygous mice (12 male, 12 female) were bilaterally injected in both dorsal and ventral hippocampus, either with the floxed GluR2 virus used in Chapter 4, or a control floxed GFP virus. Following the completion of the behavioural study, the animals were perfused and viral expression was assessed by staining for GFP or AU1, the peptide marker included in the GluR2 virus. The perfusions were performed 4 months after the viral injections; the immunoreactivity against AU1 in the GluR2 virus-injected animals was weaker than seen with animals with a shorter time window between injection and perfusion (see Chapter 4); however, immunoreactivity against AU1 or GFP was observed in the hippocampus of all animals in the study (Fig. 5.1). The anti-AU1 immunofluorescence was more diffuse throughout the neuropil when compared to the localised GFP fluorescence in individual neurons; however, anti-AU1 immunoreactivity was observed co-localised with tdTomato in PV+ interneurons in different sub-fields of both dorsal and ventral hippocampi. The post-mortem histology demonstrates successful viral transfection of my behavioural cohort, and supports the idea that divergences in behavioural phenotype between the two experimental groups are a consequence of the effects of the GluR2 virus.

5.3.2 Mild spontaneous locomotor phenotype in animals transfected with GluR2 virus

Once the animals had recovered from surgery, they were subjected to a battery of behavioural tests, including an assessment of spontaneous locomotor activity. The animals were placed in Perspex boxes for 2 hours, and movement and rearing was detected by the disruption of photobeams created by a perimeter frame. Spontaneous locomotion can be influenced by a variety of factors, including stress, anxiety, appetite, circadian activity, and various drugs and manipulations in neural circuits, including hippocampal lesions (Aoki et al., 2017; Boulle et al., 2014; Cassel et al., 1998; Salahpour et al., 2008; Verwey et al., 2013). It can also be affected by novelty, as animals will show

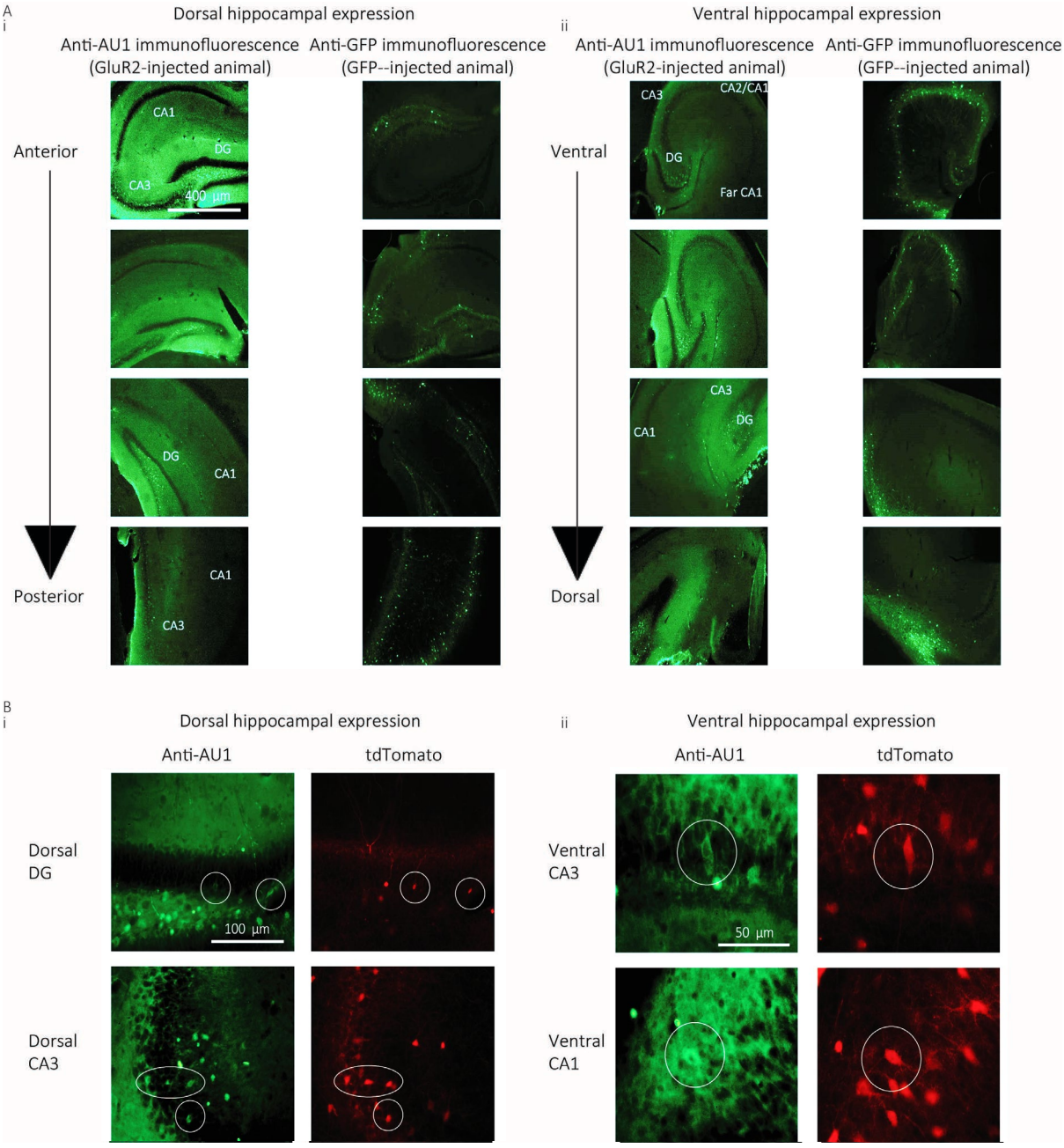

Figure 5.1. Viral expression in the hippocampus of the behavioural cohort (4 months post-injected). (A) Images (5x magnification) acquired from animals following completiong of the battery of behavioural tasks. Images taken from (i) coronal sections containing dorsal hippocampus, going (from top to bottom) anterior to posterior, and (ii) horizontal sections containing ventral hippocampus, going (from top to bottom) ventral to dorsal. Sections in the left columns represent anti-AU1 immunoreactivity in GluR2-injected animals; the right columns contain sections exhibiting anti-GFP fluorescence taken from GFP-injected animals. (B) Images acquired from (i) dorsal hippocampal sections (20x magnification) and (ii) ventral hippocampal sections (40x magnification) taken from GluR2-injected animals. Left columns present anti-AU1 immunofluorescence whilst right column presents tdTomato fluorescence. Fluorescence was weaker in animals perfused 4 months post-injection than animals in Chapter 4, but AU1 immunoreactivity was observed in PV+ cells in both dorsal and ventral hippocampus across multiple sub-fields.

increased activity in novel environments, which decreases with familiarisation with the new location

(Arenas et al., 2014). It is possible that altering the recruitment of GABAergic interneurons in a brain

region associated with novelty may result in an abnormal locomotor phenotype. Rearing in rodents is considered a protective response to stress in a novel environment, and is associated with risk assessment and anxiety (Piras et al., 2013).

2 (viral type) * 2 (gender) two-way ANOVAs were performed to determine the effect of viral treatment and gender on ambulatory and rearing activity. Full hippocampal injection of the floxed GluR2 virus had no significant main effect on overall ambulatory locomotor activity compared to control animals injected with a floxed GFP virus, as assessed by total beam breaks across 2 hours (Fig. 5.2A). Controls (n = 11 animals) reported an average of 2908.82 ± 278.9 beam breaks, whilst GluR2-injected animals (n = 12 animals) recorded 2442.92 ± 158.6 beam breaks ($F_{(1,19)} = 1.95$, $p = 0.179$). In contrast, GluR2-treated animals showed significantly lower rearing activity across the testing period than controls (226.82 ± 16 vs 176.67 ± 13.5 rears; $F_{(1,19)} = 5.161$, $p = 0.035$; Fig. 5.2B). There was no significant effect of gender on either activity, nor an interaction between gender and viral type ($p > 0.1$). When beam breaks were separated into 5-minute time bins, a 2 (viral treatment) * 24 (time bin) repeated-measures ANOVA revealed a significant virus * time bin interaction ($F_{(23,483)} = 1.751$, $p = 0.017$; Fig. 5.2C). Simple main effects were used to explore this interaction, with an adjusted significance value of 0.0044. There were no significant differences between the two groups in any of the time bins, but borderline significance was seen in the 15-to-20 minute time window (276.1 ± 24.7 vs 172.1 ± 23.6; $F_{(1,21)} = 9.285$, $p = 0.006$).

In summary, viral overexpression of GluR2 in hippocampal PV+ cells had a mild effect on locomotor activity, seemingly restricted to the early minutes following introduction to the locomotor testing chamber, and caused a significant reduction in rearing behaviour. The former may be due to altered responses to novelty, whilst the latter may represent altered expression of novelty-induced anxiety in these animals. Subsequent tests will look into anxiety phenotypes and novelty-related behaviour.

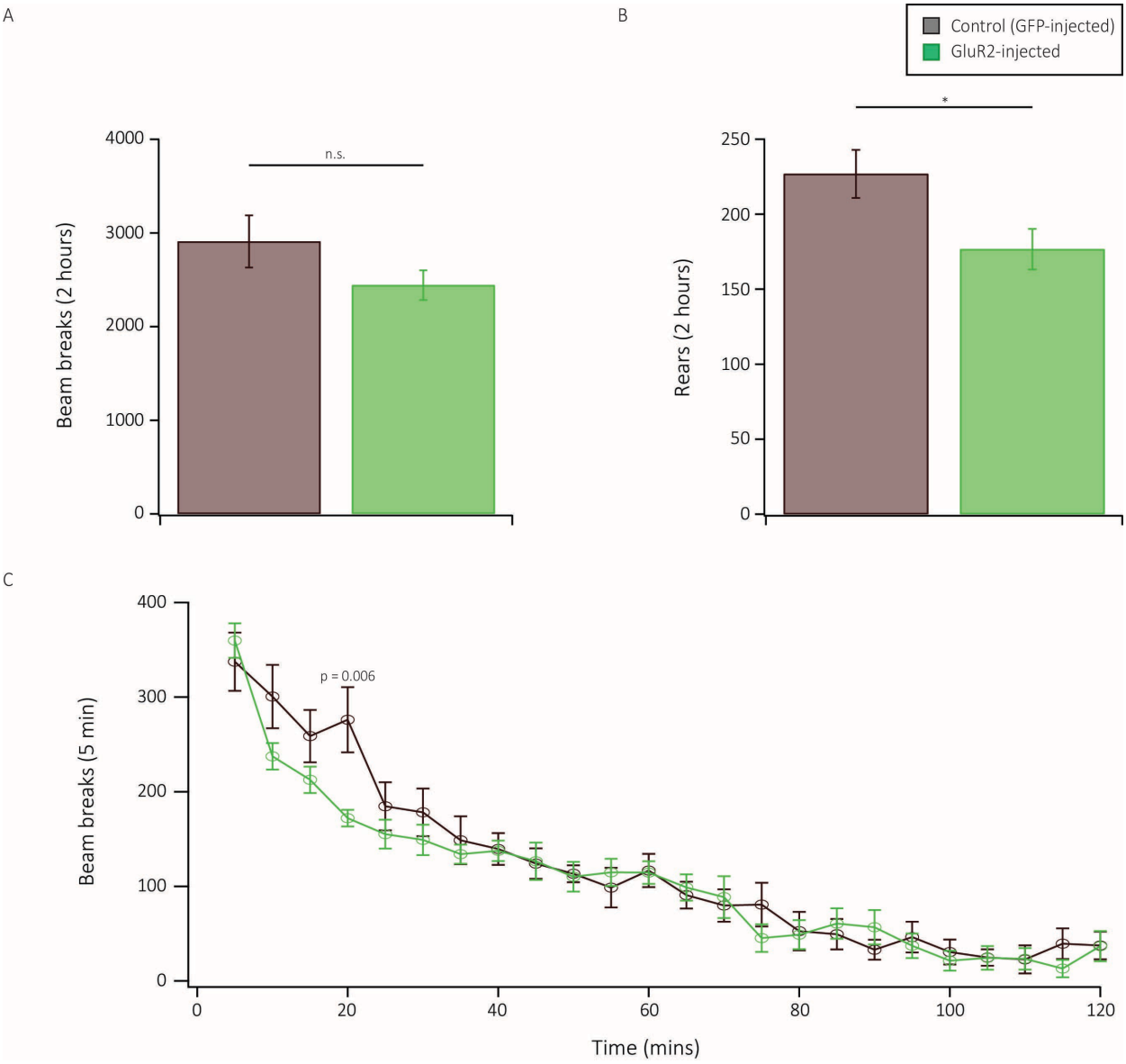

Figure 5.2. Transfection of hippocampal PV+ interneurons with GluR2 causes a mild hypolocomotor phenotype. (A) Overall horizontal beam breaks are not significantly different in controls (n = 11) compared to GluR2-injected (n = 12) animals (2908.82 vs 2442.92). (B) The GluR2-transfected animals recorded fewer vertical beam breaks (representing rearing activity) over 2 hours than GFP-injected controls (226.82 vs 176.67). (C) GluR2 animals show borderline significantly lower activity than controlswithin 20 minutes after placement in locomotor boxes, but exhibit similar locomotor activity for the remainder of the 2-hour testing period. * = $p < 0.05$; ** = $p < 0.01$; *** = $p < 0.001$. n.s. = $p \geq 0.05$. Error bars indicate standard error of the mean.

5.3.3 Unclear anxiety phenotype following transfection of PV+ interneurons with GluR2

Anxiety in rodents has been linked to activity in the ventral hippocampus, with lesions within the region resulting in reduced expression of anxiety-related behaviours (Bannerman et al., 2003b).

Given the bulk of *in vitro* experimentation during this project was performed in ventral hippocampus, I decided to test whether manipulation of PV+ interneuron AMPA receptors in this region resulted in any alteration in anxiety in the GluR2-injected cohort. To accomplish this, I performed multiple anxiety tests, including the elevated plus maze (EPM), open field test, and food neophagia.

The EPM consists of four arms of equal length; two 'closed' arms with walls, and two 'open' arms without. Mice typically prefer to dwell in the closed arms, whilst ventral hippocampal lesions and anxiolytics increase open arm time (Fig. 5.3A) (File, 1990; Kjelstrup et al., 2002). The two viral groups travelled similar distances during the 5 minutes of the task (5.74 ± 0.4 cm/s vs 5.4 ± 0.4 cm/s; $t(21) = 0.521$, $p = 0.607$). T-tests revealed that there was no effect of viral treatment on the percent time spent in the open arms (11.51 ± 3.7% vs 5.11 ± 1.4%; equal variances not assumed (Levene's test for equality of variance, $F = 7.64$, $p = 0.012$); $t(12.839) = 1.632$, $p = 0.127$; Fig. 5.3Aii), nor on the number of open arm entries (25.27 ± 7.3 entries vs 17.33 ± 3.1 entries; equal variances not assumed (Levene's test for equality of variance, $F = 5.385$, $p = 0.03$); $t(13.63) = 1.002$, $p = 0.314$; Fig. 5.3Aiii). However, a 2 (viral treatment) * 2 (gender) two-way ANOVA revealed a significant effect of viral treatment on percent time in open arms ($F_{(1,19)} = 4.519$, $p = 0.047$), as well as an effect of gender ($F_{(1,19)} = 6.367$, $p = 0.021$); there was no interaction between the two variables, although the largest percent time spent in the open arms was by the female GFP group (19.06 ± 6.4%; $F_{(1,19)} = 2.764$, $p = 0.113$; Fig. 5.3Aiv). There was also a non-significant trend towards an effect of gender on number of open arm entries ($F_{(1,19)} = 4.054$, $p = 0.058$). There were no significant effects of viral treatment on the relative time spent in open arms:closed arms, latency to first open arm entry, or other variables ($p \geq 0.1$).

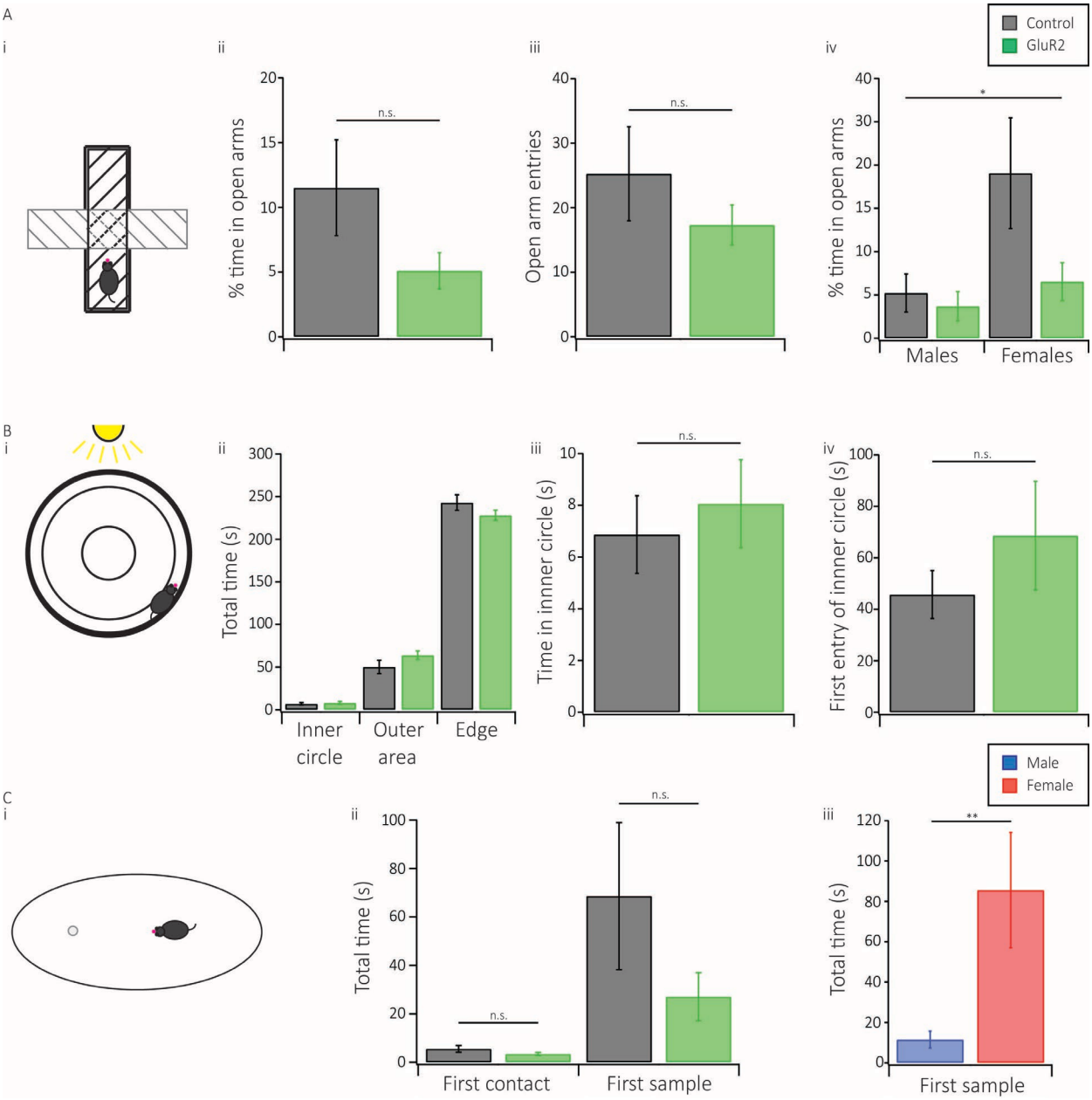

Figure 5.3. Transfection of hippocampal PV+ interneurons with a virus expressing GluR2 does not alter anxiety-related phenotypes. (A) (i) On an elevated plus maze with open and closed arms; (ii) there was not a significant difference between the two groups for % time in open arms (11.51% vs 5.11%). (iii) The animals also did not show a difference in the number of entries into open arms they made (25.27 entries vs 17.33 entries). (iv) Separating groups by viral type and gender reveals significant effect of both variables on % time spent in the open arms. (B) (i) In an open field chamber, (ii) both cohorts showed a similar preference for the edge region and unwillingness to enter the inner portion of the field; (iii) there was no significant difference in the time spent in the inner 20 cm diameter circle of the field (6.87 s vs 8.06 s). (iv) There was also no notable difference in the average time taken for animals from each cohort to first enter the inner circle (45.74 s vs 68.64 s). (C) (i) In a food neophagia test where animals were exposed to a novel foodstuff in a novel restricted environment, (ii) the two cohorts showed a similar willingness to approach the foodstuff. The GluR2-injected animals did not take a significantly different amount of time to first consume the novel foodstuff (68.6 s vs 27.08 s) (iii) In contrast, females took significantly longer to sample the novel foodstuff than males (11.53 s vs 85.57 s). N = 11 control animals, 12 GluR2 animals.

The open field test involves placing the animal in a brightly lit metallic cylinder of 60 cm diameter,

with animals preferring to stick to the edges (Fig. 5.3B). The maze was separated into three zones;

an inner circle of 10 cm radius, an outer area of 15 cm radius, and an edge region of 5 cm radius. The two experiments groups covered similar distances during the task ($t(21) = 0.073$, $p = 0.942$). Animals in both groups spent roughly equivalent lengths of time in each region, with most time spent at the edge and little time in the inner circle (Fig. 5.3Bii). A 2 (viral type) * 2 (gender) two-way ANOVA did not reveal a significant difference in the time spent in the inner circle between the two viral groups (6.87 ± 1.5 s vs 8.06 ± 1.7 s;$F_{(1,19)} = 0.247$, $p = 0.625$; Fig. 5.3Biii), nor the latency to first entry into the inner circle (45.74 ± 9.3 s vs 68.64 ± 21.1 s; $F_{(1,19)} = 0.947$, $p = 0.323$; Fig. 5.3Biv). Furthermore, there was no main effect of gender or interaction with viral type for either variable ($p > 0.1$).

Finally, I tested food neophagia in the cohort. This involved placing the animals in a restricted novel environment with a previously unencountered foodstuff, and timing how long it took for them to approach and then taste the food (Fig. 5.3C). Greater anxiety results in slower decisions to sample the food, whilst ventral hippocampal lesioned rodents have an attenuated neophobic response (Miller et al., 1986). Due to the strongly non-normal distribution of latencies to first sample ($p \leq 0.001$ for both experimental groups, Shapiro-Wilk test), the non-parametric Kruskal-Wallis test was used to compare performance on the task. The was no significant difference between the control group and the GluR2-injected group concerning the time taken to consume the novel foodstuff (68.6 ± 30.3 s vs 27.08 ± 9.9 s for first sample; $p = 0.460$; Fig. 5.3Cii). However, a marked difference was observed between the performance of males and females on the task (11.53 ± 4.2 s vs 85.57 ± 28.6 s; Fig. 5.3Ciii). There is no satisfactory non-parametric equivalent to the two-way ANOVA to effectively test the effects of both viral type and gender on performance on the neophagia task. For the sake of curiosity, however, both a Kruskal-Wallis test comparing across gender and a parametric two-way ANOVA for viral type and gender reveal a significant effect of gender on performance ($p = 0.002$ and $F_{(1,19)} = 10.457$, $p = 0.004$, respectively). Additionally, analysing the data with a two-way

ANOVA revealed a non-significant trend towards an effect of viral treatment ($F_{(1,19)} = 3.821$, $p = 0.066$).

Overall, the results from the various anxiety tests provide an unclear picture of what effects, if any, transfection of hippocampal PV+ interneurons with GluR2 may have. A significant reduction in the time spent in open arms was observed in the GluR2 group on the EPM task compared to controls; however, performance between the two groups was not significantly different in other EPM parameters, or on two other anxiety tests. In contrast, in addition to an increase in time spent in open arms on the EPM, females exhibited a significant increase in time to sample a novel foodstuff, two seemingly conflicting effects on anxiety-related performance. In conclusion, there is limited evidence suggesting that the GluR2 manipulation resulted in increased anxiety in the behavioural cohort.

5.3.4 Trend towards increased spatial novelty preference following GluR2 transfection

Rodents have a natural preference for novel objects and environments over familiar ones, and hippocampal activity has been strongly implicated in this (Sanderson et al., 2009). To test whether my manipulation had any influence on the processes underpinning novelty preference, I subjected my cohort to a spatial novelty preference task, in which animals were first exposed to two arms of a Y-shaped maze (with the third arm blocked), before being removed and subsequently replaced in the maze with the previously blocked arm now available (Fig. 5.4A). Mice typically show a preference for the novel arm over those they had previous experience in.

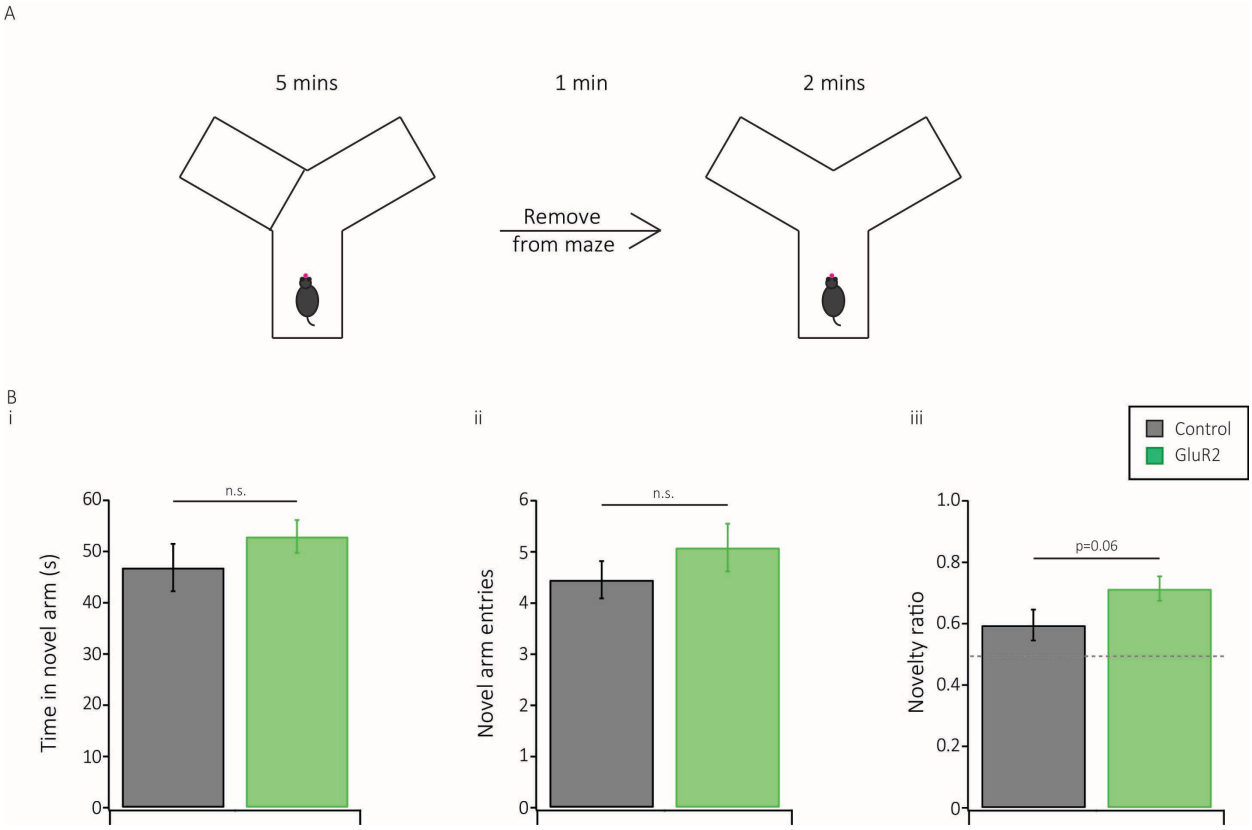

Figure 5.4. No significant effect of GluR2 viral transfection in hippocampal PV+ neurons on spatial novelty preference. (A) Test involves two phases in a Y-shaped maze, where the animal first spends 5 minutes exploring 2 out of the 3 arms of the maze, and then is replaced back in the maze with the third arm unblocked, and has to choose whether to explore the novel arm or those previously explored. (B) There was no significant difference between the GluR2-treated animals and GFP-treated controls in terms of (i) total time spent in the novel arm (46.87 s vs 52.95 s), (ii) number of entries into the novel arm (4.45 vs 5.08 entries), or (iii) ratio of time spent in the novel arm compared to the previously explored arm the animal did not start in (0.6 vs 0.71). Horizontal dashed line represents zero preference for novel over other arm. N = 11 control animals, 12 GluR2 animals.

During the 5-minute sample phase, the control and GluR2 groups exhibited very similar activity. The two groups showed no significant differences in the total number of entries into both the start and 'other' arms (27.45 ± 2.3 entries vs 28.17 ± 1.6 entries), number of 'other' arm entries (13.82 ± 1 entries vs 13.92 ± 0.9 entries), time spent in the other arm (118.41 ± 8.1 s vs 117.67 ± 5.3 s), and the ratio of time spent in the other arm compared to the start arm (0.98 ± 0.1 vs 1.06 ± 0.1). In general, the two groups showed similar levels of activity, and a similar lack of preference for either arm, during the sample phase.

A 2 (viral type) * 2 (gender) two-way ANOVA revealed that the two viral treatment groups showed no significant difference in the amount of time they spent in the novel arm during the 2-minute

choice phase (46.87 ± 4.6 s vs 52.95 ± 3.2 s; $F_{(1,19)}$ = 1.261, p = 0.275; Fig. 5.4B). Similarly, there was no difference in the number of entries made into the novel arm (4.45 ± 0.4 entries vs 5.08 ± 0.5 entries; $F_{(1,19)}$ = 1.301, p = 0.268). A final way to judge novelty preference was to calculate the ratio for the amount of time spent in the novel arm compared to the 'other' arm, the arm from which the animal did not start the test but which was explored during the initial phase of the experiment (see 5.2.3.4 for formula). If an animal spent an equivalent amount of time in the novel and other arms, the novelty ratio would come out at 0.5. One-sample t-tests comparing novelty preference in either viral experimental group to chance-level performance revealed a non-significant trend towards significance for the control GFP-transfected group against chance (0.6 ± 0.05; t(10) = 2.065, p = 0.066), and a significant level of preference in the GluR2-transfected group (0.71 ± 0.04; t(11) < 0.001). The GluR2-transfected cohort showed a borderline significant trend towards greater preference for the novel arm compared to the control group ($F_{(1,19)}$ = 3.761, p = 0.067). There was no significant effect of gender on performance based upon any variable, nor any interactions with viral group (p > 0.1).

Overall, the GluR2 virus-injected animals showed a trend towards slightly greater preference for a novel spatial location over a previously explored location compared to GFP-treated controls; however, this difference was not great enough to make any conclusive claims about greater novelty preference in these animals.

5.3.5 Delay-dependent impairment in spatial working memory following viral-driven expression of GluR2 in hippocampal PV+ interneurons

As shown in Chapter 3, activity of CP-AMPARs in dorsal hippocampus is necessary for optimal expression of spatial working memory in the rewarded alternation T-maze task. The deficit resulting from CP-AMPAR pharmacological antagonism in the experiment was likely largely mediated by reduced recruitment of PV+ cells; however, whilst general channel activity and PV+ interneuron recruitment is likely to be highly important for optimal working memory, the extent to which flexible recruitment due to excitatory plasticity in these cells contributes to working memory is unclear. To explore this, I repeated the T-maze task performed in Chapter 3 with the experimental cohort.

After several habituation sessions to become accustomed to the T-maze, the task was performed as previously, with 10 trials in a session and a 5-second delay between consuming the reward in the forced/sample trial and placement back in the maze for the choice trial. The animals had no previous experience of performing the task before the first day of testing. Across 6 sessions, there were no clear differences between the control (n = 11 animals) and experimental (n=12 animals) groups, with both groups learning the task similarly well (Fig. 5.5Ai). A 2 (viral type) * 2 (gender) * 6 (session) repeated-measures ANOVA did not reveal a main effect of viral treatment ($F_{(1,19)} = 1.405$, $p = 0.25$), nor an interaction between session and viral treatment ($F_{(5,105)} = 0.712$, $p = 0.616$); furthermore, there was no effect of gender on performance, nor any interaction with session or viral treatment

Figure 5.5 (next page). Transfection of hippocampal PV+ interneurons with the floxed GluR2 virus resulted in a delay-dependant impairment on the rewarded alternation T-maze task. (A) (i) Both groups learnt the task with a 5-second delay between the sample and choice phases at a similar rate, reaching a near-identical level of performance after 6 days (84.55% vs 85%). (ii) Splitting sessions into two halves of 5 trials, however, revealed a significant interaction between viral treatment and half of session (averaged across 6 sessions of training/testing), with controls improving with accumulating trials (73.33% vs 83.64%), and GluR2-transfected animals deteriorating (78.06% vs 70%). (B) (i) Extending the sample-choice delay to 30 seconds resulted in a substantial impairment in performance in the GluR2-expressing group only, which persisted across 2 sessions of testing. (ii) Averaging performance across the two days revealed a strongly significant decrease in % correct choices in the GluR2 group compared to controls (81.36% vs 60.42%). (iii) Separating the two sessions into 2 halves of 5 trials each revealed a decrease in performance from the first to the second half of testing sessions in the GluR2 group (65% vs 55.83%), in contrast to a small increase in controls (78.18% vs 84.55%). (C) (i) In 12-trial sessions containing interleaved short- and long-delay trials, performance remained roughly similar between the two trial types for control animals (85.61% and 82.58%), whilst the GluR2-injected animals showed a substantial drop-off in performance during long-delay trials compared to short-delay trials (88.89% vs 61.81%). (ii) The two groups exhibited similar choice latencies during trials with both short and long delays. Horizontal dashed lines represent chance (50%). $*^4$ = $p < 0.04$, $**^4$ = $p < 0.008$, $***^4$ = $p < 0.001$. N = 11 control animals, 12 GluR2 animals.

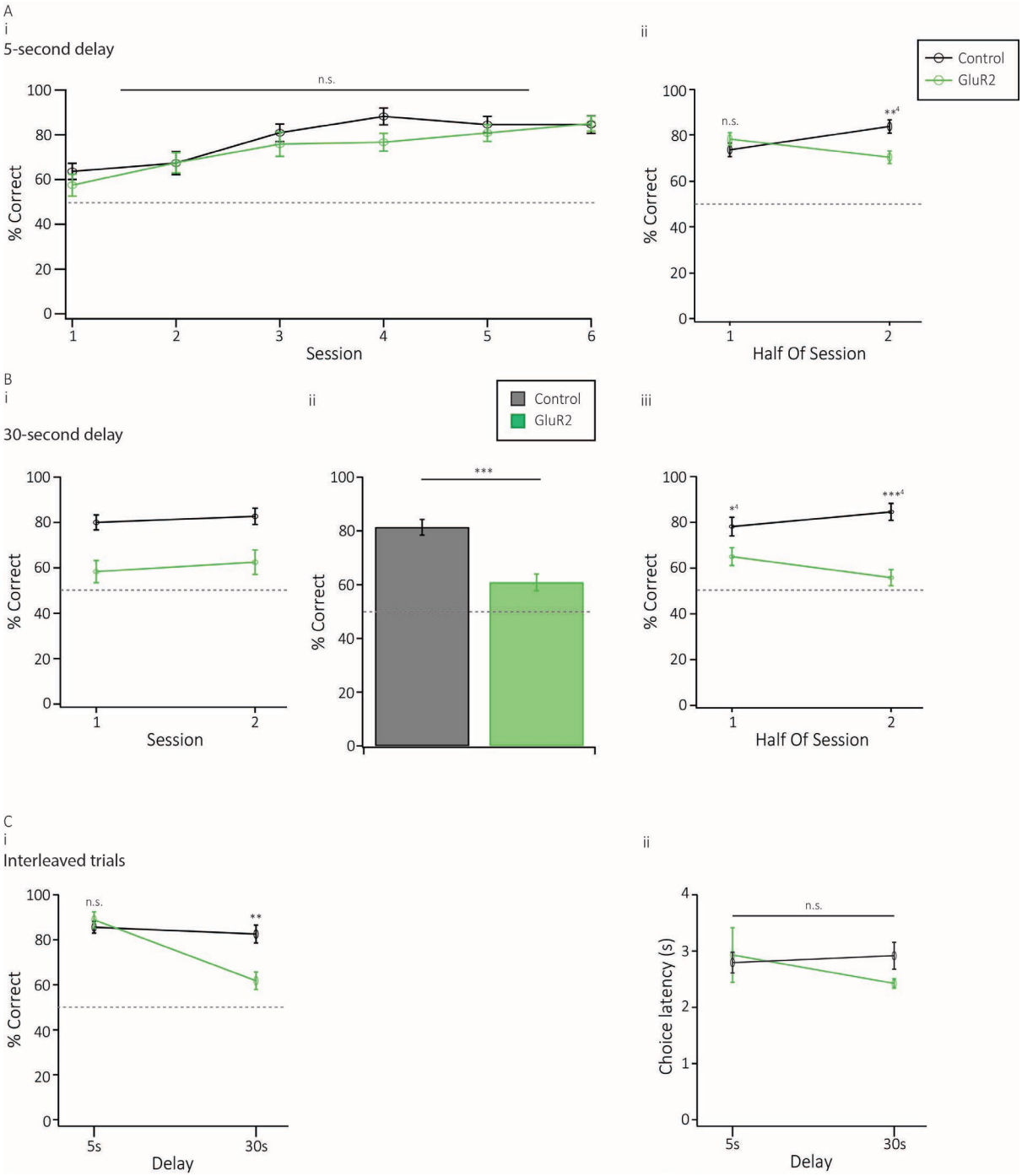

(p > 0.01). In the sixth session, performance in the two groups was almost identical (84.55 ± 3.9% vs 85 ± 3.4%).

However, when splitting session into two halves of 5 trials and adding half of session as a factor into the same ANOVA, a highly significant interaction between viral treatment and half of session

emerged ($F_{(1,21)}$ = 25.777, p < 0.001; Fig. 5.5Aii). Testing for simple effects (with a significance value of 0.04), it was found that both groups showed a significantly different % of correct choices between the first and second half of sessions across the 6 sessions, with the controls improving in the second half of sessions (73.33 ± 3% in first half vs 83.64 ± 2.9% in second half; $F_{(1,10)}$ = 15.561, p = 0.001), whilst the GluR2-transfected group made less correct choices in the second half compared to the first (78.06 ± 2.8% vs 70 ± 2.8%, as previously; $F_{(1,11)}$ = 10.377, p = 0.004). Comparing between the two viral groups, there was no significant difference between the two groups during the first half of sessions ($F_{(1,21)}$ = 1.322, p = 0.263), but a significant difference during the second half of sessions, as a result of the greater number of mistakes made by the GluR2 group compared to the control group ($F_{(1,21)}$ = 11.665, p = 0.003).

The parameters of the test were then altered, such that the 5-second delay between the sample and choice phases of the test was extended to 30 seconds, during which time the animal would be placed in an empty cage (separate from the holding cage during testing or home cage). This alteration resulted in a notable decrease in performance only in the GluR2-transfected group (Fig. 5.5B). Across two days of testing, the control group performed at a level close to what they did with the 5-second delay; however, the GluR2 group showed a decline that persisted to the second day (Fig. 5.5Bi). When performance across the two days was averaged, a 2 (viral type) * 2 (gender) ANOVA revealed that the number of correct choices made by the GluR2 group was at a strongly significantly lower level than the number recorded by the control group (81.36 ± 2.9% vs 60.42 ± 3.1%; $F_{(1,19)}$ = 23.579, p < 0.001; Fig. 5.5Bii). In contrast, there was no effect of gender ($F_{(1,19)}$ = 2.662, p = 0.119), nor an interaction between gender and viral treatment ($F_{(1,19)}$ = 0.065, p = 0.801).

Furthermore, when sessions were divided into two halves of 5 trials, a 2 (viral type) * 2 (session) * 2 (half) ANOVA revealed a significant interaction between viral treatment and half of session ($F_{(1,21)}$ =

5.649, p = 0.027; Fig. 5.5Biii). *Post hoc* simple main effects (with a significance value of 0.04) revealed whilst performance in the GFP-treated control group showed no significant change between the first and second half of sessions (78.18 ± 4.1% vs 84.55 ± 3.7%; $F_{(1,10)} = 1.818$, p = 0.192), the GluR2-transfected group showed a trend towards a significant decline in performance in the second half compared to the first (65 ± 3.9% vs 55.83 ± 3.5%; $F_{(1,11)} = 4.115$, p = 0.055). As a result, the significant difference between the two groups during the first half of sessions ($F_{(1,21)} = 5.42$, p = 0.03) expanded to a strongly significant difference during the second half of sessions ($F_{(1,21)} = 31.398$, p < 0.001). The difference in performance between the two groups on the task with the 30-second delay developed over time, as the two groups were not significantly different in performance on the first trial across the two sessions (72.73 ± 10.3% vs 62.5 ± 9%; t(21) = 0.749, p = 0.462). The impaired performance over time did not appear to be as a result of satiation, as trial choice latencies across the session were not significantly different between the two viral groups, did not significantly change between the first and second half of sessions, and there was no significant interaction between the two variables ($F_{(1,21)} \leq 0.542$, $p \geq 0.4$).

Due to the change in experimental parameters, there was the possibility that the impairment with a 30-second delay was at least partially due an increased sensitivity to changes in experimental parameters (e.g. extension of the sample-choice delay, exposure to a separate holding cage during this delay). Alternatively, with the apparent deterioration of performance with increasing trials, it was possible that an impairment may have developed with a 5-second delay with increasing numbers of sessions. To demonstrate that the decrease in correct choices made was due to a memory impairment emerging only when subjected to a prolonged sample-choice delay, I subjected the cohort to sessions containing trials with short and long sample-choice delays interleaved with each other.

During this phase of testing, the cohort was further subjected to 2 sessions containing 12 trials, 6 with a 5-second sample-choice delay and 6 with a 30-second delay, interleaved in a pseudorandom order (Fig. 5.5Ci). Both groups showed similar ability to make correct choices on short-delay trials (85.61 ± 2.6% vs 88.89 ± 2.5%), but the GluR2 group still showed a substantially reduced level of correct choice-making on 30-second delay trials compared to controls (82.58 ± 4% vs 61.81 ± 3.9%). A 2 (viral type) * 2 (session) * 2 (delay) ANOVA revealed a significant main effect of virus ($F_{(1,21)}$ = 6.277, p = 0.021), and of delay ($F_{(1,21)}$ = 22.877, p < 0.001), as well as a significant interaction between viral treatment and trial delay ($F_{(1,21)}$ = 14.595, p = 0.001). Simple main effects revealed no significant difference between the two groups with 5-second delay trials ($F_{(1,21)}$ = 0.819, p = 0.376), but a strongly significant difference when the delay is extended to 30 seconds ($F_{(1,21)}$ = 13.91, p = 0.001). The discrepancy between the two groups at the different latencies could not be explained by the time taken to make a choice, as both groups exhibited similarly short choice latencies on trials with both short and long delays. A 2 (viral treatment) * 2 (delay) ANOVA revealed no significant effect of delay nor of viral treatment on choice latency, nor an interaction between the two variables ($F_{(1,21)}$ ≤ 1.58, p ≥ 0.2; Fig. 5.5Cii).

Overall, this series of experiments indicates that, whilst the group transfected with the GluR2 virus are equally capable of performing the rewarded alternation T-maze task and performing it correctly with a short delay, increasing the working memory load by extending the period of time the animal needs to retain information regarding the sample phase of the trial brings out an impairment in the cohort compared to GFP-injected controls. This impairment appears to get worse when the animal has already performed more trials, which may indicate interference with memories of past trials that result from disruption in the ability to adjust recruitment of PV+ cells, and consequentially non-optimal network activity. That the animals could still perform the short-delay task as well as controls

whilst struggling with the long-delay task indicates it is an issue with memory, rather than task comprehension.

5.3.6 Intact spatial reference memory acquisition and retention in transfected mice in the appetitive Y-maze task

Whilst previous studies have found impairments in working memory following manipulations in PV+ cell recruitment, they have typically also reported intact spatial reference memory in the same cohort (Fuchs et al., 2007). In contrast to the short-term, flexible memory that underpins correct choice-making on the T-maze task shown in the previous section, spatial reference memory tasks require long-term memory of an association between a particular location and an outcome (e.g. food reward, escape). One such task is the elevated Y-maze reference memory task, which involves an animal being assigned a constant reward arm defined by allocentric, extramaze spatial cues, for the duration of testing, and receiving multiple trials each day in which they start from either of the two non-reward arms (Fig. 5.6A). Studies involving PV-specific knockout of GluR1 or full-brain knockout of GluR4 have shown normal performance of this task, even in the presence of working memory deficits (Caputi et al., 2012; Fuchs et al., 2007). As such, one would expect the two experimental groups in the present study to learn the task similarly.

Both groups showed similarly poor performance over the first five sessions of training/testing, with minimal improvement except for a small subsection of animals (Fig. 5.6Aii). The poor performance was due to most animals generally making the same directional turn regardless of start point, and as 50% of trials in a session started from each non-rewarded arm, these animals would consistently score 50%. Given that there was a limited time window to extract information regarding reference

memory from the cohort before moving onto the next task, it was decided that the animals would be given some assistance in understanding the rules of the task. As such, after the fifth session of training, all mice that scored 80% or less (21 out of 23 animals) were given additional training, involving a rapid succession of trials with a short inter-trial interval (minimum 1 minute), all starting from the arm that each animal would typically make an incorrect turn from, until they began to make the opposite turn and correctly enter the reward arm. Once they made 3 correct choices, the animals received a final sequence of trials from the other start arm, to ensure they still correctly found the reward arm from there. Once they had made one correct choice from this arm, they were returned to the home cage. This additional training caused an immediate improvement the following day in a majority of mice, but for those that didn't respond well (60% or fewer correct choices, 7 animals, 3 from the GFP-injected group and 4 from the GluR2-injected group), one additional session of remedial training was given after the sixth regular training session. Qualitatively, there was no systematic difference between the two groups regarding the extent of remedial training required and provided.

Both groups showed similar improvements following this additional training, and showed high levels of correct choice-making, with both groups averaging over 80% correct choices for the final four days of testing. A 2 (viral type) * 2 (gender) * 10 (session) repeated-measures ANOVA across the whole training/testing period revealed a significant effect of session (no assumption of sphericity ($\chi^2(44) = 81.611$, $p = 0.001$, G-G $\varepsilon = 0.483$); $F_{(4.347,82.591)} = 36.5346$, $p < 0.001$), but did not show an effect of virus ($F_{(1,21)} = 0.031$, $p = 0.863$), gender ($F_{(1,21)} = 1.452$, $p = 0.243$), or an interaction between virus and session ($F_{(4.347,825917)} = 0.497$, $p = 0.753$). The final testing session involved post-choice baiting, wherein the reward was only given once the animal entered the correct reward arm, thus accounting for any influence olfactory cues rom the reward itself may have had on the animals. An independent-samples t-test for this final session revealed no difference between the two

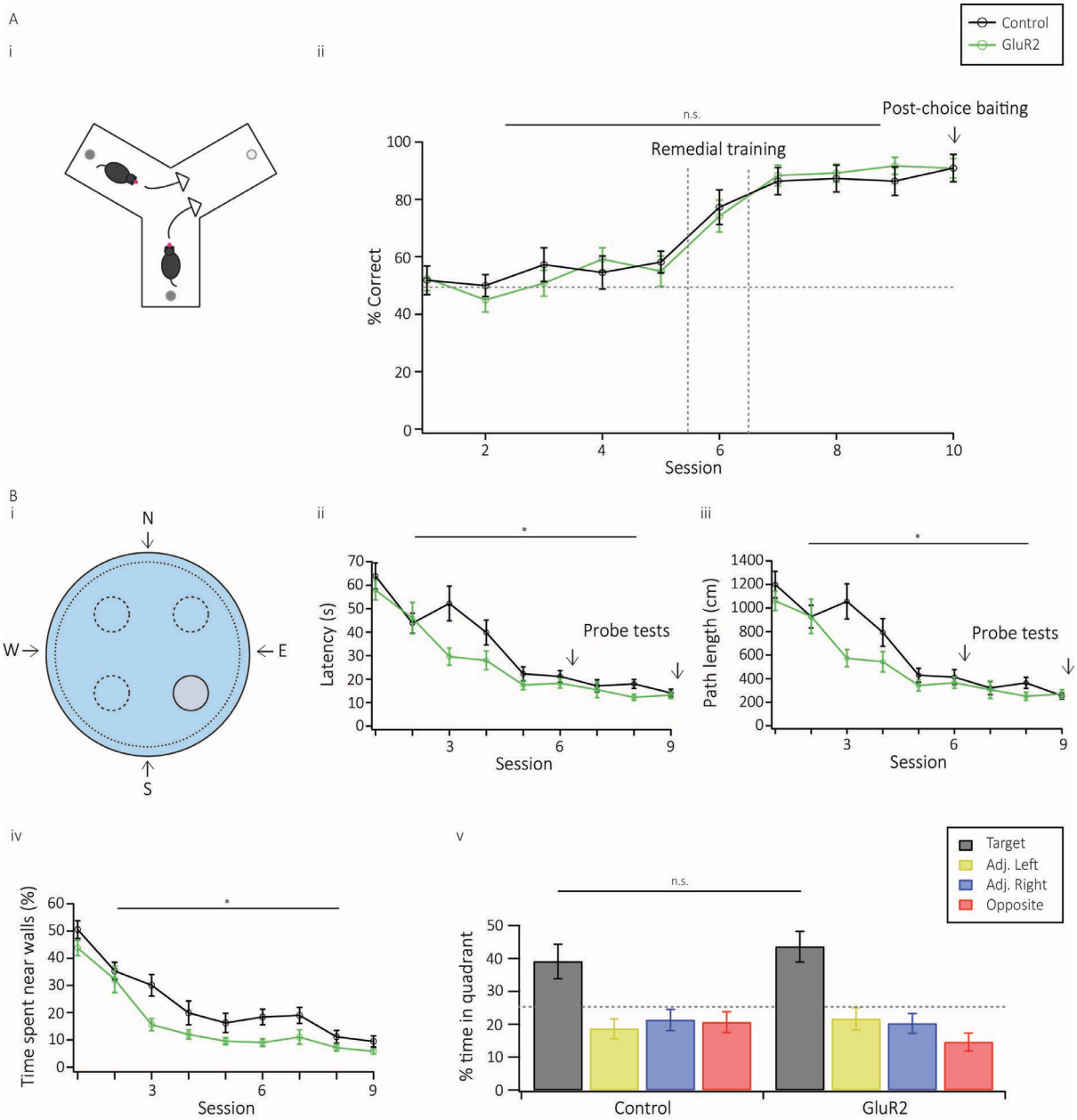

Figure 5.6. Spatial reference memory remains intact in animals transfected with the GluR2 virus. (A) (i) The appetitive spatial reference memory-dependent Y-maze task involves an animal learning to adjust its choice-making from a variable starting point to go to a static reward location. Choice-making is guided by extramaze cues. (ii) Both experimental groups showed similar performance on the task throughout the study. The majority of animals in both groups had difficulties learning the task despite multiple sessions, so blocks of remedial training were given after session 5 for any animal that scored 80% or less on that day, and after session 6 for any animal that scored 60% or less. Both groups responded similarly well to the remedial training, and reached a very similar level of performance, with the mean scores on the final day with post-choice baiting almost identical (90.91% vs 90.83%). (B) (i) The spatial reference memory version of the Morris water maze requires animals to learn to use extramaze cues to navigate towards a static hidden platform from varying start points. The performance over 9 days, measured using either (ii) latency to find platform or (iii) path length to platform demonstrate no impairment in the GluR2 group, and even better performance over the first few days. (iv) The GluR2 group showed a greater tendency to move away from the wall and explore the maze, which may in part explain the better initial performance on the task. (v) Probe tests were performed after sessions 6 and 9, in which the animal was placed into the water maze without the platform present and its affinity for its past location determined. Aggregating together performance across the two probe tests reveal similar preference for the segment containing the learned platform location (39.06% vs 43.54%). Horizontal dashed lines represent chance performance. N = 11 control animals, 12 GluR2 animals.

experimental groups (90.91 ± 4.8% vs 90.83 ± 3.4%; t(21) = 0.013, p = 0.99). Furthermore, a 2 (viral type) * 2 (session) ANOVA across the final two days of testing showed no significant effect of introducing post-choice baiting on performance ($F_{(1,21)}$ = 0.525, p = 0.477).

Overall, whilst there were difficulties encountered with both viral groups with procedural aspects of the elevated Y-maze task without assistance, both groups of animals showed similar performance once they had received remedial training. Thus, whilst spatial working memory is impaired under certain conditions in the GluR2-treated cohort, transfection of hippocampal PV+ interneurons with the GluR2-expressing virus has no clear effect upon spatial reference memory in an appetitive task with similar procedural, sensorimotor, and motivational demands.

5.3.7 Slower learning of new platform locations in Morris water maze in animals transfected with GluR2 virus

Previous studies have reported changes in hippocampal pyramidal cell-to-interneuron monosynaptic strength correlating with learning of new reward locations in a familiar environment (Dupret et al., 2013). Whilst these studies used a cheeseboard apparatus we did not possess, other studies have shown deficits in receptor knockout models when animals had to learn new escape platform locations in the Morris water maze (Nakazawa et al., 2003). As such, I decided to conclude the study with a two-part experiment utilising the water maze.

The water maze involves placing the animal into a tub filled with an opaque water:paint mix from 8 potential start points, denoted with compass directions (Fig. 5.6B). Animals received 4 trials in a session, with the starting points randomly assigned from the 8 possible options. From these start

points, animals would have to use extramaze cues to navigate towards a platform hidden just below the water surface in a fixed location. There are 4 possible platform locations, but for the initial phase of this experiment, hereby referred to as the reference memory phase, animals were assigned either southeast (SE) or northwest (NW), counterbalanced for viral type and gender. The cohort received 9 sessions of training to this single assigned platform location on consecutive days. Furthermore, the day following sessions 6 and 9, animals received probe tests, in which the platform was removed and the animal placed in the maze at the start point opposite the platform location and allowed to swim freely for 60 seconds (i.e. SE for animals trained to NW and vice versa), with the amount of time spent in each of the four quadrants of the maze assessed.

Across the reference memory phase, the GluR2-injected animals showed no impairment in learning the initial platform location; in fact, if anything, the GluR2 mice performed better during acquisition. Two measures were used to assess performance in the water maze – the latency from initial placement in the maze to climbing onto the platform, or the path length from starting position to platform. Using 2 (viral type) * 2 (gender) * 9 (session) repeated-measures ANOVAs to investigate any influence of virus on either variable, a significant main effect of virus was found for both latency ($F_{(1,19)} = 8.479$, $p = 0.009$; Fig. 5.6Bii) and path length ($F_{(1,21)} = 6.062$, $p = 0.024$; Fig. 5.6Biii). Additionally, significant main effects of gender were seen for latency ($F_{(1,19)} = 7.039$, $p = 0.016$) and path length ($F_{(1,19)} = 6.443$, $p = 0.02$). Significant interactions were found between viral type and session for latency (no assumption of sphericity ($\chi^2(35) = 102.729$, $p < 0.001$, G-G $\varepsilon = 0.536$); $F_{(4.289,81.484)} = 2.611$, $p = 0.038$) and for path length (no assumption of sphericity ($\chi^2(35) = 114.9$, $p < 0.001$, G-G $\varepsilon = 0.505$, $F_{(4.406,76.873)} = 2.784$, $p = 0.032$ for latency). There were no interactions between gender and viral treatment, or gender, virus, and session, for either latency or path length.

The main effect of viral type is due to the faster acquisition of the platform location in the GluR2 group as determined by their markedly lower latencies and path lengths during sessions 3 and 4 (for the main effect of gender, the males learned faster than females). Exploring the nature of the interactions, simple main effects revealed a significant difference in the latencies between the two viral groups restricted to day 3 ($F_{(1,19)}$ = 10.874, p = 0.004), with the same observed for path length ($F_{(1,19)}$ = 12.017, p = 0.003). The faster acquisition may be in part due to a greater tendency to explore the maze, as the GluR2 group spent less time in the immediate vicinity of the walls ($F_{(1,19)}$ = 15.590, p = 0.001; Fig. 5.6Biv). Performance in both viral treatment groups was similar from session 5 onwards, and averaging the results from both probe tests revealed a similar preference for the quadrant in which the platform had been previously located (termed the target quadrant), indicating both groups had a broadly equivalent peak reference memory capacity (Fig. 5.6Bv). Comparing each group to chance-level performance, both the control group (39.06 ± 4.5%; t(10) = 3.146, p = 0.01) and the GluR2-treated group (43.54 ± 3.6%; t(11) = 5.207, p < 0.001) showed a significantly above-chance (25%) preference for the target quadrant, and an ANOVA for virus and gender revealed there was no no effect of viral treatment on the % time spent in the target quadrant ($F_{(1,19)}$ = 0.455, p = 0.508), nor an effect of gender or interaction between the two variables (p > 0.1).

After establishing the absence of any reference memory impairment in the GluR2-transfected experimental group, the study moved onto the second phase of the water maze experiment, involving serial 'spatial reversals', in which the location of the platform was moved several times to new locations (Fig. 5.7). First, the day after the second probe test, the position of the platform was moved to the quadrant opposite its initial location (i.e. animals trained to NW now had to go to SE to find the platform), with each animal receiving three days of testing at this new location before another probe test (Fig. 5.7A). Using either latency or path length as a readout of performance, there was no major difference between the groups following this first reversal ($F_{(1,21)}$ = 0.109, p =

0.745 for latency; $F_{(1,21)} = 0.999$, $p = 0.329$ for path length). After this, the platform location was moved twice more, to NE and SW, with the order of platform positions counterbalanced for viral treatment, gender, and previous platform order (Fig. 5.7B, C). Following these reversals, the GluR2 group was less able to learn the new platform locations, with longer averaged latencies and path lengths during the first two sessions of both reversals.

When averaged across all 3 reversals, 2 (viral type) * 2 (gender) * 3 (session) * 3 (platform positions) repeated-measures ANOVAs revealed a significant main effect of viral treatment on path length ($F_{(1,19)} = 6.257$, $p = 0.022$; Fig. 5.7D), but not on latency ($F_{(1,19)} = 1.995$, $p = 0.174$). There was no effect of gender on either variable, nor any interactions between virus and gender ($p > 0.1$). The main effect of viral treatment on path length occurred in the absence of a significant interaction between viral treatment and platform position ($F_{(2,38)} = 0.709$, $p = 0.499$). Furthermore, a 2 (viral type) * 2 (gender) * 3 (session) * 3 (platform positions) revealed that there was a significant main effect of viral treatment on time spent in the quadrant containing the previous platform location during acquisition trials ($F_{(1,191)} = 6.239$, $p = 0.022$), plus an effect of session ($F_{(2,38)} = 15.509$, $p < 0.001$), but no other effects or interactions involving virus, gender, or platform. There was no observed interaction between virus and session for any variable; however, the effect on path length was strongest during the first two days of training, with the peak difference between the two groups during the second session (433.32 ± 30.7 cm vs 678.39 ± 66.6 cm). The difference between the two groups decreased substantially by the third session, chiefly due to improved performance in the GluR2 group (407.02 ± 28.6 cm vs 474.69 ± 55.8 cm).

The notion that the GluR2 group was eventually capable of learning the new platform locations to at least the same level as the control group was supported by the average performance of the two groups during the probe tests that followed each 3-session training period (Fig. 5.7E). The GluR2-

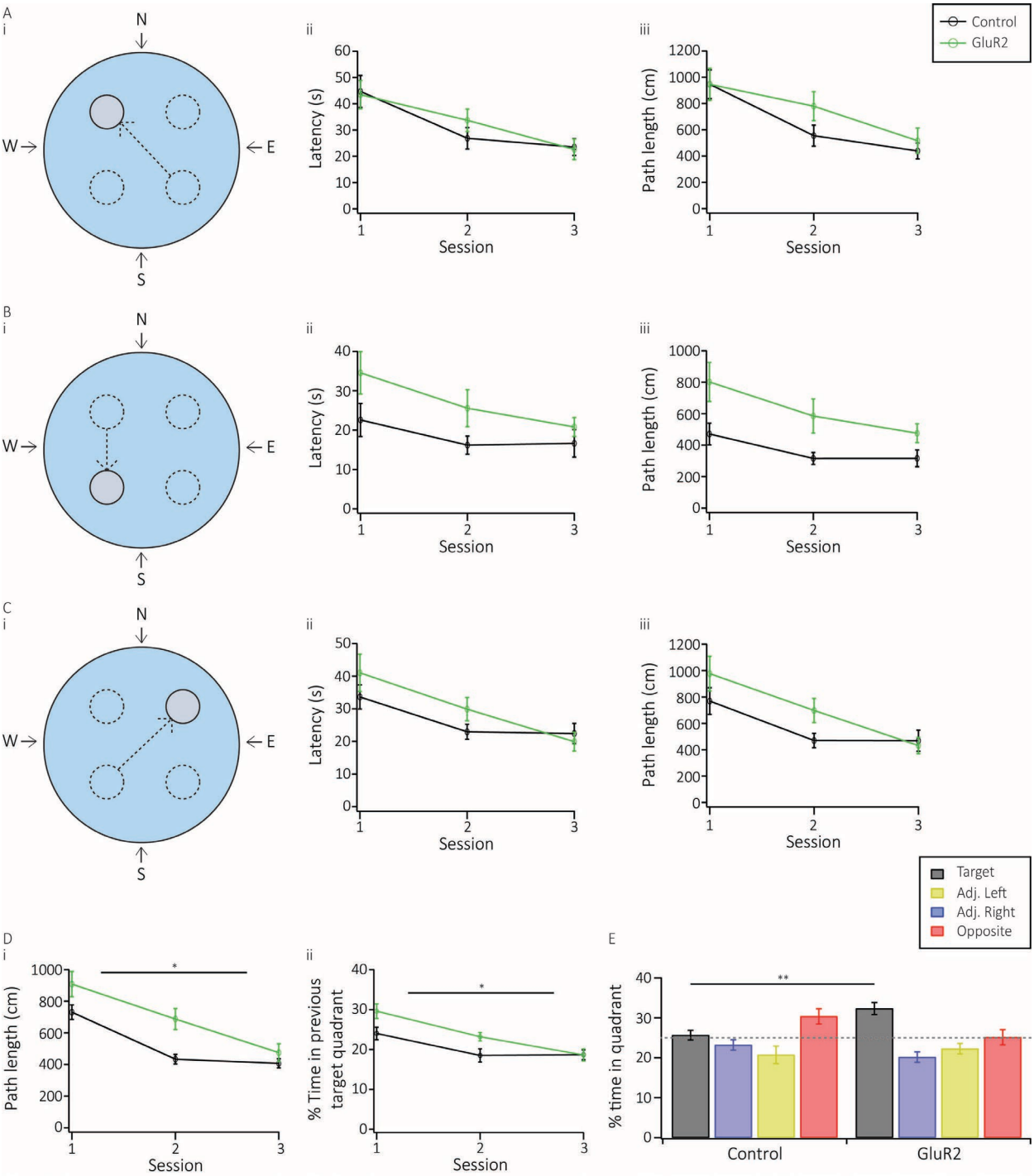

Figure 5.7. Transfection of hippocampal PV+ interneurons with a GluR2-expressing virus causes an impairment in a serial spatial reversal water maze task. (A-C) (i) Each reversal consisted of the platform being moved to a previously unused location for each animal, with the first reversal involving moving the platform opposite its initial location. (ii) Latency to reach the platform and (iii) path length to platform were recorded for each group for 3 training sessions per new location. (D) (i) Path length to platform was significantly shorter in the control group compared to the GluR2 group when averaged across the three reversals, (ii) as was the time spent in the water maze quadrant containing the previously learnt platform location. (E) The GluR2-injected group was able to adequately learn the new platform location after 3 sessions of training, as they averaged a significantly higher % time spent in the new target quadrant across the three probe tests compared to controls (25.67% vs 32.33%). N = 11 control animals, 12 GluR2 animals.

injected group showed significantly greater preference for the target quadrant compared to the

control group (25.67 ± 1.2% vs 32.33 ± 1.5%; $t(21) = 3.42$, $p = 0.003$). In fact, whilst the GluR2 group still showed a significantly above-chance preference for the target quadrant during reversal probe tests ($t(11) = 4.965$, $p < 0.001$), the control group did not show a significant preference for the target quadrant ($t(11) = 0.537$, $p = 0.603$).

Overall, the data from the water maze study indicate that whilst overexpression of GluR2 in hippocampal PV+ interneurons does not impair the general ability to learn a fixed location in an environment, animals carrying the manipulation have greater difficulty in adjusting to new locations compared to control animals. This issue can be overcome with repeated exposure to the new location, but suggests that, as in the T-maze, interference may arise in these animals from memories of previous platform locations competing with memories of the new position.

5.4 Discussion

The study has revealed that bilateral full hippocampal injection of a virus driving Cre-dependent expression of edited GluR2 into PV-Cre mice results in highly specific impairments in spatial memory, appearing to result from interference between memory traces arising due to the reduced flexibility within the hippocampus network. These impairments emerged in the absence of significant deficits in long-term reference memory or novelty preference, contrasting performance on anxiety tests, and only mild changes in locomotor and rearing behaviour. These results reveal a specific importance for the presence of CP-AMPARs at excitatory inputs onto hippocampal PV+ interneurons for certain memory processes, likely due to excitatory plasticity mediated by calcium currents flowing through these channels.

As mentioned in the introduction, the experiments performed within this Chapter were unblinded. This was a consequence of both the intrahippocampal injections and behavioural tests being performed by the same experimenter working solo, itself a consequence of time and personnel restrictions. The benefits of blinded behavioural experiments are clear, as observer bias has been widely reported as a potential confound of research (Holman et al., 2015; Tuyttens et al., 2014; van Wilgenburg and Elgar, 2013). Some experiments are more open to the influence of experimenter bias than others; the lomocotor assay is collected automatically by software and occurs over a 2-hour period in the absence of the experimenter, whilst the spatial novelty preference task requires manual timing of mouse entries and close interaction with the animals. Nevertheless, future experiments would benefit from blinding if possible.

Spontaneous locomotor exploration is known to be affected by hippocampal lesions, as well as novelty of the current environment (Arenas et al., 2014; Cassel et al., 1998). The influence of PV+ interneuron function or dysfunction upon locomotor activity has had limited study, although one group reported novelty-induced hyperactivity in an animal with PV+-specific NMDAR NR1 subunit ablation, whilst another reported age-restricted hyperactivity and reduced inhibitory activity following expression of mutant huntingtin in PV+ interneurons (Belforte et al., 2010; Dougherty et al., 2014). In this study, I saw no change in overall locomotor activity as defined by number of beam breaks across 2 hours of testing, but I saw a significant decrease restricted to the initial 20-minute period of testing. Whilst NMDAR activity in PV+ interneurons is reported as necessary for timely reductions in activity following continued exposure to novel environments, GluR2 introduction appeared to cause a quicker reduction in novelty-induced hyperactivity compared to control animals. This restricted effect may be due to altered habituation and responses to novelty within these animals, which will be touched upon again when discussing the spatial novelty preference results.

I also observed a significant reduction in rearing activity across the testing period in the experimental group when compared to control animals. Rearing activity is believed to be a risk assessment behaviour in response to stressful situations, and is associated with anxiety (Piras et al., 2013). In different animals and studies, hippocampal lesions have been shown to either decrease or increase rearing activity (Clifton et al., 1998; Glickman et al., 1970). GABAergic activity appears to make some contribution to this, but in which way is not entirely clear; anxiolytic drugs (acting on $GABA_A$ receptors) have been shown to increase rearing in a high-stress environment, and decrease rearing in a low-stress environment (McNaughton, 1985; McNaughton et al., 1984). As a novel environment, the LMA boxes might be considered a stressful environment to the experimental animals, considering their relative experimental naivety prior to being subjected to the assay. However, the lower levels activity in the GluR2-transfected animals compared to controls in the early period inside the boxes suggests that the animals might have been habituating slightly quicker to the boxes, suggesting that they may have considered the environment less stressful than the control group. Whether this might be due to changes in plasticity at interneuron synapses, or baseline excitability and drive onto interneurons is unclear. Given that selective chemical activation of hippocampal PV+ interneurons (in the dentate gyrus) has been reported to have an anxiolytic effect, it may be that the changes at synapses onto hippocampal PV+ interneurons in my model either decreased interneuron recruitment if the LMA boxes were considered a high-stress environment, or increased activity if they were considered a low-stress environment (Zou et al., 2016).

If the reduction in rearing is a result of an anxiolytic phenotype in the GluR2 animals, one might expect a significant decrease in anxiety measures on the various anxiety assays they were subjected to during this study. However, analysis revealed an effect of both viral treatment and gender on

percent time spent on open arms during the EPM task, resulting from less time spent by GluR2 animals and males compared to controls and females, whilst no significant difference between the two viral groups was observed in the other two anxiety tests, suggesting that the GluR2 animals may have exhibited greater anxiety in my cohort. Ventral hippocampal activity has been shown to have a large contribution to expression of anxiety and fear, as has GABAergic activity (Bannerman et al., 2003b; Nuss, 2015). Additionally, alterations in hippocampal PV+ interneuron function have been shown to influence anxiety-related phenotypes (Winkelmann et al., 2014; Zou et al., 2016). However, given the inconsistent relative performance of the control and experimental groups on the various anxiety tests, it is unclear whether the preserved functionality of PV+ interneurons in the GluR2-transfected animals is sufficient to maintain normal anxiety-related behaviour.

Regarding the contrast between the results in this study and those following DREADD-induced activation of PV+ interneurons, several differences are present between the two approaches used. The viral manipulation approach involves a long-term alteration in the properties of PV+ interneurons, whilst DREADD activation only lasts for a period of approximately 1 hour; as such, any long-term adaptive changes in the network resulting from alterations in PV+ interneuron AMPAR properties will not be present in DREADD-transfected mice (Zou et al., 2016). Additionally, treatment with CNO caused direct activation of PV+ interneurons and led to increased firing frequency of DREADD-transfected neurons. In contrast, the manipulation in the current study, whilst altering the excitability of neurons due to both AMPAR-mediated current properties and loss of plasticity, does not directly drive or inhibit interneuronal activity; as such, the patterns of network activity are likely to be different in CNO-treated, DREADD-transfected mice in comparison to the GluR2 virus-transfected animals in this study. Nevertheless, based on the EPM result, it is possible that if activation of hippocampal PV+ interneurons is anxiolytic, that a potentially anxiogenic phenotype in the GluR2 group represents reduced excitability of hippocampal PV+ interneurons, that may be a

consequence either of the different properties of GluR2-containing AMPARs compared to CP-AMPARs, or longer-term changes in the network resulting from the loss of interneuron plasticity.

Concerning the locomotor assay data, one possibility is that the early reduction in movement observed may have been due to altered responses to novelty in the experimental group. I decided to investigate novelty recognition in the cohort using a spatial novelty preference test. Animals with hippocampal lesions lose their ability to recognise the novel location on this task, whilst animals lacking the perineuronal net protein brevican, important for modulating synaptic function and plasticity in PV+ interneurons, also show reduced novelty preference (Favuzzi et al., 2017; Sanderson et al., 2007). However, my two groups showed no significant difference in novelty recognition, and the GluR2-injected group showed a trend towards increased novelty preference compared to the control group. This non-significant increase in preference for the novel arm over the previously explored arm could possibly due to faster habituation to the previous arms, which would tie in with the results from the locomotor assay, with the GluR2 animals showing a faster reduction in exploratory activity with exposure to the novel environment. As to why the GluR2 animals do not replicate the impaired novelty preference phenotype seen following brevican knockout, it may be that the deficits observed in those animals occur due to effects on the synapse beyond alterations in plasticity.

One point that merits some discussion in relation to the tasks discussed thus far is the group size used during the study, and the potential underpowering of certain experiments. Due to practical limitations, 12 animals were included in each initial viral group for this behavioural study. However, some anxiety tests are relatively low powered due to inter-individual variability, and can potentially require large group sizes to observe significant differences between groups in the presence of small but behaviourally relevant effect sizes. As such, with larger groups, some of the trends observed in

the previously discussed tasks may have become significant. Using the data collected in this chapter as a pilot study, it is possible to perform power calculations to estimate the sample sizes required to consistently observe significant differences between the control and GluR2-transfected group on the reported tasks. The results of such calculations, performed with the assistance of publicly available online power calculators, demonstrate the potential limitations of some behavioural tasks. For example, based on the reported beam breaks in the lomocotor assay and time to sample in the neophagia assay, for the tasks to be adequately powered such that true effects of the GluR2 manipulation would be consistently reported as significant (80% power), one would need n's of 62 animals/group and 92 animals/group, respectively. In fact, even with the borderline significant difference in novelty ratios between the two groups reported on the novelty preference task, power calculations suggest that a significant difference in spatial novelty preference would only be reliably reported with 37 animals in each group. In contrast, by using the data underpinning the strongly significant difference in performance between the two groups on the 30-second delay T-maze task, power calculations would suggest the task to have sufficient statistical power with only 3 animals in each group.

There are at least two ways one can interpret these observations. The first is that the experiments performed were insufficiently powered to detect behavioural differences between the two groups with the sample sizes used. The second is that the groups did not exhibit behavioural differences on the task. Indeed, as sample sizes get increasingly large, the chance of observing a very small yet statistically significant difference that may be behaviourally uninformative increases. For example, using the results from the open field assay as a pilot study, one might expect to reliably see a significant effect of viral type on time spent in the inner circle (a readout of anxious behaviour) with group sizes of 300 animals per viral treatment; however, it would be hard to interpret whether this difference truly reflects a substantial alteration in anxiety processes following GluR2 expression in

PV+ interneurons. Studies have managed to observe significant differences following various manipulations on tasks such as the neophagia and novelty preference assays with comparable sample sizes to those used during this study (Bannerman et al., 2003b; Favuzzi et al., 2017). As such, whilst there is certainly a question as to whether the lack of significant differences reported between the two viral groups on some of the tasks are simply a result of underpowered tests, I do not have evidence based on the data collected within this chapter to claim that anxiety processing in response to novel foodstuffs is altered following transfection of PV+ interneurons with the GluR2 virus, and the practicality of repeating some of the tasks with the recommended sample sizes would be prohibitive.

My results in Chapter 3 demonstrated that CP-AMPAR signalling within dorsal hippocampus is necessary for optimal performance on the rewarded alternation T-maze task, whilst the results in Chapter 4 suggest that the drug effects of CP-AMPAR antagonists on gamma oscillations, and potentially therefore working memory, are due to inhibition of CP-AMPARs specifically on PV+ interneurons. Therefore, within this thesis alone there is evidence for the importance of AMPAergic activity in hippocampal PV+ interneurons for expression of working memory, in addition to other studies (Caputi et al., 2012; Fuchs et al., 2007). The deficit in Chapter 3 emerged on the T-maze with a 5-second delay between the sample and choice phase of trials, a delay which failed to differentiate the two groups in the present chapter. However, extending this delay to 30 seconds caused a strongly significant decline in performance only in the GluR2 group, which worsened over the course of testing sessions with repeated trials. The impairment was present even when trials were interleaved with 5-second delay trials where the same group would perform at similar levels to the controls. Therefore, whilst working memory is preserved with minimal load, increasing working memory load reveals a substantial impairment in expression of working memory following transfection of hippocampal PV+ interneurons with GluR2. My results are supported by previous

observations that knockout of brevican results in less accurate choice-making on the T-maze task compared to wild-types with a 15-second delay between the sample and choice phase of trials (Favuzzi et al., 2017).

Is this effect due to impairments in CP-AMPAR-mediated plasticity, and if so, how could it cause this memory deficit? The anti-Hebbian plasticity protocol used in Chapter 4 elicited potentiation of post-synaptic potentials throughout 20 minutes post-pairing; however, a substantial difference in normalised amplitude emerges between control cells and GluR2-transfected PV+ interneurons within 1 minute post-pairing (Fig. 4.8). Between the start of the sample phase and the decision moment during the choice phase is likely to approach 1 minute for trials with a 30-second sample-choice delay, given the latency between initial placement in the maze until reaching the reward arms. Should excitatory plasticity in PV+ interneurons be necessary for maintenance of short-term memory during this period, the impairment in potentiation resulting from a lack of CP-AMPARs may be sufficient to impair this maintenance.

If plasticity is necessary for coping with increasing working memory load, how does it accomplish this? PV+ interneurons are believed to enable retention of short-term episodic memory by shaping the activity of pyramidal cell ensembles such that specific cell assemblies are active on distinct gamma cycles. Flexibility in the strength of synapses onto PV+ interneurons enables context-specific activation of these cells to strengthen inputs and promote the synchronisation of pyramidal cells under the control of these interneurons, leading to formation and maintenance of short-term memory, whilst facilitating the filtering out of weak stimuli (Favuzzi et al., 2017). It would appear that flexibility in the excitability of interneurons is not essential for maintenance of short-term memory with a brief delay, given the similar performance of the two groups with a 5-second delay. It is possible that other brain regions aside from the hippocampus are compensating during short-

delay trials; a delayed nonmatching-to-place radial maze task with short and long delays revealed that medial prefrontal cortex activity could compensate for inactivated hippocampus during short-delay trials, but that dorsal hippocampus activity was necessary for long-delay trials (Lee and Kesner, 2003). Indeed, it was proposed over 30 years ago that, whilst the hippocampus was necessary for intermediate-term working memory, animals with hippocampal damage appeared to have a limited-capacity, limited-duration, short-term memory system outside of the hippocampus that was capable of subserving short-term memory independent of hippocampal function (Rawlins, 1985).

However, with greater memory demand as the animal has to retain information at the forefront of its thought processes for a longer period of time, the inability to favour currently relevant memory traces by promoting the recruitment of specific PV+ interneurons may result in the memory impairments observed during this study. Curiously, it has been shown that hippocampal cell assemblies exhibit activity during the delay period of a memory task, and that similar task conditions (left/right turns) triggered similar sequences of assembly expression (Pastalkova et al., 2008). The parameters of cell-assembly dynamics were proposed to be influenced by various factors, including experience-dependent synaptic plasticity. Increasing the intra-trial delay may increase the network demands for maintaining these sequences. By reducing dynamic PV+ interneuron recruitment within the network and altering cell assembly expression, an impairment in interneuron plasticity may lead to interference between other recent episodic memories, or alternatively increase the rate of memory trace decay, either way increasing the likelihood of making an incorrect choice based on the correct recent memory. The increased number of incorrect choices made during the latter half of sessions with the 30-second intra-trial delay may be due to an increased number of memories of recent trials and a reduced ability to decipher which is the pertinent memory for the current situation.

The concept of interference impairing memory performance in changing conditions has some basis. Whilst studying the mammillary body rather than the hippocampus, another group found that lesioned mice had increasing impairments on a single-phase spontaneous alternation T-maze task with increasing numbers of trials (Béracochéa and Jaffard, 1987). On this task, trials consisted of single runs in which the animal had to enter the alternate arm to the one entered on the previous trial; lesioned mice performed worse than controls with long (30-second) but not short (5-second) delays between trials, which together with the decline in performance with accumulating trials was interpreted by the experimenters as vulnerability to proactive interference (Béracochéa and Jaffard, 1987). Both these results are comparable to the impairments I observed with the GluR2-injected experimental group. Additionally, prefrontal lesioned rats exhibited worse performance with the accumulation of trials during a session on a reference-plus-working memory T-maze task compared to sham-treated animals (Granon et al., 1994).

Concerning hippocampal function, one study found that, whilst inactivating medial prefrontal cortex (mPFC) in rats did not impair initial learning or retrieval of a spatial memory task, animals with inactivated mPFC were impaired in their ability to react to changes to the rules of the task (Guise and Shapiro, 2017). The study found that mPFC activity influenced coding within area CA1 of hippocampus during learning, and in doing so affected how quickly animals could adapt to changes in the task. The idea that optimal network activity promotes effective coding based upon currently relevant information would suggest that impairments of the dynamic nature of the network might partially disrupt this coding and cause interference between memory of new and previously established information. However, I cannot conclusively determine from my results whether the observed memory impairments resulted from deficits in encoding or retrieval. The results from the first trials during the 30-second delay sessions show that whilst the average in the GluR2 group was lower than the GFP group, it was not a significant difference, suggesting that initial encoding may be

mostly intact in the animals, and that the issues may be predominantly driven by difficulties with retrieval of currently revelant memories against competing ones.

Some might be surprised to see the discrepancy between the trend towards increased novelty preference on the spatial novelty preference task and the impaired T-maze performance in the GluR2-injected group, given that both are believed to depend on non-associative short-term memory. However, the spatial novelty preference task involves a single trial, eliminating the possibility of interference emerging. Furthermore, there is minimal strategy involved with the task, as it does not involve reward-driven motivation, but simply depends upon natural spontaneous preference for novelty over familiar locations, a basis of foraging behaviour (Sanderson and Bannerman, 2012). In contrast, whilst both the spontaneous and rewarded alternation versions of the T-maze initially depend upon the innate alternating tendency of rodents (that is likely similarly dependent upon novelty preference and recognition of (relative) familiarity to the spatial novelty task), following repeated training on the task, it is possible that behaviour is driven by decision-making based upon active retention of short-term memory and awareness of the need to alternate. As such, the tasks can be distinguished based upon both the motivation involved and the exposure to each (both number of trials and days); therefore, the response of rodents to each task in terms of approach may differ accordingly.

In contrast to the reported short-term working memory impairment, the experimental group showed no deficits in long-term memory, tested with spatial reference memory tasks such as the Y-maze and water maze. This is in keeping with studies that found performance on such tasks was preserved following PV-specific knockout of GluR1, occurring alongside working memory impairments (Fuchs et al., 2007). In fact, I even saw faster acquisition of the hidden platform in the reference memory phase of the water maze task (although this may be due to reduced thigmotaxis

in these animals enabling more efficient exploration of the maze). The brevican study found that animals impaired on short-term recognition memory exhibited greater discrimination towards a novel object in a long-term memory version of the task (Favuzzi et al., 2017). The group suggested that prolonged experience might reduce excitatory drive onto interneurons, reducing pyramidal cell inhibition and promoting memory consolidation. Other studies have reported experience-related plasticity changes in the configuration of PV+ interneuron network that appear to promote memory consolidation (Donato et al., 2015, 2013). How a lack of plasticity at PV+ interneuron excitatory inputs may improve long-term memory acquisition and consolidation is unclear, and my Y-maze results show no differentiation between my experimental and control groups. The Y-maze experiment was potentially compromised by the prolonged difficulty for many animals in understanding the rules of the task, and the requirement to administer remedial training to improve performing. However, following training, both groups showed very similar long-term memory for the reward location, as they also did in the probe tests during the reference memory phase of the water maze experiment.

A sizeable majority of the behavioural cohort exhibited difficulty in learning how to accurately perform the Y-maze spatial reference memory task. Successful acquisition of the task requires understanding that the food reward is located in a geographically consistent location throughout testing, as well as association of said location with the reward. In failing to improve performance on the task across days of testing without assistance via remedial training, these animals demonstrated a fundamental lack of spatial learning. Having previously been trained on the rewarded alternation T-maze task that required a win-shift strategy for successful completion, one may have hypothesised that, in the absence of successful learning of the rules of the task and the reward location, animals might have instinctively resorted to alternation behaviour. In reality, the poor performance during initial training on the Y-maze resulted from a strong tendency of mice to repeatedly make the same

turning (either left or right, depending on the animal), regardless of start point, suggesting that animals were not using their experience on the T-maze to inform on their behaviour during the Y-maze task, either due to the difference in context (room, maze), or due to the inability to retain memory of previous trials across the 5-minute inter-trial interval. Instead, animals appeared to stick with the reliable 50% reward response rate of a particular direction choice, without processing the link between successful outcome on a particular trial and the starting location. This instinct had become strongly ingrained in some animals, as during the remedial training sessions, some animals received a large number of trials (>20) starting from the 'incorrect' start arm in quick succession before they attempted making the opposite directional choice. However, the majority of animals appeared to adjust their behaviour upon learning that reward acquisition was dependent entry into a specific reward arm, as >50% of animals showed marked improvement on the task following 1 session of remedial training.

In contrast to the intial acquisition of reference memory on the Y-maze and water maze tasks, where the GluR2-treated animals showed a similar, or greater, ability compared to the control group to acquire a constant location within an environment and maintain that memory across days of testing, they were less capable at acquiring a new location within the same environment. This task has similar principles and likely requires similar memory processes to the cheeseboard task discussed previously, during which changes in the strength of purported monosynaptic excitatory-to-inhibitory connections in the hippocampus were detected correlating with learning of new reward locations (Dupret et al., 2013). The GluR2-transfected group had to swim longer distances to find the new platform locations, with a clear difference between the groups following the second and third reversals; furthermore, the GluR2 group spent more time during trials swimming in the water maze quadrant that contained the previous platform location. However, the GluR2 group actually showed

greater affinity towards the new target quadrant in the probe tests following 3 days of training to the new platform location.

It seems that whilst the GluR2-transfected animals struggle to learn to swim towards the new location, with sufficient exposure they are able to acquire a strong representation of the new location. If the animals have impaired excitatory-to-inhibitory plasticity in PV+ interneurons, they may exhibit less refined expression of updated spatial maps for the new platform locations, or a lesser ability to separate out previously applicable maps during retrieval, and therefore exhibit interference between the previous assemblies and new assemblies promoting memory of the current location. Reversal learning on the water maze is also known to require hippocampal NMDAR function, with AP5 infusions and dentate gyrus/CA1-specific NR1 subunit knockouts impairing performance (Bannerman et al., 2014, 2012; Morris et al., 1990). It may be that repeated exposures to the new location across days enable sufficient pyramidal cell plasticity to occur such that the new spatial map for the current platform location becomes dominant despite the lack of interneuron plasticity. When the platform is moved again, the map representing the new location again struggles to compete with the previous representation due to the lack of flexible interneuron recruitment, with the now obsolete representation remaining prominent. The memory interference following spatial reversal is comparable to the effects seen following prefrontal inactivation (Guise and Shapiro, 2017).

The increased preference for the target quadrant in the probe test following reversal training may be due to greater awareness in the control group of the consistently changing nature of the platform location, encouraging animals to search for a new location, but this is unclear. I cannot exclude the possibility that the deficits during the spatial reversals are due to the animals acquiring platform locations more strongly, due to the difference during initial acquisition, and as a result they initially

perform worse during the reversals, but outperform the control group during the reversal probe tests.

Finally, there is also scope for one to interpret the deficit within the context of the response inhibition theory of hippocampal function, given the significantly greater time spent in the water maze quadrant previously containing the escape platform. Interpretation of a similar water maze reversals deficit following cell-specific NMDAR knockout suggested that the difficulty in learning and finding the new platform location following movement from a previously learned location resulted from a failure in inhibiting the response to go to the previous platform location, and that this hippocampus-dependent response inhibition is necessary for resolving interference between competing memories of old and new platform locations (Bannerman et al., 2012). Given that the GluR2-transfected animals appear capable of acquiring long-term memory, it would seem that the deficit during the reversal phase of the water maze task is not due to an impairment in memory encoding (although, as mentioned above, they could be a result of stronger memory encoding).

One could interpret the difference during initial acquisition within this context. I suggested that the differences between the viral groups in path length and latency during acquisition may have been a consequence of reduced thigmotaxis in the GluR2-transfected group. Thigmotaxis can represent anxiety, due to the potential danger of leaving the edges and exploring the central area of the maze, so one could interpret reduced thigmotaxis as a representation of reduced anxiety; however, this may conflict with the reduced time spent in open arms by the GluR2 group on the EPM task (Pritchett et al., 2016). One could interpret a reduction in anxiety to reflect behavioural disinhibition; should the GluR2-transfected mice exhibit reduced inhibition of impulsive responses to move towards previously learned locations, they may also exhibit reduced inhibition of tendencies to leave the relative safety of the water maze edges to enter the more central regions. However, more work

would need to be done to say with greater confidence that the deficit was caused by impaired memory retrieval or a reduced ability to inhibit instinctive behavioural tendencies to move towards the previously learned platform position.

Overall, the experiments in this chapter paint a picture of a selective requirement for excitatory plasticity in fast-spiking PV+ hippocampal interneurons in order to enable flexible recruitment of interneurons in response to dynamics changes within the current environment, enabling the emergence and activity of cell assemblies representing information pertinent to the current situation. Disrupting this plasticity does not disrupt the formation of short-term or long-term memory, but leads to interference between memory traces, both within a short-term memory-dependent setting such as the trial-by-trial variability of the T-maze, as well as more long-term with the water maze serial platform reversals, resulting in sub-optimal representations of the current environment. The impairments resulting from my manipulation are specific to certain aspects of memory, as the transfected animals displayed normal levels of performance under certain conditions on short- and long-term memory-dependent tasks, as well as broadly normal anxiety expression and novelty preference. Therefore, accounts based on differences in non-mnemonic factors (e.g. sensorimotor, motivational, emotional behaviour) seem unlikely. These findings could fit within the context of proposed roles of inhibitory plasticity in maintaining E-I balance and preserving the fidelity of information transmission within networks, as excitatory plasticity in the absence of corresponding inhibitory plasticity has been predicted to lead to noise and excessive activation of newly encoded memories (Lamsa et al., 2005, Vogels et al., 2011). Combined with Chapter 4, these results suggest that my viral manipulation is an effective tool for cell-specific manipulation of AMPAR composition, and could be used in future to explore the importance of CP-AMPAR-mediated activity and plasticity in other cell types, as well as further investigating the mechanisms of PV+ interneuron plasticity and consequences of its absence on network activity during behaviour.

6 Discussion and conclusions

6.1 Summary of the project

The aims of this study were to elucidate the contributions of CP-AMPAR activity and calcium conductance in hippocampal parvalbumin-positive interneurons to the function of the hippocampal network, and the effects of dysfunction of these channels on hippocampus-dependent behaviour. By using pharmacological and genetic approaches, I have dissociated the relative contributions of distinct receptor classes to the dynamics of hippocampal gamma oscillatory activity, demonstrated a requirement of AMPA receptors for dendritic calcium currents and anti-Hebbian plasticity induction in hippocampal PV+ interneurons, and revealed selective memory impairments indicative of interference in the absence of CP-AMPAR-mediated calcium currents in these neurons. These results provide further insight into the mechanisms of network oscillations, and reveal a significant role for dynamic recruitment of fast-spiking perisomatic-targeting interneurons in short- and longer-term memory processes. The findings from each chapter will be briefly summarised and challenged, before a final discussion of the results of the project, their significance within the wider field, and potential future steps that can be taken to build on these discoveries.

6.1.1 In vitro *antagonism of hippocampal AMPARs and effects on network activity*

Chapter 2 investigated the acute effects of CP-AMPAR inhibition on carbachol-evoked gamma-frequency oscillatory activity within an *in vitro* ventral hippocampal preparation. Based on reported deficits in gamma power but not frequency in hippocampal slices following knockout of GluR4 or PV-

specific ablation of GluR1, I anticipated a selective decline in oscillation power following acute blockade of CP-AMPARs, with minimal effects on frequency (Caputi et al., 2012; Fuchs et al., 2007). In fact, I observed a reliable reduction in oscillation power area within 10 minutes post-application of commonly used CP-AMPAR antagonists philanthotoxin-433 and NASPM, with no significant coinciding change in peak oscillation frequency. However, when using a derivative of philanthotoxin with altered AMPAR affinity, philantotoxin-74, I observed substantial transformations in hippocampal activity, with a simultaneous decrease in both power area and peak frequency followed by the emergence of low-frequency, high-amplitude oscillations. Single-cell patch-clamp pharmacology suggests that these more widespread effects following exposure to philantotoxin-74 could be a result of additional antagonism of GluR2-containing AMPARs on top of CP-AMPAR inhibition.

Previous studies had reported reductions in gamma oscillation power without changes in frequency following PV+ interneuron-specific ablation of AMPAR subunits (Caputi et al., 2012; Fuchs et al., 2007). However, the specificity of the PV-Cre line used for this knockout had been brought into question, following contrasting phenotypes when using either this PV-Cre line or a different one for interneuron-specific knockout of the NMDAR NR1 subunit (Belforte et al., 2010; Bygrave et al., 2016; Korotkova et al., 2010). The results from this chapter agree with findings from those studies manipulating AMPAR subunit expression in PV+ interneurons, and support the idea that said findings were due to effects specifically on PV+ cells (Belforte et al., 2010; Bygrave et al., 2016; Caputi et al., 2012; Fuchs et al., 2007; Korotkova et al., 2010). The reduction in gamma power following a reduction in excitatory drive onto PV+ cells makes logical sense, given that oscillation peaks have been shown to reflect chloride currents following $GABA_AR$ activation mediated by PV+ cells; reduced excitation of interneurons will result in decreases in activity and GABAergic signalling (Penttonen et

al., 1998). Overall, the results I observed with highly selective antagonists such as NASPM and PhTx-433 were predicted and in agreement with common thinking within the field.

In contrast, the consistently observed consequences of PhTx-74 were unexpected, and potentially indicative of actions on receptors beyond CP-AMPARs. The initial line of investigation following this result was to query whether the dose of PhTx-74 that elicited these changes in hippocampal activity was sufficient to significantly inhibit AMPAR currents mediated by receptors containing the GluR2 subunit. The single-cell voltage-clamp pharmacology experiments revealed a similar effect of the drug at the used dose on AMPAR-mediated currents in PV+ interneurons and pyramidal cells, indicative of a lack of selectivity for CP-AMPARs that might be the underlying basis for the results I collected. Given that NBQX abolishes oscillatory activity, it is likely any effects on GluR2-containing AMPARs result from inhibiting only a portion of receptors (Cunningham et al., 2003). I posited that such partial inhibition of pyramidal cell AMPARs could result in slower activation following relief of PV+ interneuron-mediated perisomatic inhibition, which, when combined with a reduced excitatory drive onto PV+ cells, could slow down excitation within the network sufficiently to drive the decrease in frequency observed in the present study.

These results are slightly obfuscated by the observations in Chapter 4, where NASPM application reliably induced reductions in oscillation frequency alongside reductions in gamma power. The reasons for this discrepancy compared to the results in Chapter 2 are unclear, but provided the NASPM supplied for the experiments in Chapter 4 was still selective for CP-AMPARs, it reveals that frequency changes can be induced solely through antagonism of these receptors. The fact that GluR2 viral transfection of PV+ cells removed sensitivity to the effects of NASPM on oscillation power and frequency indicates these receptors are responsible for the decline in frequency; therefore, it is possible that the full range of effects of PhTx-74 could be mediated via actions on these receptors

only. The results in Chapter 4 also indicate that the effects of NASPM are due to antagonism of CP-AMPARs specifically on PV+ interneurons, rather than those found on SOM+ interneurons or (in lesser quantities) on pyramidal cells.

Ultimately, it could simply be the case that the effects on frequency of 10 µM PhTx-74 are due to greater coverage of CP-AMPARs than 10 µM PhTx-433, and that, for reasons unknown, 100 µM NASPM during the experiments in Chapter 4 was inhibiting a greater portion of CP-AMPARs in PV+ interneurons than during the same experiments in Chapter 2. If this is the case, then it would suggest that partial inhibition of CP-AMPARs on PV+ interneurons, and subsequent reduction in synaptic recruitment, reduces interneuron firing sufficiently to reduce the power of oscillations whilst preserving population firing rate, whilst antagonism of a greater number of receptors sufficiently disrupts interneuron recruitment as to slow down the network. Both PhTx-74 and NASPM (particularly in Chapter 4) showed a rebound increase in gamma power following or coinciding with the decline in frequency, which may not be surprising, as when the firing rate is slower, there are likely to be more neurons ready to fire on each cycle. To test whether this hypothesis is more applicable than the idea I posited in Chapter 2 concerning the relative influence of inhibiting CP-AMPARs compared to GluR2-containing AMPARs on hippocampal gamma-frequency oscillations, it would be necessary to perform a dose-response curve for each of the compounds, including PhTx-433. I previously did not observe any effects on oscillatory activity following application of doses of PhTx-74 or NASPM below 10 µM or 100 µM, respectively, but it may be that further experimentation would reveal something. Given the expense and potential impact of such experiments, however, the feasibility of performing such a dose-response study is low.

There is scope for exploring the action of these CP-AMPAR antagonists on other channel types, as well as CP-AMPARs on cells other than PV+ interneurons, such as SOM+ interneurons and (to a lesser

extent) pyramidal cells. However, despite the conflicting results in my different chapters, it appears that the vast majority of the actions of CP-AMPARs during hippocampal gamma-frequency oscillations influenced by acute pharmacological blockade are mediated via receptors on PV+ interneurons, so such experiments would be of greater interest within a different functional context. Depending on further characterisation of its inhibitory effects, PhTx-74 also could become a useful tool for further pharmacological study in conjunction with other compounds, given its seemingly partially non-selective actions. In contrast to the destructive effects of NBQX on gamma activity *in vitro*, something with partial inhibition such as PhTx-74 could give more useful insights into AMPAR function within circuits and contributions to network activity.

6.1.2 In vivo *inhibition of hippocampal CP-AMPARs and behavioural consequences*

In Chapter 3, I decided to move *in vivo* and investigate whether CP-AMPAR inhibition by NASPM, and subsequent reduction in gamma power, would result in impairments of memory processes dependent on gamma oscillatory activity and associated behaviour. Genetic studies had shown that PV-specific ablation of GluR1 resulted in impairments on the spatial working memory-dependent rewarded alternation T-maze, and following intrahippocampal infusion of NASPM, I also reported a dose-dependent deficit in performance on the task, restricted to the period immediately following infusion (Fuchs et al., 2007). However, I also observed notable unintended side effects of NASPM infusion, including spasms and seizures, which restricted the ability to fully complete this section of the study.

Throughout this thesis I have referenced a study that used a PV-Cre line to selectively knock out the GluR1 subunit in PV+ interneurons, in doing so substantially reducing AMPAR currents in these

neurons due to the vast majority of AMPARs in these cells being composed of GluR1 homomers or GluR1/GluR4 heteromers (Fuchs et al., 2007). Given what is known about PV+ interneuron activity within gamma oscillations, and how important gamma oscillations seem to be for accurate choice-making on the rewarded alternation T-maze task, there was a sound scientific basis for the impairments reported in the study (Cardin et al., 2009; Yamamoto et al., 2014). However, as mentioned previously, questions have been raised regarding the cellular specificity of the PV-Cre line used in the Fuchs et al*.* study, as conflicting reports have emerged regarding the consequences of PV+ interneuron-specific NR1 knockout using either that PV-Cre line, or the PV-Cre line used in this thesis, which has been shown to have comprehensive and highly specific coverage of PV+ interneurons only (Belforte et al., 2010; Bygrave et al., 2016; Korotkova et al., 2010). The present findings show that inhibition of hippocampal CP-AMPARs, most notably expressed on PV+ interneurons, reduces gamma power recorded *in vitro*, and impairs performance on the T-maze (the picture is less clear regarding gamma oscillation frequency between the different chapters). Furthermore, the gamma oscillation experiments in Chapter 4 indicate that these effects, at least *in vitro*, can be in large part attributed to antagonism of CP-AMPARs specifically in PV+ interneurons. Therefore, whilst questions remain over the PV-Cre line specificity, the evidence I provide in this thesis provides support that the deficits reported by Fuchs et al*.* can be attributed to ablation of GluR1 in PV+ interneurons, although the constitutive knockout is likely to have additional effects on PV+ interneuron maturation beyond AMPAR subunit expression.

However, this chapter also demonstrated the limitations of pharmacological approaches. The experiments with NASPM in Chapter 2 showed the dose-dependent nature of its effects on *in vitro* gamma oscillations within the hippocampus, with no consistent effect on activity up to a concentration of 50 µM, but reliable decreases in power following exposure to 100 µM NASPM. In a similar fashion, 1 mM NASPM infusion had no notable effect on spatial working memory expression,

whilst 10 mM NASPM caused substantial changes in choice-making accuracy. However, likely due to an excitation-inhibition imbalance following inhibition of excitatory channels predominantly expressed on inhibitory cells, this dose also led to spasms and seizures in some mice. A drug such as NASPM is more likely to be useful in a situation when CP-AMPARs are transiently expressed, e.g. during learning, rather than when they are continuously expressed, and necessary for maintaining network activity. Given that activity in the hippocampus appears to be the latter due to CP-AMPAR expression on PV+ interneurons, there are likely to be fundamental difficulties with any further use of NASPM that render further characterisation of the compound's effects on *in vivo* network activity and behaviour impractical.

6.1.3 In vitro *characterisation of GluR2 virus-transfected PV+ interneurons and hippocampal networks*

The multiple limitations of a pharmacological approach, including the inability to selectively isolate calcium currents and the side effects *in vivo*, required the development of a more elegant approach. I generated a viral construct that drove high levels of edited GluR2 expression in Cre-expressing cells, and injected it into PV-Cre/Ai9 mice. Experiments investigating cellular specificity of expression, current-voltage relationships, properties and drug sensitivity of gamma oscillations, dendritic calcium signals, and anti-Hebbian plasticity induction all were indicative of successful neuronal transfection and transformation of receptor properties towards an AMPAR population dominated by GluR2-containing receptors.

Expression of my virus, visualised using immunofluorescence targeted against the AU1 peptide incorporated into the construct, was primarily restricted to the extranuclear cytoplasm and visible

processes of PV+ interneurons (identified by tdTomato expression), as would be expected given that the GluR2 is synthesised and stored in the endoplasmic reticulum until assembly into AMPAR tetramers and trafficking to dendrites. However, I also observed immunofluorescence in the neuropil of injected hippocampus, even in wild-type animals with no Cre recombinase expression. This background fluorescence is surprising, and its origin is unclear, given that there was no observed immunoreactivity localised to cells in wild-type mice, but considering the large quantities of virus injected, it could be a consequence of background leakiness. There is no obvious driver of this background stain, given the aforementioned lack of cellular reactivity, which one would expect if it was driven by spontaneous loxP recombination.

I also had difficulties with histology when trying to identify transfected cells following completion of recordings *in vitro*, as despite multiple different approaches in terms of slice preparation, I was unable to elicit any anti-AU1 immunoreactivity in sections I had used for *in vitro* electrophysiology, including the previously observed neuropil immunofluorescence. It is possible that fixation in some way modifies or masks the AU1 epitope, with a greater effect of PFA on thin slices rather than the whole brain during perfusion. In any case, as a result of this, I had to include all cells recorded from injected animals into my analyses. The partial coverage of CA1 cells seen with the injection coordinates used for the oscillation and current-voltage relationship experiments are a likely explanation for the varied rectification indices and spontaneous current properties of cells recorded from transfected slices during the rectification experiment. After I altered injection coordinates to have greater coverage of PV+ cells in area CA1, the injected cell populations showed greater consistency during the calcium imaging and plasticity experiments. It would be of substantial merit to repeat the current-voltage relationship experiments in animals injected with the adjusted coordinates. However, with the cells from which I-V relationships were recorded, the PV+ neuron population transfected with my GluR2 virus showed a shift towards reduced rectification and a more

linear current-voltage relationship, in line with what was observed following similar manipulations in non-neuronal cells (Iino et al., 2001).

Transfection of hippocampal PV+ interneurons with the floxed GluR2 virus did not impair the ability to generate carbachol-evoked gamma oscillations *in vitro* in ventral hippocampal slices. However, whilst there were no significant changes in gamma power, I did observe a small but significant decrease in the peak frequency of baseline oscillations in transfected slices compared to controls. The most plausible explanation for this is the altered channel gating kinetics. However, whilst GluR2-containing AMPARs are reported to have slower deactivation kinetics than CP-AMPARs, the two subclasses of AMPARs have been reported as having identical activation kinetics (Grosskreutz et al., 2003). It may be that slower deactivation sufficiently increases the reset time before interneurons can fire such that the interneuron population firing rate and oscillation frequency decrease in the manner observed in my experiments. Nevertheless, despite this slight shift in frequency, the overall machinery required for oscillogenesis is broadly preserved following viral transfection.

Slices from animals injected with the GluR2 virus were resistant to the effects of NASPM on *in vitro* oscillations. The extent of this protection was such as to suggest that the effects of NASPM on gamma oscillations are mediated almost exclusively via inhibition of CP-AMPARs on PV+ interneurons. However, as mentioned before, the effects observed following NASPM treatment diverged from those observed during experiments performed in Chapter 2, both in terms of the time course of NASPM effects, and the changes in oscillation frequency following drug application. The reasons for the different time course, range, and potency of effects between the two experiments, performed approximately 18 months apart, are not entirely clear. The most likely candidates in terms of differences between the two experiments are the genotype (wild-type vs PVCre/Ai9 homozygous mice), time point of drug application (NASPM was often applied 45-60 minutes

following first placement within the recording chamber in Chapter 2, whilst all slices in Chapter 4 were left for at least 1 hour to record baseline properties before experiments were performed), or an unknown change in the production of NASPM by Tocris between Spring 2016 and Summer 2017. Regardless of the cause of the difference, there is at least one consistent feature between the recordings made in each chapter; any effects of NASPM on oscillation frequency occurred after the peak of the effects on gamma power. In contrast, changes in power and frequency following PhTx-74 treatment occurred simultaneously.

Following alterations of the viral injection coordinates, I performed other experiments that revealed further properties indicative of GluR2 inclusion into AMPARs, namely an inability to stimulate NASPM-sensitive dendritic calcium signals, and a reduced ability to induce plasticity following pairing of presynaptic activity with post-synaptic hyperpolarisation. These single-cell properties are in line with my predictions of what overexpression of GluR2 in PV+ interneuron would lead to. I observed the stimulation of dendritic Ca^{2+} signals in non-transfected PV+ interneurons, with a nonlinear relationship between input stimulation amplitude and signal size that is likely due to Ca^{2+}-induced Ca^{2+} release based upon previous work inducing dendritic calcium responses (Camiré and Topolnik, 2014). I could not induce a similar input response curve in transfected cells; however, interpretation of the results was slightly hampered by the stimulation of smaller currents with high-amplitude stimulation compared to control cells, despite using the same protocol and without a significant difference between threshold stimulation-induced current amplitude between the two cell populations. Whilst normalising Ca^{2+} signal size to evoked current area still demonstrated a significant difference between the two cell types with respect to dendritic Ca^{2+} signal size, a repeat of the experiment with more rigorous control of current response may assist to further underline the consequences of the viral manipulation on dendritic calcium currents.

Our plasticity experiments were partially performed by a project student (Mina Moniri), and as plasticity experiments can be low yield due to the prolonged recording period and shifts in input resistance and holding current that occur during this period, the experimental protocol was simplified to aid data collection. To this end, unlike for previous experiments in Chapter 4, neither NMDAR blockers (e.g. DL-AP5) nor $GABA_AR$ antagonists (e.g. gabazine) were included in the perfusing aCSF. Instead, cells were injected with slow current to maintain a resting membrane potential, and hyperpolarised via current injection to -90 mV for pairing with theta burst stimulation. Under these conditions, we were able to elicit potentiation of subthreshold responses in controls cells only, with plasticity conforming to anti-Hebbian rules (Lamsa et al., 2007). Whilst we used an anti-Hebbian pairing protocol, due to the lack of NMDAR inhibition and the possibility that dendrites were not as hyperpolarised as the cell soma, we cannot rule out NMDARs having some influence over plasticity proceedings. Performing the same protocol in the presence of DL-AP5 and gabazine could further underline the AMPAergic mechanism of this plasticity.

Le Roux et alet al. reported that distinct plasticity mechanisms occurred at feedforward and feedback inputs onto PV+ interneurons in area CA1 (Le Roux et al., 2013). By placing the stimulation electrode in stratum oriens, we were preferentially activating feedback afferents. One additional experiment that might be of interest to perform would be to investigate whether Hebbian plasticity at feedback synapses is preserved in GluR2-transfected PV+ interneurons, and whether there are any compensatory changes in NMDAR expression that lead to the emergence of Hebbian plasticity at feedforward synapses.

6.1.4 Effects of viral transfection of hippocampal PV+ interneurons on behaviour and spatial memory

The final experimental chapter involved taking the virus generated in Chapter 4 and observing the effects that PV-specific transfection of the virus within hippocampus has on behaviour and learning and memory. Following full bilateral hippocampal injection of the virus, I observed mild effects on locomotor phenotypes, and no significant differences in expression of anxiety and novelty preference when compared to a control group injected with a GFP-expressing virus. However, I saw a highly significant delay-dependent impairment on the spatial working memory-dependent rewarded alternation T-maze task, and an impairment in learning new platform locations within the water maze following serial spatial reversals. Together, these results are indicative of an interference phenotype in these animals, with inflexibility in the recruitment of PV+ cells preventing the sufficient dynamic regulation of pyramidal cell assemblies necessary for disambiguation of memories of currently relevant information from those of previously useful information.

During a locomotor assay measuring free spontaneous movement, I observed a significant interaction between viral treatment and time for beam breaks, used as a readout of movement, with a significant difference between the two groups restricted to a single time bin in the first 20 minutes of testing, with lower numbers of beam breaks in the GluR2 experimental group. Given the relationship between hippocampal function, novelty, and locomotor activity, I was curious as to whether my viral manipulation of hippocampal activity had any influence on novelty recognition/preference; however, whilst the GluR2 group showed a notable trend towards greater preference for a novel spatial location over a previously explored one in a spatial novelty preference assay compared to the control group, this did not come out as significant (Arenas et al., 2014; Cassel et al., 1998; Favuzzi et al., 2017; Sanderson et al., 2007). Given that I saw only a minor effect on ambulatory locomotor activity, with a borderline significant difference between the two groups restricted to a very narrow time window, it may not be surprising to see only a non-significant trend towards novelty preference or recognition. If a slight preference for a novel location requires slightly

greater memory of, and potentially habituation towards, a previously explored location, such habituation may result in a faster decline in novelty-induced hyperactivity. The trend towards greater novelty preference is surprising, however, given the reduced novelty preference seen in animals lacking brevican, important for modulating PV+ interneuron synaptic function (Favuzzi et al., 2017). It may be of some interest to further explore novelty recognition in these animals, for example using a novel object recognition task.

During the locomotor assay, I also observed a reduction in numbers of rears; rearing is an anxiety-associated risk assessment behaviour. However, the results of three separate assays of anxiety gave an uncertain picture of anxiety in the animals, with one task indicating a possible anxiogenic phenotype whilst the other two did not (Piras et al., 2013). Rearing has a complex phenotype, with anxiolytic drugs having differing effects on levels of rearing dependent on stress within the current environment (McNaughton, 1985; McNaughton et al., 1984). What the change in rearing observed in the present study might indicate is unclear, particularly given the uncertainty resulting from anxiety tests. It may be of interest to explore the fear conditioning phenotype within these animals, and see whether there is a more substantial phenotype in a GluR2-transfected cohort when learning is incorporated into the behavioural paradigm, particularly a spatial fear conditioning task.

Perhaps the most exciting result within this thesis was the highly significant impairment in performance on the spatial working memory-dependent T-maze task, but only with a lengthy delay between sample and choice. As posited in section 5.4, a lack of excitatory plasticity in PV+ interneurons being responsible for this is plausible, given the onset of potentiation observed in Chapter 4 and the time span of trials and sessions for behavioural testing on the T-maze. The lack of flexible recruitment of PV+ interneurons may hinder optimal expression of cell assemblies representing currently relevant information, and interference between competing memory traces

may result in impaired performance on the rewarded alternation task. Such an impairment may only become notable with increasing working memory load, such as increasing the sample-choice delay. As mentioned in Chapter 5, hippocampal cell assemblies have been shown to exhibit activity during the delay period of a memory task, and that expression of these assemblies may be influenced by plasticity lacking in GluR2 virus-transfected animals (Pastalkova et al., 2008). There is clear scope for further exploring what impact the manipulation has on network activity during performance on this task by performing *in vivo* recordings from dorsal hippocampus in transfected animals performing the task. Given the reported influence of prefrontal cortical activity upon working memory and reacting to changing task conditions, it may also be of merit to explore interactions between hippocampus and prefrontal cortex during the tasks performed in this chapter, in controls and GluR2-transfected animals (Granon et al., 1994; Guise and Shapiro, 2017). Additionally, it may be interesting to see how animals injected with the GluR2 virus perform on other working memory-dependent tasks, such as the working memory variant of the radial arm maze, to see in which conditions the loss of PV+ interneuron plasticity brings out significant impairments in expression of working memory.

I observed no impairment in spatial reference memory, which was expected given the preservation of reference memory following PV-specific GluR1 ablation (Fuchs et al., 2007). The difficulties I had with poor task learning with my Y-maze experiment were likely a consequence of extensive learning of a different task on the T-maze prior to acquisition of the Y-maze task. Therefore, to confirm similar learning between the two groups in addition to peak memory performance, it may be nice to repeat the experiment with a cohort experimentally naïve to spatial testing. Repeating the Y-maze task to observe rates of learning in the two experimental groups is of greater interest, given the faster learning of platform location by the experimental group than controls in the reference memory phase of my water maze study, an effect I may have missed on the Y-maze task with the

remedial training. The result on the water maze was partially complicated by the differences in thigmotaxis between the two groups, as the faster acquisition of platform location may have been partly due to a greater tendency to explore the central areas of the maze where the platform positions resided, rather than purely spatial learning. Whilst there are still questions that could be asked regarding possible improvements in long-term spatial learning following artificial GluR2 expression in PV+ interneurons, it seems clear that they show no deficits in their capacity to express spatial reference memory.

Whilst the GluR2-injected animals were as capable as controls of learning the initial platform location in the water maze, if not more so, multiple movements of platform location brought out an impairment in learning the new platform locations, as exhibited by a significant increase in trial path length across three days of testing, averaged for three spatial reversals. The impairment exhibited a limited duration, as after three days of training to a new location, the GluR2 animals had learned the new location sufficiently as to spend significantly more time in the target quadrant than controls during probe tests. This result fits in line with the presence of excitatory-to-inhibitory plasticity in dorsal hippocampus during learning of new reward locations on a day-to-day basis in a study using a cheeseboard apparatus (Dupret et al., 2013).

To further explore the deficit observed in the animals, it would likely be necessary to move away from using the water maze for multiple reasons. First, any attempts to use *in vivo* electrophysiology would require an experimental design without substantial amounts of water. Second, the water maze used during this study has been used previously, and it has been found that mice have a natural bias towards one quadrant (SW) and against another (NE), without notable bias towards either NW or SE. As I used either NW or SE for the reference memory phase of testing, the reversals experiments involved training animals to go to SW and NE at one point during the study, with a

visible preference observed in some animals. Although the sequence of platform locations for each mouse was counterbalanced across the cohort to limit any influence upon results, it would be preferable for any future experiments to use a set-up without such an in-built bias in the testing apparatus. Given the experiments already performed using the cheeseboard set-up, designing a quantifiable measurement for learning on the cheeseboard would make it an ideal candidate for further exploring the impact of GluR2 overexpression in PV+ cells on network activity and day-to-day spatial learning.

6.2 Hippocampal CP-AMPARs in gamma oscillations

The first major stated goal of this project was to investigate the importance of activity of CP-AMPARs within the hippocampus for optimal network function, in particular gamma oscillatory activity. Other studies had used genetic ablation of AMPAR subunits to study AMPAergic activity during oscillations, but using selective AMPAR antagonists enables a specific acute view into channel activity during network activity independent of any compensatory changes occurring at a genetic level (Caputi et al., 2012; Fuchs et al., 2007). By applying agents such as NASPM and philanthotoxin to an *in vitro* preparation, I could see real-time changes in various properties.

Application of CP-AMPAR-selective antagonists resulted in consistent and robust decreases in the power of carbachol-evoked oscillations recorded in area CA3 of ventral hippocampus *in vitro*. Furthermore, the experiments in Chapter 4 indicate that this effect is principally due to inhibition of CP-AMPARs on PV+ interneurons. These fit well with established knowledge of PING mechanisms of hippocampal oscillogenesis, that excitatory recruitment of PV+ interneurons by pyramidal cells is a

necessary component of generating and maintaining peak oscillatory activity (Tiesinga and Sejnowski, 2009).

The data collected in Chapters 2 and 4 paint a less clear picture regarding the frequency of gamma oscillations and the impact of glutamate receptor antagonism on it. I have already discussed at length how PhTx-74 may be acting through heteromeric AMPARs to bring about its effects, and without the results from Chapter 4, my data offered a clean distinction between the function of CP-AMPAR-mediated signalling within the hippocampus and its effects on network activity, and the additional contribution of other ionotropic glutamate receptors in modulating the rate of activity within the network. However, given the supposedly extremely high specificity of NASPM for CP-AMPARs, the data from Chapter 4 raises questions over whether there are particular conditions under which CP-AMPAR blockade may or may not influence the frequency of oscillations.

Whilst I do not have conclusive answers regarding how exactly activation of CP-AMPARs within the hippocampus shapes activity within the network, it is clear that impaired function of these channels results in substantial deficits in the functionality of the hippocampal network. A subsequent aim of this project was to ascertain whether such disruption would have behavioural consequences, particularly on tasks associated with hippocampal gamma oscillations. Intrahippocampal infusion of NASPM resulted in a significant reduction in the number of correct choices, down to near-chance levels, albeit with unintended side effects. If PV+ interneuron activity is necessary to shape pyramidal cell assemblies providing representations of recent memory, impaired recruitment of these interneurons and less strict regulation of pyramidal cell activity will reduce the specificity of memory representations and disrupt accurate recall of short-term memory. In summary, the pharmacological experiments provide an acute insight into the mechanisms of hippocampal function and working memory that falls in line with previous literature and knowledge within the field.

Whilst these experiments confirm the necessity of CP-AMPAR activity for hippocampal oscillations, it hasn't previously been established whether the distinct subunit composition of these receptors is essential for gamma activity, or whether GluR2-containing AMPARs could fulfil the same role. In addition to demonstrating the contribution of CP-AMPARs specifically within PV+ cells to the deficits brought about by NASPM exposure, floxed GluR2 viral transfection broadly conserves oscillatory function within the hippocampus. Whilst CP-AMPARs with fast channel gating kinetics enable rapid, precise recruitment of interneurons, they are less important to the fast-spiking properties of these neurons than K_v3 potassium channels (Hu et al., 2014; Rudy and McBain, 2001). With the preservation of these channels, GluR2-expressing PV+ cells retain the ability to fire at high-frequency, even if their firing rate is slowed down slightly by their AMPAR properties. These results demonstrate that, whilst the properties of AMPARs within PV+ interneurons shape patterns of activity observed within the hippocampus, their lack of GluR2 expression is not an essential component for the generation of gamma oscillations within the region.

Overall, the data collected within this study aligns with the well-established literature covering excitatory-inhibitory models of hippocampal gamma oscillogenesis, with fast excitatory recruitment of PV+ interneurons necessary to maintain high-frequency synchronous activity within the region (Buzsáki and Wang, 2012). However, the role of plasticity within the network in shaping neural ensemble activity and memory processes is difficult to determine *in vitro*, as network activity is not guided by external stimuli within the environment, but persistent non-specific cholinergic drive. *In vivo* recordings during awake behaviour are likely to be a more informative approach for investigating this.

6.3 Dynamic hippocampal network requires flexible recruitment of PV+ cells

The second major aim of this thesis was to develop an approach to selectively alter PV+ interneuron AMPARs in a way that removed calcium permeability whilst broadly conserving overall excitability, and using this approach to reveal the significance of AMPAR-mediated interneuron plasticity for hippocampus-dependent behaviour. To this end, I developed a virus to drive Cre-dependent expression of edited GluR2, and found in PV-Cre animals that it reduced inward rectification, dendritic calcium signals, and the ability to induce anti-Hebbian plasticity, whilst seeming to mostly conserve channel conductance. By observing the behavioural consequences of transfection of hippocampal PV+ interneurons with this virus, I was able to demonstrate specific memory impairments resulting from this loss of excitatory plasticity within fast-spiking perisomatic-targeting interneurons.

To attempt to pinpoint potential processes and substrates driving mnemonic impairments, a brief recap of hippocampal circuitry may be beneficial. Activity within the hippocampal network is complex, due to the number of neuronal cell types and array of local and long-distance connections. A trisynaptic loop of excitation travelling from entorhinal cortex through dentate gyrus, area CA3, and area CA1 before returning to entorhinal cortex is complemented by direct entorhinal inputs to areas CA1 and CA3, as well as recurrent collateral connectivity within areas CA3 and CA1 (Amaral et al., 2007; Amaral and Lavenex, 2007; Andersen, 1975; Canto et al., 2008; Insausti and Amaral, 2004; Le Duigou et al., 2014). This excitation is also highly regulated by an array of interneuron classes and subclasses, with a range of distinct properties (Tukker et al., 2007). The interplay between these different neuronal groups and pathways make the circuit mechanisms underpinning gamma oscillations within the region more complex than a simple loop of excitation and inhibition between pyramidal cells and PV+ interneurons.

Oscillations within area CA1 of hippocampus have been recorded at low and high frequencies, with slow gamma oscillations entrained by inputs from area CA3, and higher-frequency oscillations entrained by entorhinal inputs or possibly occurring independent of external inputs (Colgin et al., 2009; Colgin and Moser, 2010; Montgomery and Buzsáki, 2007; Remondes and Schuman, 2002; Yamamoto et al., 2014; Zemankovics et al., 2013). Excitation of PV+ interneurons within area CA1, either via feedforward inputs or feedback local recurrent collaterals, causes perisomatic inhibition within target pyramidal cells (Le Roux et al., 2013; Mann et al., 2005b). Inactivation of PV+ interneurons disinhibits target pyramidal cells, which are now able to fire synchronously. Whether cells fire depends on their excitatory drive, however, which is influenced by both excitatory inputs from pyramidal cells and additional inhibition, proposed to come from perisomatic-targeting cholecystokinin-positive basket cells and dendritic inhibition from SOM+ interneurons (Bartos and Elgueta, 2012; Klausberger and Somogyi, 2008; Müller and Remy, 2014; Tukker et al., 2007). With all these inputs influencing the pyramidal cell excitability and the composition of synchronously firing pyramidal cell assemblies, as well as uncertainty over which inputs are more significant for PV+ interneuron recruitment during gamma activity, I was uncertain regarding the extent to which CP-AMPAR-mediated plasticity in PV+ cells would influence oscillation-associated memory processes such as spatial working memory, and behavioural expression of this memory.

Whilst my manipulation did not affect overall performance on the working memory task involving low working memory load, increasing the difficulty of the task by extending the intra-trial delay resulted in the emergence of a strongly significant decrease in choice accuracy. Additionally, more mistakes were made with increasing numbers of trials across sessions containing either short- or long-delay trials. As discussed previously, I have proposed that this is an interference phenotype, with a lack of disambiguation between memory traces concerning what is currently relevant

information. At a circuit level, this would suggest that AMPAR-mediated plasticity, occurring at either feedforward or feedback inputs (or both), and flexible changes in PV+ interneuron excitability allows dynamic control over the expression of pyramidal cell assemblies in a manner that is necessary for optimal memory retrieval and expression of working memory, even when excitatory inputs onto pyramidal cells and non-parvalbumin-expressing interneurons are unaffected. These changes in synaptic strength occur over a very brief time window (<1 minute), but accumulation (or a lack of) over time of plasticity in parallel to changes at inputs onto pyramidal cells may lead to increasing obfuscation of memory processes. As performance was not significantly different between the two groups on the very first trial of long-delay sessions, and performance significantly deteriorated over accumulating trials in the GluR2-transfected group compared to controls even during sessions with short-delay trials, there is a possibility that this impairment may be arising at the level of retrieval rather than encoding.

The impairment I observed in the water maze following multiple shifts in the platform location is again possibly indicative of interference resulting from competition between memory traces, whether due to disrupted retrieval of the new location or failures in inhibiting movement towards the previously relevant location, although it is also possible the impairment resulted from stronger initial encoding disrupting learning of later locations. In a study utilising a 'matching-to-multiple-places' cheeseboard-based task that potentially involves similar memory processes, Dupret et alet al. showed competing expression of old and new spatial maps on separate gamma and theta cycles in the hippocampus, with the new map emerging in prominence as monosynaptic connections between purported pyramidal and inhibitory neurons shifted in strength; if similar cognitive processes are required for effective platform learning and performance during serial spatial reversal testing on the water maze, then the impairment may be occurring at a retrieval level, should the assemblies representing currently relevant platform locations not be expressed as a result of

competition with older representations associated with previously correct platform locations (Dupret et al., 2013).

I cannot rule out the possibility that the processes underpinning the water maze impairment are potentially distinct from those driving the working memory impairment shown here, given the different memory demands of each task. The rewarded alternation T-maze requires brief retention of memory on a trial-by-trial basis, whilst the water maze task is more of a reference memory task, with multiple trials in a day and multiple days in a row with the same static platform location to remember. Nevertheless, although the two tasks have different cognitive requirements, the impairments appear to share a common interference component.

A further point to consider is that whilst I was manipulating receptors proposed to mediate anti-Hebbian plasticity, Dupret et alet al. reported the excitatory-to-inhibitory synaptic plasticity occurring in their study to follow Hebbian learning rules (Dupret et al., 2013). However, anti-Hebbian LTP (i.e. plasticity in the absence of post-synaptic spiking) would be difficult to detect using extracellular techniques such as those used in the study.

Our viral injections were targeted to drive expression throughout the full hippocampus. Whilst I predict the behavioural impairments on the spatial memory tasks were dependent on manipulations of dorsal hippocampal activity, I cannot make any claims regarding which cells or sub-fields were the locus of impaired memory expression, as PV+ interneurons can be found throughout the different hippocampal sub-fields. Should the impairment on the T-maze result from deficits in memory retrieval, one might predict that plasticity in PV+ interneurons either in area CA3 or in area CA1 and recruited by CA3 neurons to be important, given the implication of CA3-to-CA1 connections in

memory retrieval and the reported coherence of oscillatory activity between the two regions during choice-making on the T-maze (Gilbert and Kesner, 2006; Montgomery and Buzsáki, 2007).

The Dupret et alet al. study recorded from, and reported changes in synaptic strength in, neurons in area CA1 (Dupret et al., 2013). As such, I might expect that the impairment in learning new platform locations on the water maze resulted from a loss of plasticity in PV+ interneurons in area CA1. Furthermore, Bannerman et al. indicates a significant contribution of CA1 activity towards the disambiguation of memories (Bannerman et al., 2012). However, given the critical role of the dentate gyrus in pattern separation, and thus in disambiguation of inputs, I cannot discount a role for parvalbumin-expressing interneurons in the DG, and flexible recruitment of said neurons, in maintaining the distinction between sensory input necessary for optimal memory processing (Leutgeb et al., 2007).

To more properly grasp the mechanisms driving the behavioural deficits observed in the GluR2-transfected mice, the logical next step is to repeat the experiments in animals implanted with electrodes in dorsal hippocampus, with interest in recording, amongst other parameters, oscillatory activity and coherence between sub-fields, neuronal firing patterns, and neuronal connectivity and changes in synaptic strength. Whilst the T-maze task is well-suited for recordings during behaviour, given the obvious issues in performing electrode recordings in animals in the water maze, an alternative experimental approach will likely have to be used in its stead. A quantifiable design based upon the cheeseboard experiments performed by Dupret et al. would be a good candidate, given the data already obtained from electrophysiological recordings in these animals.

6.4 Future steps

During the work undertaken in this project, I have generated a virus capable of driving Cre-dependent expression of an edited GluR2 construct that alters single-cell properties in a way indicative of GluR2 synthesis and incorporation into AMPARs. After *in vitro* characterisation, I used the virus to explore the consequences of abolishing AMPAR-mediated calcium conductance in PV+ interneurons on behaviour and memory processes, in doing so identifying multiple memory deficits in transfected animals.

Our viral tool, as useful as it has proven to be, is not without caveats. Expression of the construct is inflexible following transfection. Developing a version with inducible expression following transfection (e.g. via tamoxifen) could enable one to explore the consequences of viral expression at different phases of task learning. Furthermore, based upon the spontaneous current properties observed during the current-voltage relationship experiments, and the reduced current sizes following high amplitude stimulation during the calcium signal experiments, there appears to be some alteration to baseline synaptic transmission, which is unsurprising given the known properties of GluR2-containing AMPARs compared to CP-AMPARs. It is unlikely that there are further manipulations of AMPARs one could employ to counteract this, so if one wanted to manipulate anti-Hebbian plasticity in PV+ interneurons whilst fully preserving AMPAergic transmission, one would likely have to search for downstream pathways to target. Finally, the limitations of the AU1 tag have been covered thus far in this thesis, so developing a version of the virus with an in-built fluorescent tag would have clear merit, provided the fluorescent tag did not disrupt receptor assembly.

Having discussed the complexities of hippocampal structure and signalling, it would be of real interest to be able to pinpoint the pathways and sub-fields of the hippocampus primarily responsible for the memory impairments resulting from my manipulation. The first logical next step for this work would be to use *in vivo* electrophysiology during awake behaviours to correlate memory impairments with abnormalities in network activity. Beyond this, the tool could be used to selectively target hippocampal sub-fields, rather than the full-brain transfection used during this thesis' work, and to subsequently begin to elucidate the relative importance of plasticity within interneuron populations of the different sub-fields to the memory processes impaired by artificial GluR2 expression.

The virus could also be used to explore interneuron plasticity in other brain regions, as well as other cell types. In particular, somatostatin-expressing interneurons are also known to express CP-AMPARs, and plasticity mediated by these receptors has been induced in SOM+ cells (Szabo et al., 2012). As with PV+ cells, other plasticity pathways have been demonstrated in these cells, with metabotropic glutamate receptor-dependent potentiation recorded in CA1 SOM+ neurons (Vasuta et al., 2015). Given the reported roles for hippocampal and prefrontal cortical SOM+ interneurons in, amongst other things, contextual fear memory and working memory, there may be interest in exploring contributions of flexible recruitment of these cells mediated by CP-AMPARs to behaviours and memory processes of interest (Kim et al., 2016; Stefanelli et al., 2016).

6.5 Concluding remarks

The work undertaken during the project described in this thesis involved using two separate approaches to investigate patterns of hippocampal activity both *in vitro* and *in vivo*. My

pharmacological experiments provide a new insight into acute mechanisms of oscillatory activity and support previous genetic-based work in the field, but uncertainty over the basis for the divergent effects of philanthotoxin-433 and philanthotoxin-74, as well as the conflicting observations seen with NASPM at different time points in the study, need to be answered in the future.

The virus-based experiments demonstrate the possibilities of using such an approach to selectively manipulate AMPAR composition in neuronal cells, and reveal the significance of AMPAR-mediated hippocampal interneuron plasticity for specific memory processes. My data point towards a previously undiscussed role of interneuron plasticity in preventing interference between competing memory traces, and future work can look to further explore the memory phenotype in my model to gain greater understanding of short-term hippocampus-dependent memory processes.

There has been an intense interest in the role of synaptic plasticity in various memory processes in the decades since its first discovery, and whilst many findings have implicated its importance in various processes and aspects of memory, in many ways the landscape has become increasingly complex and uncertain, with subtle manipulations identifying dissociations between different forms of memory based on the underlying regions, neurons, and connections held responsible for their expression. The recent discovery of excitatory plasticity in inhibitory cells provided a logical mechanism to compensate for the increased activity with a network resulting from plasticity in excitatory circuits and maintain functional, high-fidelity processing. In addition, it raised the possibility of a novel mechanism via which optimal memory processing could occur; however, functional implications of this plasticity had only received limited focus, to the best of my knowledge. The findings of the present study reveal that, within a brain region long associated with various aspects of memory, the ability to exhibit activity-dependent modulation of excitation of a specific class of inhibitory cells appears necessary to maintain the segregation of overlapping

memories to avoid the development of interference. These observations provide novel insights into the role of inhibitory-excitatory balance in the expression of certain aspects of hippocampus-dependent memory, and suggest that greater understanding of the relative contributions of excitatory and inhibitory activity to memory processes may lead to new approaches in tackling situations of memory dysfunction.

7 Bibliography

Adesnik, H., Nicoll, R.A., 2007. Conservation of glutamate receptor 2-containing AMPA receptors during long-term potentiation. J. Neurosci. 27, 4598–4602.

Alger, B.E., Teyler, T.J., 1976. Long-term and short-term plasticity in the CA1, CA3, and dentate regions of the rat hippocampal slice. Brain Res. 110, 463–480.

Altman, J., Brunner, R.L., Bayer, S.A., 1973. The hippocampus and behavioral maturation. Behav. Biol. 8, 557–596.

Amaral, D.G., 1978. A golgi study of cell types in the hilar region of the hippocampus in the rat. J. Comp. Neurol. 182, 851–914.

Amaral, D.G., Lavenex, P., 2007. Hippocampal neuroanatomy, in: Andersen, P., Morris, R., Amaral, D.G., Bliss, T., O'Keefe, J. (Eds.), The Hippocampus Book. Oxford University Press, New York, pp. 37–114.

Amaral, D.G., Scharfman, H.E., Lavenex, P., 2007. The dentate gyrus: fundamental neuroanatomical organization (dentate gyrus for dummies). Prog. Brain Res. 163, 3–22.

Andersen, P., 1975. Organization of Hippocampal Neurons and their interconnections, in: Isaacson, R.L., Pribram, K.H. (Eds.), The Hippocampus. Springer US, pp. 155–175.

Andersen, P., Bliss, T.V., Lomo, T., Olsen, L.I., Skrede, K.K., 1969. Lamellar organization of hippocampal excitatory pathways. Acta Physiol. Scand. 76, 4A–5A.

Andersen, P., Morris, R., Amaral, D., Bliss, T., O'Keefe, J. (Eds.), 2006. The Hippocampus Book. Oxford University Press.

Andersen, P., Sundberg, S.H., Sveen, O., Wigström, H., 1977. Specific long-lasting potentiation of synaptic transmission in hippocampal slices. Nature 266, 736–737.

Anggono, V., Huganir, R.L., 2012. Regulation of AMPA receptor trafficking and synaptic plasticity. Curr. Opin. Neurobiol. 22, 461–469.

Anis, N., Sherby, S., Goodnow, R., Niwa, M., Konno, K., Kallimopoulos, T., Bukownik, R., Nakanishi, K., Usherwood, P., Eldefrawi, A., 1990. Structure-activity relationships of philanthotoxin analogs and polyamines on N-methyl-D-aspartate and nicotinic acetylcholine receptors. J. Pharmacol. Exp. Ther. 254, 764–773.

Aoki, C., Chowdhury, T.G., Wable, G.S., Chen, Y.-W., 2017. Synaptic changes in the hippocampus of adolescent female rodents associated with resilience to anxiety and suppression of food restriction-evoked hyperactivity in an animal model for anorexia nervosa. Brain Res. 1654, 102–115.

Araki, Y., Lin, D.-T., Huganir, R.L., 2010. Plasma membrane insertion of the AMPA receptor GluA2 subunit is regulated by NSF binding and Q/R editing of the ion pore. Proc. Natl. Acad. Sci. U. S. A. 107, 11080–11085.

Ardid, S., Wang, X.-J., Gomez-Cabrero, D., Compte, A., 2010. Reconciling coherent oscillation with modulation of irregular spiking activity in selective attention: gamma-range synchronization between sensory and executive cortical areas. J. Neurosci. 30, 2856–2870.

Arenas, M.C., Daza-Losada, M., Vidal-Infer, A., Aguilar, M.A., Miñarro, J., Rodríguez-Arias, M., 2014. Capacity of novelty-induced locomotor activity and the hole-board test to predict sensitivity to the conditioned rewarding effects of cocaine. Physiol. Behav. 133, 152–160.

Aschauer, D.F., Kreuz, S., Rumpel, S., 2013. Analysis of transduction efficiency, tropism and axonal transport of AAV serotypes 1, 2, 5, 6, 8 and 9 in the mouse brain. PLOS ONE 8, e76310.

Axmacher, N., Henseler, M.M., Jensen, O., Weinreich, I., Elger, C.E., Fell, J., 2010. Cross-frequency coupling supports multi-item working memory in the human hippocampus. Proc. Natl. Acad. Sci. U. S. A. 107, 3228–3233.

Ayalon, G., Stern-Bach, Y., 2001. Functional assembly of AMPA and kainate receptors is mediated by several discrete protein-protein interactions. Neuron 31, 103–113.

Baker, K.B., Kim, J.J., 2002. Effects of stress and hippocampal NMDA receptor antagonism on recognition memory in rats. Learn. Mem. 9, 58–65.

Bannerman, D.M., Bus, T., Taylor, A., Sanderson, D.J., Schwarz, I., Jensen, V., Hvalby, Ø., Rawlins, J.N.P., Seeburg, P.H., Sprengel, R., 2012. Dissecting spatial knowledge from spatial choice by hippocampal NMDA receptor deletion. Nat. Neurosci. 15, 1153–1159.

Bannerman, D.M., Deacon, R.M.J., Offen, S., Friswell, J., Grubb, M., Rawlins, J.N.P., 2002. Double dissociation of function within the hippocampus: spatial memory and hyponeophagia. Behav. Neurosci. 116, 884–901.
Bannerman, D.M., Deacon, R.M.J., Seeburg, P.H., Rawlins, J.N.P., 2003a. GluR-A-Deficient mice display normal acquisition of a hippocampus-dependent spatial reference memory task but are impaired during spatial reversal. Behav. Neurosci. 117, 866–870.
Bannerman, D.M., Good, M.A., Butcher, S.P., Ramsay, M., Morris, R.G., 1995. Distinct components of spatial learning revealed by prior training and NMDA receptor blockade. Nature 378, 182–186.
Bannerman, D.M., Grubb, M., Deacon, R.M.J., Yee, B.K., Feldon, J., Rawlins, J.N.P., 2003b. Ventral hippocampal lesions affect anxiety but not spatial learning. Behav. Brain Res. 139, 197–213.
Bannerman, D.M., Niewoehner, B., Lyon, L., Romberg, C., Schmitt, W.B., Taylor, A., Sanderson, D.J., Cottam, J., Sprengel, R., Seeburg, P.H., Köhr, G., Rawlins, J.N.P., 2008. NMDA receptor subunit NR2A is required for rapidly acquired spatial working memory but not incremental spatial reference memory. J. Neurosci. 28, 3623–3630.
Bannerman, D.M., Sprengel, R., Sanderson, D.J., McHugh, S.B., Rawlins, J.N.P., Monyer, H., Seeburg, P.H., 2014. Hippocampal synaptic plasticity, spatial memory and anxiety. Nat. Rev. Neurosci. 15, 181–192.
Bannerman, D.M., Yee, B.K., Good, M.A., Heupel, M.J., Iversen, S.D., Rawlins, J.N., 1999. Double dissociation of function within the hippocampus: a comparison of dorsal, ventral, and complete hippocampal cytotoxic lesions. Behav. Neurosci. 113, 1170–1188.
Barker, G.R.I., Banks, P.J., Scott, H., Ralph, G.S., Mitrophanous, K.A., Wong, L.-F., Bashir, Z.I., Uney, J.B., Warburton, E.C., 2017. Separate elements of episodic memory subserved by distinct hippocampal-prefrontal connections. Nat. Neurosci. 20, 242–250.
Barnes, C.A., 1979. Memory deficits associated with senescence: a neurophysiological and behavioral study in the rat. J. Comp. Physiol. Psychol. 93, 74–104.
Bartos, M., Elgueta, C., 2012. Functional characteristics of parvalbumin- and cholecystokinin-expressing basket cells. J. Physiol. 590, 669–681.
Bartos, M., Vida, I., Jonas, P., 2007. Synaptic mechanisms of synchronized gamma oscillations in inhibitory interneuron networks. Nat. Rev. Neurosci. 8, 45–56.
Bear, M.F., Abraham, W.C., 1996. Long-term depression in hippocampus. Annu. Rev. Neurosci. 19, 437–462.
Belforte, J.E., Zsiros, V., Sklar, E.R., Jiang, Z., Yu, G., Li, Y., Quinlan, E.M., Nakazawa, K., 2010. Postnatal NMDA receptor ablation in corticolimbic interneurons confers schizophrenia-like phenotypes. Nat. Neurosci. 13, 76–83.
Béracochéa, D.J., Jaffard, R., 1987. Impairment of spontaneous alternation behavior in sequential test procedures following mammillary body lesions in mice: evidence for time-dependent interference-related memory deficits. Behav. Neurosci. 101, 187–197.
Bi, G., Poo, M., 2001. Synaptic modification by correlated activity: Hebb's postulate revisited. Annu. Rev. Neurosci. 24, 139–166.
Bi, G.Q., Poo, M.M., 1998. Synaptic modifications in cultured hippocampal neurons: dependence on spike timing, synaptic strength, and postsynaptic cell type. J. Neurosci. 18, 10464–10472.
Bianchin, M., Walz, R., Ruschel, A.C., Zanatta, M.S., Da Silva, R.C., Bueno e Silva, M., Paczko, N., Medina, J.H., Izquierdo, I., 1993. Memory expression is blocked by the infusion of CNQX into the hippocampus and/or the amygdala up to 20 days after training. Behav. Neural Biol. 59, 83–86.
Bieri, K.W., Bobbitt, K.N., Colgin, L.L., 2014. Slow and fast gamma rhythms coordinate different spatial coding modes in hippocampal place cells. Neuron 82, 670–681.
Billingslea, E.N., Tatard-Leitman, V.M., Anguiano, J., Jutzeler, C.R., Suh, J., Saunders, J.A., Morita, S., Featherstone, R.E., Ortinski, P.I., Gandal, M.J., Lin, R., Liang, Y., Gur, R.E., Carlson, G.C., Hahn, C.-G., Siegel, S.J., 2014. Parvalbumin cell ablation of NMDA-R1 causes increased resting network cxcitability with associated social and self-care deficits. Neuropsychopharmacology 39, 1603–1613.
Bird, C.M., Burgess, N., 2008. The hippocampus and memory: insights from spatial processing. Nat. Rev. Neurosci. 9, 182–194.
Bird, K.D., 2004. Analysis of Variance via confidence dntervals. SAGE Publications, Thousand Oaks, California.
Blaschke, M., Keller, B.U., Rivosecchi, R., Hollmann, M., Heinemann, S., Konnerth, A., 1993. A single amino acid determines the subunit-specific spider toxin block of alpha-amino-3-hydroxy-5-methylisoxazole-4-propionate/kainate receptor channels. Proc. Natl. Acad. Sci. U. S. A. 90, 6528–6532.
Blasco-Ibáñez, J.M., Freund, T.F., 1995. Synaptic input of horizontal interneurons in stratum oriens of the hippocampal CA1 subfield: structural basis of feed-back activation. Eur. J. Neurosci. 7, 2170–2180.

Bliss, T.V., Collingridge, G.L., 1993. A synaptic model of memory: long-term potentiation in the hippocampus. Nature 361, 31–39.
Bliss, T.V., Lomo, T., 1973. Long-lasting potentiation of synaptic transmission in the dentate area of the anaesthetized rabbit following stimulation of the perforant path. J. Physiol. 232, 331–356.
Bloodgood, B.L., Giessel, A.J., Sabatini, B.L., 2009. Biphasic synaptic Ca influx arising from compartmentalized electrical signals in dendritic spines. PLoS Biol. 7, e1000190.
Bochet, P., Audinat, E., Lambolez, B., Crepel, F., Rossier, J., Iino, M., Tsuzuki, K., Ozawa, S., 1994. Subunit composition at the single-cell level explains functional properties of a glutamate-gated channel. Neuron 12, 383-388.
Börgers, C., Kopell, N., 2003. Synchronization in networks of excitatory and inhibitory neurons with sparse, random connectivity. Neural Comput. 15, 509–538.
Boulle, F., Massart, R., Stragier, E., Païzanis, E., Zaidan, L., Marday, S., Gabriel, C., Mocaer, E., Mongeau, R., Lanfumey, L., 2014. Hippocampal and behavioral dysfunctions in a mouse model of environmental stress: normalization by agomelatine. Transl. Psychiatry 4, e485.
Boulter, J., Hollmann, M., O'Shea-Greenfield, A., Hartley, M., Deneris, E., Maron, C., Heinemann, S., 1990. Molecular cloning and functional expression of glutamate receptor subunit genes. Science 249, 1033–1037.
Bowie, D., Lange, G.D., Mayer, M.L., 1998. Activity-dependent modulation of glutamate receptors by polyamines. J. Neurosci. 18, 8175–8185.
Bowie, D., Mayer, M.L., 1995. Inward rectification of both AMPA and kainate subtype glutamate receptors generated by polyamine-mediated ion channel block. Neuron 15, 453–462.
Boyett, J.M., Buckmaster, P.S., 2001. Somatostatin-immunoreactive interneurons contribute to lateral inhibitory circuits in the dentate gyrus of control and epileptic rats. Hippocampus 11, 418–422.
Brackley, P.T., Bell, D.R., Choi, S.K., Nakanishi, K., Usherwood, P.N., 1993. Selective antagonism of native and cloned kainate and NMDA receptors by polyamine-containing toxins. J. Pharmacol. Exp. Ther. 266, 1573–1580.
Bragin, A., Jandó, G., Nádasdy, Z., Hetke, J., Wise, K., Buzsáki, G., 1995. Gamma (40-100 Hz) oscillation in the hippocampus of the behaving rat. J. Neurosci. 15, 47–60.
Brankack, J., Stewart, M., Fox, S.E., 1993. Current source density analysis of the hippocampal theta rhythm: associated sustained potentials and candidate synaptic generators. Brain Res. 615, 310–327.
Brill, J., Huguenard, J.R., 2008. Sequential changes in AMPA receptor targeting in the developing neocortical excitatory circuit. J. Neurosci. 28, 13918–13928.
Broadbent, N.J., Gaskin, S., Squire, L.R., Clark, R.E., 2010a. Object recognition memory and the rodent hippocampus. Learn. Mem. 17, 5–11.
Broadbent, N.J., Squire, L.R., Clark, R.E., 2010b. Sustained dorsal hippocampal activity is not obligatory for either the maintenance or retrieval of long-term spatial memory. Hippocampus 20, 1366–1375.
Broadbent, N.J., Squire, L.R., Clark, R.E., 2004. Spatial memory, recognition memory, and the hippocampus. Proc. Natl. Acad. Sci. U. S. A. 101, 14515–14520.
Bromfield, E.B., Cavazos, J.E., Sirven, J.I., 2006. Basic mechanisms underlying seizures and epilepsy. American Epilepsy Society.
Brown, M.W., Aggleton, J.P., 2001. Recognition memory: what are the roles of the perirhinal cortex and hippocampus? Nat. Rev. Neurosci. 2, 51–61.
Brun, V.H., Otnass, M.K., Molden, S., Steffenach, H.-A., Witter, M.P., Moser, M.-B., Moser, E.I., 2002. Place cells and place recognition maintained by direct entorhinal-hippocampal circuitry. Science 296, 2243–2246.
Brunel, N., 2000. Dynamics of sparsely connected networks of excitatory and inhibitory spiking neurons. J. Comput. Neurosci. 8, 183–208.
Brunel, N., Hakim, V., 1999. Fast global oscillations in networks of integrate-and-fire neurons with low firing rates. Neural Comput. 11, 1621–1671.
Brunel, N., Wang, X.-J., 2003. What determines the frequency of fast network oscillations with irregular neural discharges? I. Synaptic dynamics and excitation-inhibition balance. J. Neurophysiol. 90, 415–430.
Buhl, E.H., Han, Z.S., Lörinczi, Z., Stezhka, V.V., Karnup, S.V., Somogyi, P., 1994. Physiological properties of anatomically identified axo-axonic cells in the rat hippocampus. J. Neurophysiol. 71, 1289–1307.
Burgess, N., Maguire, E.A., O'Keefe, J., 2002. The human hippocampus and spatial and episodic memory. Neuron 35, 625–641.
Buschman, T.J., Denovellis, E.L., Diogo, C., Bullock, D., Miller, E.K., 2012. Synchronous oscillatory neural ensembles for rules in the prefrontal cortex. Neuron 21, 838-846.

Butler, J.L., Paulsen, O., 2015. Hippocampal network oscillations - recent insights from in vitro experiments. Curr. Opin. Neurobiol. 31, 40-44.
Buzsáki, G., 2002. Theta oscillations in the hippocampus. Neuron 33, 325–340.
Buzsáki, G., 1996. The hippocampo-neocortical dialogue. Cereb. Cortex 1991 6, 81–92.
Buzsáki, G., 1986. Hippocampal sharp waves: their origin and significance. Brain Res. 398, 242–252.
Buzsáki, G., Buhl, D.L., Harris, K.D., Csicsvari, J., Czéh, B., Morozov, A., 2003. Hippocampal network patterns of activity in the mouse. Neuroscience 116, 201–211.
Buzsáki, G., Draguhn, A., 2004. Neuronal oscillations in cortical networks. Science 304, 1926–1929.
Buzsáki, G., Leung, L.W., Vanderwolf, C.H., 1983. Cellular bases of hippocampal EEG in the behaving rat. Brain Res. 287, 139–171.
Buzsáki, G., Wang, X.-J., 2012. Mechanisms of Gamma Oscillations. Annu. Rev. Neurosci. 35, 203–225.
Bygrave, A.M., Masiulis, S., Nicholson, E., Berkemann, M., Barkus, C., Sprengel, R., Harrison, P.J., Kullmann, D.M., Bannerman, D.M., Kätzel, D., 2016. Knockout of NMDA-receptors from parvalbumin interneurons sensitizes to schizophrenia-related deficits induced by MK-801. Transl. Psychiatry 6, e778.
Camiré, O., Topolnik, L., 2014. Dendritic Calcium Nonlinearities Switch the Direction of Synaptic Plasticity in Fast-Spiking Interneurons. J. Neurosci. 34, 3864–3877.
Canolty, R.T., Edwards, E., Dalal, S.S., Soltani, M., Nagarajan, S.S., Kirsch, H.E., Berger, M.S., Barbaro, N.M., Knight, R.T., 2006. High gamma power is phase-locked to theta oscillations in human neocortex. Science 313, 1626–1628.
Canto, C.B., Wouterlood, F.G., Witter, M.P., 2008. What does the anatomical organization of the entorhinal cortex tell us? Neural Plast. 2008.
Caputi, A., Fuchs, E.C., Allen, K., Magueresse, C.L., Monyer, H., 2012. Selective reduction of AMPA currents onto hippocampal interneurons impairs network oscillatory activity. PLOS ONE 7, e37318.
Cardin, J.A., Carlén, M., Meletis, K., Knoblich, U., Zhang, F., Deisseroth, K., Tsai, L.-H., Moore, C.I., 2009. Driving fast-spiking cells induces gamma rhythm and controls sensory responses. Nature 459, 663–667.
Carter, A.G., Regehr, W.G., 2002. Quantal events shape cerebellar interneuron firing. Nat. Neurosci. 5, 1309–1318.
Cassel, J.C., Cassel, S., Galani, R., Kelche, C., Will, B., Jarrard, L., 1998. Fimbria-fornix vs selective hippocampal lesions in rats: effects on locomotor activity and spatial learning and memory. Neurobiol. Learn. Mem. 69, 22–45.
Castillo, P.E., Malenka, R.C., Nicoll, R.A., 1997. Kainate receptors mediate a slow postsynaptic current in hippocampal CA3 neurons. Nature 388, 182–186.
Catarzi, D., Colotta, V., Varano, F., 2007. Competitive AMPA receptor antagonists. Med. Res. Rev. 27, 239–278.
Ceranik, K., Bender, R., Geiger, J.R.P., Monyer, H., Jonas, P., Frotscher, M., Lübke, J., 1997. A novel type of GABAergic interneuron connecting the input and the output regions of the hippocampus. J. Neurosci. 17, 5380–5394.
Chen, H.X., Otmakhov, N., Lisman, J., 1999. Requirements for LTP induction by pairing in hippocampal CA1 pyramidal cells. J. Neurophysiol. 82, 526–532.
Chow, A., Erisir, A., Farb, C., Nadal, M.S., Ozaita, A., Lau, D., Welker, E., Rudy, B., 1999. K(+) channel expression distinguishes subpopulations of parvalbumin- and somatostatin-containing neocortical interneurons. J. Neurosci. 19, 9332–9345.
Clark, R.E., Zola, S.M., Squire, L.R., 2000. Impaired recognition memory in rats after damage to the hippocampus. J. Neurosci. 20, 8853–8860.
Clarkson, J., Dwyer, D., Flecknell, P., Leach, M., Rowe, C., 2018. Handling method alters the hedonic value of reward in laboratory mice. Sci. Rep. 8, 1–8.
Clements, J.D., Bekkers, J.M., 1997. Detection of spontaneous synaptic events with an optimally scaled template. Biophys. J. 73, 220-229.
Clifton, P.G., Vickers, S.P., Somerville, E.M., 1998. Little and often: ingestive behavior patterns following hippocampal lesions in rats. Behav. Neurosci. 112, 502–511.
Colgin, L.L., 2013. Mechanisms and Functions of Theta Rhythms. Annu. Rev. Neurosci. 36, 295–312.
Colgin, L.L., Denninger, T., Fyhn, M., Hafting, T., Bonnevie, T., Jensen, O., Moser, M.-B., Moser, E.I., 2009. Frequency of gamma oscillations routes flow of information in the hippocampus. Nature 462, 353–357.
Colgin, L.L., Moser, E.I., 2010. Gamma oscillations in the hippocampus. Physiology 25, 319–329.

Collingridge, G.L., Kehl, S.J., McLennan, H., 1983. Excitatory amino acids in synaptic transmission in the Schaffer collateral-commissural pathway of the rat hippocampus. J. Physiol. 334, 33–46.
Colosimo, A., Goncz, K.K., Holmes, A.R., Kunzelmann, K., Novelli, G., Malone, R.W., Bennett, M.J., Gruenert, D.C., 2000. Transfer and expression of foreign genes in mammalian cells. Biotechniques 29, 314-331.
Conrad, K.L., Tseng, K.Y., Uejima, J.L., Reimers, J.M., Heng, L.-J., Shaham, Y., Marinelli, M., Wolf, M.E., 2008. Formation of accumbens GluR2-lacking AMPA receptors mediates incubation of cocaine craving. Nature 454, 118–121.
Contractor, A., Mulle, C., Swanson, G.T., 2011. Kainate receptors coming of age: milestones of two decades of research. Trends Neurosci. 34, 154–163.
Cowan, N., 2008. What are the differences between long-term, short-term, and working memory? Prog. Brain Res. 169, 323-338.
Csicsvari, J., Hirase, H., Czurko, A., Buzsáki, G., 1998. Reliability and state dependence of pyramidal cell-interneuron synapses in the hippocampus: an ensemble approach in the behaving rat. Neuron 21, 179–189.
Csicsvari, J., Jamieson, B., Wise, K.D., Buzsáki, G., 2003. Mechanisms of gamma oscillations in the hippocampus of the behaving rat. Neuron 37, 311–322.
Cunningham, M.G., O'Connor, R.P., Wong, S.E., 2008. Construction and implantation of a microinfusion system for sustained delivery of neuroactive agents. J. Vis. Exp. 17.
Cunningham, M.O., Davies, C.H., Buhl, E.H., Kopell, N., Whittington, M.A., 2003. Gamma oscillations induced by kainate receptor activation in the entorhinal cortex in vitro. J. Neurosci. 23, 9761–9769.
Cutsuridis, V., Hasselmo, M., 2011. Spatial memory sequence encoding and replay during modeled theta and ripple oscillations. Cogn. Comput. 3, 554–574.
Cutsuridis, V., Taxidis, J., 2013. Deciphering the role of CA1 inhibitory circuits in sharp wave-ripple complexes. Front. Syst. Neurosci. 7.
Czéh B., Varga Z.K., Henningsen, K., Kovács, G.L., Miseta, A., Wiborg, O., 2015. Chronic stress reduces the number of GABAergic interneurons in the adult rat hippocampus, dorsal-ventral and region-specific differences. Hippocampus 25, 393-405.
Davies, R.W., Morris, B., 2004. Molecular Biology of the Neuron. OUP Oxford.
Deacon, R.M.J., Bannerman, D.M., Kirby, B.P., Croucher, A., Rawlins, J.N.P., 2002. Effects of cytotoxic hippocampal lesions in mice on a cognitive test battery. Behav. Brain Res. 133, 57–68.
Deacon, R.M.J., Rawlins, J.N.P., 2006. T-maze alternation in the rodent. Nat. Protoc. 1, 7–12.
Deacon, R.M.J., Rawlins, J.N.P., 2002. Learning impairments of hippocampal-lesioned mice in a paddling pool. Behav. Neurosci. 116, 472–478.
Deller, T., Adelmann, G., Nitsch, R., Frotscher, M., 1996. The alvear pathway of the rat hippocampus. Cell Tissue Res. 286, 293–303.
D'Esposito, M., 2007. From cognitive to neural models of working memory. Philos. Trans. R. Soc. Lond. B. Biol. Sci. 362, 761–772.
Ding, X., Qiao, Y., Piao, C., Zheng, X., Liu, Z., Liang, J., 2014. N-methyl-D-aspartate receptor-mediated glutamate transmission in nucleus accumbens plays a more important role than that in dorsal striatum in cognitive flexibility. Front. Behav. Neurosci. 8.
Dingledine, R., Borges, K., Bowie, D., Traynelis, S.F., 1999. The glutamate receptor ion channels. Pharmacol. Rev. 51, 7–61.
Donato, F., Chowdhury, A., Lahr, M., Caroni, P., 2015. Early- and late-born parvalbumin basket cell subpopulations exhibiting distinct regulation and roles in learning. Neuron 85, 770–786.
Donato, F., Rompani, S.B., Caroni, P., 2013. Parvalbumin-expressing basket-cell network plasticity induced by experience regulates adult learning. Nature 504, 272–276.
Donevan, S.D., Rogawski, M.A., 1995. Intracellular polyamines mediate inward rectification of Ca(2+)-permeable alpha-amino-3-hydroxy-5-methyl-4-isoxazolepropionic acid receptors. Proc. Natl. Acad. Sci. U. S. A. 92, 9298–9302.
Dong, H.W., Swanson, L.W., Chen, L., Fanselow, M.S., Toga, A.W., 2009. Genomic-anatomic evidence for distinct functional domains in hippocampal field CA1. Proc. Natl. Acad. Sci. U. S. A. 106, 11794-11799.
Dougherty, S.E., Hollimon, J.J., McMeekin, L.J., Bohannon, A.S., West, A.B., Lesort, M., Hablitz, J.J., Cowell, R.M., 2014. Hyperactivity and cortical disinhibition in mice with restricted expression of mutant huntingtin to parvalbumin-positive cells. Neurobiol. Dis. 62.
Dragoi, G., Carpi, D., Recce, M., Csicsvari, J., Buzsáki, G., 1999. Interactions between hippocampus and medial septum during sharp waves and theta oscillation in the behaving rat. J. Neurosci. 19, 6191-6199.

Dupret, D., O'Neill, J., Csicsvari, J., 2013. Dynamic reconfiguration of hippocampal interneuron circuits during spatial learning. Neuron 78, 166–180.
Dupret, D., O'Neill, J., Pleydell-Bouverie, B., Csicsvari, J., 2010. The reorganization and reactivation of hippocampal maps predict spatial memory performance. Nat. Neurosci. 13, 995–1002.
Duva, C.A., Floresco, S.B., Wunderlich, G.R., Lao, T.L., Pinel, J.P., Phillips, A.G., 1997. Disruption of spatial but not object-recognition memory by neurotoxic lesions of the dorsal hippocampus in rats. Behav. Neurosci. 111, 1184–1196.
Ehrhardt, A., Xu, H., Kay, M.A., 2003. Episomal persistence of recombinant adenoviral vector genomes during the cell cycle in vivo. J. Virol. 77, 7689-7695.
Edmonds, B., Gibb, A.J., Colquhoun, D., 1995. Mechanisms of activation of glutamate receptors and the time course of excitatory synaptic currents. Annu. Rev. Physiol. 57, 495–519.
Ego-Stengel, V., Wilson, M.A., 2010. Disruption of ripple-associated hippocampal activity during rest impairs spatial learning in the rat. Hippocampus 20, 1–10.
Ekstrom, A.D., Kahana, M.J., Caplan, J.B., Fields, T.A., Isham, E.A., Newman, E.L., Fried, I., 2003. Cellular networks underlying human spatial navigation. Nature 425, 184–188.
Ellender, T.J., Nissen, W., Colgin, L.L., Mann, E.O., Paulsen, O., 2010. Priming of hippocampal population bursts by individual perisomatic-targeting interneurons. J. Neurosci. 30, 5979–5991.
Ermentrout, G.B., Kopell, N., 1998. Fine structure of neural spiking and synchronization in the presence of conduction delays. Proc. Natl. Acad. Sci. U. S. A. 95, 1259–1264.
Eschenko, O., Ramadan, W., Mölle, M., Born, J., Sara, S.J., 2008. Sustained increase in hippocampal sharp-wave ripple activity during slow-wave sleep after learning. Learn. Mem. 15, 222–228.
Fanselow, M.S., Dong, H.W., 2010. Are the dorsal and ventral hippocampus functionally distinct structures? Neuron 65, 7-19.
Farrant, M., Nusser, Z., 2005. Variations on an inhibitory theme: phasic and tonic activation of GABA(A) receptors. Nat. Rev. Neurosci. 6, 215–229.
Favuzzi, E., Marques-Smith, A., Deogracias, R., Winterflood, C.M., Sánchez-Aguilera, A., Mantoan, L., Maeso, P., Fernandes, C., Ewers, H., Rico, B., 2017. Activity-dependent gating of parvalbumin interneuron function by the perineuronal net protein brevican. Neuron 95, 639–655.e10.
Fell, J., Klaver, P., Lehnertz, K., Grunwald, T., Schaller, C., Elger, C.E., Fernández, G., 2001. Human memory formation is accompanied by rhinal–hippocampal coupling and decoupling. Nat. Neurosci. 4, 1259–1264.
File, S.E., 1990. One-trial tolerance to the anxiolytic effects of chlordiazepoxide in the plus-maze. Psychopharmacology (Berl.) 100, 281–282.
Fisahn, A., Contractor, A., Traub, R.D., Buhl, E.H., Heinemann, S.F., McBain, C.J., 2004. Distinct roles for the kainate receptor subunits GluR5 and GluR6 in kainate-induced hippocampal gamma oscillations. J. Neurosci. 24, 9658–9668.
Fisahn, A., Pike, F.G., Buhl, E.H., Paulsen, O., 1998. Cholinergic induction of network oscillations at 40 Hz in the hippocampus in vitro. Nature 394, 186–189.
Florez, C.M., McGinn, R.J., Lukankin, V., Marwa, I., Sugumar, S., Dian, J., Hazrati, L.-N., Carlen, P.L., Zhang, L., Valiante, T.A., 2015. In vitro recordings of human neocortical oscillations. Cereb. Cortex 25, 578-597.
Fox, S.E., Wolfson, S., Ranck, J.B., 1986. Hippocampal theta rhythm and the firing of neurons in walking and urethane anesthetized rats. Exp. Brain Res. 62, 495–508.
Frerking, M., Malenka, R.C., Nicoll, R.A., 1998. Synaptic activation of kainate receptors on hippocampal interneurons. Nat. Neurosci. 1, 479–486.
Freudenberg, F., Resnik, E., Kolleker, A., Celikel, T., Sprengel, R., Seeburg, P.H., 2016. Hippocampal GluA1 expression in Gria1-/- mice only partially restores spatial memory performance deficits. Neurobiol. Learn. Mem. 135, 83–90.
Freund, T.F., Buzsáki, G., 1996. Interneurons of the hippocampus. Hippocampus 6, 347–470.
Freund, T.F., Katona, I., 2007. Perisomatic inhibition. Neuron 56, 33–42.
Fuchs, E.C., Zivkovic, A.R., Cunningham, M.O., Middleton, S., LeBeau, F.E.N., Bannerman, D.M., Rozov, A., Whittington, M.A., Traub, R.D., Rawlins, J.N.P., Monyer, H., 2007. Recruitment of parvalbumin-positive interneurons determines hippocampal function and associated behavior. Neuron 53, 591–604.
Fukuda, T., Kosaka, T., 2000. Gap junctions linking the dendritic network of GABAergic interneurons in the hippocampus. J. Neurosci. 20, 1519–1528.

Fuster, J.M., 2000. Cortical dynamics of memory. Int. J. Psychophysiol. Off. J. Int. Organ. Psychophysiol. 35, 155–164.
Fuster, J.M., Alexander, G.E., 1971. Neuron activity related to short-term memory. Science 173, 652–654.
Fyhn, M., Molden, S., Hollup, S., Moser, M.-B., Moser, E., 2002. Hippocampal neurons responding to first-time dislocation of a target object. Neuron 35, 555–566.
Fyhn, M., Molden, S., Witter, M.P., Moser, E.I., Moser, M.-B., 2004. Spatial representation in the entorhinal cortex. Science 305, 1258–1264.
Gabriel, 1969. Simultaneous test procedures - some theory of multiple comparisons. Ann. Math. Stat. 40, 224–250.
Gaiarsa, J.-L., Caillard, O., Ben-Ari, Y., 2002. Long-term plasticity at GABAergic and glycinergic synapses: mechanisms and functional significance. Trends Neurosci. 25, 564–570.
Ganter, P., Szücs, P., Paulsen, O., Somogyi, P., 2004. Properties of horizontal axo-axonic cells in stratum oriens of the hippocampal CA1 area of rats in vitro. Hippocampus 14, 232–243.
Geiger, J.R., Lübke, J., Roth, A., Frotscher, M., Jonas, P., 1997. Submillisecond AMPA receptor-mediated signaling at a principal neuron-interneuron synapse. Neuron 18, 1009–1023.
Geiger, J.R.P., Melcher, T., Koh, D.-S., Sakmann, B., Seeburg, P.H., Jonas, P., Monyer, H., 1995. Relative abundance of subunit mRNAs determines gating and Ca2+ permeability of AMPA receptors in principal neurons and interneurons in rat CNS. Neuron 15, 193–204.
Geisler, C., Brunel, N., Wang, X.-J., 2005. Contributions of intrinsic membrane dynamics to fast network oscillations with irregular neuronal discharges. J. Neurophysiol. 94, 4344–4361.
Gensler, S., Sander, A., Korngreen, A., Traina, G., Giese, G., Witzemann, V., 2001. Assembly and clustering of acetylcholine receptors containing GFP-tagged ε or γ subunits. Eur. J. Biochem. 268, 2209–2217.
Gerrow, K., Triller, A., 2010. Synaptic stability and plasticity in a floating world. Curr. Opin. Neurobiol. 20, 631–639.
Gilbert, P.E., Kesner, R.P., 2006. The role of the dorsal CA3 hippocampal subregion in spatial working memory and pattern separation. Behav. Brain Res. 169, 142–149.
Givens, B., Olton, D.S., 1994. Local modulation of basal forebrain: effects on working and reference memory. J. Neurosci. 14, 3578–3587.
Gleeson, R., Dragunow, M., Kirton, N., Villiger, J., Chute, D., 1980. Intracranial cannulation of small animals. Behav. Res. Methods Instrum. 12, 346–348.
Glickman, S.E., Higgins, T.J., Isaacson, R.L., 1970. Some effects of hippocampal lesions on the behavior of Mongolian gerbils. Physiol. Behav. 5, 931–938.
Gloveli, T., Dugladze, T., Rotstein, H.G., Traub, R.D., Monyer, H., Heinemann, U., Whittington, M.A., Kopell, N.J., 2005a. Orthogonal arrangement of rhythm-generating microcircuits in the hippocampus. Proc. Natl. Acad. Sci. U. S. A. 102, 13295–13300.
Gloveli, T., Dugladze, T., Saha, S., Monyer, H., Heinemann, U., Traub, R.D., Whittington, M.A., Buhl, E.H., 2005b. Differential involvement of oriens/pyramidale interneurones in hippocampal network oscillations in vitro. J. Physiol. 562, 131–147.
Godavarthi, S.K., Sharma, A., Jana, N.R., 2014. Reversal of reduced parvalbumin neurons in hippocampus and amygdala of Angelman syndrome model mice by chronic treatment of fluoxetine. J. Neurochem. 130, 444–454.
Goffer, Y., Xu, D., Eberle, S.E., D'amour, J., Lee, M., Tukey, D., Froemke, R.C., Ziff, E.B., Wang, J., 2013. Calcium-permeable AMPA receptors in the nucleus accumbens regulate depression-like behaviors in the chronic neuropathic pain state. J. Neurosci. 33, 19034–19044.
Gonzalez-Burgos, G., Lewis, D.A., 2012. NMDA Receptor Hypofunction, Parvalbumin-positive neurons, and cortical gamma oscillations in schizophrenia. Schizophr. Bull. 38, 950–957.
Good, M.A., Barnes, P., Staal, V., McGregor, A., Honey, R.C., 2007. Context- but not familiarity-dependent forms of object recognition are impaired following excitotoxic hippocampal lesions in rats. Behav. Neurosci. 121, 218–223.
Gould, T.J., Rowe, W.B., Heman, K.L., Mesches, M.H., Young, D.A., Rose, G.M., Bickford, P.C., 2002. Effects of hippocampal lesions on patterned motor learning in the rat. Brain Res. Bull. 58, 581–586.
Granon, S., Vidal, C., Thinus-Blanc, C., Changeux, J.P., Poucet, B., 1994. Working memory, response selection, and effortful processing in rats with medial prefrontal lesions. Behav. Neurosci. 108, 883–891.
Gray, J.A., McNaughton, N., 2000. The Neuropsychology Of Anxiety, 2nd ed. Oxford University Press.
Greger, I.H., Akamine, P., Khatri, L., Ziff, E.B., 2006. Developmentally regulated, combinatorial RNA processing modulates AMPA receptor biogenesis. Neuron 51, 85–97.

Greger, I.H., Khatri, L., Kong, X., Ziff, E.B., 2003. AMPA receptor tetramerization is mediated by Q/R editing. Neuron 40, 763–774.
Greger, I.H., Khatri, L., Ziff, E.B., 2002. RNA editing at Arg607 controls AMPA receptor exit from the endoplasmic reticulum. Neuron 34, 759–772.
Greger, I.H., Ziff, E.B., Penn, A.C., 2007. Molecular determinants of AMPA receptor subunit assembly. Trends Neurosci. 30, 407–416.
Grosskreutz, J., Zoerner, A., Schlesinger, F., Krampfl, K., Dengler, R., Bufler, J., 2003. Kinetic properties of human AMPA-type glutamate receptors expressed in HEK293 cells. Eur. J. Neurosci. 17, 1173–1178.
Guire, E.S., Oh, M.C., Soderling, T.R., Derkach, V.A., 2008. Recruitment of calcium-permeable AMPA receptors during synaptic potentiation is regulated by CaM-Kinase I. J. Neurosci. 28, 6000–6009.
Guise, K.G., Shapiro, M.L., 2017. Medial prefrontal cortex reduces memory interference by modifying hippocampal encoding. Neuron 94, 183–192.
Gulyás, A.I., Megías, M., Emri, Z., Freund, T.F., 1999. Total number and ratio of excitatory and inhibitory synapses converging onto single interneurons of different types in the CA1 area of the rat hippocampus. J. Neurosci. 19, 10082–10097.
Gulyás, A.I., Miles, R., Hájos, N., Freund, T.F., 1993. Precision and variability in postsynaptic target selection of inhibitory cells in the hippocampal CA3 region. Eur. J. Neurosci. 5, 1729–1751.
Gulyás, A.I., Szabó, G.G., Ulbert, I., Holderith, N., Monyer, H., Erdélyi, F., Szabó, G., Freund, T.F., Hájos, N., 2010. Parvalbumin-containing fast-spiking basket cells generate the field potential oscillations induced by cholinergic receptor activation in the hippocampus. J. Neurosci. 30, 15134–15145.
Hahn, T.T.G., Sakmann, B., Mehta, M.R., 2006. Phase-locking of hippocampal interneurons' membrane potential to neocortical up-down states. Nat. Neurosci. 9, 1359–1361.
Haj-Dahmane, S., Béïque, J.C., Shen, R.-Y., 2017. GluA2-lacking AMPA receptors and nitric oxide signaling gate spike-timing dependent potentiation of glutamate synapses in the dorsal raphe nucleus. eNeuro 4.
Hájos, N., Pálhalmi, J., Mann, E.O., Németh, B., Paulsen, O., Freund, T.F., 2004. Spike timing of distinct types of GABAergic interneuron during hippocampal gamma oscillations in vitro. J. Neurosci. 24, 9127–9137.
Hájos, N., Paulsen, O., 2009. Network mechanisms of gamma oscillations in the CA3 region of the hippocampus. Neural Netw. 22, 1113–1119.
Han, Z.S., Buhl, E.H., Lörinczi, Z., Somogyi, P., 1993. A high degree of spatial selectivity in the axonal and dendritic domains of physiologically identified local-circuit neurons in the dentate gyrus of the rat hippocampus. Eur. J. Neurosci. 5, 395–410.
Hangya, B., Borhegyi, Z., Szilágyi, N., Freund, T.F., Varga, V., 2009. GABAergic neurons of the medial septum lead the hippocampal network during theta activity. J. Neurosci. 29, 8094–8102.
Hao, L., Yang, Z., Lei, J., 2018. Underlying mechanisms of cooperativity, input specificity, and associativity of long-term potentiation through a postive feedback of local protein synthesis. Front. Comput. Neurosci. 12.
Hannula, D.E., Greene, A., 2012. The hippocampus reevaluated in unconscious learning and memory: at a tipping point? Front. Hum. Neurosci. 6.
Harris, R.J., 2001. A primer of multivariate statistics, 3rd ed. Lawrence Erlbaum Associates, Inc., Mahwah, New Jersey.
Hasenstaub, A., Shu, Y., Haider, B., Kraushaar, U., Duque, A., McCormick, D.A., 2005. Inhibitory postsynaptic potentials carry synchronized frequency information in active cortical networks. Neuron 47, 423–435.
Hasselmo, M.E., Bodelón, C., Wyble, B.P., 2002. A proposed function for hippocampal theta rhythm: separate phases of encoding and retrieval enhance reversal of prior learning. Neural Comput. 14, 793–817.
He, Y., Janssen, W.G., Vissavajjhala, P., Morrison, J.H., 1998. Synaptic distribution of GluR2 in hippocampal GABAergic interneurons and pyramidal cells: a double-label immunogold analysis. Exp. Neurol. 150, 1–13.
Hebb, D.O., 1949. Organisation of behavior. John Wiley & Sons, New York.
Henley, J.M., Wilkinson, K.A., 2013. AMPA receptor trafficking and the mechanisms underlying synaptic plasticity and cognitive aging. Dialogues Clin. Neurosci. 15, 11–27.
Hippenmeyer, S., Vrieseling, E., Sigrist, M., Portmann, T., Laengle, C., Ladle, D.R., Arber, S., 2005. A developmental switch in the response of DRG neurons to ETS transcription factor signalling. PLoS Biol. 3, e159.
Ho, M.T.-W., Pelkey, K.A., Topolnik, L., Petralia, R.S., Takamiya, K., Xia, J., Huganir, R.L., Lacaille, J.-C., McBain, C.J., 2007. Developmental expression of Ca2+-permeable AMPA receptors underlies depolarization-induced long-Term depression at mossy fiber–CA3 pyramid synapses. J. Neurosci. 27, 11651–11662.

Hock, B.J., Bunsey, M.D., 1998. Differential effects of dorsal and ventral hippocampal lesions. J. Neurosci. 18, 7027–7032.
Hoffmann, T., Stadler, L.K.J., Busby, M., Song, Q., Buxton, A.T., Wagner, S.D., Davis, J.J., Ko Ferrigno, P., 2010. Structure-function studies of an engineered scaffold protein derived from stefin A. I: Development of the SQM variant. Protein Eng. Des. Sel. 23, 403–413.
Holdstock, J.S., Mayes, A.R., Roberts, N., Cezayirli, E., Isaac, C.L., O'Reilly, R.C., Norman, K.A., 2002. Under what conditions is recognition spared relative to recall after selective hippocampal damage in humans? Hippocampus 12, 341–351.
Holman, L., Head, M.L., Lanfear, R., Jennions, M.D., 2002. Evidence of experimental bias in the life sciences: why we need blind data recording. PLoS Biol. 13, e1002190.
Honey, R.C., Watt, A., Good, M., 1998. Hippocampal lesions disrupt an associative mismatch process. J. Neurosci. 18, 2226–2230.
Hong, I., Kim, J., Kim, J., Lee, S., Ko, H.-G., Nader, K., Kaang, B.-K., Tsien, R.W., Choi, S., 2013. AMPA receptor exchange underlies transient memory destabilization on retrieval. Proc. Natl. Acad. Sci. U. S. A. 110, 8218–8223.
Hormuzdi, S.G., Pais, I., LeBeau, F.E., Towers, S.K., Rozov, A., Buhl, E.H., Whittington, M.A., Monyer, H., 2001. Impaired electrical signaling disrupts gamma frequency oscillations in connexin 36-deficient mice. Neuron 31, 487–495.
Howard, A., Tamas, G., Soltesz, I., 2005. Lighting the chandelier: new vistas for axo-axonic cells. Trends Neurosci. 28, 310–316.
Howard, M.W., Rizzuto, D.S., Caplan, J.B., Madsen, J.R., Lisman, J., Aschenbrenner-Scheibe, R., Schulze-Bonhage, A., Kahana, M.J., 2003. Gamma oscillations correlate with working memory load in humans. Cereb. Cortex 13, 1369–1374.
Hu, H., Gan, J., Jonas, P., 2014. Fast-spiking, parvalbumin+ GABAergic interneurons: From cellular design to microcircuit function. Science 345, 1255263.
Huang, S., Uusisaari, M.Y., 2013. Physiological temperature during brain slicing enhances the quality of acute slice preparations. Front. Cell. Neurosci. 7.
Huerta, P.T., Lisman, J.E., 1995. Bidirectional synaptic plasticity induced by a single burst during cholinergic theta oscillation in CA1 in vitro. Neuron 15, 1053–1063.
Huganir, R.L., Nicoll, R.A., 2013. AMPARs and synaptic plasticity: the last 25 years. Neuron 80, 704–717.
Iglói, K., Doeller, C.F., Berthoz, A., Rondi-Reig, L., Burgess, N., 2010. Lateralized human hippocampal activity predicts navigation based on sequence or place memory. Proc. Natl. Acad. Sci. U. S. A. 107, 14466–14471.
Iino, M., Goto, K., Kakegawa, W., Okado, H., Sudo, M., Ishiuchi, S., Miwa, A., Takayusa, Y., Saito, I., Tsuzuki, K., Ozawa, S., 2001. Glia-synapse interaction through Ca2+-permeable AMPA receptors in Bergmann glia. Science 292, 926–929.
Insausti, R., Amaral, D.G., 2004. Chapter 23 - Hippocampal Formation, in: Mai, G.P.K. (Ed.), The Human Nervous System (Second Edition). Academic Press, San Diego, pp. 871–914.
Isaac, J.T.R., Ashby, M.C., McBain, C.J., 2007. The role of the GluR2 subunit in AMPA receptor function and synaptic plasticity. Neuron 54, 859–871.
Ishiuchi, S., Tsuzuki, K., Yoshida, Y., Yamada, N., Hagimura, N., Okado, H., Miwa, A., Kurihara, H., Nakazato, Y., Tamura, M., Sasaki, T., Ozawa, S., 2002. Blockage of Ca2+-permeable AMPA receptors suppresses migration and induces apoptosis in human glioblastoma cells. Nat. Med. 8, 971–978.
Izquierdo, I., Bianchin, M., Silva, M.B., Zanatta, M.S., Walz, R., Ruschel, A.C., Da Silva, R.C., Paczko, N., Medina, J.H., 1993. CNQX infused into rat hippocampus or amygdala disrupts the expression of memory of two different tasks. Behav. Neural Biol. 59, 1–4.
Jahr, C.E., Stevens, C.F., 1993. Calcium permeability of the N-methyl-D-aspartate receptor channel in hippocampal neurons in culture. Proc. Natl. Acad. Sci. U. S. A. 90, 11573–11577.
Jeneson, A., Kirwan, C.B., Hopkins, R.O., Wixted, J.T., Squire, L.R., 2010. Recognition memory and the hippocampus: A test of the hippocampal contribution to recollection and familiarity. Learn. Mem. 17, 63–70.
Jensen, O., Colgin, L.L., 2007. Cross-frequency coupling between neuronal oscillations. Trends Cogn. Sci. 11, 267–269.
Johnson, A., Redish, A.D., 2007. Neural ensembles in CA3 transiently encode paths forward of the animal at a decision point. J. Neurosci. 27, 12176–12189.
Johnson, J.W., Ascher, P., 1987. Glycine potentiates the NMDA response in cultured mouse brain neurons. Nature 325, 529–531.

Jonas, P., Bischofberger, J., Fricker, D., Miles, R., 2004. Interneuron diversity series: Fast in, fast out--temporal and spatial signal processing in hippocampal interneurons. Trends Neurosci. 27, 30–40.
Jonas, P., Burnashev, N., 1995. Molecular mechanisms controlling calcium entry through AMPA-type glutamate receptor channels. Neuron 15, 987–990.
Jonas, P., Lisman, J., 2014. Structure, function, and plasticity of hippocampal dentate gyrus microcircuits. Front. Neural Circuits 8.
Jones, M.G., Anis, N.A., Lodge, D., 1990. Philanthotoxin blocks quisqualate-, AMPA- and kainate-, but not NMDA-, induced excitation of rat brainstem neurones in vivo. Br. J. Pharmacol. 101, 968–970.
Jung, M.W., McNaughton, B.L., 1993. Spatial selectivity of unit activity in the hippocampal granular layer. Hippocampus 3, 165–182.
Jutras, M.J., Fries, P., Buffalo, E.A., 2009. Gamma-band synchronization in the macaque hippocampus and memory formation. J. Neurosci. 29, 12521–12531.
Kamboj, S.K., Swanson, G.T., Cull-Candy, S.G., 1995. Intracellular spermine confers rectification on rat calcium-permeable AMPA and kainate receptors. J. Physiol. 486, 297–303.
Kamondi, A., Acsády, L., Buzsáki, G., 1998a. Dendritic spikes are enhanced by cooperative network activity in the intact hippocampus. J. Neurosci. 18, 3919–3928.
Kamondi, A., Acsády, L., Wang, X.J., Buzsáki, G., 1998b. Theta oscillations in somata and dendrites of hippocampal pyramidal cells in vivo: activity-dependent phase-precession of action potentials. Hippocampus 8, 244–261.
Kang, K., Shelley, M., Henrie, J.A., Shapley, R., 2010. LFP spectral peaks in V1 cortex: network resonance and cortico-cortical feedback. J. Comput. Neurosci. 29, 495–507.
Kiernan, J.A., 2012. Anatomy of the temporal lobe. Epilepsy Res. Treat. 2012.
Kim, D., Jeong, H., Lee, J., Ghim, J.-W., Her, E.S., Lee, S.-H., Jung, M.W., 2016. Distinct roles of parvalbumin- and somatostatin-expressing interneurons in working memory. Neuron 92, 902–915.
Kinney, J.W., Davis, C.N., Tabarean, I., Conti, B., Bartfai, T., Behrens, M.M., 2006. A specific role for NR2A-containing NMDA receptors in the maintenance of parvalbumin and GAD67 immunoreactivity in cultured interneurons. J. Neurosci. 26, 1604–1615.
Kitajima, T., Hara, K.-I., 1991. A model of the mechanism of cooperativity and associativity of long-term potentiation in the hippocampus: a fundamental mechanism of assoiative memory and learning. Biol. Cybern. 64, 365-371.
Kjelstrup, K.G., Tuvnes, F.A., Steffenach, H.-A., Murison, R., Moser, E.I., Moser, M.-B., 2002. Reduced fear expression after lesions of the ventral hippocampus. Proc. Natl. Acad. Sci. 99, 10825–10830.
Klausberger, T., Magill, P.J., Márton, L.F., Roberts, J.D.B., Cobden, P.M., Buzsáki, G., Somogyi, P., 2003. Brain-state- and cell-type-specific firing of hippocampal interneurons in vivo. Nature 421, 844–848.
Klausberger, T., Márton, L.F., Baude, A., Roberts, J.D.B., Magill, P.J., Somogyi, P., 2004. Spike timing of dendrite-targeting bistratified cells during hippocampal network oscillations in vivo. Nat. Neurosci. 7, 41–47.
Klausberger, T., Marton, L.F., O'Neill, J., Huck, J.H.J., Dalezios, Y., Fuentealba, P., Suen, W.Y., Papp, E., Kaneko, T., Watanabe, M., Csicsvari, J., Somogyi, P., 2005. Complementary roles of cholecystokinin- and parvalbumin-expressing GABAergic neurons in hippocampal network oscillations. J. Neurosci. 25, 9782–9793.
Klausberger, T., Somogyi, P., 2008. Neuronal diversity and temporal dynamics: the unity of hippocampal circuit operations. Science 321, 53–57.
Kloosterman, F., van Haeften, T., Lopes da Silva, F.H., 2004. Two reentrant pathways in the hippocampal-entorhinal system. Hippocampus 14, 1026–1039.
Kloosterman, F., Van Haeften, T., Witter, M.P., Lopes Da Silva, F.H., 2003. Electrophysiological characterization of interlaminar entorhinal connections: an essential link for re-entrance in the hippocampal-entorhinal system. Eur. J. Neurosci. 18, 3037–3052.
Knowles, W.D., Schwartzkroin, P.A., 1981. Axonal ramifications of hippocampal CA1 pyramidal cells. J. Neurosci. 1, 1236–1241.
Kocsis, B., Bragin, A., Buzsáki, G., 1999. Interdependence of multiple theta generators in the hippocampus: a partial coherence analysis. J. Neurosci. 19, 6200–6212.
Koh, D.S., Geiger, J.R., Jonas, P., Sakmann, B., 1995. Ca(2+)-permeable AMPA and NMDA receptor channels in basket cells of rat hippocampal dentate gyrus. J. Physiol. 485, 383–402.
Köhr, G., De Koninck, Y., Mody, I., 1993. Properties of NMDA receptor channels in neurons acutely isolated from epileptic (kindled) rats. J. Neurosci. 13, 3612–3627.

Koike, M., Iino, M., Ozawa, S., 1997. Blocking effect of 1-naphthyl acetyl spermine on Ca(2+)-permeable AMPA receptors in cultured rat hippocampal neurons. Neurosci. Res. 29, 27–36.
Koike, M., Tsukada, S., Tsuzuki, K., Kijima, H., Ozawa, S., 2000. Regulation of kinetic properties of GluR2 AMPA receptor channels by alternative splicing. J. Neurosci. 20, 2166–2174.
Korotkova, T., Fuchs, E.C., Ponomarenko, A., von Engelhardt, J., Monyer, H., 2010. NMDA receptor ablation on parvalbumin-positive interneurons impairs hippocampal synchrony, spatial representations, and working memory. Neuron 68, 557–569.
Kotin, R.M., Siniscalco, M., Samulski, R.J., Zhu, X.D., Hunter, L., Laughlin, C.A., McLaughlin, S., Muzyczka, N., Rocchi, M., Berns, K.I., 1990. Site-specific integration by adeno-associated virus. Proc. Natl. Acad. Sci. U. S. A. 87, 2211-2215.
Kramer, J.H., Schuff, N., Reed, B.R., Mungas, D., Du, A.-T., Rosen, H.J., Jagust, W.J., Miller, B.L., Weiner, M.W., Chui, H.C., 2004. Hippocampal volume and retention in Alzheimer's disease. J. Int. Neuropsychol. Soc. 10, 639–643.
Kromann, H., Krikstolaityte, S., Andersen, A.J., Andersen, K., Krogsgaard-Larsen, P., Jaroszewski, J.W., Egebjerg, J., Strømgaard, K., 2002. Solid-phase synthesis of polyamine toxin analogues: potent and selective antagonists of Ca2+-permeable AMPA receptors. J. Med. Chem. 45, 5745–5754.
Kuenzi, F.M., Fitzjohn, S.M., Morton, R.A., Collingridge, G.L., Seabrook, G.R., 2000. Reduced long-term potentiation in hippocampal slices prepared using sucrose-based artificial cerebrospinal fluid. J. Neurosci. Methods 100, 117–122.
Kügler, S., Kilic, E., Bähr, M., 2003. Human synapsin 1 gene promoter confers highly neuron-specific long-term transgene expression from an adenoviral vector in the adult rat brain depending on the transduced area. Gene Ther. 10, 337–347.
Kumar, S.S., Bacci, A., Kharazia, V., Huguenard, J.R., 2002. A developmental switch of AMPA receptor subunits in neocortical pyramidal neurons. J. Neurosci. 22, 3005–3015.
Kumaran, D., Maguire, E.A., 2006. An unexpected sequence of events: Mismatch detection in the human hippocampus. PLOS Biol. 4, e424.
Kunec, S., Hasselmo, M.E., Kopell, N., 2005. Encoding and retrieval in the CA3 region of the hippocampus: a model of theta-phase separation. J. Neurophysiol. 94, 70–82.
Kwag, J., Paulsen, O., 2009. Bidirectional control of spike timing by GABA(A) receptor-mediated inhibition during theta oscillation in CA1 pyramidal neurons. Neuroreport 20, 1209-1213.
Lamsa, K., Heeroma, J.H., Kullmann, D.M., 2005. Hebbian LTP in feed-forward inhibitory interneurons and the temporal fidelity of input discrimination. Nat. Neurosci. 8, 916–924.
Lamsa, K.P., Heeroma, J.H., Somogyi, P., Rusakov, D.A., Kullmann, D.M., 2007. Anti-Hebbian long-term potentiation in the hippocampal feedback inhibitory circuit. Science 315, 1262–1266.
Larson, J., Munkácsy, E., 2015. Theta-burst LTP. Brain Res. 1621, 38–50.
Lau, P.Y.-P., Katona, L., Saghy, P., Newton, K., Somogyi, P., Lamsa, K.P., 2017. Long-term plasticity in identified hippocampal GABAergic interneurons in the CA1 area in vivo. Brain Struct. Funct. 222, 1809–1827.
Lavenex, P., Amaral, D.G., 2000. Hippocampal-neocortical interaction: a hierarchy of associativity. Hippocampus 10, 420–430.
Lawrence, J.J., Grinspan, Z.M., McBain, C.J., 2004. Quantal transmission at mossy fibre targets in the CA3 region of the rat hippocampus. J. Physiol. 554, 175–193.
Lawrence, J.J., McBain, C.J., 2003. Interneuron diversity series: containing the detonation--feedforward inhibition in the CA3 hippocampus. Trends Neurosci. 26, 631–640.
Le Duigou, C., Simonnet, J., Teleñczuk, M.T., Fricker, D., Miles, R., 2014. Recurrent synapses and circuits in the CA3 region of the hippocampus: an associative network. Front. Cell. Neurosci. 7.
Leão, R.N., Mikulovic, S., Leão, K.E., Munguba, H., Gezelius, H., Enjin, A., Patra, K., Eriksson, A., Loew, L.M., Tort, A.B.L., Kullander, K., 2012. OLM interneurons differentially modulate CA3 and entorhinal inputs to hippocampal CA1 neurons. Nat. Neurosci. 15, 1524–1530.
Le Roux, N., Cabezas, C., Böhm, U.L., Poncer, J.C., 2013. Input-specific learning rules at excitatory synapses onto hippocampal parvalbumin-expressing interneurons. J. Physiol. 591, 1809–1822.
LeBeau, F.E.N., Towers, S.K., Traub, R.D., Whittington, M.A., Buhl, E.H., 2002. Fast network oscillations induced by potassium transients in the rat hippocampus in vitro. J. Physiol. 542, 167–179.
Lee, A.-R., Kim, J.-H., Cho, E., Kim, M., Park, M., 2017. Dorsal and ventral hippocampus differentiate in functional pathways and differentially associate with neurological disease-related genes during postnatal development. Front. Mol. Neurosci. 10, 331.

Lee, H.-K., Takamiya, K., Han, J.-S., Man, H., Kim, C.-H., Rumbaugh, G., Yu, S., Ding, L., He, C., Petralia, R.S., Wenthold, R.J., Gallagher, M., Huganir, R.L., 2003. Phosphorylation of the AMPA receptor GluR1 subunit is required for synaptic plasticity and retention of spatial memory. Cell 112, 631–643.
Lee, I., Kesner, R.P., 2003. Time-dependent relationship between the dorsal hippocampus and the prefrontal cortex in spatial memory. J. Neurosci. 23, 1517–1523.
Lei, S., McBain, C.J., 2002. Distinct NMDA receptors provide differential modes of transmission at mossy fiber-interneuron synapses. Neuron 33, 921–933.
Lei, S., Pelkey, K.A., Topolnik, L., Congar, P., Lacaille, J.-C., McBain, C.J., 2003. Depolarization-induced long-term depression at hippocampal mossy fiber-CA3 pyramidal neuron synapses. J. Neurosci. 23, 9786–9795.
Lerma, J., 2003. Roles and rules of kainate receptors in synaptic transmission. Nat. Rev. Neurosci. 4, 481–495.
Leutgeb, J.K., Leutgeb, S., Moser, M.-B., Moser, E.I., 2007. Pattern separation in the dentate gyrus and CA3 of the hippocampus. Science 315, 961–966.
Lewis, D.A., Hashimoto, T., Volk, D.W., 2005. Cortical inhibitory neurons and schizophrenia. Nat. Rev. Neurosci. 6, 312–324.
Li, Y., Stam, F.J., Aimone, J.B., Goulding, M., Callaway, E.M., Gage, F.H., 2013. Molecular layer perforant path-associated cells contribute to feed-forward inhibition in the adult dentate gyrus. Proc. Natl. Acad. Sci. U. S. A. 110, 9106–9111.
Lisman, J., 2010. Working memory: the importance of theta and gamma oscillations. Curr. Biol. 20, R490-492.
Lisman, J., 1989. A mechanism for the Hebb and the anti-Hebb processes underlying learning and memory. Proc. Natl. Acad. Sci. U. S. A. 86, 9574–9578.
Lisman, J.E., Jensen, O., 2013. The theta-gamma neural code. Neuron 77, 1002–1016.
Liu, S.J., Cull-Candy, S.G., 2002. Activity-dependent change in AMPA receptor properties in cerebellar stellate cells. J. Neurosci. 22, 3881–3889.
Lomeli, H., Mosbacher, J., Melcher, T., Höger, T., Geiger, J.R., Kuner, T., Monyer, H., Higuchi, M., Bach, A., Seeburg, P.H., 1994. Control of kinetic properties of AMPA receptor channels by nuclear RNA editing. Science 266, 1709–1713.
Lu, W., Shi, Y., Jackson, A.C., Bjorgan, K., During, M.J., Sprengel, R., Seeburg, P.H., Nicoll, R.A., 2009. Subunit composition of synaptic AMPA receptors revealed by a single-cell genetic approach. Neuron 62, 254–268.
Lüscher, C., Malenka, R.C., 2012. NMDA receptor-dependent long-term potentiation and long-term depression (LTP/LTD). Cold Spring Harb. Perspect. Biol. 4.
Lynch, G., Baudry, M., 1984. The biochemistry of memory: a new and specific hypothesis. Science 224, 1057–1063.
Maccaferri, G., 2005. Stratum oriens horizontal interneurone diversity and hippocampal network dynamics. J. Physiol. 562, 73–80.
Madisen, L., Zwingman, T.A., Sunkim, S.M., Oh, S.W., Zariwala, H.A., Gu, H., Ng, L.L., Palmiter, R.D., Hawrylycz, M.J., Jones, A.R., Lein, E.S., Zeng, H., 2010. A robust and high-throughput Cre reporting and characterization system for the whole mouse brain. Nat. Neurosci. 13, 133-140.
Mahanty, N.K., Sah, P., 1998. Calcium-permeable AMPA receptors mediate long-term potentiation in interneurons in the amygdala. Nature 394, 683–687.
Malin, E.L., McGaugh, J.L., 2006. Differential involvement of the hippocampus, anterior cingulate cortex, and basolateral amygdala in memory for context and footshock. Proc. Natl. Acad. Sci. U. S. A. 103, 1959-1963.
Mann, E.O., Mody, I., 2010. Control of hippocampal gamma oscillation frequency by tonic inhibition and excitation of interneurons. Nat. Neurosci. 13, 205–212.
Mann, E.O., Radcliffe, C.A., Paulsen, O., 2005a. Hippocampal gamma-frequency oscillations: from interneurones to pyramidal cells, and back. J. Physiol. 562, 55–63.
Mann, E.O., Suckling, J.M., Hajos, N., Greenfield, S.A., Paulsen, O., 2005b. Perisomatic feedback inhibition underlies cholinergically induced fast network oscillations in the rat hippocampus in vitro. Neuron 45, 105–117.
Mansour, M., Nagarajan, N., Nehring, R.B., Clements, J.D., Rosenmund, C., 2001. Heteromeric AMPA receptors assemble with a preferred subunit stoichiometry and spatial arrangement. Neuron 32, 841–853.
Marrosu, F., Portas, C., Mascia, M.S., Casu, M.A., Fà, M., Giagheddu, M., Imperato, A., Gessa, G.L., 1995. Microdialysis measurement of cortical and hippocampal acetylcholine release during sleep-wake cycle in freely moving cats. Brain Res. 671, 329–332.

Martin, S.J., Grimwood, P.D., Morris, R.G., 2000. Synaptic plasticity and memory: an evaluation of the hypothesis. Annu. Rev. Neurosci. 23, 649–711.
Matsumura, N., Nishijo, H., Tamura, R., Eifuku, S., Endo, S., Ono, T., 1999. Spatial- and task-dependent neuronal responses during real and virtual translocation in the monkey hippocampal formation. J. Neurosci. 19, 2381–2393.
Mátyás, F., Freund, T.F., Gulyás, A.I., 2004. Convergence of excitatory and inhibitory inputs onto CCK-containing basket cells in the CA1 area of the rat hippocampus. Eur. J. Neurosci. 19, 1243–1256.
Mayer, M.L., 2006. Glutamate receptors at atomic resolution. Nature 440, 456–462.
Mayer, M.L., Westbrook, G.L., Guthrie, P.B., 1984. Voltage-dependent block by Mg2+ of NMDA responses in spinal cord neurones. Nature 309, 261–263.
Mayes, A.R., Holdstock, J.S., Isaac, C.L., Hunkin, N.M., Roberts, N., 2002. Relative sparing of item recognition memory in a patient with adult-onset damage limited to the hippocampus. Hippocampus 12, 325–340.
Mayes, A.R., Holdstock, J.S., Isaac, C.L., Montaldi, D., Grigor, J., Gummer, A., Cariga, P., Downes, J.J., Tsivilis, D., Gaffan, D., Gong, Q., Norman, K.A., 2004. Associative recognition in a patient with selective hippocampal lesions and relatively normal item recognition. Hippocampus 14, 763–784.
McBain, C.J., Dingledine, R., 1993. Heterogeneity of synaptic glutamate receptors on CA3 stratum radiatum interneurones of rat hippocampus. J. Physiol. 462, 373–392.
McBain, C.J., Fisahn, A., 2001. Interneurons unbound. Nat. Rev. Neurosci. 2, 11–23.
McBain, C.J., Mayer, M.L., 1994. N-methyl-D-aspartic acid receptor structure and function. Physiol. Rev. 74, 723–760.
McCown, T.J., Xiao, X., Li, J., Breese, G.R., Jude Samulski, R., 1996. Differential and persistent expression patterns of CNS gene transfer by an adeno-associated virus (AAV) vector. Brain Res. 713, 99–107.
McHugh, S.B., Niewoehner, B., Rawlins, J.N.P., Bannerman, D.M., 2008. Dorsal hippocampal N-methyl-d-aspartate receptors underlie spatial working memory performance during non-matching to place testing on the T-maze. Behav. Brain Res. 186, 41–47.
McHugh, T.J., Blum, K.I., Tsien, J.Z., Tonegawa, S., Wilson, M.A., 1996. Impaired hippocampal representation of space in CA1-specific NMDAR1 knockout mice. Cell 87, 1339–1349.
McHugh, T.J., Jones, M.W., Quinn, J.J., Balthasar, N., Coppari, R., Elmquist, J.K., Lowell, B.B., Fanselow, M.S., Wilson, M.A., Tonegawa, S., 2007. Dentate gyrus NMDA receptors mediate rapid pattern separation in the hippocampal network. Science 317, 94–99.
McNaughton, N., 1985. The effects of systemic and intraseptal injections of sodium amylobarbitone on rearing and ambulation in rats. Aust. J. Psychol. 37, 15–27.
McNaughton, N., Gray, J.A., 2000. Anxiolytic action on the behavioural inhibition system implies multiple types of arousal contribute to anxiety. J. Affect. Disord. 61, 161–176.
McNaughton, N., Owen, S., Boarder, M., Gray, J.A., Fillenz, M., 1984. Responses to novelty in rats with lesions of the dorsal noradrenergic bundle. N. Z. J. Psychol. 13, 16–24.
Meyer, A.H., Katona, I., Blatow, M., Rozov, A., Monyer, H., 2002. In vivo labeling of parvalbumin-positive interneurons and analysis of electrical coupling in identified neurons. J. Neurosci. 22, 7055–7064.
Miller, J., Nonneman, A., Kelly, K., Neisewander, J., Isaac, W., 1986. Disruption of neophobia, conditioned odor aversion, and conditioned taste aversion in rats with hippocampal lesions - ScienceDirect. Behav. Neural Biol. 45, 240–253.
Miller, K.M., Price, C.C., Okun, M.S., Montijo, H., Bowers, D., 2009. Is the N-Back task a valid neuropsychological measure for assessing working memory? Arch. Clin. Neuropsychol. 24, 711–717.
Milukovic, S., Restrepo, C.E., Siwani, S., Bauer, P., Pupe, S., Tort, A.B.L., Kullander, K., Leão, R.N., 2018. Ventral hippocampal OLM cells control type 2 theta oscillations and response to predator odor. Nat. Commun. 9, 3638.
Mitchell, S.J., Silver, R.A., 2003. Shunting inhibition modulates neuronal gain during synaptic excitation. Neuron 38, 433–445.
Miyake, K., Miyake, N., Shimada, T., 2015. Gene delivery into the central nervous system (CNS) using AAV vectors.
Miyake, N., Miyake, K., Yamamoto, M., Hirai, Y., Shimada, T., 2011. Global gene transfer into the CNS across the BBB after neonatal systemic delivery of single-stranded AAV vectors. Brain Res. 1389, 19–26.
Modlinska, K., Stryjek, R., 2016. Food neophobia in wild rats (Rattus norvegicus) inhabiting a changeable environment - a field study. PLOS ONE 11, e0156741.

Mölle, M., Yeshenko, O., Marshall, L., Sara, S.J., Born, J., 2006. Hippocampal sharp wave-ripples linked to slow oscillations in rat slow-wave seep. J. Neurophysiol. 96, 62–70.
Montgomery, S.M., Buzsáki, G., 2007. Gamma oscillations dynamically couple hippocampal CA3 and CA1 regions during memory task performance. Proc. Natl. Acad. Sci. U. S. A. 104, 14495–14500.
Montoya, C.P., Sainsbury, R.S., 1985. The effects of entorhinal cortex lesions on type 1 and type 2 theta. Physiol. Behav. 35, 121–126.
Monyer, H., Seeburg, P.H., Wisden, W., 1991. Glutamate-operated channels: developmentally early and mature forms arise by alternative splicing. Neuron 6, 799–810.
Morris, R.G., Anderson, E., Lynch, G.S., Baudry, M., 1986. Selective impairment of learning and blockade of long-term potentiation by an N-methyl-D-aspartate receptor antagonist, AP5. Nature 319, 774–776.
Morris, R.G., Davis, S., Butcher, S.P., 1990. Hippocampal synaptic plasticity and NMDA receptors: a role in information storage? Philos. Trans. R. Soc. Lond. B. Biol. Sci. 329, 187–204.
Morris, R.G., Garrud, P., Rawlins, J.N., O'Keefe, J., 1982. Place navigation impaired in rats with hippocampal lesions. Nature 297, 681–683.
Moser, E., Moser, M.B., Andersen, P., 1993. Spatial learning impairment parallels the magnitude of dorsal hippocampal lesions, but is hardly present following ventral lesions. J. Neurosci. 13, 3916–3925.
Moser, E.I., Kropff, E., Moser, M.-B., 2008. Place cells, grid clls, and the brain's spatial representation system. Annu. Rev. Neurosci. 31, 69–89.
Moser, M.-B., Moser, E.I., 1998. Functional differentiation in the hippocampus. Hippocampus 8, 608–619.
Moser, M.B., Moser, E.I., Forrest, E., Andersen, P., Morris, R.G., 1995. Spatial learning with a minislab in the dorsal hippocampus. Proc. Natl. Acad. Sci. 92, 9697–9701.
Müller, C., Remy, S., 2014. Dendritic inhibition mediated by O-LM and bistratified interneurons in the hippocampus. Front. Synaptic Neurosci. 6.
Müller, W., Misgeld, U., 1986. Slow cholinergic excitation of guinea pig hippocampal neurons is mediated by two muscarinic receptor subtypes. Neurosci. Lett. 67, 107–112.
Murray, A.J., Sauer, J.-F., Riedel, G., McClure, C., Ansel, L., Cheyne, L., Bartos, M., Wisden, W., Wulff, P., 2011. Parvalbumin-positive CA1 interneurons are required for spatial working but not for reference memory. Nat. Neurosci. 14, 297–299.
Nabekura, J., Ebihara, S., Akaike, N., 1993. Muscarinic receptor activation of potassium channels in rat dentate gyrus neurons. J. Neurophysiol. 70, 1544–1552.
Nadel, L., O'Keefe, J., Black, A., 1975. Slam on the brakes: A critique of Altman, Brunner, and Bayer's response-inhibition model of hippocampal function. Behav. Biol. 14, 151–162.
Nakagawa, T., 2010. The biochemistry, ultrastructure, and subunit assembly mechanism of AMPA receptors. Mol. Neurobiol. 42, 161–184.
Nakashiba, T., Young, J.Z., McHugh, T.J., Buhl, D.L., Tonegawa, S., 2008. Transgenic inhibition of synaptic transmission reveals role of CA3 output in hippocampal learning. Science 319, 1260–1264.
Nakazawa, K., Quirk, M.C., Chitwood, R.A., Watanabe, M., Yeckel, M.F., Sun, L.D., Kato, A., Carr, C.A., Johnston, D., Wilson, M.A., Tonegawa, S., 2002. Requirement for hippocampal CA3 NMDA receptors in associative memory recall. Science 297, 211–218.
Nakazawa, K., Sun, L.D., Quirk, M.C., Rondi-Reig, L., Wilson, M.A., Tonegawa, S., 2003. Hippocampal CA3 NMDA receptors are crucial for memory acquisition of one-time experience. Neuron 38, 305–315.
Nascimento Häckl, L.P., Carobrez, A.P., 2007. Distinct ventral and dorsal hippocampus AP5 anxiolytic effects revealed in the elevated plus-maze task in rats. Neurobiol. Learn. Mem. 88, 177–185.
Neher, E., Sakaba, T., 2008. Multiple roles of calcium ions in the regulation of neurotransmitter release. Neuron 59, 861–872.
Nicoll, R.A., Schmitz, D., 2005. Synaptic plasticity at hippocampal mossy fibre synapses. Nat. Rev. Neurosci. 6, 863–876.
Nissen, W., Szabo, A., Somogyi, J., Somogyi, P., Lamsa, K.P., 2010. Cell type-specific long-term plasticity at glutamatergic synapses onto hippocampal interneurons expressing either parvalbumin or CB1 cannabinoid receptor. J. Neurosci. 30, 1337–1347.
Niswender, C.M., Conn, P.J., 2010. Metabotropic glutamate receptors: Physiology, pharmacology, and disease. Annu. Rev. Pharmacol. Toxicol. 50, 295–322.
Nitz, D., McNaughton, B., 2004. Differential modulation of CA1 and dentate gyrus interneurons during exploration of novel environments. J. Neurophysiol. 91, 863–872.
Nuss, P., 2015. Anxiety disorders and GABA neurotransmission: a disturbance of modulation. Neuropsychiatr. Dis. Treat. 11, 165–175.

Nyíri, G., Stephenson, F.A., Freund, T.F., Somogyi, P., 2003. Large variability in synaptic N-methyl-D-aspartate receptor density on interneurons and a comparison with pyramidal-cell spines in the rat hippocampus. Neuroscience 119, 347–363.
Ognjanovski, N., Schaeffer, S., Wu, J., Mofakham, S., Maruyama, D., Zochowski, M., Aton, S.J., 2017. Parvalbumin-expressing interneurons coordinate hippocampal network dynamics required for memory consolidation. Nat. Commun. 8.
Oh, M.C., Derkach, V.A., 2005. Dominant role of the GluR2 subunit in regulation of AMPA receptors by CaMKII. Nat. Neurosci. 8, 853–854.
O'Keefe, J., Dostrovsky, J., 1971. The hippocampus as a spatial map. Preliminary evidence from unit activity in the freely-moving rat. Brain Res. 34, 171–175.
O'Keefe, J., Nadel, L., 1978. The hippocampus as a cognitive map. Clarendon Press, Oxford.
O'Reilly, K.C., Alarcon, J.M., Ferbinteanu, J., 2014. Relative contributions of CA3 and medial entorhinal cortex to memory in rats. Front. Behav. Neurosci. 8.
Pastalkova, E., Itskov, V., Amarasingham, A., Buzsáki, G., 2008. Internally generated cell assembly sequences in the rat hippocampus. Science 321, 1322–1327.
Penn, A.C., Greger, I.H., 2009. Sculpting AMPA receptor formation and function by alternative RNA processing. RNA Biol. 6, 517–521.
Penttonen, M., Kamondi, A., Acsády, L., Buzsáki, G., 1998. Gamma frequency oscillation in the hippocampus of the rat: intracellular analysis in vivo. Eur. J. Neurosci. 10, 718–728.
Pierson, J.L., Pullins, S.E., Quinn, J.J., 2015. Dorsal hippocampus infusions of CNQX into the dentate gyrus disrupt expression of trace fear conditioning. Hippocampus 25, 779–785.
Pietersen, A.N.J., Ward, P.D., Hagger-Vaughan, N., Wiggins, J., Jefferys, J.G.R., Vreugdenhil, M., 2014. Transition between fast and slow gamma modes in rat hippocampus area CA1 in vitro is modulated by slow CA3 gamma oscillations. J. Physiol. 592, 605–620.
Pioli, E.Y., Gaskill, B.N., Gilmour, G., Tricklebank, M.D., Dix, S.L., Bannerman, D.M., Garner, J.P., 2014. An automated maze task for assessing hippocampus-sensitive memory in mice. Behav. Brain Res 261, 249-257.
Piras, G., Rattazzi, L., McDermott, A., Deacon, R., D'Acquisto, F., 2013. Emotional change-associated T Cell mobilization at the early stage of a mouse model of multiple sclerosis. Front. Immunol. 4.
Plant, K., Pelkey, K.A., Bortolotto, Z.A., Morita, D., Terashima, A., McBain, C.J., Collingridge, G.L., Isaac, J.T.R., 2006. Transient incorporation of native GluR2-lacking AMPA receptors during hippocampal long-term potentiation. Nat. Neurosci. 9, 602–604.
Pouille, F., Scanziani, M., 2004. Routing of spike series by dynamic circuits in the hippocampus. Nature 429, 717–723.
Poulsen, M.H., Lucas, S., Strømgaard, K., Kristensen, A.S., 2014. Evaluation of PhTX-74 as subtype-selective inhibitor of GluA2-containing AMPA receptors. Mol. Pharmacol. 85, 261–268.
Pratt, J., Winchester, C., Dawson, N., Morris, B., 2012. Advancing schizophrenia drug discovery: optimizing rodent models to bridge the translational gap. Nat. Rev. Drug Discov. 11, 560–579.
Pritchett, D., Taylor, A.M., Barkus, C., Engle, S.J., Brandon, N.J., Sharp, T., Foster, R.G., Harrison, P.J., Peirson, S.N., Dannerman, D.M., 2016. Searching for cognitive enhancement in the Morris water maze: better and worse performance in D-amino acid oxidase knockout (Dao(-/-)) mice. Eur. J. Neurosci 43, 979-989.
Punnakkal, P., Jendritza, P., Köhr, G., 2012. Influence of the intracellular GluN2 C-terminal domain on NMDA receptor function. Neuropharmacology 62, 1985–1992.
Raben, N., Nagaraju, K., Lee, E., Plotz, P., 2000. Modulation of disease severity in mice with targeted disruption of the acid alpha-glucosidase gene. Neuromuscul. Disord. NMD 10, 283–291.
Raghavachari, S., Kahana, M., Rizzuto, D., Caplan, J., Kirschen, M., Bourgeois, B., Madsen, J., Lisman, J., 2001. Gating of human theta oscillations by a working memory task. J. Neurosci. 21, 3175–3183.
Ranganath, C., 2006. Working memory for visual objects: complementary roles of inferior temporal, medial temporal, and prefrontal cortex. Neuroscience 139, 277–289.
Rasch, B., Born, J., 2013. About sleep's role in memory. Physiol. Rev. 93, 681–766.
Rawlins, J.N., 1985. Associations across time: The hippocampus as a temporary memory store. Behav. Brain Sci. 8, 479–496.
Reisel, D., Bannerman, D.M., Schmitt, W.B., Deacon, R.M.J., Flint, J., Borchardt, T., Seeburg, P.H., Rawlins, J.N.P., 2002. Spatial memory dissociations in mice lacking GluR1. Nat. Neurosci. 5, 868–873.

Remondes, M., Schuman, E.M., 2002. Direct cortical input modulates plasticity and spiking in CA1 pyramidal neurons. Nature 416, 736–740.
Rex, C.S., Colgin, L.L., Jia, Y., Casale, M., Yanagihara, T.K., Debenedetti, M., Gall, C.M., Kramar, E.A., Lynch, G., 2009. Origins of an intrinsic hippocampal EEG pattern. PLoS ONE 4, e7761.
Ribak, C.E., 1992. Local circuitry of GABAergic basket cells in the dentate gyrus. Epilepsy Res. Suppl. 7, 29–47.
Ribak, C.E., Seress, L., 1983. Five types of basket cell in the hippocampal dentate gyrus: a combined Golgi and electron microscopic study. J. Neurocytol. 12, 577–597.
Ribak, C.E., Vaughn, J.E., Saito, K., 1978. Immunocytochemical localization of glutamic acid decarboxylase in neuronal somata following colchicine inhibition of axonal transport. Brain Res. 140, 315–332.
Richmond, M.A., Yee, B.K., Pouzet, B., Veenman, L., Rawlins, J.N., Feldon, J., Bannerman, D.M., 1999. Dissociating context and space within the hippocampus: effects of complete, dorsal, and ventral excitotoxic hippocampal lesions on conditioned freezing and spatial learning. Behav. Neurosci. 113, 1189–1203.
Riedel, G., Micheau, J., Lam, A.G., Roloff, E.L., Martin, S.J., Bridge, H., de Hoz, L., Poeschel, B., McCulloch, J., Morris, R.G., 1999. Reversible neural inactivation reveals hippocampal participation in several memory processes. Nat. Neurosci. 2, 898–905.
Rolls, E.T., 1999. Spatial view cells and the representation of place in the primate hippocampus. Hippocampus 9, 467–480.
Rozov, A., Burnashev, N., 1999. Polyamine-dependent facilitation of postsynaptic AMPA receptors counteracts paired-pulse depression. Nature 401, 594–598.
Rozov, A., Sprengel, R., Seeburg, P.H., 2012. GluA2-lacking AMPA receptors in hippocampal CA1 cell synapses: evidence from gene-targeted mice. Front. Mol. Neurosci. 5.
Rudy, B., McBain, C.J., 2001. Kv3 channels: voltage-gated K+ channels designed for high-frequency repetitive firing. Trends Neurosci. 24, 517–526.
Ruppersberg, J.P., Kitzing, E. v., Schoepfer, R., 1994. The mechanism of magnesium block of NMDA receptors. Semin. Neurosci. 6, 87–96.
Sakimura, K., Kutsuwada, T., Ito, I., Manabe, T., Takayama, C., Kushiya, E., Yagi, T., Aizawa, S., Inoue, Y., Sugiyama, H., 1995. Reduced hippocampal LTP and spatial learning in mice lacking NMDA receptor epsilon 1 subunit. Nature 373, 151–155.
Salahpour, A., Ramsey, A.J., Medvedev, I.O., Kile, B., Sotnikova, T.D., Holmstrand, E., Ghisi, V., Nicholls, P.J., Wong, L., Murphy, K., Sesack, S.R., Wightman, R.M., Gainetdinov, R.R., Caron, M.G., 2008. Increased amphetamine-induced hyperactivity and reward in mice overexpressing the dopamine transporter. Proc. Natl. Acad. Sci. 105, 4405–4410.
Sambandan, S., Sauer, J.-F., Vida, I., Bartos, M., 2010. Associative plasticity at excitatory synapses facilitates recruitment of fast-spiking interneurons in the dentate gyrus. J. Neurosci. 30, 11826–11837.
Sancho-Bielsa, F.J., Navarro-López, J.D., Alonso-Llosa, G., Molowny, A., Ponsoda, X., Yajeya, J., López-García, C., 2012. Neurons of the dentate molecular layer in the rabbit hippocampus. PLoS ONE 7.
Sanderson, D.J., Bannerman, D.M., 2012. The role of habituation in hippocampus-dependent spatial working memory tasks: evidence from GluA1 AMPA receptor subunit knockout mice. Hippocampus 22, 981–994.
Sanderson, D.J., Good, M.A., Skelton, K., Sprengel, R., Seeburg, P.H., Rawlins, J.N.P., Bannerman, D.M., 2009. Enhanced long-term and impaired short-term spatial memory in GluA1 AMPA receptor subunit knockout mice: Evidence for a dual-process memory model. Learn. Mem. 16, 379–386.
Sanderson, D.J., Gray, A., Simon, A., Taylor, A.M., Deacon, R.M.J., Seeburg, P.H., Sprengel, R., Good, M.A., Rawlins, J.N.P., Bannerman, D.M., 2007. Deletion of glutamate receptor-A (GluR-A) AMPA receptor subunits impairs one-trial spatial memory. Behav. Neurosci. 121, 559–569.
Sanderson, D.J., McHugh, S.B., Good, M.A., Sprengel, R., Seeburg, P.H., Rawlins, J.N.P., Bannerman, D.M., 2010. Spatial working memory deficits in GluA1 AMPA receptor subunit knockout mice reflect impaired short-term habituation: Evidence for Wagner's dual-process memory model. Neuropsychologia 48, 2303–2315.
Sans, N., Vissel, B., Petralia, R.S., Wang, Y.-X., Chang, K., Royle, G.A., Wang, C.-Y., O'Gorman, S., Heinemann, S.F., Wenthold, R.J., 2003. Aberrant formation of glutamate receptor complexes in hippocampal neurons of mice lacking the GluR2 AMPA receptor subunit. J. Neurosci. 23, 9367–9373.
Schaefers, A.T.U., Winter, Y., 2011. Rapid task acquisition of spatial-delayed alternation in an automated T-maze by mice. Behav. Brain Res. 225, 56–62.

Schlingloff, D., Káli, S., Freund, T., Háajos, N., Gulyás, A.I., 2014. Mechanisms of sharp wave initiation and ripple generation. J. Neurosci. 34, 11385-11398.
Schmitt, W.B., Deacon, R.M., Seeburg, P.H., Rawlins, J.N., Bannerman, D.M., 2003. A within-subjects, within-task demonstration of intact spatial reference memory and impaired spatial working memory in glutamate receptor-A-deficient mice. J. Neurosci. 23, 3953-3959.
Scoville, W.B., Milner, B., 1957. Loss of recent memory after bilateral hippocampal lesions. J. Neurol. Neurosurg. Psychiatry 20, 11–21.
Sederberg, P.B., Schulze-Bonhage, A., Madsen, J.R., Bromfield, E.B., McCarthy, D.C., Brandt, A., Tully, M.S., Kahana, M.J., 2007. Hippocampal and neocortical gamma oscillations predict memory formation in humans. Cereb. Cortex 1991 17, 1190–1196.
Selden, N.R., Everitt, B.J., Jarrard, L.E., Robbins, T.W., 1991. Complementary roles for the amygdala and hippocampus in aversive conditioning to explicit and contextual cues. Neuroscience 42, 335–350.
Senior, T.J., Huxter, J.R., Allen, K., O'Neill, J., Csicsvari, J., 2008. Gamma oscillatory firing reveals distinct populations of pyramidal cells in the CA1 region of the hippocampus. J. Neurosci. 28, 2274–2286.
Shepherd, J.D., 2012. Memory, plasticity and sleep - a role for calcium permeable AMPA receptors? Front. Mol. Neurosci. 5.
Shevtsova, Z., Malik, J.M.I., Michel, U., Schöll, U., Bähr, M., Kügler, S., 2006. Evaluation of epitope tags for protein detection after in vivo CNS gene transfer. Eur. J. Neurosci. 23, 1961–1969.
Shi, C.J., Cassell, M.D., 1999. Perirhinal cortex projections to the amygdaloid complex and hippocampal formation in the rat. J. Comp. Neurol. 406, 299-328.
Shipton, O.A., El-Gaby, M., Apergis-Schoute, J., Deisseroth, K., Bannerman, D.M., Paulsen, O., Kohl, M.M., 2014. Left-right dissociation of hippocampal memory processes in mice. Proc. Natl. Acad. Sci. U. S. A. 111, 15238-15243.
Sik, A., Penttonen, M., Buzsáki, G., 1997. Interneurons in the hippocampal dentate grus: an in vivo intracellular study. Eur. J. Neurosci. 9, 573–588.
Sik, A., Penttonen, M., Ylinen, A., Buzsáki, G., 1995. Hippocampal CA1 interneurons: an in vivo intracellular labeling study. J. Neurosci. 15, 6651–6665.
Smith, D.M., Mizumori, S.J.Y., 2006. Hippocampal place cells, context, and episodic memory. Hippocampus 16, 716–729.
Soderling, T.R., Derkach, V.A., 2000. Postsynaptic protein phosphorylation and LTP. Trends Neurosci. 23, 75–80.
Sohal, V.S., Zhang, F., Yizhar, O., Deisseroth, K., 2009. Parvalbumin neurons and gamma rhythms enhance cortical circuit performance. Nature 459, 698–702.
Solstad, T., Boccara, C.N., Kropff, E., Moser, M.-B., Moser, E.I., 2008. Representation of geometric borders in the entorhinal cortex. Science 322, 1865–1868.
Soltesz, I., Deschênes, M., 1993. Low- and high-frequency membrane potential oscillations during theta activity in CA1 and CA3 pyramidal neurons of the rat hippocampus under ketamine-xylazine anesthesia. J. Neurophysiol. 70, 97–116.
Sommer, B., Keinänen, K., Verdoorn, T.A., Wisden, W., Burnashev, N., Herb, A., Köhler, M., Takagi, T., Sakmann, B., Seeburg, P.H., 1990. Flip and flop: a cell-specific functional switch in glutamate-operated channels of the CNS. Science 249, 1580–1585.
Sommer, B., Köhler, M., Sprengel, R., Seeburg, P.H., 1991. RNA editing in brain controls a determinant of ion flow in glutamate-gated channels. Cell 67, 11–19.
Somogyi, P., Smith, A.D., Nunzi, M.G., Gorio, A., Takagi, H., Wu, J.Y., 1983. Glutamate decarboxylase immunoreactivity in the hippocampus of the cat: distribution of immunoreactive synaptic terminals with special reference to the axon initial segment of pyramidal neurons. J. Neurosci. 3, 1450–1468.
Soriano, E., Frotscher, M., 1989. A GABAergic axo-axonic cell in the fascia dentata controls the main excitatory hippocampal pathway. Brain Res. 503, 170–174.
Spruston, N., Lübke, J., Frotscher, M., 1997. Interneurons in the stratum lucidum of the rat hippocampus: An anatomical and electrophysiological characterization. J. Comp. Neurol. 385, 427–440.
Squire, L.R., Zola-Morgan, S., 1991. The medial temporal lobe memory system. Science 253, 1380–1386.
Steele, R.J., Morris, R.G., 1999. Delay-dependent impairment of a matching-to-place task with chronic and intrahippocampal infusion of the NMDA-antagonist D-AP5. Hippocampus 9, 118–136.
Stefanelli, T., Bertollini, C., Lüscher, C., Muller, D., Mendez, P., 2016. Hippocampal somatostatin interneurons control the size of neuronal memory ensembles. Neuron 89, 1074–1085.

Steffenach, H.-A., Sloviter, R.S., Moser, E.I., Moser, M.-B., 2002. Impaired retention of spatial memory after transection of longitudinally oriented axons of hippocampal CA3 pyramidal cells. Proc. Natl. Acad. Sci. U. S. A. 5, 3194-3198.

Stent, G.S., 1973. A physiological mechanism for Hebb's postulate of learning. Proc. Natl. Acad. Sci. U. S. A. 70, 997-1001.

Stewart, M., Fox, S.E., 1990. Do septal neurons pace the hippocampal theta rhythm? Trends Neurosci. 13, 163–169.

Struble, R.G., Desmond, N.L., Levy, W.B., 1978. Anatomical evidence for interlamellar inhibition in the fascia dentata. Brain Res. 152, 580–585.

Sullivan, D., Csicsvari, J., Mizuseki, K., Montgomery, S., Diba, K., Buzsáki, G., 2011. Relationships between hippocampal sharp waves, ripples, and fast gamma oscillation: Influence of dentate and entorhinal cortical activity. J. Neurosci. 31, 8605–8616.

Swanson, G.T., Kamboj, S.K., Cull-Candy, S.G., 1997. Single-channel properties of recombinant AMPA receptors depend on RNA editing, splice variation, and subunit composition. J. Neurosci. 17, 58–69.

Szabo, A., Somogyi, J., Cauli, B., Lambolez, B., Somogyi, P., Lamsa, K.P., 2012. Calcium-permeable AMPA receptors provide a common mechanism for LTP in glutamatergic synapses of distinct hippocampal interneuron types. J. Neurosci. 32, 6511–6516.

Tallent, M.K., 2007. Somatostatin in the dentate gyrus. Prog. Brain Res. 163, 265–284.

Tallon-Baudry, C., Kreiter, A., Bertrand, O., 1999. Sustained and transient oscillatory responses in the gamma and beta bands in a visual short-term memory task in humans. Vis. Neurosci. 16, 449–459.

Taube, J.S., Muller, R.U., Ranck, J.B., 1990. Head-direction cells recorded from the postsubiculum in freely moving rats. I. Description and quantitative analysis. J. Neurosci. 10, 420–435.

Terashima, A., Cotton, L., Dev, K.K., Meyer, G., Zaman, S., Duprat, F., Henley, J.M., Collingridge, G.L., Isaac, J.T.R., 2004. Regulation of synaptic strength and AMPA receptor subunit composition by PICK1. J. Neurosci. 24, 5381–5390.

Tiesinga, P., Sejnowski, T.J., 2009. Cortical enlightenment: are attentional gamma oscillations driven by ING or PING? Neuron 63, 727–732.

Tort, A.B.L., Komorowski, R.W., Manns, J.R., Kopell, N.J., Eichenbaum, H., 2009. Theta-gamma coupling increases during the learning of item-context associations. Proc. Natl. Acad. Sci. U. S. A. 106, 20942–20947.

Tort, A.B.L., Kramer, M.A., Thorn, C., Gibson, D.J., Kubota, Y., Graybiel, A.M., Kopell, N.J., 2008. Dynamic cross-frequency couplings of local field potential oscillations in rat striatum and hippocampus during performance of a T-maze task. Proc. Natl. Acad. U. S. A. 105, 20517-20522.

Tóth, K., Freund, T.F., Miles, R., 1997. Disinhibition of rat hippocampal pyramidal cells by GABAergic afferents from the septum. J. Physiol. 500 (Pt 2), 463–474.

Tóth, K., McBain, C.J., 1998. Afferent-specific innervation of two distinct AMPA receptor subtypes on single hippocampal interneurons. Nat. Neurosci. 1, 572–578.

Traub, R.D., Jefferys, J.G., Whittington, M.A., 1997. Simulation of gamma rhythms in networks of interneurons and pyramidal cells. J. Comput. Neurosci. 4, 141–150.

Traub, R.D., Whittington, M.A., Colling, S.B., Buzsáki, G., Jefferys, J.G., 1996a. Analysis of gamma rhythms in the rat hippocampus in vitro and in vivo. J. Physiol. 493 (Pt 2), 471–484.

Traub, R.D., Whittington, M.A., Stanford, I.M., Jefferys, J.G., 1996b. A mechanism for generation of long-range synchronous fast oscillations in the cortex. Nature 383, 621–624.

Trevelyan, A.J., Bruns, W., Mann, E.O., Crepel, V., Scanziani, M., 2013. The information content of physiological and epileptic brain activity. J. Physiol. 591, 799–805.

Treves, A., Rolls, E.T., 1994. Computational analysis of the role of the hippocampus in memory. Hippocampus 4, 374–391.

Tsien, J.Z., Huerta, P.T., Tonegawa, S., 1996. The Essential Role of Hippocampal CA1 NMDA Receptor–Dependent Synaptic Plasticity in Spatial Memory. Cell 87, 1327–1338.

Tsintsadze, V., Minlebaev, M., Suchkov, D., Cunningham, M.O., Khazipov, R., Ontogeny of kainate-induced gamma oscillations in the rat CA3 hippocampus in vitro. Front. Cell. Neurosci. 9.

Tukker, J.J., Fuentealba, P., Hartwich, K., Somogyi, P., Klausberger, T., 2007. Cell type-specific tuning of hippocampal interneuron firing during gamma oscillations in vivo. J. Neurosci. 27, 8184–8189.

Tuyttens, F.A.M., de Graaf, S., Heerkens, J.L.T., Jacobs, L., Nalon, E., Ott, S., Stadig, L., Van Laer, E., Ampe, B., 2014. Observer bias in animal behaviour research: can we believe what we score, if we score what we believe? Animal Behav. 90, 273-280.

van Groen, T., Miettinen, P., Kadish, I., 2003. The entorhinal cortex of the mouse: organization of the projection to the hippocampal formation. Hippocampus 13, 133–149.
van Vugt, M.K., Schulze-Bonhage, A., Litt, B., Brandt, A., Kahana, M.J., 2010. Hippocampal gamma oscillations increase with memory load. J. Neurosci. 30, 2694–2699.
van Wilgenburg, E., Elgar, M.A., 2013. Confirmation bias in studies of nestmate recognition: a cautionary tale for research into the behaviour of animals. PLoS One 8, e53548.
Vargha-Khadem, F., Gadian, D.G., Watkins, K.E., Connelly, A., Paesschen, W.V., Mishkin, M., 1997. Differential effects of early hippocampal pathology on episodic and semantic memory. Science 277, 376–380.
Vasuta, C., Artinian, J., Laplante, I., Hébert-Seropian, S., Elayoubi, K., Lacaille, J.-C., 2015. Metaplastic regulation of CA1 Schaffer collateral pathway plasticity by Hebbian MGluR1a-mediated plasticity at excitatory synapses onto somatostatin-expressing interneurons. eNeuro 2.
Veit, J., Hakim, R., Jadi, M.P., Sejnowski, T.J., Adesnik, H., 2017. Cortical gamma band synchronization through somatostatin interneurons. Nat. Neurosci. 20, 951-959.
Venance, L., Rozov, A., Blatow, M., Burnashev, N., Feldmeyer, D., Monyer, H., 2000. Connexin expression in electrically coupled postnatal rat brain neurons. Proc. Natl. Acad. Sci. U. S. A. 97, 10260–10265.
Verdoorn, T.A., Burnashev, N., Monyer, H., Seeburg, P.H., Sakmann, B., 1991. Structural determinants of ion flow through recombinant glutamate receptor channels. Science 252, 1715–1718.
Verwey, M., Robinson, B., Amir, S., 2013. Recording and analysis of circadian rhythms in running-wheel activity in rodents. J. Vis. Exp. 24.
Vida, I., Bartos, M., Jonas, P., 2006. Shunting inhibition improves robustness of gamma oscillations in hippocampal interneuron networks by homogenizing firing rates. Neuron 49, 107–117.
Vogels, T.P., Sprekeler, H., Zenke, F., Clopath, C., Gerstner, W., 2011. Inhibitory plasticity balances excitation and inhibition in sensory pathways and memory networks. Science 334, 1569–1573.
Walker, H.C., Lawrence, J.J., McBain, C.J., 2002. Activation of kinetically distinct synaptic conductances on inhibitory interneurons by electrotonically overlapping afferents. Neuron 35, 161–171.
Wang, J.Q., Arora, A., Yang, L., Parelkar, N.K., Zhang, G., Liu, X., Choe, E.S., Mao, L., 2005. Phosphorylation of AMPA receptors: mechanisms and synaptic plasticity. Mol. Neurobiol. 32, 237–249.
Wang, X.J., Buzsáki, G., 1996. Gamma oscillation by synaptic inhibition in a hippocampal interneuronal network model. J. Neurosci. 16, 6402–6413.
Washburn, M.S., Dingledine, R., 1996. Block of alpha-amino-3-hydroxy-5-methyl-4-isoxazolepropionic acid (AMPA) receptors by polyamines and polyamine toxins. J. Pharmacol. Exp. Ther. 278, 669–678.
Washburn, M.S., Numberger, M., Zhang, S., Dingledine, R., 1997. Differential dependence on GluR2 expression of three characteristic features of AMPA receptors. J. Neurosci. 17, 9393–9406.
Wenthold, R.J., Petralia, R.S., Blahos J, I.I., Niedzielski, A.S., 1996. Evidence for multiple AMPA receptor complexes in hippocampal CA1/CA2 neurons. J. Neurosci. 16, 1982–1989.
West, A.E., Chen, W.G., Dalva, M.B., Dolmetsch, R.E., Kornhauser, J.M., Shaywitz, A.J., Takasu, M.A., Tao, X., Greenberg, M.E., 2001. Calcium regulation of neuronal gene expression. Proc. Natl. Acad. Sci. U. S. A. 98, 11024-11031.
Whitehead, G., Jo, J., Hogg, E.L., Piers, T., Kim, D.-H., Seaton, G., Seok, H., Bru-Mercier, G., Son, G.H., Regan, P., Hildebrandt, L., Waite, E., Kim, B.-C., Kerrigan, T.L., Kim, K., Whitcomb, D.J., Collingridge, G.L., Lightman, S.L., Cho, K., 2013. Acute stress causes rapid synaptic insertion of Ca2+ -permeable AMPA receptors to facilitate long-term potentiation in the hippocampus. Brain J. Neurol. 136, 3753–3765.
Whittington, M.A., Cunningham, M.O., LeBeau, F.E.N., Racca, C., Traub, R.D., 2011. Multiple origins of the cortical gamma rhythm. Dev. Neurobiol. 71, 92–106.
Whittington, M.A., Traub, R.D., Jefferys, J.G., 1995. Synchronized oscillations in interneuron networks driven by metabotropic glutamate receptor activation. Nature 373, 612–615.
Wiltgen, B.J., Zhou, M., Cai, Y., Balaji, J., Karlson, M.G., Parivash, S.N., Li, W., Silva, A.J., 2010. The hippocampus plays a selective role in the retrieval of detailed context memories. Curr. Biol. 20, 1336–1344.
Winkelmann, A., Maggio, N., Eller, J., Caliskan, G., Semtner, M., Häussler, U., Jüttner, R., Dugladze, T., Smolinsky, B., Kowalczyk, S., Chronowska, E., Schwarz, G., Rathjen, F.G., Rechavi, G., Haas, C.A., Kulik, A., Gloveli, T., Heinemann, U., Meier, J.C., 2014. Changes in neural network homeostasis trigger neuropsychiatric symptoms. J. Clin. Invest. 124, 696–711.
Winson, J., 1978. Loss of hippocampal theta rhythm results in spatial memory deficit in the rat. Science 201, 160–163.

Winters, B.D., Forwood, S.E., Cowell, R.A., Saksida, L.M., Bussey, T.J., 2004. Double dissociation between the effects of peri-postrhinal cortex and hippocampal lesions on tests of object recognition and spatial memory: heterogeneity of function within the temporal lobe. J. Neurosci. 24, 5901–5908.
Wisden, W., Seeburg, P.H., 1993. Mammalian ionotropic glutamate receptors. Curr. Opin. Neurobiol. 3, 291–298.
Witter, M.P., Groenewegen, H.J., Lopes da Silva, F.H., Lohman, A.H., 1989. Functional organization of the extrinsic and intrinsic circuitry of the parahippocampal region. Prog. Neurobiol. 33, 161–253.
Witter, M.P., Naber, P.A., van Haeften, T., Machielsen, W.C., Rombouts, S.A., Barkhof, F., Scheltens, P., Lopes da Silva, F.H., 2000. Cortico-hippocampal communication by way of parallel parahippocampal-subicular pathways. Hippocampus 10, 398–410.
Wolf, M.E., Tseng, K.Y., 2012. Calcium-permeable AMPA receptors in the VTA and nucleus accumbens after cocaine exposure: when, how, and why? Front. Mol. Neurosci. 5, 72.
Wright, A., Vissel, B., 2012. The essential role of AMPA receptor GluR2 subunit RNA editing in the normal and diseased brain. Front. Mol. Neurosci. 5.
Yamamoto, J., Suh, J., Takeuchi, D., Tonegawa, S., 2014. Successful execution of working memory linked to synchronized high-frequency gamma oscillations. Cell 157, 845–857.
Ylinen, A., Soltész, I., Bragin, A., Penttonen, M., Sik, A., Buzsáki, G., 1995. Intracellular correlates of hippocampal theta rhythm in identified pyramidal cells, granule cells, and basket cells. Hippocampus 5, 78–90.
Yonelinas, A.P., Kroll, N.E.A., Quamme, J.R., Lazzara, M.M., Sauvé, M.-J., Widaman, K.F., Knight, R.T., 2002. Effects of extensive temporal lobe damage or mild hypoxia on recollection and familiarity. Nat. Neurosci. 5, 1236–1241.
Yuan, M., Meyer, T., Benkowitz, C., Savanthrapadian, S., Ansel-Bollepalli, L., Foggetti, A., Wulff, P., Alcami, P., Elgueta, C., Bartos, M., 2017. Somatostatin-positive interneurons in the dentate gyrus of mice provide local- and long-range septal synaptic inhibition. eLife 6.
Zarnadze, S., 2016. Gamma oscillation-induced plasticity in area CA3 of the hippocampus. PhD Thesis, Charité – Universitätsmedizin Berlin.
Zemankovics, R., Veres, J.M., Oren, I., Hájos, N., 2013. Feedforward inhibition underlies the propagation of cholinergically induced gamma oscillations from hippocampal CA3 to CA1. J. Neurosci. 33, 12337–12351.
Zeng, H., Chattarji, S., Barbarosie, M., Rondi-Reig, L., Philpot, B.D., Miyakawa, T., Bear, M.F., Tonegawa, S., 2001. Forebrain-specific calcineurin knockout selectively impairs bidirectional synaptic plasticity and working/episodic-like memory. Cell 107, 617–629.
Zou, D., Chen, L., Deng, D., Jiang, D., Dong, F., McSweeney, C., Zhou, Y., Liu, L., Chen, G., Wu, Y., Mao, Y., 2016. DREADD in parvalbumin interneurons of the dentate gyrus modulates anxiety, social interaction and memory extinction. Curr. Mol. Med. 16, 91–102.